STUDIES TOWARD THE SYNTHESIS OF (–) AGELASTATIN A
AND
MECHANISTIC INVESTIGATIONS OF THE UNCATALYZED CHLOROCYCLIZATION OF 4-PHENYL-4-PENTENOIC ACID

By

Emily R. Dzurka

A DISSERTATION

Submitted to
Michigan State University
in partial fulfillment of the requirements
for the degree of

Chemistry – Doctor of Philosophy

2022

ABSTRACT

STUDIES TOWARD THE SYNTHESIS OF (–) AGELASTATIN A
AND
MECHANISTIC INVESTIGATIONS OF THE UNCATALYZED CHLOROCYCLIZATION
OF 4-PHENYL-4-PENTENOIC ACID

By

Emily R. Dzurka

This thesis presents an investigation into efforts towards the total synthesis of agelastatin A, as well as a mechanistic study of the uncatalyzed chlorocyclization reaction of 4-phenyl-4-pentenoic acid.

Chapter 1 introduces all the prior total syntheses completed to date of agelastatin A. This chapter details the benefits, and similarities between each synthesis, as well as serves as an introduction into why a different, and novel route to the molecule is beneficial. Chapter 2 presents the current studies towards synthesizing the molecule utilizing chemistry that was developed in the Borhan lab. Within this chapter, different synthetic routes to access the molecule are described.

Chapter 3 focuses on the mechanistic studies to determine the molecularities that lead to the *syn*- and *anti*-chlorolactonization. Chemical kinetics were a central part of this investigation, as well as concentration studies. This information provided key insights into the postulated transition states that lead either the *syn*-addition or *anti*-addition product.

For My Family

ACKNOWLEDGEMENTS

I am incredibly grateful for so many people supporting me though my journey and time here at Michigan State University.

First and foremost, I'd like to thank my advisor Babak Borhan. Almost five years ago, I joined the Borhan lab and since then you have helped develop me into the scientist that I am today. I am forever grateful for your constant guidance and support, and for granting me the independence in lab to lead my research projects in the direction that I found most exciting. Babak is an extremely supportive mentor and teacher, and I appreciate you for supporting me inside, and outside of the laboratory. Due to your support and guidance, the development of Women in Chemistry group at Michigan State University was successful, and I am eternally appreciative that you trusted me to lead this group as well as my research projects simultaneously. Babak's guidance and support has allowed me to grow into a collaborative researcher, and now as an educator. I am forever thankful.

I am grateful to Dr. Dan Holmes and Dr. Li Xie for their patience and willingness to answer all my questions, and for training me on the numerous NMR instruments. They were incredibly helpful in helping me learn how to effectively collect data for my kinetic experiments. They were also incredibly helpful with answering any NMR question that I may have.

To my committee members, Dr. William Wulff, Dr. Robert Maleczka, and Dr. Milton Smith, thank you for providing feedback and willingness to answer my questions relating to my research projects, seminar preparation, or class material. Dr. Wulff, I'd like to specifically thank you for the opportunity to meet and work with you on a weekly basis

(pre-COVID) to contribute to the database. These interactions were not only a great way to learn from you and discuss new chemistry and new reactions, but it also taught me how to search the chemical literature. I always looked forward to our discussions during these meetings, or on Friday evenings, as it was always a pleasure to chat with you about chemistry, or just life in general.

Dr. Karen Draths and Dr. Chysoula Vasileiou, I cannot tell you how much I enjoyed contributing to Women in Chemistry with you. Those were some of my fondest memories, and I am extremely grateful for your support to develop the group and build it into the important stature that it is today within the department. Specifically, Chysoula, I'd like to thank you for your support throughout all of graduate school. You are such a huge part of the Borhan lab, and I always enjoyed our chats in your office about cats, plants, and anything else that we wanted to talk about. You are always more than willing to help, and for your guidance and support I will always be grateful.

To my lab mates, it has been a pleasure to work alongside, and to learn from you. Dr. Hadi Gholami, Dr. Saeedeh Torabi Kohlbouni, Dr. Ali Mohammadlou, Dr. Aritra Sarkar, Dr. Rahele Esmatpour Salmani, Dr. Dan Steigerwald, Dr. Xin Liang Ding, Dr. Wei Sheng, and Dr. Jun Zhang, thank you for your guidance and support. Debarshi Chakraborty, Ankush Chakraborty, and Mitch Maday you were great mentors and friends. Thank you for keeping 526 fun and enjoyable. Behad Masoudi, Aria, Vahdani, Jiaojiao Wang, Sophie Bedford, Mehdi Moemeni, Ishita Chandra, Soham Maity; thank you for laughs, and for being such wonderful lab mates.

To my parents, Mom and Dad, you have always supported me in my academic endeavors, and I am forever grateful for your continued love and support, which has been

invaluable throughout these years. This accomplishment, and my successes would not have been possible without you and your support. I love you both!

Finally, I'd like to thank my amazing fiancé, Drew. You have been my main supporters all these years and encouraged me when it seemed too difficult. At the lows and at the highs, you were always there guiding me, helping me, and supporting me. Drew, you are the best person I know, and I am fortunate to share my life with you and our girls, Olly and Murphy. You make everything around you better, including me, and you make me want to do the best I can. I am constantly grateful for you, your love, our cat family, and the life we have built together. I love you, nug bug.

TABLE OF CONTENTS

LIST OF TABLES

LIST OF FIGURES

LIST OF SCHEMES

LIST OF ABBREVIATIONS

Ac_2O	acetic anhydride
AcOH	acetic acid
Ad_E3	termolecular electrophilic addition
AIBN	azobisisobutyronitrile
Bu	butyl
Bn	benzyl
CAN	ceric ammonium nitrate
Cbz	benzyl formate
CD	circular dichroism
CDI	carbonyldiimidazole
CH_2Cl_2	dichloromethane
$CHCl_3$	chloroform
CuTC	copper(I) thiophene-2-carboxylate
D_2O	deuterium oxide
DABCO	1,4-diazobicyclooctane
DBU	1,8-diazabicyclo(5.4.0)undec-7-ene
DCDMH	1,3-dichloro-5,5-dimethylhydantoin
DCDPH	1,3-dichloro-5,5-diphenylhydantoin
DCE	1,2-dichloroethane
DEAD	diethyl azodicarboxylate
DHP	3,4-dihydropyran

$(DHQD)_2PHAL$	hydroquinidine 1,4-phthalazinediyl diether
Di. Ch. T.	dichloroamide T
DIAD	diisopropyl azodicarboxylate
DIBAL	diisobutylaluminum hydride
DIPEA	diisopropylethylamine
DIPEA	*N,N*-diisopropylethylamine
DMAP	4-dimethylaminopyridine
DMF	dimethylformamide
DMSO	dimethylsulfoxide
DTBMP	2,6-di-*tert*-butyl-4-methylpyridine
EDCI	1-ethyl-3-(3-dimethylaminopropyl)carbodiimide
eq.	equation
equiv	equivalent
Et	ethyl
Et_2O	diethyl ether
EtOAc	ethyl acetate
EtOH	ethanol
Exp	experiment
g	gram
HalA	halenium affinity
H-bonding	hydrogen bonding
Hex	hexane
HFIP	hexafluoro-2-propanol

HMPT	hexamethylphosphoramide
HOBt	hydroxybenzotriazole
h	hour
IBX	2-idoxybenzoic acid
J	coupling constant
KHMDS	potassium bis(trimethylsilyl)amide
KIE	kinetic isotopic effect
LDA	lithium diisopropylamide
MCDMH	3-chloro-5,5-dimethylhydantoin
*m*CPBA	*m*-chloroperbenzoic acid
Me	methyl
MeCN	acetonitrile
MeOH	methanol
mg	milligram
mL	milliliter
mmol	millimole
MOA	mechanism of action
mol	mole
MsCl	methanesulfonyl chloride
NAAA	nucleophile assisted alkene activation
NBS	*N*-bromosuccinimide
NcSac	chlorosaccharin
NMO	*N*-methylmorpholine *N*-oxide

NMR	nuclear magnetic resonance
NOE	nuclear overhauser effect
PDC	pyridinium dichromate
PhH	benzene
PhMe	toluene
PPTS	pyridinium *p*-toluenesulfonate
SAR	structure activity relationship
SES	2-trimethylsilylethanesulfonyl
*t*AmOH	*tert*-amyl alcohol
TBAF	tetrabutylammonium fluoride
t-BuOH	*tert*-butyl alcohol
TCCA	trichloroisocyanuric acid
Tf_2O	trifluoromethane sulfonic anhydride
TFA	trifluoroacetic acid
THF	tetrahydrofuran
TIPS-	triisopropylsilyl
TIPSCl	triisopropylsilyl chloride
TLC	thin layer chromatography
TMSI	trimethylsilyl iodide
$TMSN_3$	trimethylsilyl azide
TPAP	tetrapropylammonium perruthenate
Ts	tosyl
VTNA	variable time normalized analysis

Chapter 1 – Significance and Prior Syntheses of (–) Agelastatin A

1.1. Isolation, Characterization, and Biological Activity

The agelastatin family of alkaloids (Figure 1.1) are a group of cytotoxic molecules that exhibit a unique, complex tetracyclic framework possessing multiple contiguous stereocenters. Agelastatins A (**1**) and B (**2**) were isolated from the Coral Sea marine sponge, *Agelas dendromorpha* in 1993 near New Caledonia.[1] Agelastatins C (**3**) and D (**4**) were isolated in 1998 from the West Australian sponge, *Cymbastela sp.*[2] In 2010, agelastatins E (**5**) and F (**6**) were isolated from the New Caledonian sponge *A. dendromorpha* (Figure 1.1).[3]

Figure 1.1. Molecular structures of all agelastatin alkaloids (**1-6**)

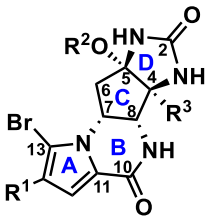

$R^1 = R^2 = R^3 = H$, $R^4 = Me$	(-)-agelastatin A (**1**)
$R^1 = Br$, $R^2 = R^3 = H$, $R^4 = Me$	(-)-agelastatin B (**2**)
$R^1 = R^2 = H$, $R^3 = OH$, $R^4 = Me$	(-)-agelastatin C (**3**)
$R^1 = R^2 = R^3 = R^4 = H$	(-)-agelastatin D (**4**)
$R^1 = R^3 = H$, $R^2 = R^4 = Me$	(-)-agelastatin E (**5**)
$R^1 = Br$, $R^2 = R^3 = R^4 = H$	(-)-agelastatin F (**6**)

Characterization of agelastatin A (**1**) was accomplished using extensive nuclear magnetic resonance (NMR) studies as well as comparison of degradative studies.[1] *Cis* stereochemistry between C5-C4 and C7-C8 was elucidated using NOE, and *trans*-fusion

stereochemistry was established by the small coupling between H(C4) and H(C8). Other extensive NOE within the molecule confirmed these results.[1] Utilizing molecular modeling and CD exciton-coupling method, the absolute stereochemistry was found to be *S* configuration at C4 and C5, and *S* configuration at C8 and *R* configuration at C7.[4]

Agelastatin A (**1**) represents several complex, unmet synthetic challenges, but it also exhibits a broad array of potent biological activities. Specifically, (–) agelastatin A (**1**) exhibits antitumor effects against a range of human tumor cells, such as human bladder, skin, colon, and breast carcinomas, and it was found to be 1.5 to 1.6 times more potent than cisplatin for malignant cell growth inhibition.[5] Though a series of cell assays and *in vitro* experiments, it was demonstrated that agelastatin A blocks protein synthesis by directly inhibiting ribosome elongation.[6] *In vivo* studies also indicated that upon administration of agelastatin A (**1**) to mice with leukemia, an increase in lifespan was observed.[5] Computational docking studies showed that hydrogen bonds in the D-ring with amino acid residues in close proximity of the binding pocket, as well as π-π stacking between the pyrrole ring and neighboring aromatic amino acids contribute to the molecular interactions and potency of the molecule.[6] Other than potency against various cancers, agelastatin A has shown potential as a small molecule treatment for Alzheimer's disease. In this case, the primary mode of action (MOA) was observed though inhibition of the glycogen synthase kinase 3β.[7] This enzyme has been shown to contribute to abnormal phosphorylation of the protein *tau*, which is hypothesized to be one of the primary causes for triggering Alzheimer's disease.[8] This enzyme has also been shown to have a role in bipolar disorder. Thus, the ability for agelastatin A (**1**) to inhibit the glycogen

synthase kinase 3β could also provide potential therapeutic options for Alzheimer's and bipolar disorder.

The unique and complex 5,6,5,5 tetracyclic core of the agelastatin family, coupled with the cytotoxicity associated with these molecules have prompted considerable efforts toward the total synthesis of agelastatin A (**1**). Currently, numerous total syntheses of agelastatin A (**1**) have been reported to date.[9,10,11,12,13,14,15,16,17,18,19,20] The fused ring system, specifically for the C-ring with 4 contiguous nitrogen-substituted stereogenic centers has proved most challenging in the prior syntheses, and only two of these syntheses involve late-stage construction of the densely functionalized C-ring.[19,20] The development of a concise, modular synthetic platform to construct the complex agelastatin core could provide access to these natural products in an asymmetric fashion without the use of precursors from the chiral pool. Late-stage core construction as well as introduction of the stereocenters also provides access to unprecedented analogs in an efficient manner for more in-depth structural activity relationship (SAR) as well as MOA analysis.

1.2. Prior Syntheses

The first total synthesis of agelastatin A (**1**) was completed in 1999 by Weinreb et *al*. highlighted by a hetero cycloaddition and a Sharpless/Kresze allylic amination protocol, shown in Scheme 1.1.[9] First, a hetero-Diels-Alder cyclization between cyclopentadiene and *N*-sulfinyl methyl carbamate formed bicyclic amino-sulfoxide **I-7.**[21] **I-7** is then immediately reacted with PhMgBr to form sulfoxide **I-8**, which is prone to

undergo a sigmatropic reaction to produce the allylic sulfoxide **I-11**. Upon heating, this intermediate readily undergoes a 2,3-sigmatropic allylic rearrangement to construct the amine-alcohol cyclopentene **I-10**. Carbamate formation and Boc protection allowed for a Sharpless/Kresze allylic amination[22] to successfully provide amino-carbamate **I-14** in good yield. Reduction with sodium borohydride, followed by amide coupling with **I-16**, and desilylation with TBAF afforded pyrrole **I-18**. Hydrolysis with LiOH, PDC oxidation of the newly formed carbinol and then 1,4-aza-Michael addition of the pyrrole afforded **I-19**, successfully constructing the A, B, and C rings of the core in a diastereoselective manner. *Ipso* bromo-desilylation using NBS smoothly installed the bromide on the pyrrole, and Boc deprotection was then achieved using TMSI at ambient temperature. The use of acids, such as TFA, caused dimerization. Lastly, subjection of the amino-ketone to sodium hydroxide and methyl isocyanate provided the urea, constructing the D ring diastereoselectively and completing the first total synthesis of agelastatin A (**1**) in an asymmetric route of 16 overall steps. Ring closure of the D-ring was hypothesized to be selective for *cis* because *cis*-fusion of the C and D ring is calculated to be approximately 20 kcal/mol more stable than the *trans* isomer.[2]

Scheme 1.1. Weinreb's total synthesis of (±) agelastatin A (**1**)

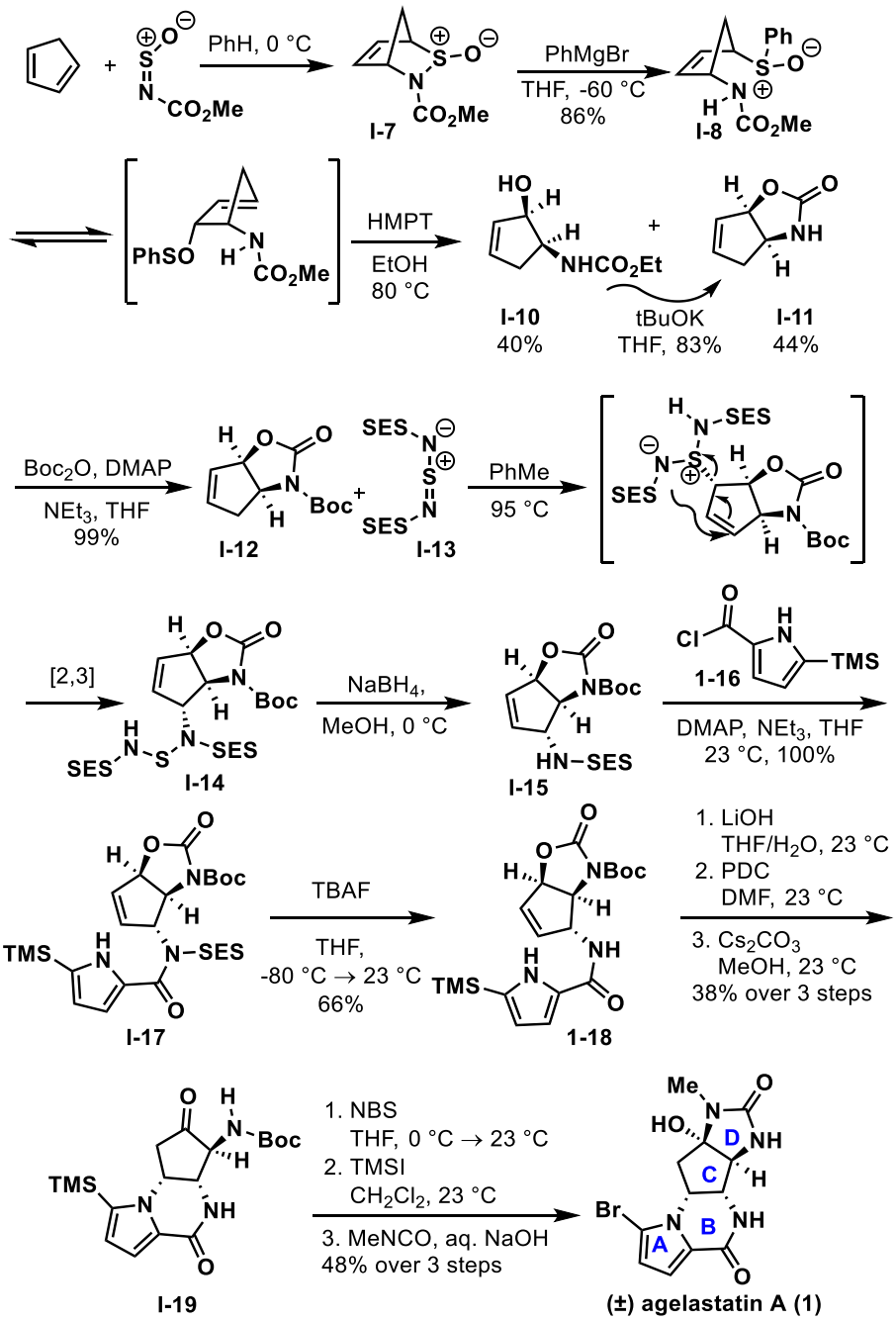

The first asymmetric total synthesis of agelastatin A (**1**) was completed by Feldman *et al.* in 2002 (Scheme 1.2).[10] The synthesis commenced with chiral epoxyalkyne **I-20**, which is selectively opened with sodium azide, and the resultant carbinol was subjected to oxazolidinone synthesis using PMe_3, *n*-BuLi and CO_2 successfully providing the cyclic carbamate **I-21**. The silylalkyne was converted to the stannane **I-22** in a three-step sequence, which upon exposure to PhI(CN)OTf (Stang's reagent),[23] alkynyliodonium salt **I-23** was accessed. This intermediate readily reacts with sodium *p*-toluenesulfinate to form the putative alkylidenecarbene intermediate that undergoes a 1,5 C-H insertion to form the cyclopentene **I-24** in modest yield. The cyclization yields the cis-fused product diastereoselectively, setting one of the four C-N stereocenters. High selectivity is observed because the *cis*-isomer is calculated to be approximately 20 kcal/mol lower in energy than the *trans* isomer.[2]

Conjugate addition of *o*-nitrobenzylamine onto the α, β-unsaturated sulfone, and then acylation with pyrrolic acid chloride **I-25** provided amide **I-26** in good yield and diastereoselectivity. Stereochemistry for the B and C rings was hypothesized to be established by the concave framework upon conjugate addition of *o*-nitrobenzylamine onto the sulfone, and therefore set the second of four C-N stereocenters on the central C-ring. The unfunctionalized pyrrole was used to avoid issues throughout the remaining steps in the synthesis. Cs_2CO_3 mediated hydrolysis of the oxazolidinone followed by Swern oxidation provided ketone **I-28** in good yield. Upon oxidation to the ketone, it was discovered that the traditional Swern conditions also facilitated a 1,4-aza Michael addition to construct the B-ring, forming the tricycle in a one-pot process. Long-wave irradiation followed by selective mono-bromination, using precisely one equivalent of NBS in the

solvent mixture of MeOH/THF successfully completed the first asymmetric total synthesis of (–) agelastatin A in 14 overall steps.

Scheme 1.2. Feldman's asymmetric total synthesis of (–) agelastatin A (**1**)

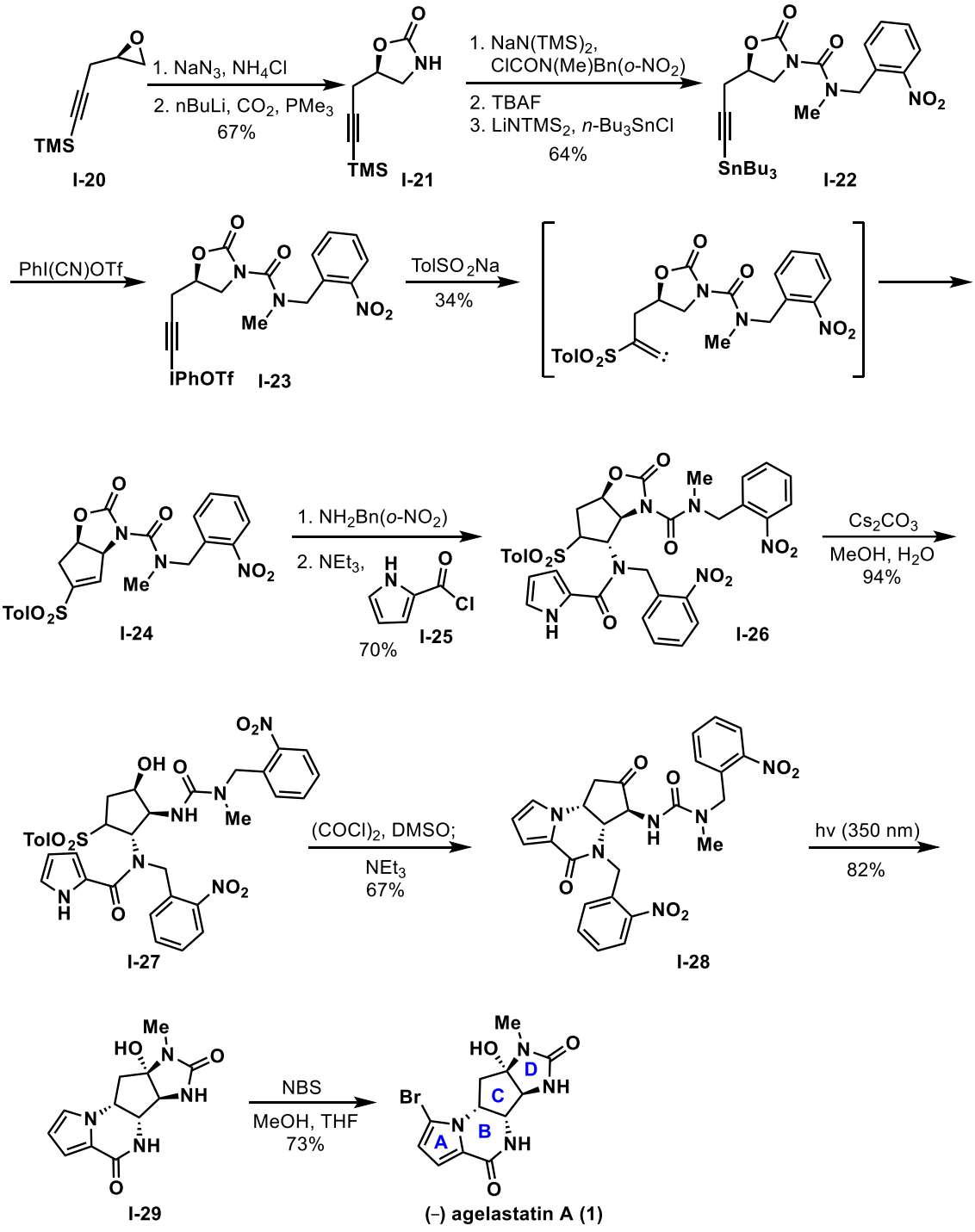

In a strategy reminiscent of the pioneering work conducted by Weinreb, Hale and co-workers published an enantiospecific total synthesis of (–) agelastatin A (**1**) starting from chiral oxazolidinone (–) **I-15** (Scheme 1.3).[11] Chiral (–) **I-15** was prepared from D-glucosamine in 17 steps.[24] Racemic **15** was previously used as an advanced intermediate in the Weinrab synthesis of racemic agelastatin A (**1**), however, in this synthesis, the use of chiral (–) **I-15** constitutes an enantiospecific total synthesis of agelastatin A.[11] This synthesis sought an alternative route to (–) agelastatin A (**1**) from Weinreb et *al*. due to their use of highly dangerous methyl isocyanate.

Boc deprotection using trifluoroacetic acid, followed by *N*-carbamoylation with the acid chloride[25] to form the urea **I-31** was achieved in high yield using the combination of *n*-BuLi and DABCO. A second *N*-acylation, followed by treatment with $HSnBu_3$ and AIBN mediated deprotection, and then subsequent hydrolysis, PDC oxidation and selective NBS-mediated 1,4-aza Michael cyclization afforded bromo-tricycle **I-35** in five steps. Unlike previous syntheses,[9,10] treatment of enone **I-34** with bases such as Et_3N, NaH, KHMDS, Cs_2CO_3 and PBu_3 all proved ineffective, only returning back the starting enone. However, upon subjecting the pyrrole-enone to NBS, *ipso*-bromodesilylation and further bromination of the pyrrole affords a more acidic pyrrole intermediate, which then readily undergoes the desired 1,4-aza Michael cyclization in the presence of Hunig's base. pK_a studies conducted by Hale and co-workers indicated this as a plausible explanation as to why successful cyclization occurs upon bromination.[24] **I-35** exists as a mixture of brominated compounds, however, dehalogenation readily occurs using Pd/C in the presence of H_2 and NaOAc to form **I-36**. Hydrogenative benzyl deprotection followed by selective mono-bromination completed the synthesis to afford (–) agelastatin A (**1**).

Scheme 1.3. Hale's asymmetric synthesis of (–) agelastatin A (**1**)

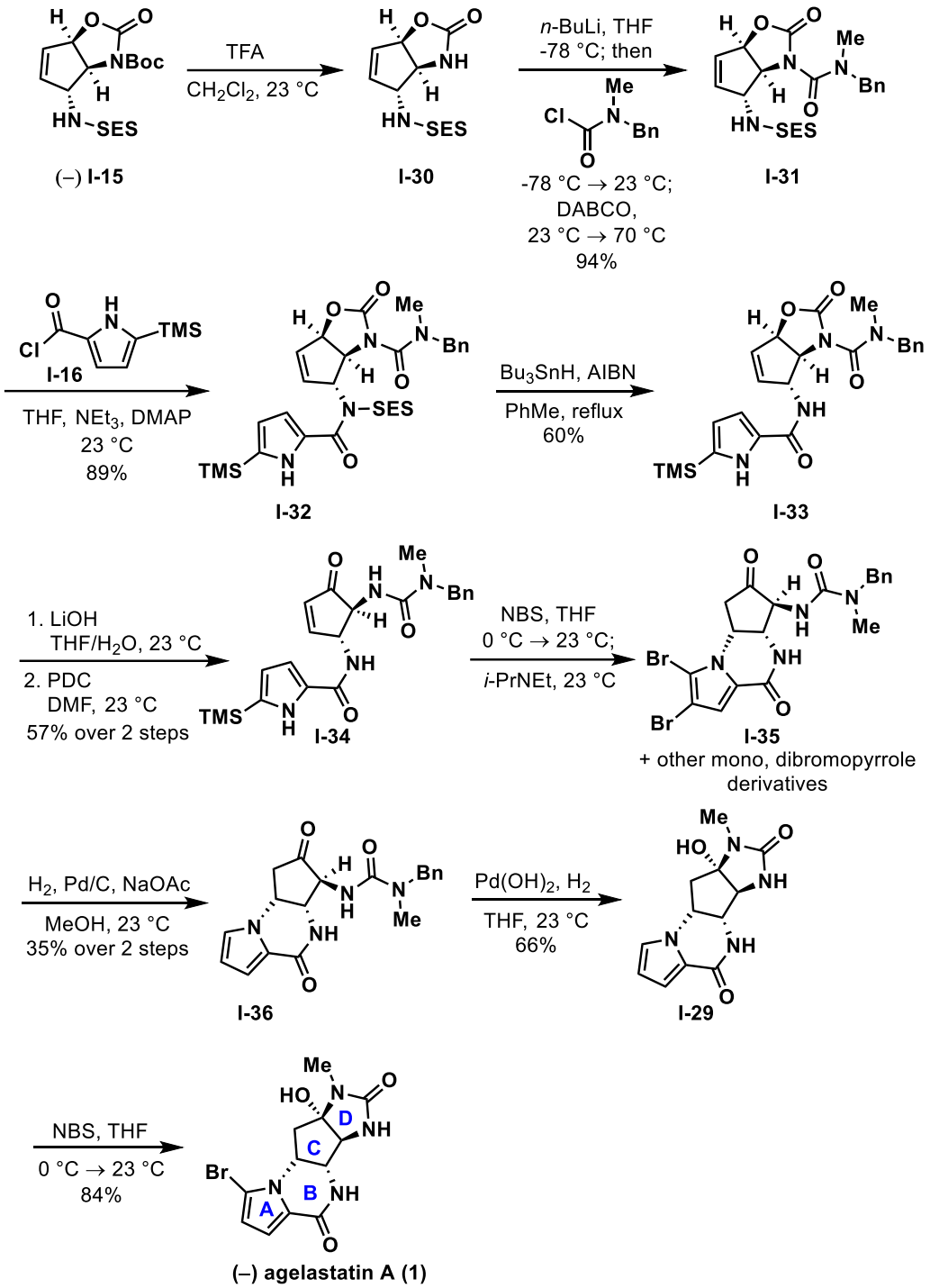

The next asymmetric enantioselective total synthesis of (–) agelastatin A (**1**) was developed by Davis, highlighted by the construction of core intermediates though an enantioselective and diastereoselective alkylation, cross-metathesis, and a diastereoselective 1,4-aza Michael addition.[12]

Scheme 1.4. Davis' asymmetric synthesis of (–) agelastatin A (**1**)

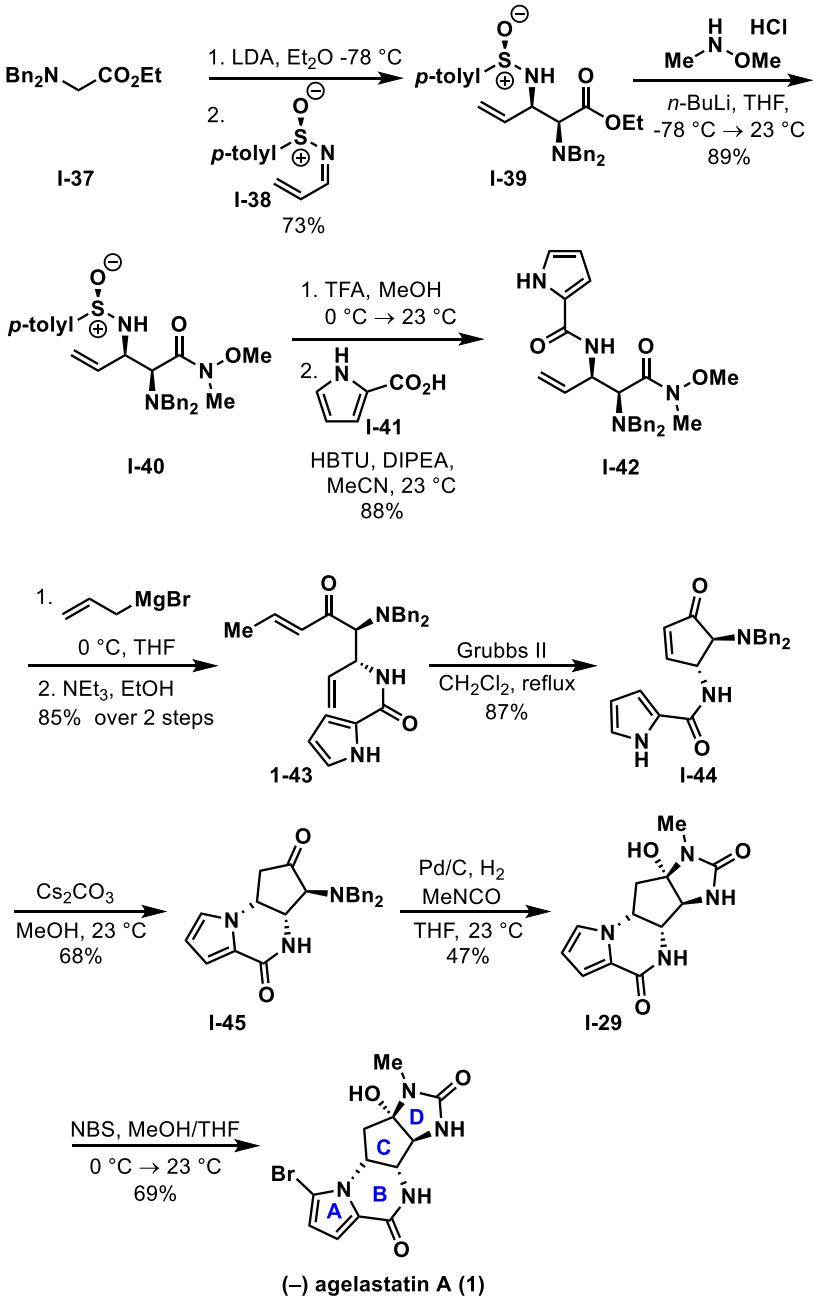

The synthesis began with the preparation of the chiral precursor, α, β diamino ester **I-39**, accomplished using enantioselective alkylation of **I-37** with enantiopure sulfinimine **I-38.** (Scheme 1.4). Chiral sulfinimine **I-38** was prepared from commercially available (1*R*,2*S*,5*R*)-(–)-menthyl (*S*)-*p*-toluenesulfinate, or (1*R*,2*S*,5*R*)-(–)-menthyl (*R*)-*p*-toluenesulfinate.[26] Thee of the four possible diastereomers were isolated in a ratio of 18:1:5, with the major *syn* diastereomer (**1-39**) being isolated in 73% yield. High selectivity was predicted due to the chair like transition state during the alkylation of the enolate (Scheme 1.5). *E*-enolate formation of **I-37** leads to the proposed transition state, which provides *syn* selectivity because of the lower energy associated with the depicted diastereomeric transition state shown in Scheme 1.5.[27]

Scheme 1.5. Determination of Stereochemistry

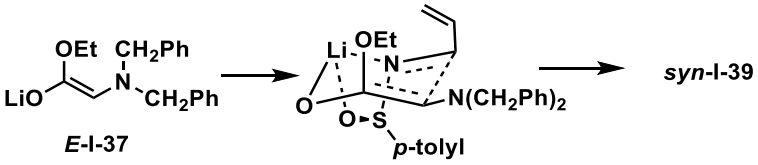

Ester **I-39** was then converted to the desired asymmetric metathesis precursor **I-43** in a high yielding, five step sequence. Ring closing metathesis of diene **I-43** was successfully achieved using Grubb's second-generation catalyst to afford the diamino-enone **I-44**. Similar to the previous Weinreb synthesis of agelastatin A,[9] the enone smoothly underwent 1,4-aza Michael addition cyclization to form **I-45**, constructing the tricyclic core in a high diastereoselectivity. Although, as previously mentioned, Hale *et al*. reported that Cs_2CO_3 did not induce cyclization on a similar substrate, both Weinrab and Davis found success in achieving the 1,4-aza Michael cyclization using Cs_2CO_3 under

ambient conditions. Hydrogenative debenzylation using Pd/C with H_2,, followed by treatment with methyl isocyanate afforded the final D-ring (**I-29**).[9] Lastly, to conclude Davis' synthesis of (–) agelastatin A (**1**), selective monobromination of the pyrrole was achieved using NBS.[10]

Trost and coworkers also successfully developed an asymmetric, enantioselective synthesis of the enantiomer, (+) agelastatin A (**1**), highlighted by two different Tsuji-Trost asymmetric allylic alkylations (AAA) to construct the core and simultaneously establish multiple stereocenters (Scheme 1.6).[13] Their synthesis began from cyclopentene-1,4-diol that was Boc protected to form **I-46**, which undergoes selective alkylation using bromo-2-pyrrole carboxylate **I-47** in the presence of ligand **I-54**, $[Pd(C_3H_5)Cl]_2$ and Cs_2CO_3 to afford pyrrole **I-48**. Hydrolysis using LiOH, followed by acid chloride formation, and then exposure to NH_2OMe•HCl provided Weinreb's amide **I-49** in good yield over two steps.

Another intramolecular Pd-catalyzed asymmetric allylic alkylation (AAA) was performed to access piperazinone **I-50**. Although, in this instance, the chiral ligand was not necessary for the cyclization, however it was found to provide a higher yield when used. Aziridination of the alkene using *N*-heterocyclic carbene complex **I-55** installed the tosylaziridine, which underwent $In(OTf)_3$/DMSO mediated ring opening and oxidation to afford the α-amino ketone **I-52.**[28,29] Similar to previous syntheses,[9,12] exposure of the amino-ketone to methyl isocyanate triggers cyclization and installs the D-ring (**I-53**) with the correct stereochemical relationship. Completion of the synthesis was then accomplished using a SmI_2 mediated cleavage of *N*-OMe and *N*-Ts to provide (+) agelastatin A (**1**).

Scheme 1.6. Trost's asymmetric synthesis of (+) agelastatin A (**1**)

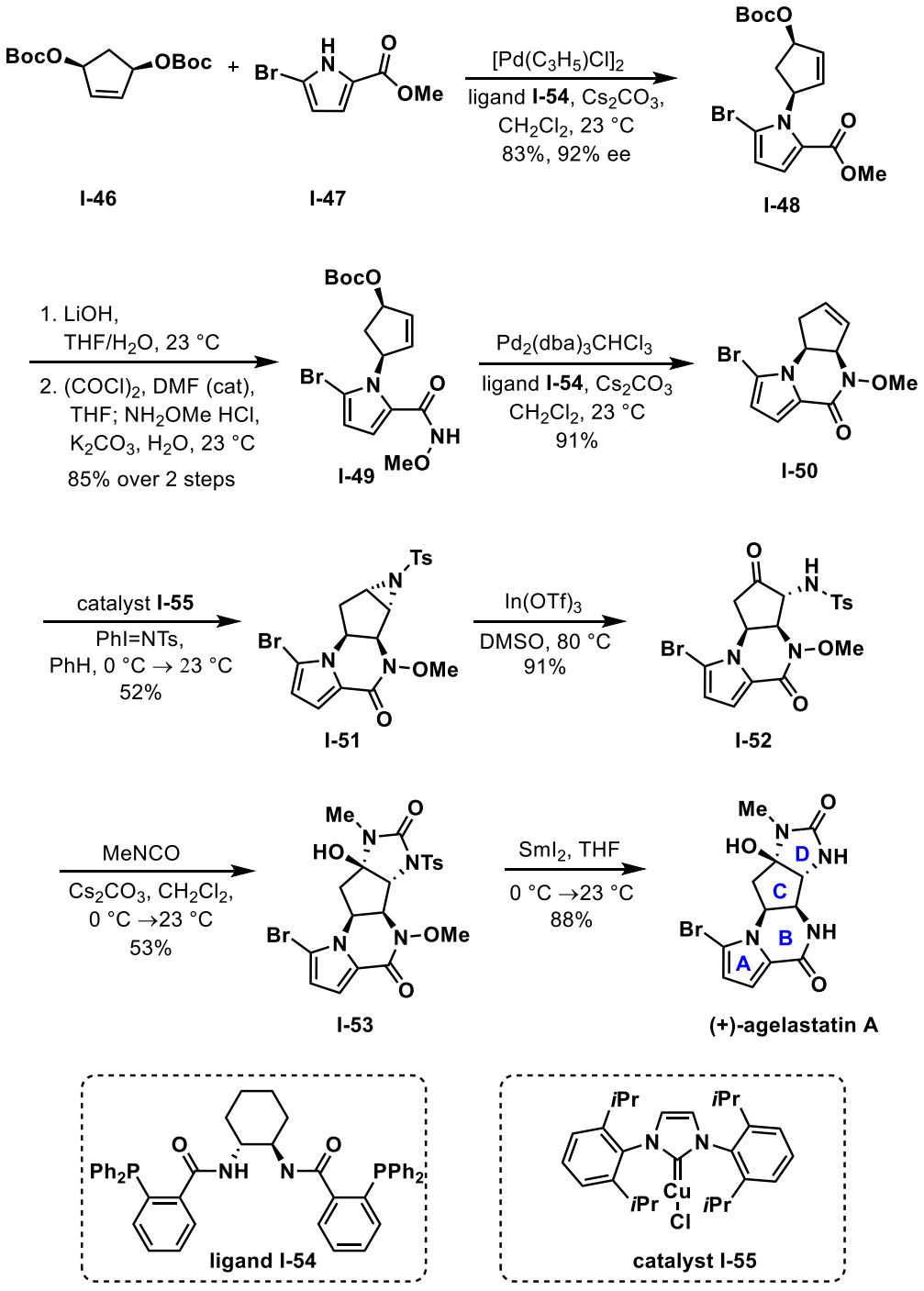

Ichikawa and co-workers developed an alternative asymmetric strategy to access (–) agelastatin A (**1**) (Scheme 1.7).[14] Starting from **I-56**, which was readily derived from L-arabitol,[30] selective deprotection of the terminal acetonide, followed by mesylation, elimination, hydrolysis, IBX oxidation, and then olefination with carbethoxymethylene-triphenylphosphorane afforded the dienoate **I-58** over five steps in good yield.[31]

DIBAL reduction, and then oxidation provided the aldehyde **I-59**, which undergoes enantioselective addition using diethylzinc to access allyl alcohol **I-60** with 92:8 selectivity.[32] Reaction with trichloroacetyl isocyanate, followed by hydrolysis gave the carbamate, which set the stage for the [3,3]-sigmatropic rearrangement. Dehydration[33] generated the cyanate, which instantly rearranged into the isocyanate. Subsequent exposure to benzyloxy-tributylstannane gave the Cbz protected amine (**I-63**). Dowex deprotection, followed by ring closing metathesis using Grubb's catalyst generated cyclopentenyl amino-diol I**-65** in high yield. Exposure to 2,2-dimethoxypropane gave a mixture of diol protection and oxygen-nitrogen protection, however, the diol protected acetonide was readily hydrolyzed with wet silica gel. The resultant alcohol was then treated with trichloroacetyl isocyanate to form cyclopentene **I-67**, which undergoes a [3,3] Sigmatropic rearrangement, and the resultant isocyanate is then trapped with 2,2,2-trichloroethanol to give the rearranged protected amine **I-68** selectively, in good yield. Troc deprotection followed by amidation and another Dowex mediated deprotection afforded amino-alcohol **I-70** in good yield over three steps.

Scheme 1.7. Ichikawa's asymmetric synthesis of (–) agelastatin A (**1**)

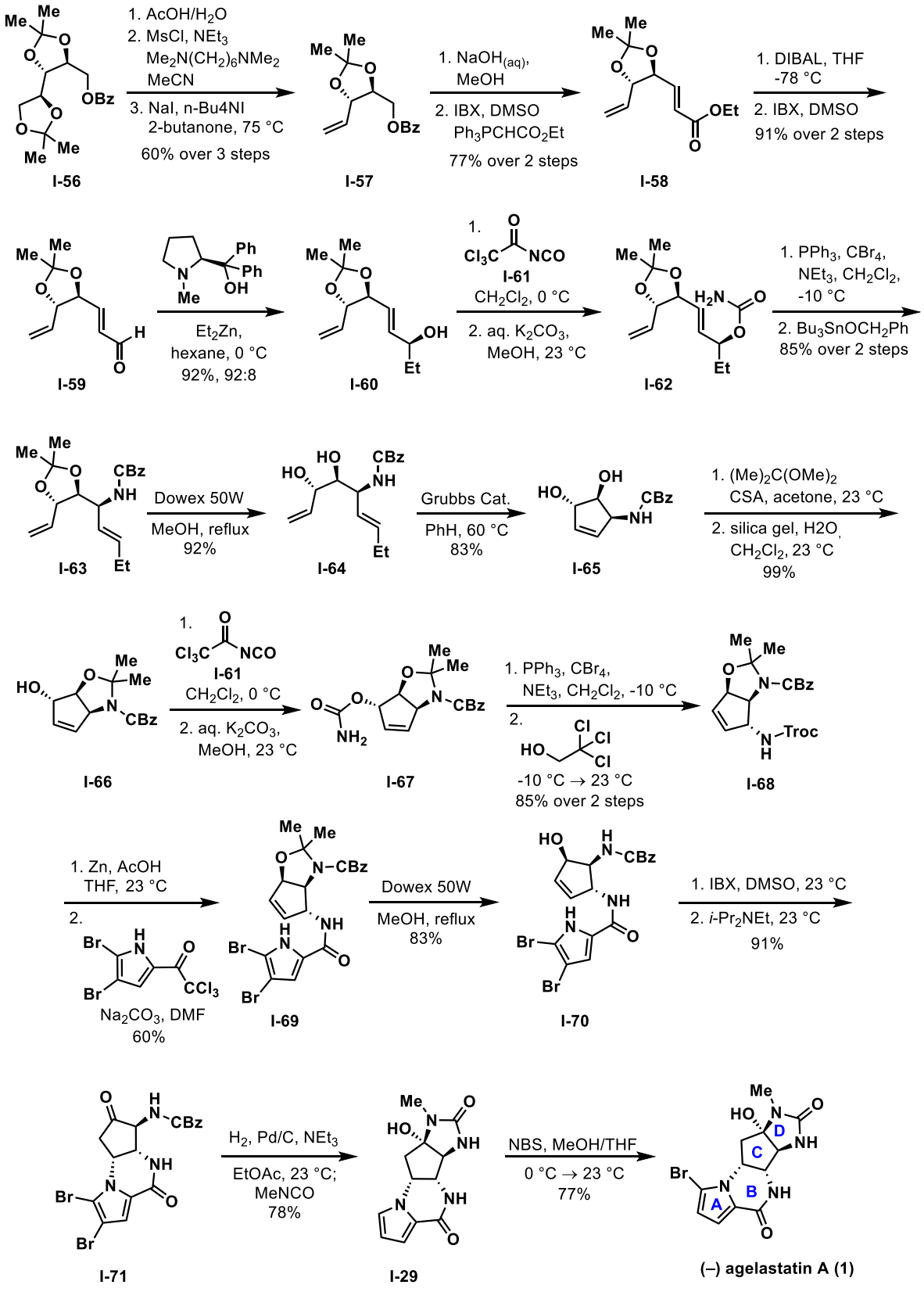

Subsequent IBX oxidation to the enone allowed for the desired 1,4-aza Michael addition/cyclization upon subjection to Hunig's base, thus constructing the B-ring and the tricyclic core in a diastereoselective fashion.[11] Exposure to Pd/C and H_2 simultaneously dehalogenated the pyrrole ring, and provided the free, unprotected amine, which was immediately reacted with methyl isocyanate *in situ* to construct the final D-ring diastereoselectively. Lastly, selective monobromination of the pyrrole provided (–) agelastatin A(**1**) in an overall 27 step total synthesis.[10]

In an alternative fashion, Yoshimitsu and coworkers developed an asymmetric enantioselective synthesis from achiral starting materials and utilized an enzymatic resolution to provide enantiopure intermediates along the path to completing the total synthesis of (–) agelastatin A (**1**).[15] They began their synthesis by reacting cyclopentadiene with Boc-protected nitrosyl amine in a hetero Diels-Alder reaction to produce bicycle **I-72** (Scheme 1.8). Reductive cleavage of the N-O bond produced *cis*-**I-73**, and enzymatic resolution of amino alcohol **I-73** provided **I-74** in 99% *ee*. Hydrolysis, followed by Mitsunobu inversion, provided the *trans*-amino cyclopentene **I-76**. Simultaneous Boc-deprotection and conversion of the amine to the desire pyrrole was efficiently synthesized using the Clauson-Kaas pyrrole synthesis in the presence of 2,5-dimethoxytetrahydrofuran and TFA.[34,35] Carbomylation at the 2-position of the pyrrole ring was achieved using trichloroacetyl isocyanate, followed by cleavage of the trichloroacetyl group using mildly acidic conditions to access amide **I-79**. Nitrile formation using $POCl_3$ followed by methanolysis afforded carbinol **I-80** in good yield, which was converted to azide **I-81** using CDI and $TMSN_3$ in the presence of H_2O. Water proved necessary to promote full conversion of the carbamate and reduce undesired side product formation.

Scheme 1.8. Yoshimitsu's synthesis of (–) agelastatin A (**1**)

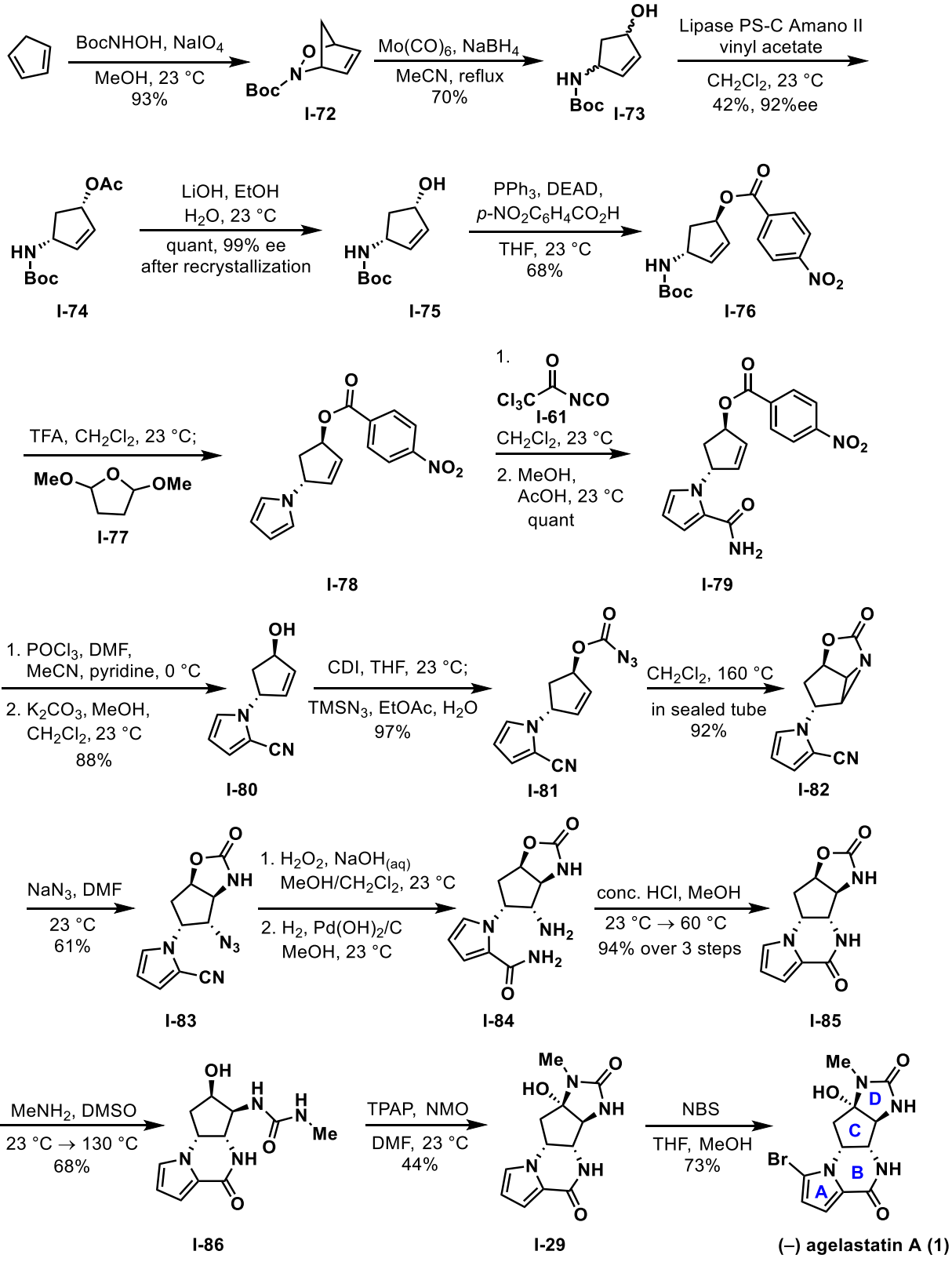

With the azide in hand, aziridination was carried out at 160 ℃ in dichloromethane to generate **I-82**, which was readily ring opened regioselectivity using NaN_3 to give azide **1-83**. Hydrolysis of the nitrile followed by hydrogenation generated amino-amide **I-84**, which cyclizes under acidic media at elevated temperature to afford lactam **I-85**. Transamidation of the carbamate using methylamine, followed by TPAP oxidation of the resultant alcohol afforded the desired cyclized urea (**I-29**), thus installing the D-ring and tetracyclic core in a diastereoselective manner. Weinreb, Feldman, Davis, Hale, Trost, and Ichikawa all used a similar approach to cyclize the D-ring, which involved either deprotection and *in situ* cyclization,[10,11] or deprotection followed by exposure to methyl isocyanate.[9,12,14] Lastly, the overall 19 step total synthesis of (–) agelastatin A was completed using a selective monobromination of the pyrrole.[10]

Wardrop *et al*. developed an alternative racemic total synthesis of agelastatin A (**1**) starting from *cis*-hydroxyacetate **I-87**,[16] which is readily prepared from cyclopentadiene (Scheme 1.9).[36] Imidate **I-88** was formed though reaction with trichloroacetonitrile in the presence of DBU, whereby heating in xylenes effected the [3,3] sigmatropic rearrangement to form *cis*-amido-acetate **I-89** in good yield and selectivity, with the *cis*-configuration being established using NOESY.

Exposure to *N*-bromoacetamide triggered a bromo-etherification/cyclization to form bromide **I-90**, which readily undergoes elimination in the presence of DBU to form the allylic acetate. Hydrolysis mediated by *p*-toluenesulfonic acid, followed by Mitsunobu and amidation using *N*-methylbenzylamide provided urea **I-94** in good yield over three steps.

Hydrazinolysis of the phthalimide using N_2H_4 provided the free amine, which was directly coupled with 2-pyrrole carboxylic acid to form amide **I-95**. Acetate hydrolysis, IBX oxidation**,** and then K_2CO_3 mediated 1,4-aza Michael addition/cyclization installed the B-ring and tricyclic core.[9] In the same procedure used by Hale,[11] benzyl deprotection caused a spontaneous *in situ* cyclization of the amine onto the ketone to form the final D-ring (**I-29**) in a diastereoselective manner. Lastly, monobromination occurred using Feldman's conditions to provide (±) agelastatin A (**1**).[10]

Scheme 1.9. Wardrop's total synthesis of (±) agelastatin A (**1**).

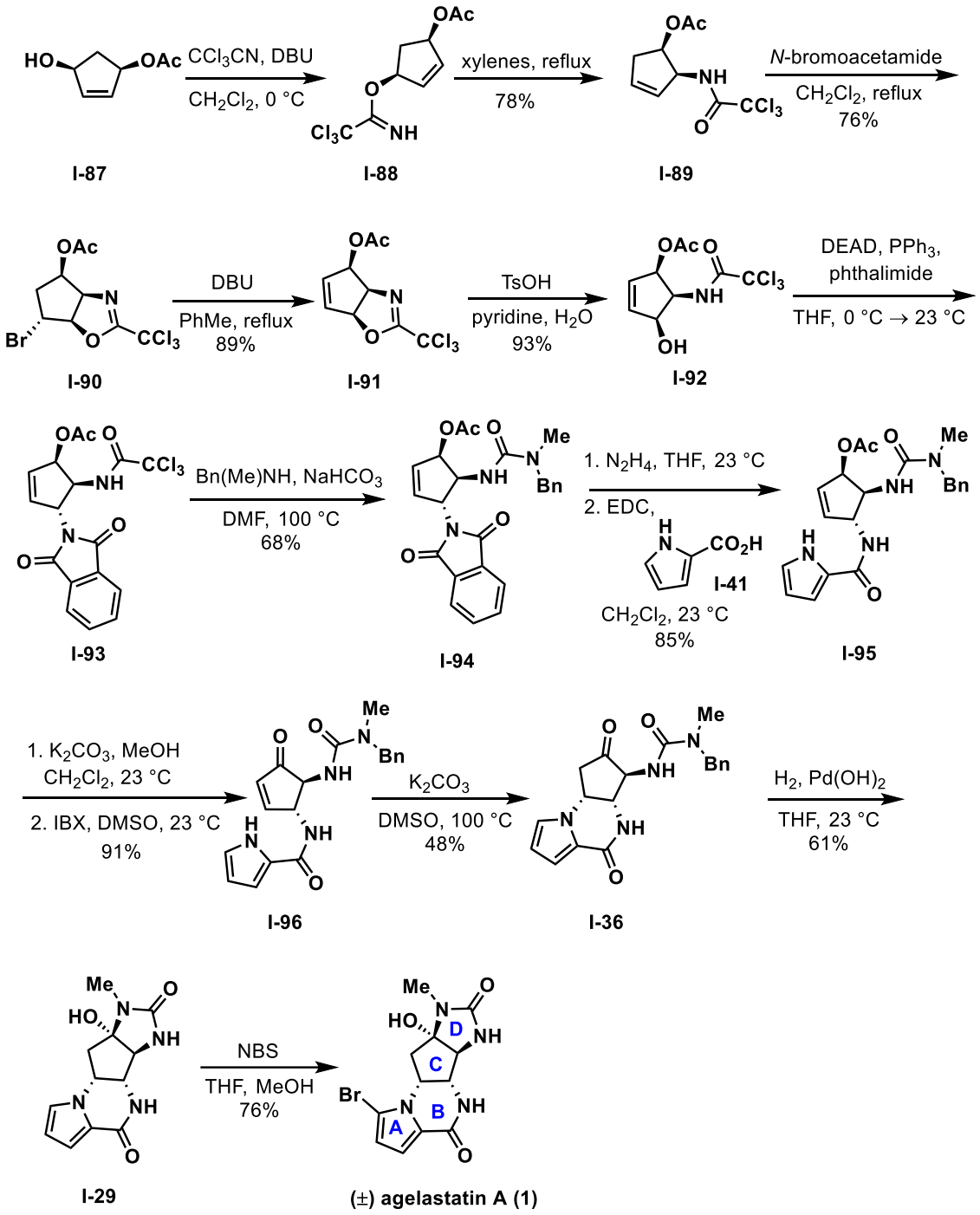

Chida and co-workers also developed an asymmetric total synthesis of (–) agelastatin A (**1**) starting from enantiopure diol **I-97** with the key steps that utilize a double Overman rearrangement followed by a ring-closing metathesis to establish stereocenters of both amines of the C-ring (Scheme 1.9).[17] Monotosylation of commercially available **I-97**, followed by installation of the thioether gave **I-98** (Scheme 1.10). Swern oxidation and Wittig olefination then provided the diene with high *Z*-selectivity but was readily isomerized to the desired *E*-alkene using AIBN and thiophenol. Acetonide deprotection using acetic acid followed by exposure to trichloroacetonitrile and DBU afforded the bistrichloroacetimidate **I-102** in modest yield. This set the stage for one of the key steps, double Overman rearrangement. **I-102** was heated in *o*-xylenes to undergo the rearrangement in a highly stereoselective manner, and **I-103** was isolated as the sole product in good yield.[37] The allylic sulfide was then oxidized to the sulfoxide, which underwent the Mislow-Evans rearrangement using $P(OMe)_3$ to generate the allylic alcohol **I-105** as a mixture of diastereomers. Ring closing metathesis using Grubb's catalyst successfully generated cyclopentene **I-106,** constructing the central C-ring and setting both amine stereocenters in the process. Mesylation of the alcohol occurred using MsCl and NEt_3 triggered *in situ* cyclization to provide oxazoline **I-107**. It is important to note that both isomers of the allylic alcohol were used, but closure of the oxazoline ring provided a single diastereomer due to the *cis* stereochemistry being lower in energy.[2]

Scheme 1.10. Chida's total synthesis of (–) agelastatin A (**1**)

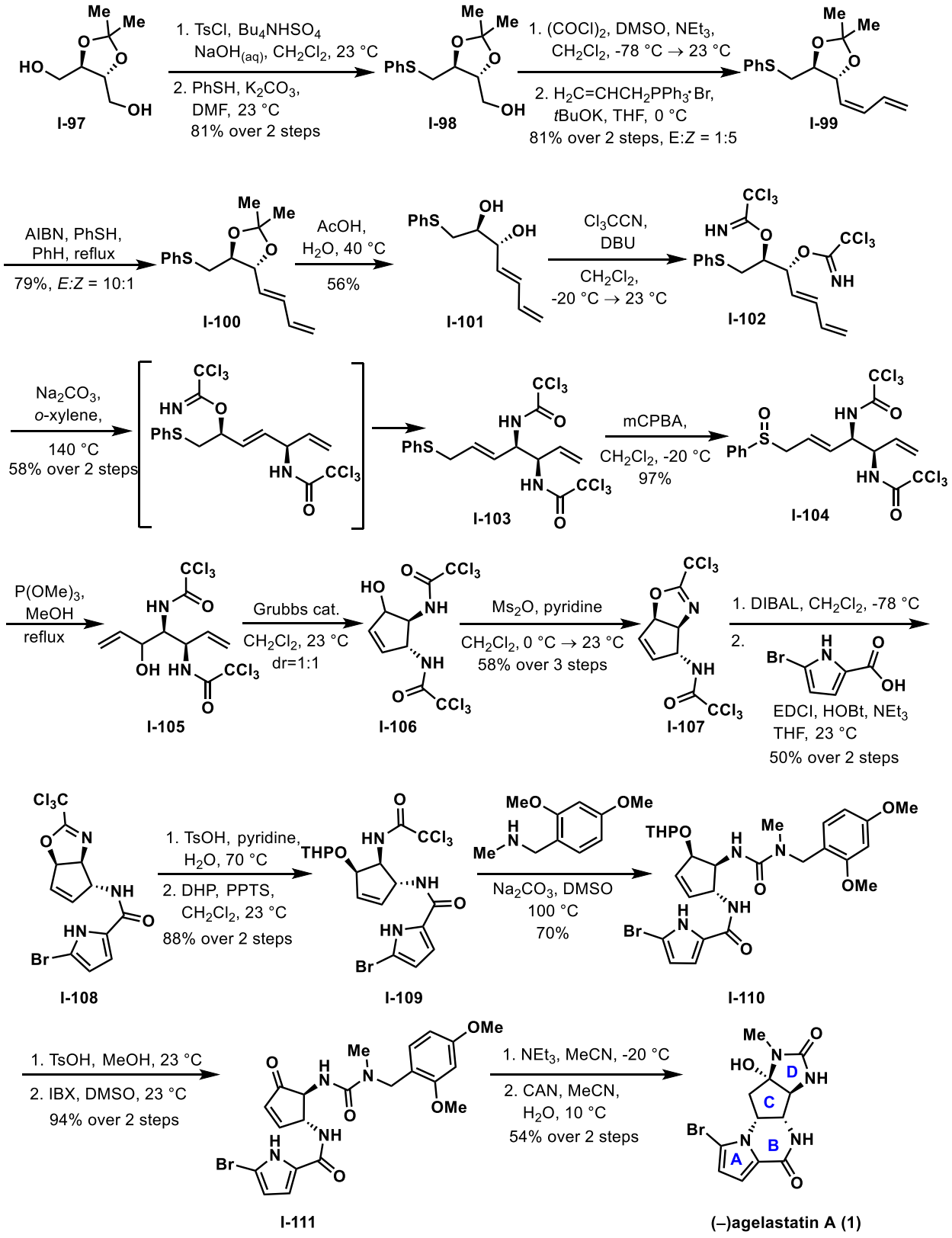

Removal of the trichloroacetyl group with DIBAL and coupling of the 2-bromopyrrole carboxylic acid provided **I-108**. The oxazoline ring was hydrolyzed and the resulting alcohol was protected as the pyran **I-109**. Amidation of the trichloroacetamide with 2,4-dimethoxybenzylmethyl amine afforded urea **I-110,** which the THP protection was then removed, and oxidation of the resultant alcohol afforded enone **I-111**. In similar fashion to previous syntheses, treatment of the pyrrole with NEt_3 induced 1,4-aza Michael addition/cyclization to construct the B-ring in a diastereoselective manner. Final deprotection using CAN afforded the cyclic urea D-ring, and thus completed the total synthesis of (–) agelastatin A (**1**) in 22 overall steps from erythitol.

Du Bois *et al.* also successfully developed an enantioselective total synthesis of (–) agelastatin A (**1**), but unlike previous syntheses, the D-ring was constructed earlier in the synthesis (Scheme1.11).[18] Starting from commercially available, enantioenriched lactam **I-112**, Boc protection, followed by $NaBH_4$ reduction provided enantiopure cyclopentenyl alcohol **I-114**. Sulfamoylation followed by Rh-catalyzed aziridination quickly afforded aziridine **I-116** as a single diastereomer in high yield.[38,39] Treatment with NaN_3 regioselectivity opened the aziridine ring, the resultant sulfonamide was acylated, and the oxathiazepane was then displaced to produce selenide **I-118** in high yield.

Boc deprotection, and Clauson-Kaas pyrrole synthesis afforded the pyrrole **I-119**. Staudinger conditions were then employed to reduce the azide, which was immediately treated with methyl isocyanate to provide urea **I-120**. *m*CPBA oxidation triggered selenoxide elimination to produce the exocyclic cyclopentene **I-121,** which upon oxidative cleavage with OsO_4 and $NaIO_4$ led to the cyclic urea, resulting in the hemiaminal, and formation of the D-ring diastereoselectively. *t*BuOK in the presence of *t*-amyl alcohol smoothly generated the 6-membered lactam ring (B-ring), triggering cyclization selectively over hydrolysis. Lastly, to complete the synthesis, selective monobromination of the pyrrole following Feldman's procedure completed the synthesis to (–) agelastatin A (**1**) in 14 overall steps from lactam **I-112**.[10]

Scheme 1.11. Du Bois' total synthesis of (–) agelastatin A (**1**)

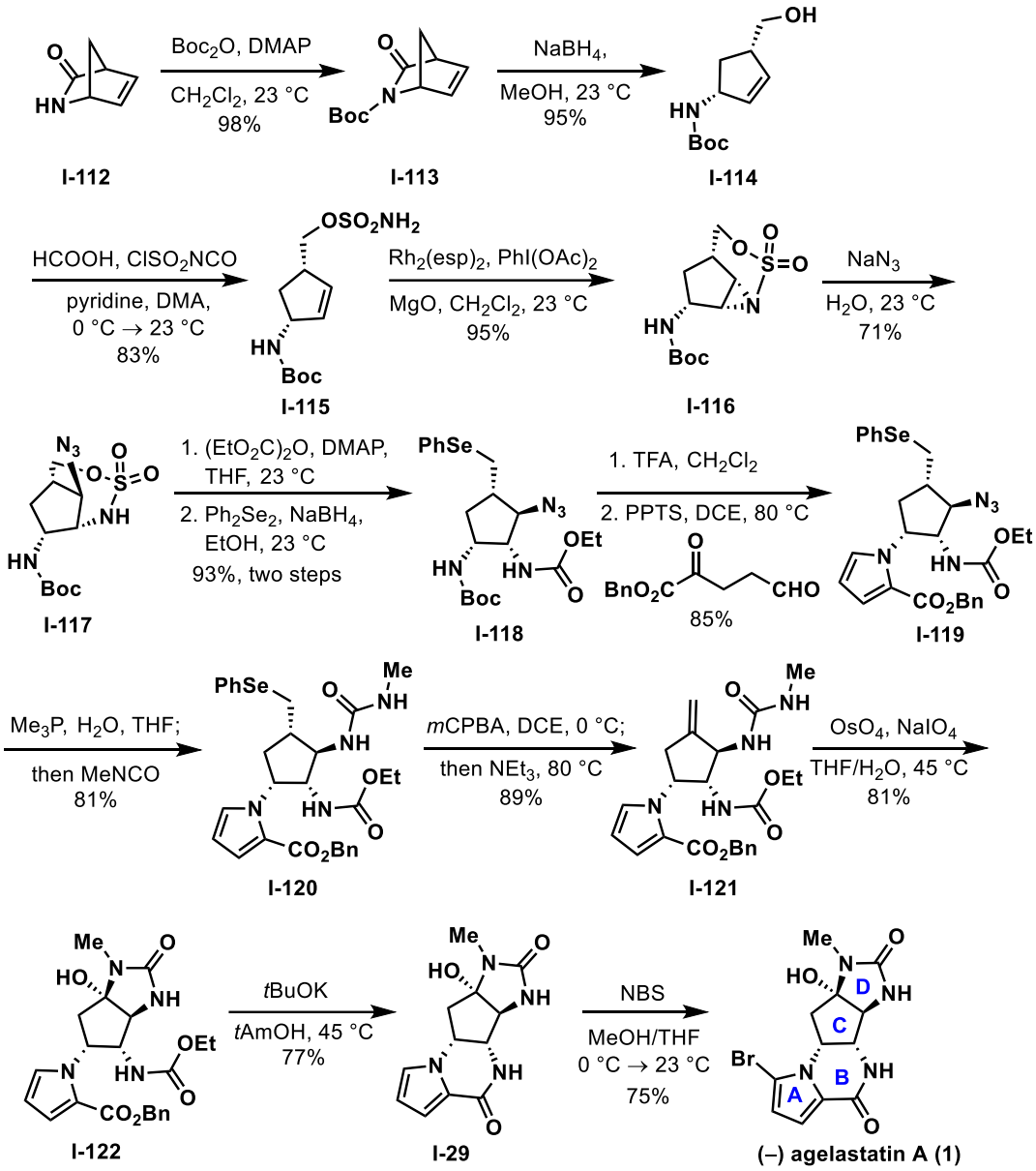

Movassaghi and coworkers also developed an enantioselective total synthesis of (–) agelastatin A (**1**), highlighted by a unique Cu-mediated cross-coupling and two acid mediated diastereoselective cyclizations to construct the B, C, and D rings of the tetracyclic framework.[19] Starting from enantiopure D-aspartic acid diester **I-123** the pyrrole was selectively monobrominated using NBS and DTBMP.[40] Treatment of the pyrrole with chlorosulfonyl isocyanate afforded the amide **I-125**, which upon addition of sodium borohydride in methanol, followed by addition of *p*-toluenesulfonic acid, delivered **I-126** as a single diastereomer. This occurs *via* formation of an imide intermediate, and subsequent reduction to product **I-126**.

Next, Movassaghi et *al*. explored routes to couple **I-127** with triazone **I-128** to introduce the imidazolone substructure. Using direct addition along with the use transmetallated deriviates of the triazone proved to be difficult and did not afford any of the desired coupled product due to either lack of reactivity, by-product formation, or decomposition. Thus, a stable metal derivative of the triazone was needed, and the cross-coupling of thioester **1-127** with stannyl derivative **I-128** proved to be fruitful. To that end, **I-128** is synthesized in two steps from commercially available material.[41] **I-126** was converted to the thioester using trimethylaluminium and 4-methylbenzenethiol. Use of CuTC efficiently coupled together the triazone and thioester to provide **I-129**.[42] Triazone was exposed to HCl, which unraveled the 6-membered ring, and underwent spontaneous cyclization to provide the imidazolone D-ring **I-130** in 89% yield and 99% *ee*. To complete the synthesis of (–) agelastatin A (**1**), **I-130** was heated in an aqueous solution of methanesulfonic acid to trigger cyclization, constructing the C-ring to provide (–) agelastatin A (**1**). ^{1}H NMR studies found that upon cyclization, (–) agelastatin A (**1**) is the

thermodynamically favored product, and the reaction equilibrates to form the natural product under these conditions.

Scheme 1.12. Movassaghi's total synthesis of (–) agelastatin A (**1**)

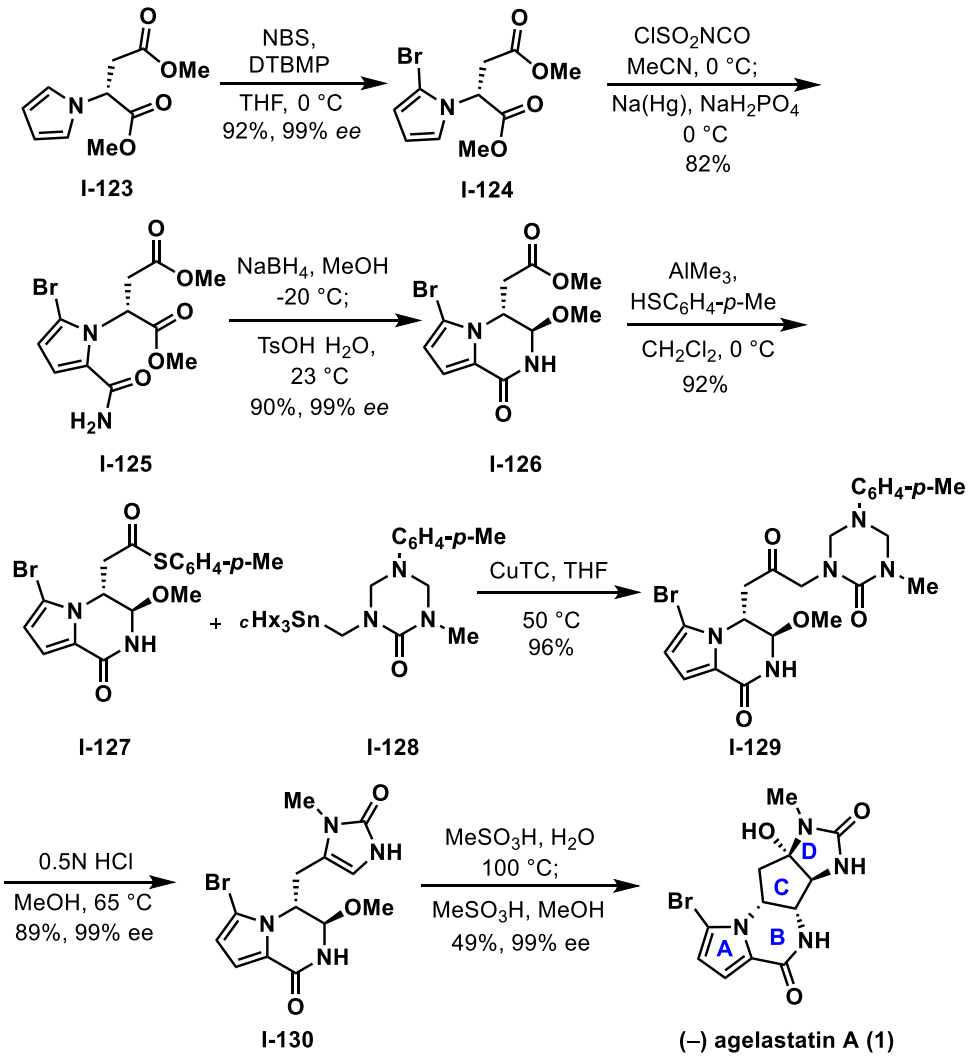

Lastly, Romo and coworkers developed a diastereoselective racemic synthesis to (±) agelastatin A (**1**), highlighted by two late-stage separate acid-mediated diastereoselective cyclizations to construct the B and C rings of the tetracyclic framework.[20] Unlike most previous syntheses, Romo started the synthesis with the formation of the D-ring urea **I-133** from tartaric acid **1-131** and N-methyl urea **I-132**.[43] Carboxylic acid **I-133** was then converted to the ester using K_2CO_3 and MeI, followed by amine protection. The ester was reduced using DIBAL-H, and oxidized to provide aldehyde **I-134**. Using the Ohira-Bestmann reagent (**I-135**) under modified Seyferth-Gilbert conditions, the terminal alkyne intermediate was formed in good yield.[44,45] This was then subjected to Zn^{II}-mediated acetalization to furnish the alkynyl acetal **I-136**.

Coupling of acetal, **I-136** with pyrrole **I-137** by activation with $SnCl_4$ provided **I-138**. The methoxy group was critical for efficient coupling presumably because of the α-effect, which renders the amide nitrogen more nucleophilic, providing a selective reaction.

Cleavage of the methoxy group using SmI_2, followed by alkyne reduction using Lindlar's catalyst to form the alkene **I-140** set the stage for cyclization and formation of the tetracyclic core. Exposure to TFA formed the *N*-acyliminium intermediate **I-141**, which upon formation undergoes nucleophilic addition from the D-ring urea, to construct the C-ring diastereoselectively (**I-142**). Regioselective addition of water to the iminium ion afforded **I-143** in high yield.

To complete the synthesis, KHMDS was used to remove Tse protecting group. Initially, Reyes *et al*. attempted to open the D-ring cyclic urea to form a cyclopentenone, undergo aza-Michael addition, followed by the subsequent D-ring closure to yield agelastatin A (**1**). This is similar to prior syntheses. However, they had found that neat

silica gel with gentle heating effects the transformation and cyclization of the B-ring diastereoselectively in good yield to provide agelastatin A (**1**).

Scheme 1.13. Reyes' total synthesis of (±) agelastatin A (**1**)

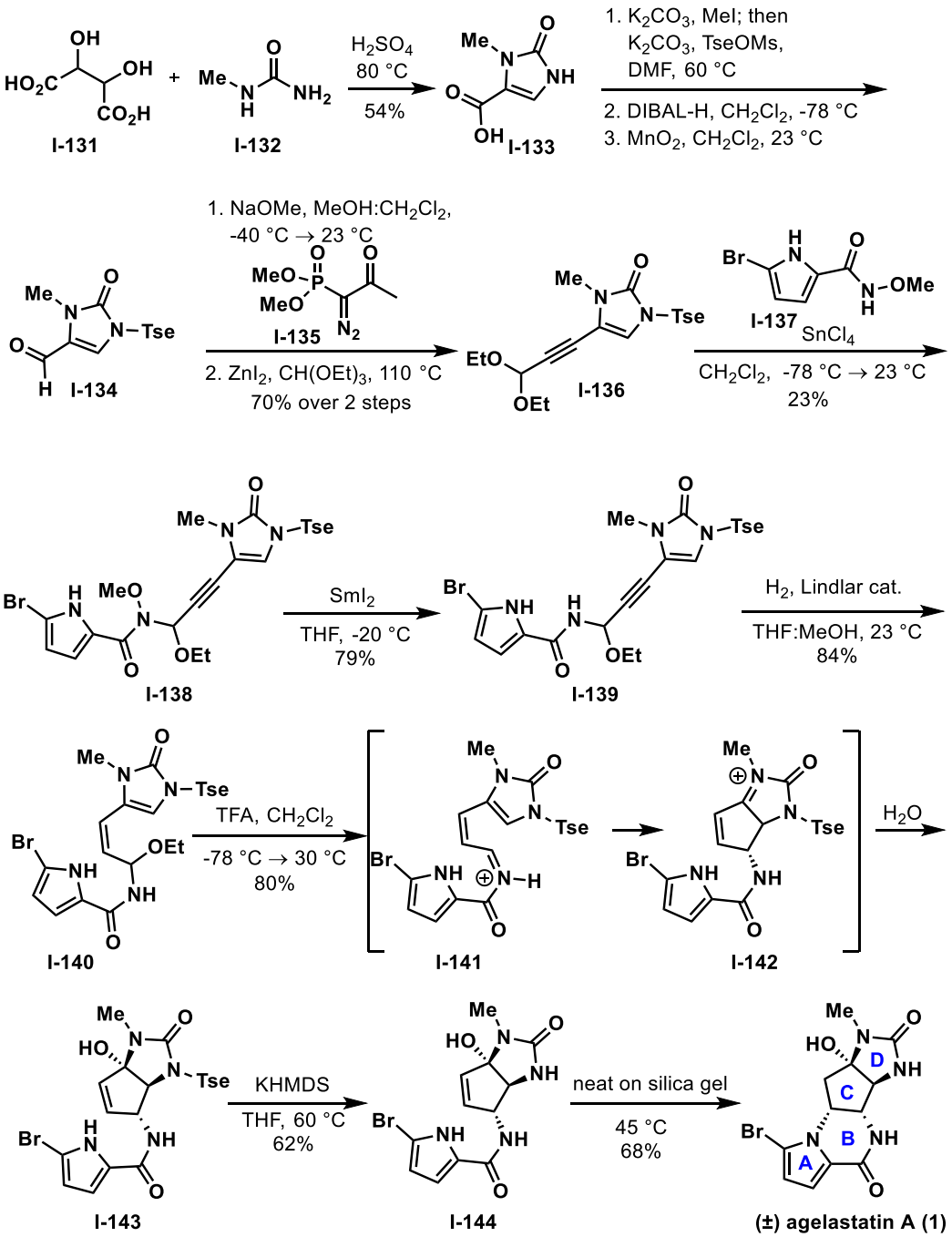

1.3. Conclusion

The total synthesis of agelastatin A (**1**) has evolved though myriad of new, successful approaches to access the natural product as well as other natural compounds in the agelastatin family. From the first total synthesis completed by Weinreb *et al* in 1999, and the first asymmetric synthesis completed in 2002 by Feldman *et al.*, agelastatin A (**1**) has been synthesized in various ways that utilize unique chemistry. However, only two of these syntheses involve late-stage construction of the densely functionalized C-ring,[19,20] with only one of those total syntheses being asymmetric.[19] Movassaghi *et al*. showed an elegant approach to the natural product that constructs the C-ring in a late-stage strategy, which set three of the four stereocenters in a diastereoselective fashion via iminium induced cyclization using methanesulfonic acid. The other 10 total syntheses construct the C-ring early in the synthesis, and 8 of the total syntheses construct the B-ring in a similar fashion as the Weinreb synthesis via a 1,4-aza Michael addition into the ketone. Also, 12 of the previous total syntheses constructed the urea D-ring in the later stages, typically implementing amide deprotection and subsequent cyclization. Due to considerable efforts towards the total synthesis of agelastatin A (**1**), any new strategies must offer significant innovation if it is to serve as a competitive route. Therefore, developing an asymmetric, modular synthesis, without the use of motifs from the chiral pool that forms the functionalized C-ring in the late-stage of the synthesis, and implements new chemistry and strategies that can simultaneously construct the core as well as install chirality in one step, warrants an investigation as this can be applicable to other natural products.

Chapter 2 – Studies Toward the Total Synthesis of (–) Agelastatin A

2.1. Introduction

Catalytic alkene functionalization is a rapidly growing field in organic chemistry. In particular, halofunctionalization has shown great utility, and has become a widely used transformation in organic synthesis. This well-known reaction, where a halogen adds to an alkene or alkyne, is a reaction that is often taught in sophomore organic chemistry classes at the collegiate level. Our group, as well as others, have studied this transformation in depth, and previous reports have showcased its versatility as a tool to functionalize small, complex organic molecules to provide access to a myriad of different scaffolds.[46,47,48]

2.2. Background

One of the very first catalytic asymmetric halofunctionalization reactions was published in 2010 by Borhan and coworkers and consisted of an asymmetric chlorolactionization.[49] Catalyzed by $(DHQD)_2PHAL$, in the presence of dichloro-diphenylhydantion (DCDPH), simultaneous chlorination and cyclization, or chlorolactonization of carboxylic acids with pendant 1,1-disubstituted alkenes provided the chlorolactones (Figure 2.1).[49] Since then, numerous other methodologies from our lab, as well other research groups, have been reported.[50,51,52,53,54]

Figure 2.1. Catalytic asymmetric halofunctionalization of alkene carboxylic acids

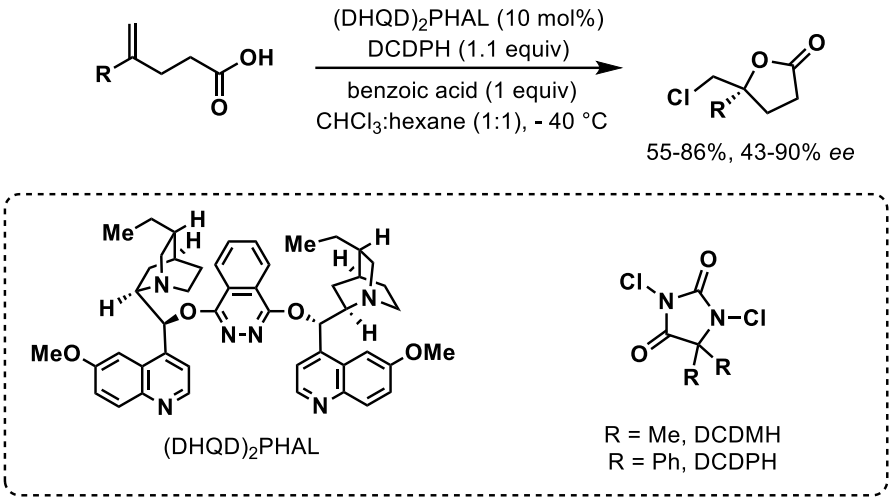

To help predict the outcome of halogenation reactions, mechanistic investigations using a computational tool and method developed in our research group, referred to as *HalA* (halenium affinity), allows us to understand the nuances that determine regio- and chemoselectivity of electrophilic alkene halogenation reactions.[55] Previously, our group developed a computationally derived scale to predict the halogenation reaction in the presence of several Lewis bases, which was validated by numerous experiments. Though an idea analogous to proton affinity values, we were able to quantify the propensity of an alkene to undergo halogenation. For a given Lewis base, the *HalA* value is defined as the DFT calculated energy upon reacting with the halenium ion (X^+). Depending on the outcome, the Lewis base may be neutral or anionic, giving rise to two scenarios:

$$\text{neutral acceptor: } \Delta H_{rxn}(X^+ + LB \rightarrow X - LB^+)$$

$$\text{anionic acceptor: } \Delta H_{rxn}(X^+ + LB^- \rightarrow X - LB)$$

The *HalA* values are calculated in kcal/mol where $T = 298.15K$ in equation 1.

$$HalA = -\Delta E_{(elec)} - \Delta ZPE - \Delta E'_{(vib)} + \frac{5}{2}RT \qquad \text{(equation 1)}$$

where, $\Delta E_{(elec)} = E_{(electronic)}$(X-LB adduct) – [$E_{(electronic)}$ (:LB) – $E_{(electronic)}(X^+)$], ΔZPE = ZPE (X−LB adduct) − ZPE (:LB), $\Delta E'_{(vib)} = E'_{(vib)}$(X−LB adduct) − E'(vib)(:LB), and (5/2) RT as translational degree of freedom.

To showcase the utility and practicality of *HalA*, our strategy was to compute the likelihood of a Lewis base, such as an alkene, to undergo halenium capture, and this predictive model was then validated experimentally with the exact same molecules that were used in the computational model. Additionally, *HalA* values take into account the influence of sterics and electronic variations, thereby providing a quantitative assessment for more than just chemical intuition. The factors that dictate kinetic and stereochemical stability of chiral halonium ions have been well studied and established that transfer of a chlorenium is irreversible.[56,57,58,59] As an illustration of *HalA* applicability, the halenium affinity for two double bonds in a single molecule were computed to predict the regio- and chemoselectivity of this reaction (Figure 2.2). In this scenario there are two possible pathways the reaction could proceed to yield two different products. The experimental results suggest that the 1,1-disubstituted olefin was chlorinated selectively, initially forming a benzylic tertiary carbocation upon chlorination, which then triggers a nucleophilic attack of the 1,2-disubstitiuted alkene in an ene-type cyclization to form an exo-cyclic benzylic carbocation. This intermediate then undergoes subsequent Friedel Crafts cyclization to form the 6,5,5-tricycle in a 55% isolated yield and 5:1 diastereoselectivity.[55] The observed regioselectivity of this reaction (path A favored) enables predictions of the major product, where no observed product was seen from Path B, along with any side products that arise from chlorination *via* Path B. In terms of

practicality, the small difference in *HalA* values between the two olefins seems negligible for chemoselectivity. However, this example shows the utility of using the *HalA* method for accurate prediction of chemoselectivity of alkene halogenation reactions. The experimental confirmation of the theoretically predicted chemoselectivity suggests that even small energetic differences (≤2 kcal/mol) can be reliably determined using the *HalA* method.

Figure 2.2. Chlorocyclization of diene is predicted by the higher *HalA* of the 1,1-disubstituted olefin

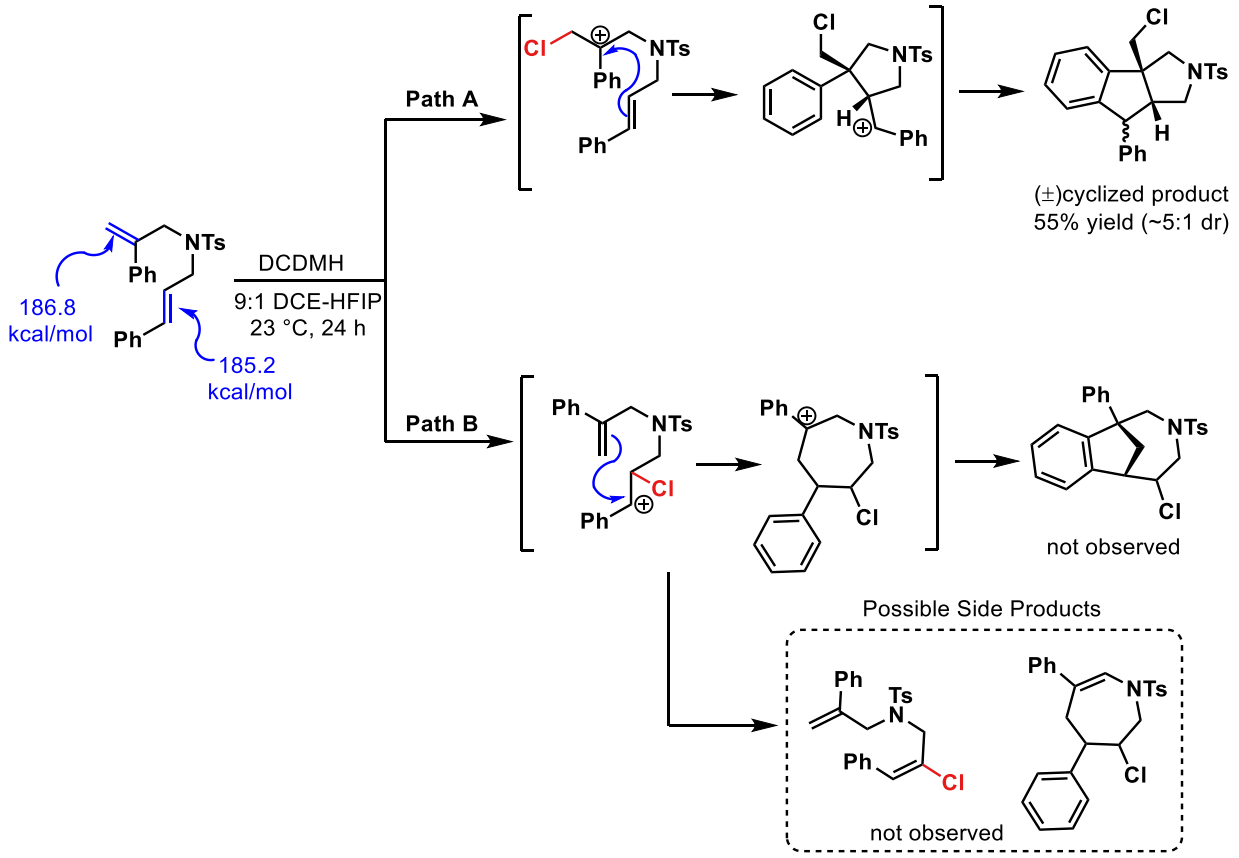

2.3. Overall Approach to (–) agelastatin A (1)

Based off this prior work, it was envisioned that the 5,6,5,5 tetracyclic core of agelastatin A (**1**) could be accessed from amide **II-2** though an asymmetric halenium-ion initiated cascade simultaneously establishing all four contiguous stereocenters diastereoselectively in a single operation from an achiral starting material (Scheme 2.1).

Scheme 2.1. Proposed mechanism for halofunctionaliztion in the synthesis of agelastatin A (**1**)

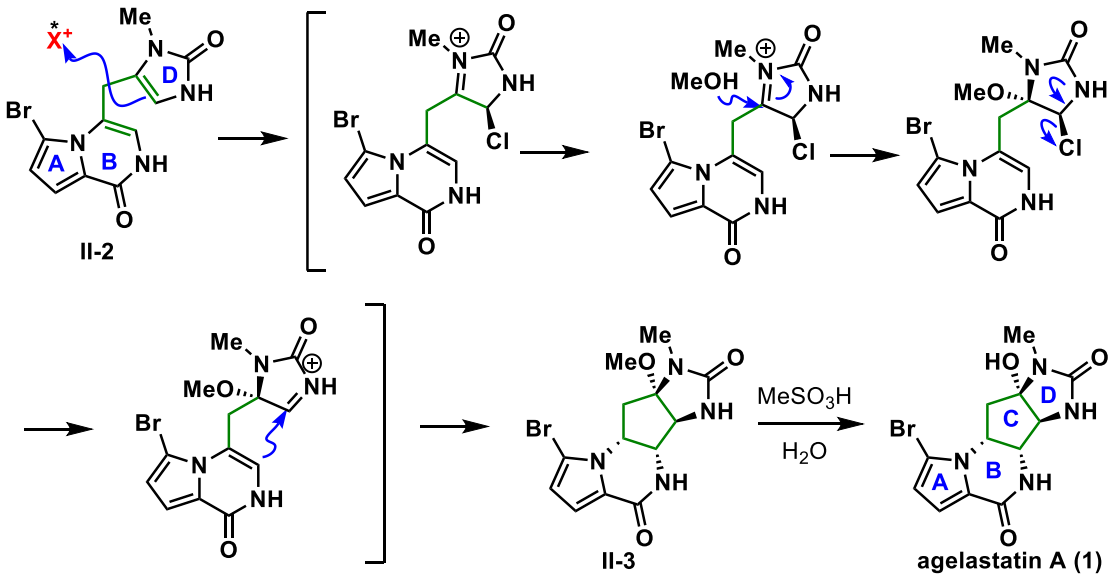

We hypothesize that upon exposure of intermediate **II-2** to a halogenating reagent in methanol, the subsequent incipient halenium ion would undergo methanolysis followed by a second ionization to form an iminium intermediate which induces a 5-exo-trig cyclization to form methylether **II-3** in a single operation.

This proposed mechanism to access agelastatin A in a single transformation is similar to the overall approach used in Movassaghi's total synthesis. Movassaghi used

an elegant approach to the natural product that constructs the C-ring in a late-stage strategy, which set three of the four stereocenters in a diastereoselective fashion via iminium induced cyclization using methanesulfonic acid (Scheme 2.2).[19] However, our approach differs by using the halocyclization on an achiral motif to construct the tetracyclic core in an asymmetric fashion. Using our group's aforementioned asymmetric halofunctionalization chemistry, this would not only allow us to construct the core and set multiple contiguous chiral centers, but also introduce chirality at the end of the synthesis. This strategy could allow us to potentially simplify the early stage of the synthesis, and provide efficient access to an array of molecules that could be used to not only access the natural product, but serve as a platform to produce a variety of other compounds in the agelastatin family as well as analogs.

Scheme 2.2. Movassaghi's approach to agelastatin A (**1**)

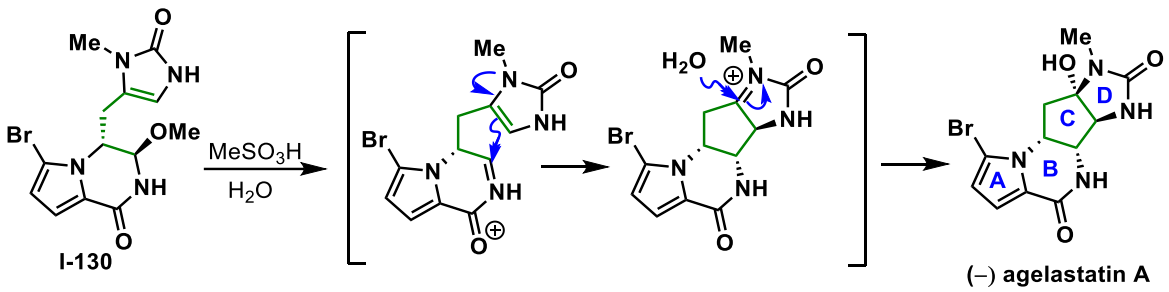

2.4. Computational Studies

Computational studies predict that the D ring olefin undergoes halogenation selectively over the B ring olefin, forestalling competitive halogenation. In our key step of the synthesis, *HalA* values are calculated to help determine the chemo- and regioselectivity of halogenation and subsequent halenium ion induced cyclization (Figure 2.3).

Figure 2.3. Chemo- and regioselectivity issues with the proposed synthesis

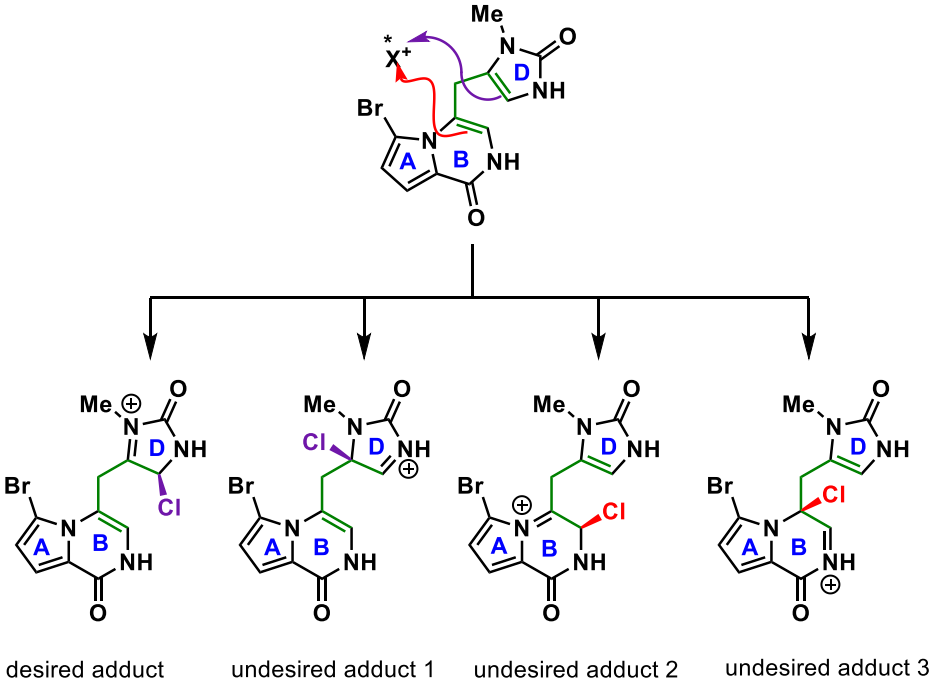

From our previous work, the *HalA* values were calculated by choosing DFT as the method, and B3LYP/6-31G* as the basis for a chlorenium ion. In the first step of the calculation, the Lewis base is subjected to a conformer distribution search to find the most

stable conformer with minimum energy. Then, calculations were performed on the lowest energy conformer. Next, the calculations are performed on the chlorenium ion in its triplet state (s^2p^4) to yield the most stable ion. The same calculations used for the Lewis base are applied to the Lewis base-halenium complex as well. For the molecule in question, there are 4 possible products (Figure 2.3), therefore, separate calculations must be considered for each nucleophilic site to where the chlorenium ion can suitably be attached. The thee energetic values, electronic energy, zero-point energy, and vibrational energy can all be extracted from the output file of the calculations from Lewis base and Lewis base- chlorenium ion complex. The electronic energy of the chlorenium ion is also extracted from the output files (Table 2.1).

Table 2.1. Electronic energy, zero-point energy, and vibration energy (kcal/mol)

Compound	**$E_{(elec)}$**	**ZPE**	**$E'_{(vib)}$**
Lewis base	-2138073.749	134.9342	9.9242
Cl^+	-288439.3721	-	-
desired adduct	-2426694.318	136.6089	10.4033
undesired adduct 1	-2426677.989	135.8912	10.4025
undesired adduct 2	-2426682.052	136.1305	10.4028
undesired adduct 3	-2426674.512	135.7075	10.4023

These values were substituted into equation **1** to calculate the *HalA* for each possible outcome of halogenation. The *HalA* values of our desired adduct is at least 11.9 kcal/mol higher as compared to the undesired adducts and is predicted to be formed preferentially, thereby potentially leading to the desired product; data which preliminarily supports our hypothesis (Figure 2.4).

Figure 2.4. Calculated *HalA* values for each outcome

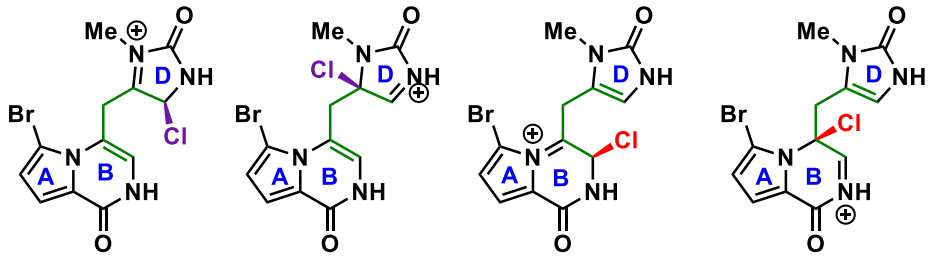

2.5. Retrosynthesis Route 1

Predicated on the calculated *HalA* values, our retrosynthesis was designed to target the advanced enamide **II-2,** which we hypothesized could undergo enantioselective halogenation to build the fused-tetracyclic framework for agelastatin A (**1**) in a single asymmetric operation. Enamide **II-2** is derived from the oxidative cleavage of the olefin in amide **II-4**, which is afforded from methyl ester **II-5** though carboxylate interconversions to produce the amide. Urea formation was envisioned to come from Boc deprotection, acylation, and exposure to ammonia could produce the desired urea **II-4**. Ester **II-5** was envisioned to be accessed in three steps from the Boc-protected amino alcohol **II-6**, which is synthesized from cyclopentadiene in a known two step protocol that utilizes a hetero-Diels-Alder cycloaddition.[60]

Scheme 2.3. Retrosynthetic plan for agelastatin A (**1**)

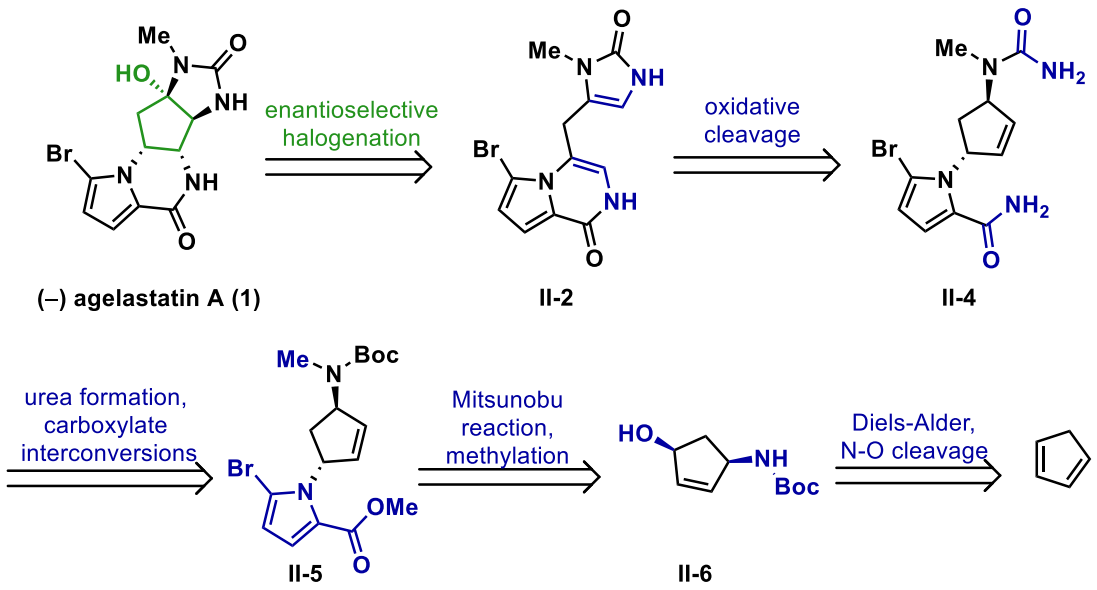

2.6. Synthetic Route 1

To begin the synthesis, sodium *meta*-periodate and *N*-Boc-hydroxylamine reacted with freshly cracked dicyclopentadiene in a MeOH/water mixture at room temperature to undergo a Diels-Alder cycloaddition to provide bicycle **II-7** in 70% yield. Reductive cleavage of the N-O bond using bis(cyclopentadienyl)titanium(IV) dichloride and zinc dust, or Nugent's reagent, provided the amino alcohol **II-6** in 86% yield (Scheme 2.4).[61] The use of sodium borohydride and molybdenum hexacarbonyl was also shown to cleave the N-O bond, however further exploration led to the use of Nugent's reagent which improved the yield to 86%. The use of sodium borohydride and molybdenum hexacarbonyl also suffered from poor scalability and reproducibility.

Scheme 2.4. Synthesis of amino alcohol

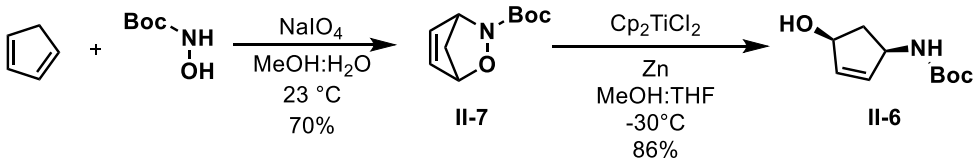

It is worth noting, homolysis of the hydroxyl group upon activation of the titanium Lewis acid at temperatures greater than -30 °C is precedented, occurring though a radical deoxygenation pathway (Scheme 2.5).[62] In an effort to prevent this undesired reactivity, an immersion cooler was used to maintain the temperature at -30 °C until complete conversion of starting material was observed by TLC, upon which the reaction was quenched with a saturated solution of potassium carbonate, and then allowed to warm to ambient temperature.

Scheme 2.5. Proposed Mechanism for Ti(III)-Mediated Alcohol Deoxygenation-Reduction

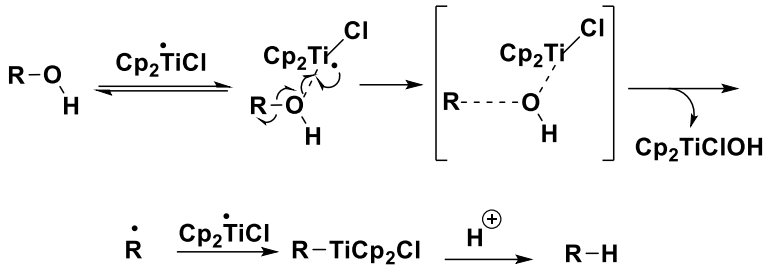

Lithium aluminum hydride reduction of **II-6** afforded the methylated amino alcohol **II-8**, which was then selectively re-protected using di-*tert*-butyl dicarbonate to provide alcohol **II-9** (Scheme 2.6)**.** Proper cooling of a mixture of di-*tert*-butyl dicarbonate and triethylamine in dichloromethane prior to addition of starting material was necessary to avoid undesired double protection. This produced compound **II-9** in 4 scalable steps from cyclopentadiene and provided multiple gram quantities. Unfortunately, direct methylation of **II-6** was not achievable in a single step due to methylation of the alcohol.

Scheme 2.6. Synthesis of **II-9**

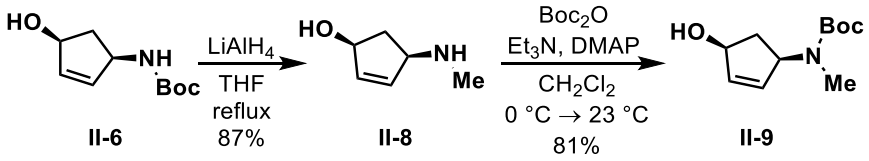

Alcohol **II-9** was then subjected to a Mitsunobu reaction employing the bromopyrrole as the nucleophile, and a strong base, such as KHMDS proved necessary to promote conversion of starting material. This afforded the pyrrole **II-10** with high *trans*-diastereoselectivity of the carbamate and pyrrole (Scheme 2.7). The purification of **II-10**

was complicated because of the bromo pyrrole **I-47** had a similar polarity to the product **II-10**. However, using diethylether in hexanes, and a larger, longer silica gel column proved sufficient to separate the two molecules. Saponification of the methyl ester proceeded using lithium hydroxide in THF/water to generate the carboxylic acid and the resultant acid was converted to the amide in high yield over two steps. Initial activation of the acid with oxalyl chloride to form the acyl chloride *in situ* proved necessary, and the acyl chloride was immediately reacted with a saturated solution of ammonia in THF to form amide **II-11**. Initially, carbonyldiimidazole was used in an attempt to form the carbamate, which was then treated directly with ammonium hydroxide to form the amide, however, this led to a far lower yield (54%).

Scheme 2.7. Synthesis of amide **II-11**

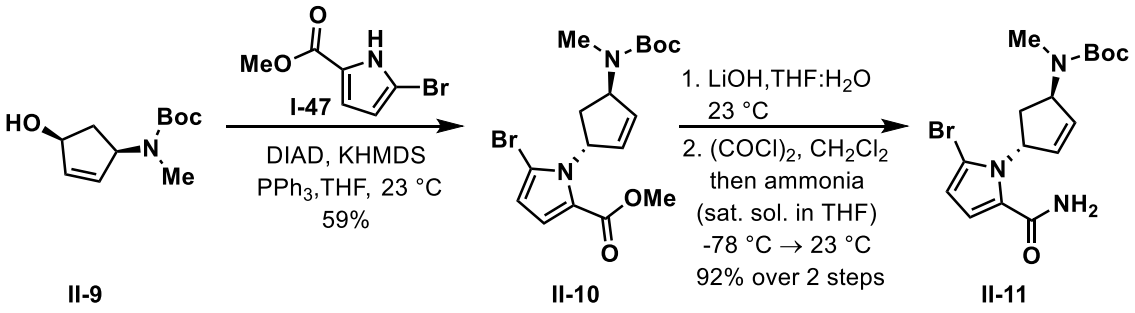

Exposure of amide **II-11** to trifluoracetic acid in dichloromethane afforded the deprotected amine **II-12** in an isolated 77% yield. The next step, installation of the desired urea (**II-13**), proved to be synthetically challenging. Previously, Dr. Hadi Gholami used potassium isocyanate in the presence of HCl in EtOH/water to convert the amine to urea **II-13**. However, this reaction was not reproducible (Scheme 2.8).

Scheme 2.8. Synthesis of urea **II-13**

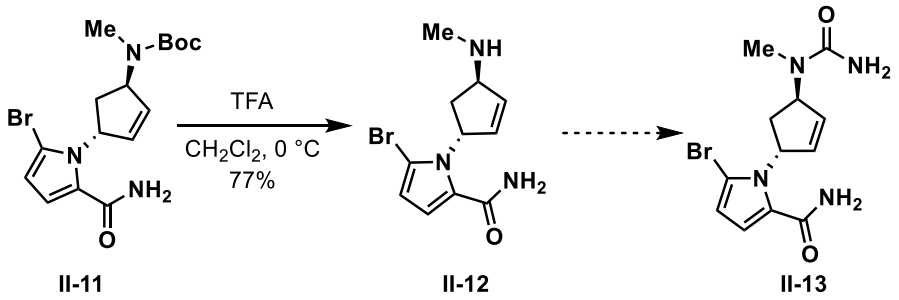

II-11 II-12 II-13

Prior use of potassium isocyanate did provide access to urea **II-13**. It was envisioned that oxidative cleavage of the double bond in **II-13** would yield the bisaldehyde, which could undergo intramolecular cyclization *in situ* to form the advanced key intermediate, enamide **II-2**, in a single operation (Scheme 2.9). However, Dr. Hadi Gholami attempted ozonolysis, dihydroxylation, and other oxidation conditions and only starting material was recovered upon attempted cleavage of **II-13**.

Scheme 2.9. Oxidative cleavage of cyclopentene and *in situ* cyclization

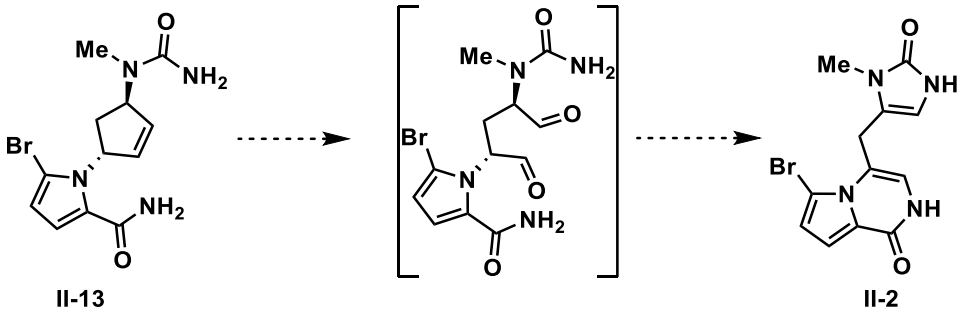

Due to the difficulty in cleaving the double bond, it was hypothesized that the *trans*-configuration of the two bulky substituents leads to an environment that is sterically inaccessible, and thus giving low reactivity with several oxidizing reagents (Figure 2.5). Therefore, it was hypothesized that the *syn*-isomer would allow one face of the olefin to be more open, and therefore improve the reactivity of the olefin to oxidative cleavage.

Figure 2.5. *Trans* and *syn* isomers

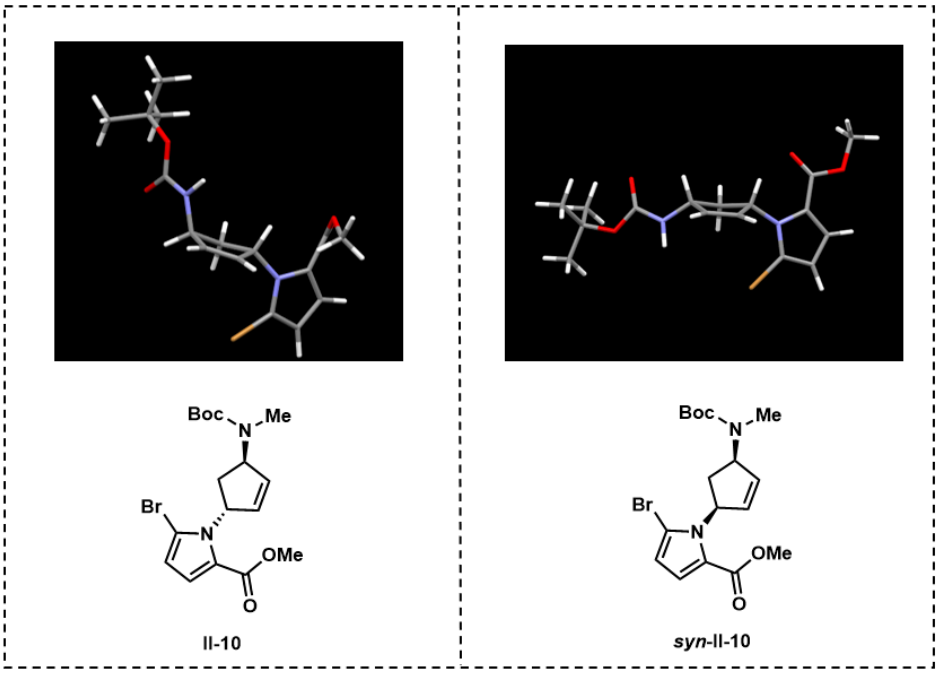

To test this hypothesis, a new synthetic strategy was implemented to access the *syn*-diastereomer **II-10.** The Appel reaction using carbon tetrabromide and triphenylphosphine was thought to convert the alcohol to the allylic bromide to achieve an overall stereochemical inversion. Then, subjection of the bromide to the pyrrole under basic conditions could provide **II-10** with the desired *syn* diastereomer.

Scheme 2.10. Retrosynthesis of *syn*-**II-10**

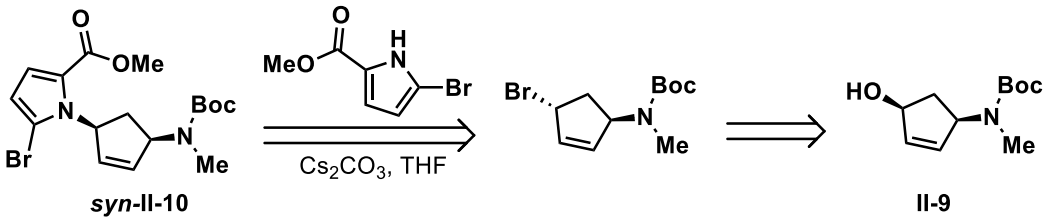

However, bromination of the alcohol under standard Appel conditions did not render the desired brominated product. Other halogenating reagents were evaluated, and the major isoloated product was found to be bicycle **II-14**. This molecule presumably arises from an intramolecular S_N2' displacement of the halide to form bicyclic carbamate **II-14** in good yields (Table 2.2).

Table 2.2. Halogenation of allylic alcohol

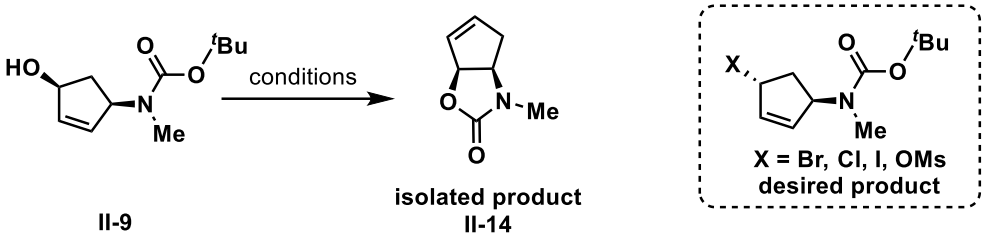

II-9 isolated product II-14

Entry	Reagent(s)	Solvent	Temperature (°C)	Yield (%)
1	PBr_3	CH_2Cl_2	0℃ → 23℃	82
2	MsCl, NEt_3	CH_2Cl_2	0℃ → 23℃	62
3	CBr_4, PPh_3	CH_2Cl_2	23℃	71
4	I_2, DIAD, PPh_3	THF	23℃	74

The formation of bicycle **II-14** due to rapid intramolecular cyclization upon activation of the allylic alcohol indicated another approach was necessary to access the intermediate needed to evaluate our key halo-cyclization strategy. The strategy was modified to access the *syn*-isomer **II-10**. Predicated on Trost's approach to agelastatin A (**1**), a Boc protected alcohol could undergo allylation with the brominated pyrrole (**I-47**) to afford the desired C-N bond, while maintaining the stereochemistry (Scheme 1.6).[63] Employing the Tsuji-Trost allylation strategy, the *syn* isomer **II-10** was successfully generated in an isolated 77% yield (Scheme 2.11). Conversion of the allylic amino alcohol **II-9** to the Boc protected amino alcohol was accomplished using excess Boc anhydride and triethylamine in 22% yield. Originally, I sought to utilize the same reaction setup that was employed by Trost *et al.* After stirring for 24 h at room temperature, TLC analysis showed only starting material. Upon gentle heating to 40℃ for 12 h, TLC analysis confirmed conversion of starting material, and the desired product was isolated in 77%

yield after silica gel chromatography. Using variable temperature NMR studies and comparing the NOE of the *anti* and *syn* isomers, the *syn*-isomer **II-10** was determined to be the configuration of the product formed via the Tsuji-Trost allylation between pyrrole **I-47** and the allylic carbonate **II-15** (see Experimental Section).

Scheme 2.11. Asymmetric allylation for the synthesis of the *syn*-isomer

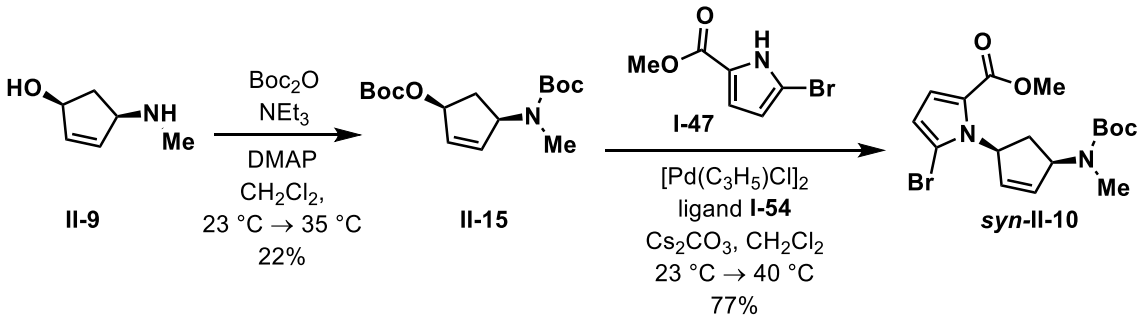

Initially, one of the limiting factors of this route to access *syn*-**II-10** was that only minimal quantities of the di-Boc protected starting material could be generated due to formation of **II-16**, which was the major isolated byproduct (Scheme 2.12). This occurred despite adding excess Boc anhydride, or running the reaction in dilute conditions. Interestingly, switching to the conditions used by Trost *et al.*, which used Boc anhydride in the presence of 30% aqueous sodium hydroxide, DMAP, and tetrabutylammonium hydrogensulfate did not generate any dimer, and the desired product **II-15** was reproducibly synthesized in 59-64% yield.[13]

Scheme 2.12. Boc protection of **II-9**

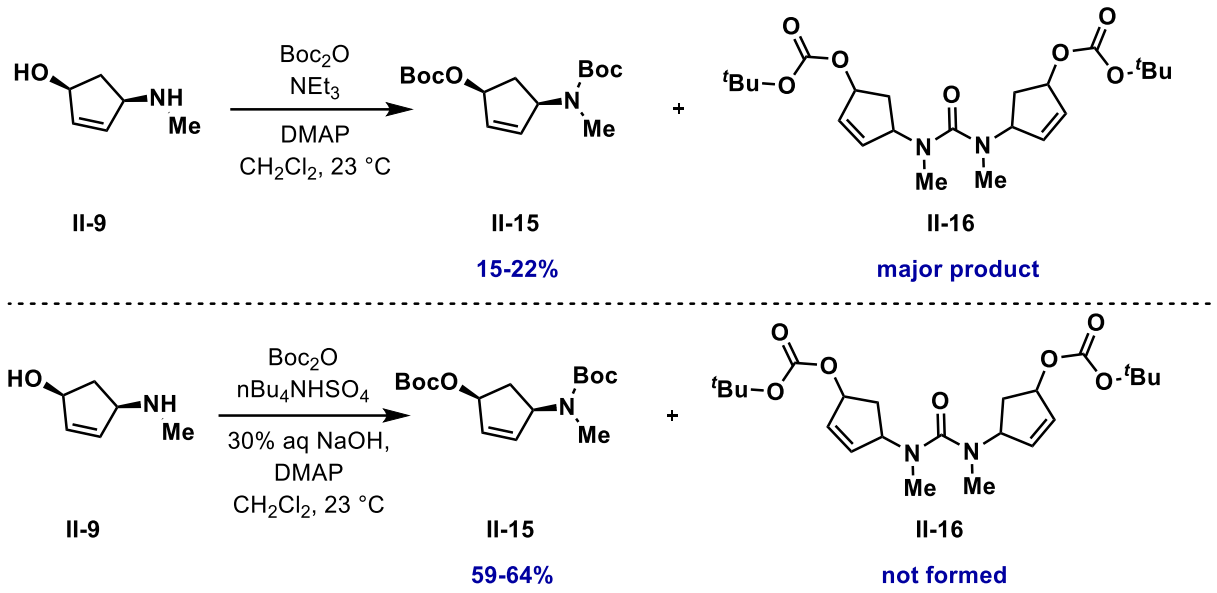

For proof of concept, I attempted to oxidatively cleave the double bond on the methyl ester substrate *syn*-**II-10**. Previously, the cleavage was conducted on the late stage intermediate **II-13** after conversion to the amide and addition of the urea functionality. However, since the desired isomer was obtained, we wanted to assess our original hypothesis regarding steric hinderance of the olefin functionalization (Figure 2.5). Initially, *syn*-**II-10** was exposed to ozonolysis, however, the material was recalcitrant to these oxidant conditions. Though investigation of other oxidants, it was found that stoichiometric osmium tetroxide in combination with 4-methylmorpholine *N*-oxide in dichloromethane provided the desired diol in an isolated 87% yield. The unoptimized reaction is sluggish, needing 5 days to reach completion, however, the successful oxidation supports our hypothesis that the double bond of the *syn*-diastereomer can be successfully oxidized under conditions that were previously unreactive for the *trans*-isomer.

Scheme 2.13. Dihydroxylation of the *syn*-isomer

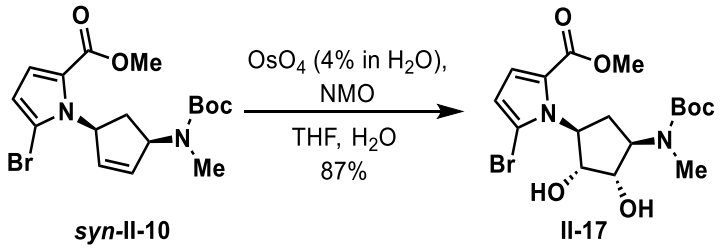

With access to *syn* isomer **II-10** and proof that the olefin is reactive to oxidizing conditions for the *syn* isomer, *syn* **II-10** was subjected to the same transformations to access the *syn* isomer for the urea compound **II-13** (Scheme 2.14).

Scheme 2.14. Formation of *syn* isomer **II-12**

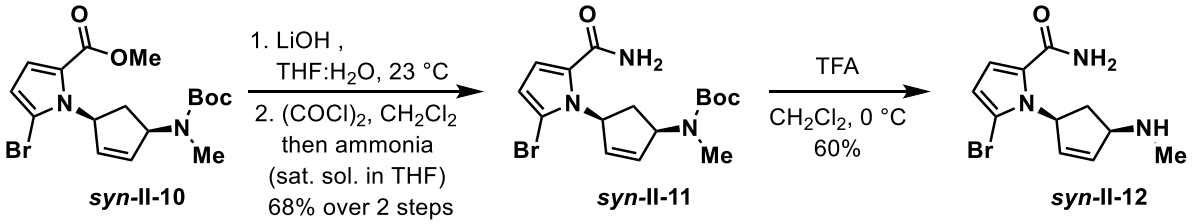

Methyl ester *syn*-**II-10** was converted into the amide by first forming the carboxylic acid using lithium hydroxide in THF/water. Activation of the carboxylic acid with oxalyl chloride afforded the acid chloride (NMR analysis confirmed acid chloride formation). Since the acid chloride is sensitive to hydrolysis and isolation, the crude solution of the acid chloride was concentrated under nitrogen, THF was added, and this solution was then directly added dropwise to a saturated solution of ammonia in THF at -78℃ to provide the amide *syn*-**II-11** in good yield. Lastly, deprotection of the Boc group using trifluoroacetic acid in dichloromethane at 0℃ afforded the amine *syn*-**II-12** in good yield.

Due to the difficulty with isolating and purifying the Boc deprotected amine *syn*-**II-12**, a three-step protocol was developed to transform the Boc protected amine to the urea *syn*-**II-13**.[64] The deprotected amine was confirmed via NMR, added to a precooled solution of triphosgene in dichloromethane, followed by the addition of Hunigs base, and stirred for 1 h. ^{1}H NMR confirmed formation of the acetylated product, and this crude solution was then directly added to a solution of ammonia in THF, which was precooled to -78 °C. The reaction was stirred for 12 h and slowly warmed to room temperature to generate the urea *syn*-**II-13**. It is important to note, the urea product is difficult to purify due to the polarity of the molecule and the four nitrogen atoms that are present. An aqueous workup is not feasible and a significant loss of product to the water layer is observed. Similarly, column conditions must be basic to ensure the urea **II-13** elutes though the silica. This, however, does not remove Hunigs base from the product and thus, has caused issues to remove. Multiple columns must be performed in order to ensure complete removal of Hunigs base.

Scheme 2.15. Formation of urea *syn*-**II-13**

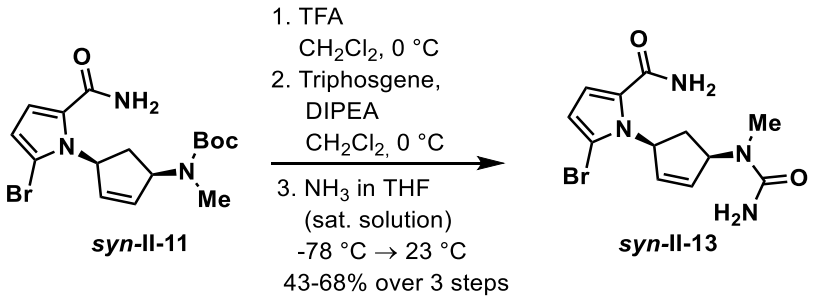

With the urea in hand, oxidative cleavage and cyclization to generate our key intermediate, enamide **II-2** was investigated. With the successful oxidation *syn*-**II-10**

(Scheme 2.13), we hypothesized that the desired oxidation, and/or consecutive oxidation/cyclization of urea *syn*-**II-13** could be feasible. In the presence of osmium tetroxide and NMO in THF/water at 23 °C, the diol was successfully formed from the urea *syn*-**II-13** (Scheme 2.16). Oxidation of alkene to the diol was successful, as observed by ^{1}H NMR. The protons corresponding to the olefin completely disappear from the NMR spectra, and the appearance of the diol α-hydrogens were observed in the spectra. Also, to further verify the formation of the diol, the spectra for diol **II-18** was compared to the isolated diol **II-17,** made from the methyl ester *syn*-**II-10**.

Scheme 2.16. Dihydroxylation of the urea *syn*-**II-13**

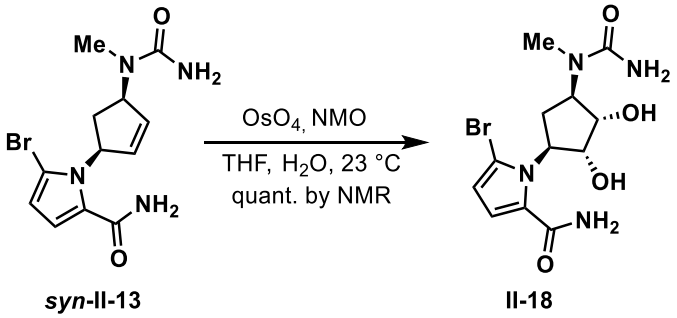

***syn*-II-13** **II-18**

While diol formation occurred smoothly, attempts to cleave the diol was problematic (Table 2.3). Complex NMRs and decomposition was observed with minimal-to-no observation of the desired product. Other conditions, such as ozonolysis and ruthenium trichloride with $NaIO_4$ also only led to decomposition of the starting material with no observation of the desired oxidized product. Interestingly, AD-mix-α only returned starting material.

Table 2.3. Attempts at oxidative cleavage of the *syn*-isomer

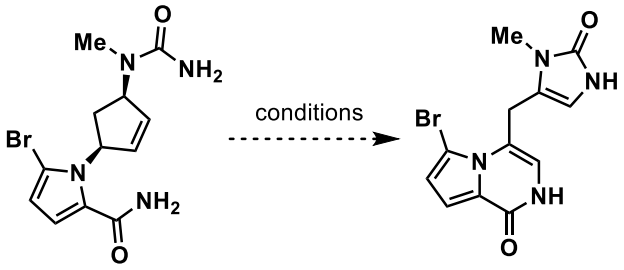

***syn*-II-13** **II-2**

Entry	Conditions	Result(s)
1	OsO_4, $NaIO_4$ THF, H_2O, 23 ℃	Complete consumption of starting material; Complex product(s) formed; No desired product or hemi-aminal observed
2	OsO_4, $Pb(OAc)_4$ THF, H_2O, 23 ℃	Complete consumption of starting material; Complex product(s) formed; No desired product or hemi-aminal observed
3	OsO_4, HIO_4 THF, H_2O, 23 ℃	Complete consumption of starting material; Complex product(s) formed; No desired product or hemi-aminal observed
4	AD-mix-α, *t*-BuOH 23 ℃	Starting material was recovered
5	O_3, $CH_3CH_2Cl_2$, -78 ℃	Decomposed (unidentifiable byproducts)

The current hypothesis as to why cleavage has been presently unsuccessful centers on the amide and urea functional groups, which can potentially coordinate with the oxidant, thus precluding diol coordination and subsequent oxidation. Oxidation of the amido- and urea functionality is also possible and cannot be ruled out.

Due to the ongoing difficulty in the oxidative cleavage of the cyclopentene to synthesize enamide **II-2**, as well as the scalability and purification issues associated with this synthesis, an alternate approach to access enamide **II-2** was developed.

2.7. Retrosynthesis Route 2

Targeting enamide **II-2**, it was envisioned that fragments **II-19** and **II-20** could be coupled together to forge the new methylene bond. The allylic halide **II-19** was envisioned to come from carboxylic acid **II-21** *via* reduction to the alcohol, and then halogenation. The preparation of carboxylic acid **II-21** is a known procedure from tartaric acid and methyl urea.[20] Fragment **II-20** was proposed to come from bis amide **II-22**, which can be accessed from **II-23** after exposure to base to induce cyclization. The formation of **II-23** is a known procedure that is afforded from the reaction between 2-trichloroacetyl pyrrole and glycine methyl ester.[65]

Scheme 2.17. Retrosynthetic scheme route 2

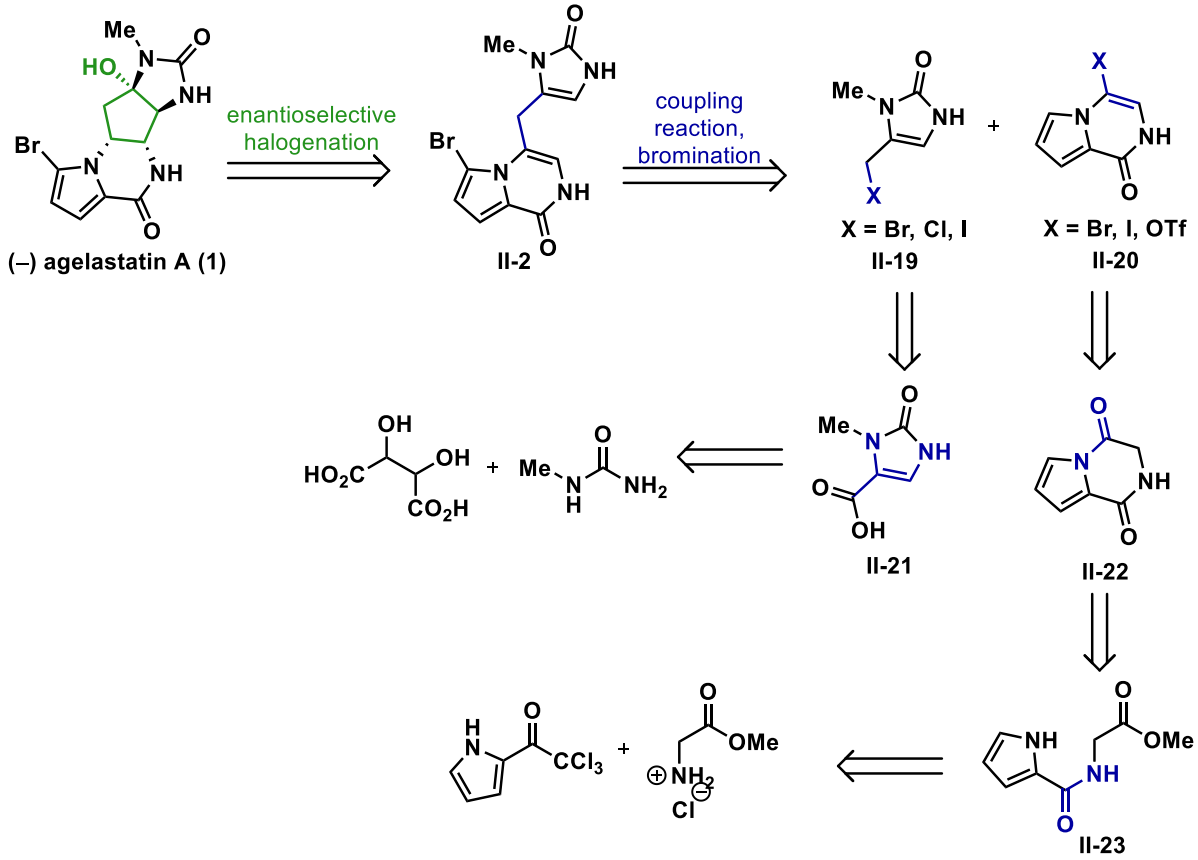

2.8. Synthetic Route 2

Targeting **II-21**, tartaric acid and *N*-methyl urea are heated in the presence of sulfuric acid to provide the cyclic urea **II-21** (Scheme 2.18).[20] This was taken directly to the next step, protection, without further purification. Protection of the amide was deemed necessary later in the synthesis in the course of coupling the two fragments together. The protection was also envisioned to help forego elimination of the activated coupling precursor due to potential instability of this moiety.

The carboxylic acid was converted into the methyl ester **II-24** using one equivalent of potassium carbonate, and one equivalent of methyl iodide, with the methyl iodide slowly added dropwise over a few min.[20] This slow addition is done to prevent *N*-methylation, and the precise use of one equivalent of base preferentially deprotonates the carboxylic acid, while slow dropwise addition provides preferential methyl ester formation.

Scheme 2.18. Methyl ester formation

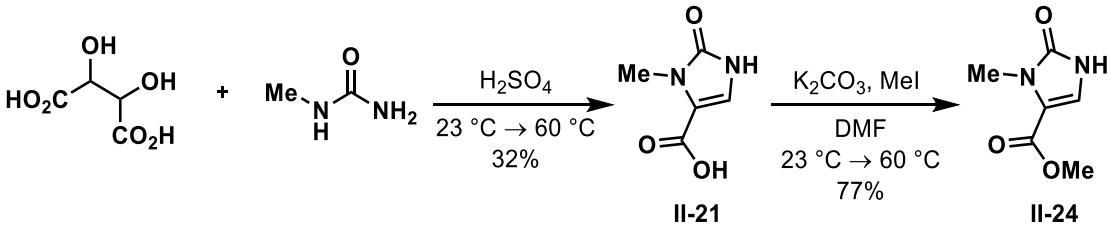

Isolation of methyl ester **II-24** proved to be difficult, and removal of DMF was also an issue. An aqueous work-up to remove DMF also caused the loss of product due to its high solubility in the aqueous layer. To circumvent this issue, and increase the isolated yield of the product, formation of methyl ester was confirmed *via* ^{1}H NMR. Upon

completion as observed by NMR, the reaction was concentrated under a flow of nitrogen gas. The crude reaction mixture was suspended in ethyl acetate and filtered over celite to remove the potassium carbonate, and the methyl ester **II-24** was taken to the next step without further purification.

Next, amide protection was attempted by alkylating the oxygen of the amide selectively using trimethyl oxonium tetrafluoroborate in dichloromethane at ambient temperature to provide the desired *O*-methylated product **II-25** (Scheme 2.19). This was confirmed via comparison of the carbon NMR for the *N* vs. *O*-methylated product. *N*-methylated product was obtained *via* the side product of methyl ester formation **II-24**, which uses methyl iodide as the methylating reagent (Scheme 2.18). **II-25** was taken to the next step without further purification.

Scheme 2.19. Methyl ether formation

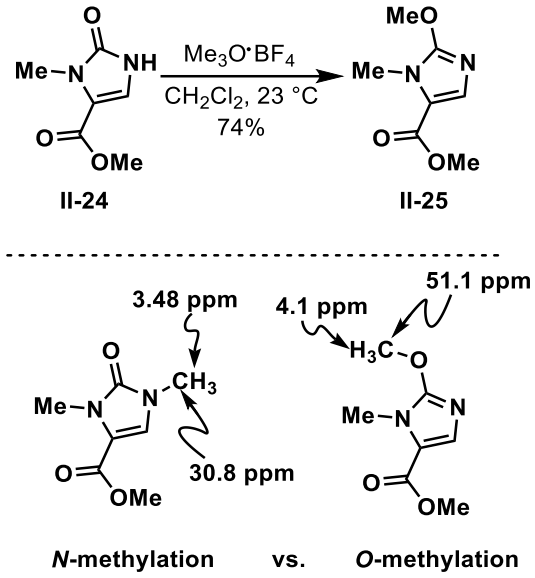

The ester was reduced with lithium aluminum hydride in ether to access the imidazyl alcohol selectively in 68% yield (Scheme 2.20).

Scheme 2.20. Imidazyl alcohol formation

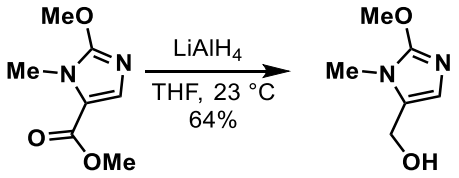

II-25 **II-26**

Next, I attempted to convert the alcohol into a suitable coupling partner. Initial attempts to effect this transformation only returned back starting material, or complex undesired byproduct formation as observed by NMR spectrum (Table 2.4).

Table 2.4. Attempts to form imidazyl halide or tosylate for coupling

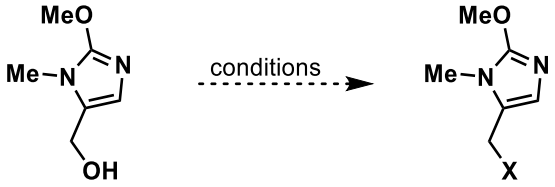

II-26 **II-27**

Entry	Conditions	Result(s)
1	PBr_3, CH_2Cl_2, 0 ℃ → 23 ℃	Full conversion; Starting material was recovered upon isolation
2	TsCl, DMAP, CH_2Cl_2, 23 ℃	Complete consumption of starting material; complex NMR

The issues of forming the imidazyl halide/tosylate are presumably due to an intramolecular elimination to displace the now good leaving group (Figure 2.6). Upon workup this reforms the allylic alcohol, which is observed upon bromination using PBr_3.

Figure 2.6. Proposed mechanism for elimination

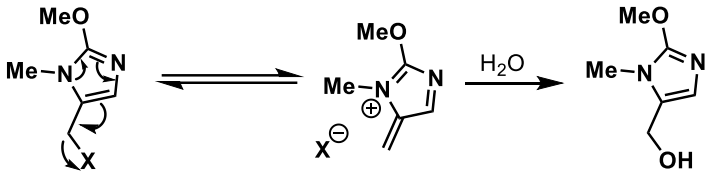

As a result of these observations, it was proposed that formation of the corresponding salt of **II-26** would circumvent the elimination issues due to deactivating the imidazole ring. Thus, exposure of alcohol **II-26** to thionyl chloride in dichloromethane provided the desired chloride **II-27** as the HCl salt without further purification (Scheme 2.21). This reaction was not subjected to an aqueous workup, it was simply concentrated under nitrogen and taken onto the next step.

Scheme 2.21. Formation of the coupling partner **II-27**

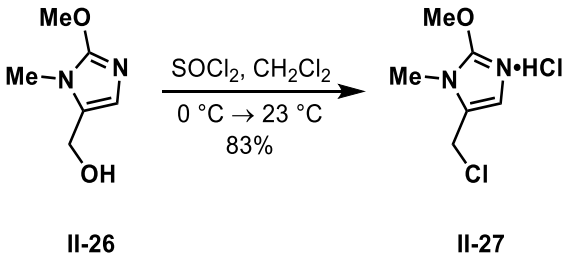

II-26 **II-27**

Upon sonication or exposure to base such as DBU, decomposition of the product **II-27** is readily observed. Due to the sensitivity of the molecule, it was stored cold, in a

refrigerator under a nitrogen atmosphere, and used within a week of synthesizing to ensure proper reactivity.

With the first coupling partner in hand, a strategy to synthesize the other coupling partner **II-20** was evaluated. Starting from 2-trichloroacetyl pyrrole and glycine methyl ester, amide **II-23** was isolated in good yield (Scheme 2.22). Literature precedent states that exposure of **II-23** in the presence of sodium hydride will produce the bicycle **II-22**.[65] However, numerous attempts resulted in recovered starting material, and the desired product was not formed. To circumvent this, the amide **II-23** was exposed to lithium hydroxide in THF/water to convert the methyl ester to the carboxylic acid **II-28** in 71% yield. The carboxylic acid **II-28** was then stirred in neat acetic anhydride and heated to 50℃ to successfully perform the cyclization and provide the acetate product **II-29**. Cleavage of the acetate group was then done using 1M HCl in a mixture of methanol and dichloromethane at ambient temperature. Addition of methanol proved necessary to afford the complete cleavage of the acetate group. Initially, potassium carbonate in the presence of methanol was attempted to cleave the acetate, however, these conditions solely provided the initial starting uncyclized amide **II-23**.

Scheme 2.22. Synthesis of **II-22**

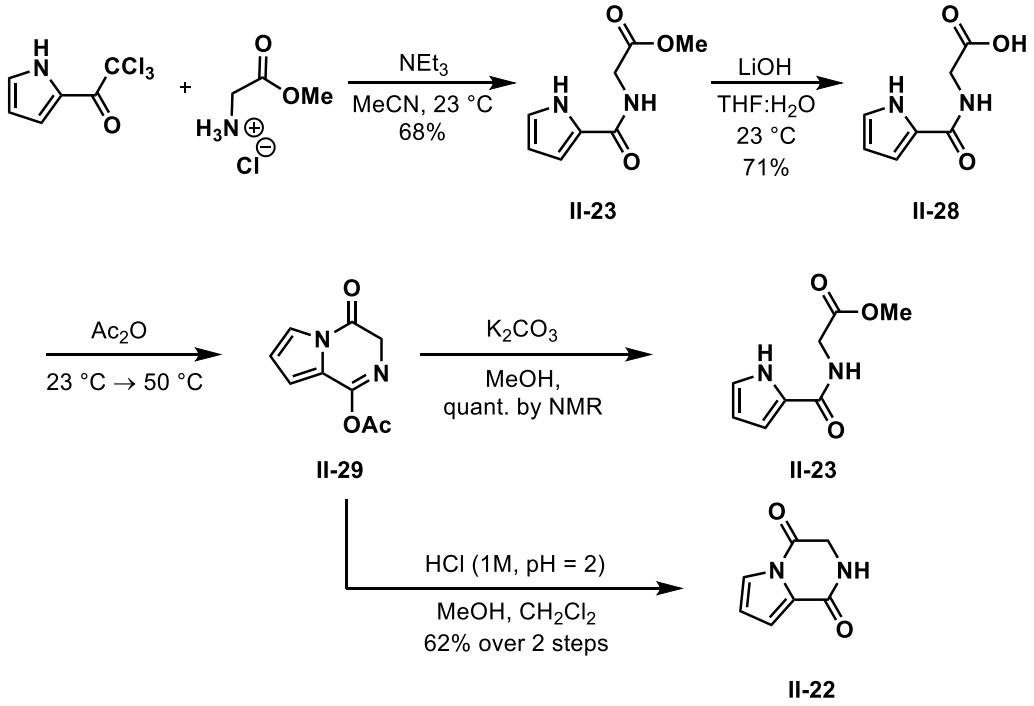

After cleavage of the acetate group, the amide was protected using the same reagent that was used prior for coupling partner **II-25**. Thus, exposure to trimethyl oxonium tetrafluoroborate in dichloromethane at room temperature selectively provided the *O*-methylated product **II-30** in good yield (Scheme 2.23).

Scheme 2.23. Protection of amide to form **II-30**

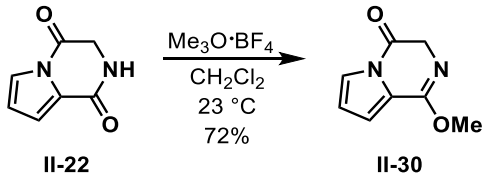

Next, conditions were evaluated to access a suitable coupling partner. Synthesis of the triflate was first attempted using KHMDS with phenyl triflimide, however, the desired triflate was not formed and these conditions only caused decomposition (Table 2.5). Similarly, using triflic anhydride with triethylamine also caused decomposition of the starting material with no identifiable product(s) observed. However, following a modified literature procedure,[66] the aryl tosylate was synthesized in 86% yield using DMAP, triethylamine, and tosyl chloride in toluene at ambient temperature.

Table 2.5. Attempts to form coupling partner **II-31**

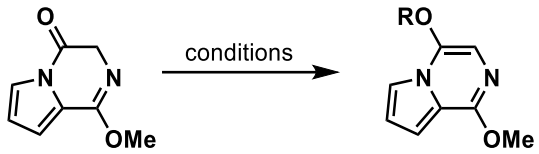

R = Tf, Ts

II-30 **II-31**

Entry	Conditions	Result(s)
1	KHMDS, Tf_2NPh THF, -78 ℃	Complete consumption of starting material; complex NMR
2	Tf_2O, NEt_3, CH_2Cl_2, 23 ℃	Complete consumption of starting material; complex NMR
3	TsCl, DMAP, NEt_3, PhMe, 23 ℃	Desired aryl tosylate (**II-31**), 86% yield

With a scalable and efficient route to both coupling partners, attempts to couple the two fragments were evaluated. Initially, as a test cross-coupling reaction, tosylate **II-31** was reacted with phenyl boronic acid using a modified literature procedure, which employed $Pd(OAc)_2$, BrettPhos, and K_3PO_4 in *t*-AmOH at 80 °C (Scheme 2.24).[67] These

conditions did indeed successfully afford the desired coupled product **II-32** in an isolated 57% yield. This result was encouraging and proved that the aryl tosylate **II-31** could undergo oxidative addition without issues and participate in cross-coupling reactions with appreciable success.

Scheme 2.24. Coupling reaction with phenyl boronic acid

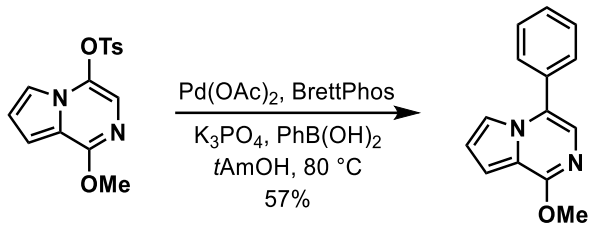

II-31 **II-32**

Using the proven aforementioned conditions, next, I attempted to convert aryl tosylate **II-31** to the boronate ester **II-33** with B_2Pin_2 (Scheme 2.25). However, the reaction did not yield the desired boronate ester product, and only the dimer of the starting material **II-33** was isolated in 72% yield.

Scheme 2.25. Formation of dimer **II-33**

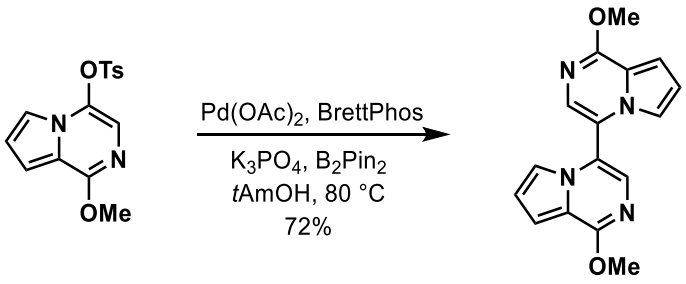

II-31 **II-33**

Due to dimer formation, different conditions were screened (Table 2.6). Addition of LiCl (entry 1) only caused decomposition. Solvent switch to dioxane, as well as modifying the palladium catalyst in different solvents (entries 2-4) only caused decomposition and no identifiable products were observed. Utilizing a different method,[68] formation of the boronate using HBPin with triethylamine, $Pd(PPh_3)Cl_2$ in dichloroethane was attempted, but only decomposition was observed (entry 5). Modification of the palladium catalyst to $Pd(OAc)_2$ and the solvent to *t*AmOH only afforded starting material at room temperature (entry 6), and upon heating, only decomposition was observed indicating a clear temperature effect and slim operating window to be able to successfully undergo oxidative addition and competent coupling without decomposition. To promote the formation of the boronate ester **II-34** and decrease dimer formation, the reaction was performed under dilute conditions (0.005M) and excess B_2Pin_2 (15 equiv). However, unfortunately, only the dimer **II-33** was isolated in 39% yield with no observable desired product (entry 7).

Table 2.6. Screening conditions for BPin formation

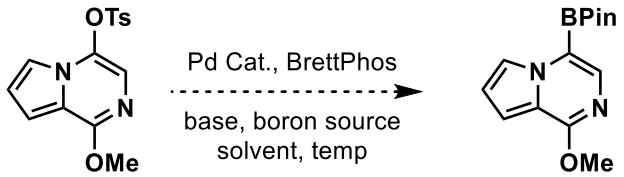

II-31 **II-34**

Entry	Solvent	Pd Catalyst	Additive	Base	Boron	Temp.	Result(s)
1	*t*AmOH	$Pd(OAc)_2$	LiCl	K_3PO_4	B_2Pin_2	23 → 80 ℃	Decomposition
2	Dioxane	$Pd(OAc)_2$	-----	K_3PO_4	B_2Pin_2	23 → 80 ℃	Decomposition
3	Dioxane	$Pd(amphos)Cl_2$	-----	K_3PO_4	B_2Pin_2	23 → 80 →110 ℃	Decomposition
4	*t*AmOH	$Pd(amphos)Cl_2$	-----	K_3PO_4	B_2Pin_2	23 → 80 ℃	Decomposition
5	DCE	$Pd(PPh_3)_2Cl_2$	-----	NEt_3	HBPin	23 → 80 ℃	Decomposition
6	*t*AmOH	$Pd(OAc)_2$	-----	NEt_3	HBPin	23 ℃→80 ℃	Decomposition
7	*t*AmOH (0.005M)	$Pd(OAc)_2$	-----	K_3PO_4	B_2Pin_2 (15 equiv)	23 → 80 ℃	Dimer **II-33** formed, 39%

Based on these observations, my hypothesis is that the boronate ester **II-34** is forming in solution, but it is then directly undergoing a rapid *in-situ* Suzuki reaction with residual starting tosylate **II-31** to form the dimer **II-33**. This indicates that the boronate ester **II-34** is highly reactive under conditions that successfully allow for initial oxidative addition of the tosylate. However, once formed it either participates in the cross-coupling reaction to form the dimer, or decomposes (Table 2.6, entries 1-6). To test this hypothesis, I ran the same conditions that were used in Scheme 2.25 *without* the B_2Pin_2 (Scheme 2.26). After heating the reaction at 80℃ for 2 h, only starting material was present, whereas in the presence of B_2Pin_2 dimer product **II-33** was solely formed. Upon heating to 110℃, there was complete decomposition of the starting material, confirming the hypothesis that **II-34** must be forming in solution and then undergoing rapid cross-coupling reaction to form the dimer **II-33.**

Scheme 2.26. Dimer formation attempt without B_2Pin_2

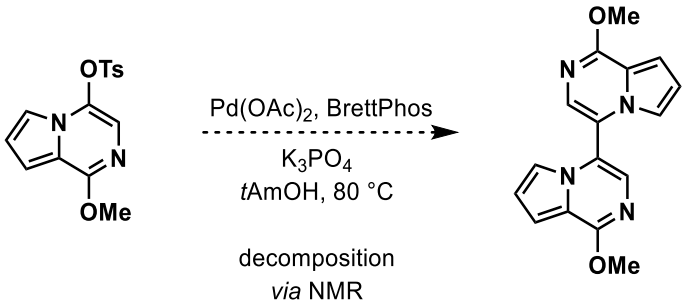

II-31 **II-33**

Since the tosylate **II-31** was undergoing an *in-situ* Suzuki reaction, I hypothesized that after formation of the boronate ester from **II-31**, then a cross coupling could occur in with imidzayl chloride **II-27**. This would effectively undergo a conversion to the boronate ester, followed by Suzuki reaction all in one pot. To test this, I ran the reaction with the same conditions described above, except now I added **II-27** to the round bottom flask. Unfortunately, after heating for 4 h only decomposition of both starting materials, **II-31** and **II-27** was observed.

Scheme 2.27. Attempted one pot boronate ester formation followed by Suzuki reaction

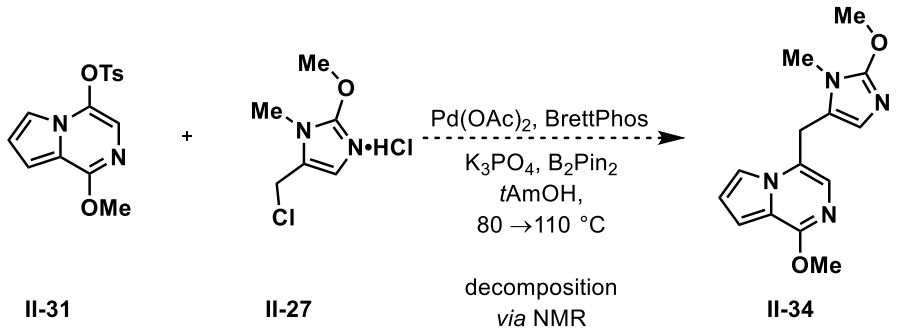

II-31 **II-27** **II-34**

Next, I attempted to form the boronate ester utilizing the other coupling fragment, the chloride **II-27**.[69] Since the chloride was isolated as a salt, and exposure to base, such as DBU, causes decomposition, consideration of the base for the Miyaura borylation reaction is important. Protonated imidazole has a pK_a of approximately 7, and in molecule **II-27** it is slightly higher than 7 due the electronically rich imidazole. Potassium acetate was therefore selected as the base to attempt formation of the boronate ester. Unfortunately, changing the palladium catalyst or solvent did not affect the outcome of the reaction, and decomposition of the starting material was observed (Table 2.7, entries 1-6).

Table 2.7. Attempted formation of imidazyl BPin **II-35**

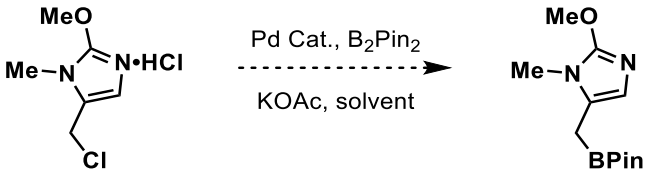

II-27 **II-35**

Entry	Solvent	Pd Catalyst	Temperature	Result(s)
1	Dioxane	$Pd(OAc)_2$	23 ℃	Decomposition
2	PhMe	$Pd(OAc)_2$	23 → 50 → 80 ℃	Decomposition
3	Dioxane	$Pd(amphos)Cl_2$	23 ℃	Decomposition
4	PhMe	$Pd(amphos)Cl_2$	23 ℃	Decomposition
5	Dioxane	$Pd(dppf)Cl_2$	23 → 50 ℃	Decomposition
6	PhMe	$Pd(dppf)Cl_2$	23 ℃	Decomposition

Due to the difficulties associated with forming the boronate species on either coupling fragment, other coupling strategies were explored. Conversion of the aryl tosylate **II-31** to the aryl bromide **II-36** would allow for lithium-halogen exchange and provide another route to the targeted enamide **II-2**. Following a modified literature procedure,[70] the aryl tosylate, nickel catalyst, zinc, COD, lithium bromide, and DMA/THF was reacted together at room temperature for 24 h. NMR monitoring of the reaction only showed starting material (Scheme 2.28). The reaction was then heated to 50 ℃ for 4 h, and monitoring of the reaction by NMR only indicated starting material. The temperature

was then increased to 80 ℃, and after 1 h, NMR indicated complete decomposition with no identifiable products observed (Scheme 2.28).

Scheme 2.28. Attempted formation of aryl bromide **II-36**

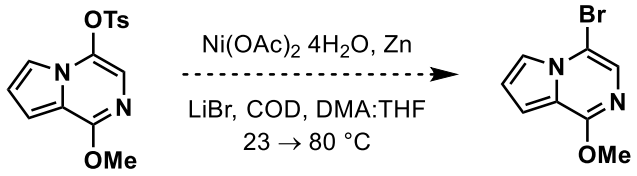

II-31 **II-36**

With problematic boronate formation and aryl bromide formation, a Stille coupling was next evaluated as an alternative strategy.[71] To this end, lithium tri-*n*-butylstannane in THF was generated by freshly using prepared lithium diisopropylamine with tri-*n*-butyltin hydride at -78 °C (Scheme 2.29). Chloride **II-27** was added to the freshly prepared tri-*n*-butylstannane in one portion at -78℃, and after 2 h the reaction was neutralized. Due to product instability on silica gel, the crude product was used directly in the next reaction to attempt the Stille coupling. ^{1}H NMR spectra indicated the stannane may have successfully worked, however, due to purification issues, and removal of the tin byproducts from the reaction, this made it very difficult to verify successful stannane formation. The freshly generated stannane **II-37** was added to a deoxygenated round bottom flask that contained tosylate **II-31**, $Pd(OAc)_2$, XPhos, CsF, and *tert*-butanol. After stirring at room temperature for 2 h, NMR of an aliquot indicated only starting materials. The reaction was then heated to 80℃ for 4 h, and NMR confirmed conversion of starting material via NMR. Unfortunately, upon workup, NMR of the crude mixture indicated only dimer **II-33** as the major product with no desired product observed.

Scheme 2.29. Attempted Stille Coupling

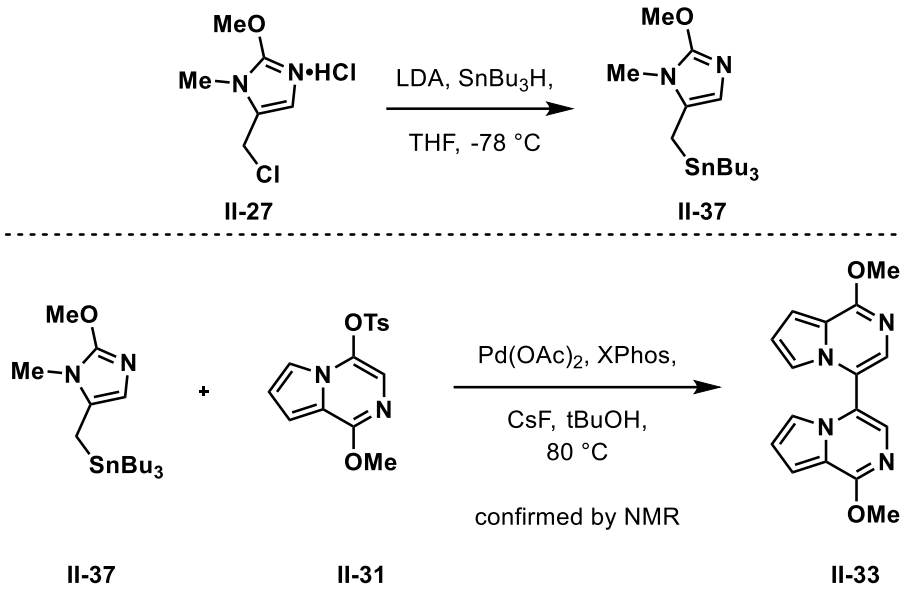

Kumada and Negishi couplings were next evaluated as alternatives (Table 2.8). Initially the Kumada coupling was explored using isopropylmagnesium chloride, which in this case was used to undergo magnesium halogen exchange with **II-36**. This mixture in THF was then added to a solution of **II-27** and reacted with $Pd(PPh_3)_4$, $Ni(dppf)Cl_2$, and $Pd(OAc)_2$ as the catalysts (entries 1-3). Unfortunately, in each reaction, only starting tosylate **II-27** was recovered. There was no sign of successful cross-coupling, or any remaining chloride **II-36**.

Negishi coupling was evaluated next. However, the Negishi coupling conditions showed the same results. The only difference was observed with the use of $Pd(OAc)_2$ as the catalyst, which caused decomposition of the tosylate **II-27** as well as the chloride **II-36** with no identifiable products**.** Presumably, chloride **II-36**, when exposed to base such as the isopropylmagnesium chloride, decomposes due to the instability of its compound.

Table 2.8. Attempted Kumada and Negishi Couplings

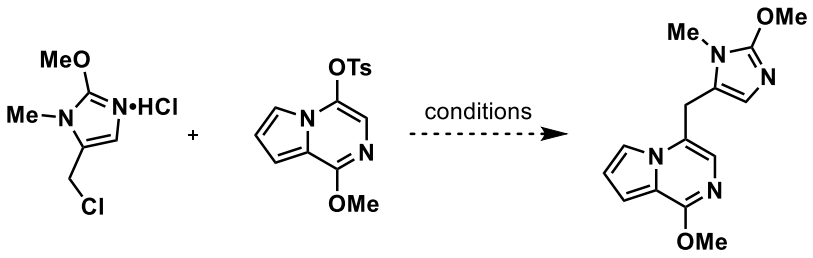

II-36 **II-27** **II-34**

Entry	Solvent	Catalyst	MgX	ZnX	Temp.	Result(s)
1	THF	$Pd(PPh_3)_4$	*i*PrMgCl	-----	23℃→80℃	Decomposition upon heating
2	THF	$Ni(dppf)Cl_2$	*i*PrMgCl	-----	23℃→80℃	Decomposition upon heating
3	THF	$Pd(OAc)_2$	*i*PrMgCl	-----	23℃→80℃	Decomposition upon heating
4	THF	$Pd(PPh_3)_4$	*i*PrMgCl	$ZnCl_2$	23℃→80℃	Decomposition upon heating
5	THF	$Ni(dppf)Cl_2$	*i*PrMgCl	$ZnCl_2$	23℃→80℃	Decomposition upon heating
6	THF	$Pd(OAc)_2$	*i*PrMgCl	$ZnCl_2$	23℃→80℃	Decomposition upon heating

2.9. Conclusion

Currently, efforts toward accessing the key intermediate to test the penultimate enantioselective halo-cyclization to access the tetracyclic core of agelastatin A (**1**) are ongoing. The enantioselective halo-cyclization event in the total synthesis, if successful, can be exploited as a traceless source of chirality, and applicable to other total syntheses. Initially, our attempts to access the key intermediate to test our halo-cyclization strategy starting from cyclopentadiene was highlighted by a diastereoselective Tsuji-Trost allylation to access a key pyrrole substituted cyclopentene. Although it was shown that we could selectively oxidize the alkene, the residual oxidized C-C bond proved to be recalcitrant in undergoing successful oxidative cleavage. It is hypothesized that this is due to deleterious reactivity with the amide and urea functionality in close proximity. This route is also difficult to scale up, and therefore, a second strategy was developed that commences from simple starting materials, and offers an efficient, scalable route to each of the fragments. Unfortunately, the final cross-coupling to access the desired intermediate has not worked so far, and suitable conditions have yet to be developed. Future work will consist of using a coupling strategy that is similar to Movassaghi's synthesis that entails a thioester and a stannane for efficient coupling.[19] A new strategy to synthesize the enamide **II-2** from the imidazyl chloride **II-36** and tosylate **II-27** fragments is currently under development.

2.10. Experimental Section

2.10.1. General Information

Unless otherwise mentioned, solvents were purified as follows. Toluene and CH_2Cl_2 were dried over CaH_2 whereas THF and Et_2O were dried over sodium (dryness was monitored by color of benzophenone ketyl radical); they were freshly distilled prior to use. NMR spectra were obtained using 500 MHz Varian NMR spectrometers and referenced using the residual 1H peak from the deuterated solvent. Waters 2795 (Alliance HT) instrument was used for HMS analysis with polyethylene glycol (PEG-400-600) as a reference. Column chromatography was performed using Silicycle 60Å, 35-75 μm silica gel. Pre-coated 0.25 mm thick silica gel 60 F254 plates were used for analytical TLC and visualized using UV light or potassium permanganate stain.

2.10.2. Experimental Procedure for Route 1 Synthesis

Prepared following literature precedent.[60]

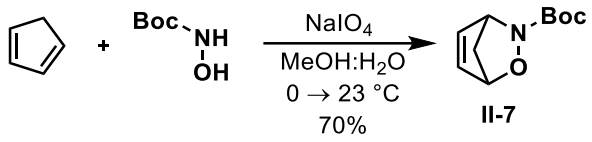

Dicyclopentadiene was placed in a three-neck round-bottom flask equipped with a condenser and placed in a sand bath heated to approximately 180 ℃. The receiving flask is a three-membered round-bottom flask that is placed in a -78 ℃ ice bath to collect the monomer. Cyclopentadiene (20 mL, 244 mmol, 1.5 equiv) was added directly to the clear stirring solution of *N*-Boc-hydroxylamine (21.6 g, 162 mmol, 1 equiv) in MeOH (600 mL) at 0 ℃. Sodium (meta)periodate (18.9 g, 178 mmol, 1.1 equiv) was added directly afterwards and the solution turned a bright yellow. The reaction was allowed to stir for 1 h at 0 ℃. After evaporation of the solvent, the crude product was dissolved in ethyl acetate and water, partitioned, and the residual organics were extracted from the aqueous layer with ethyl acetate (3 x 300 mL). The combined organics were washed with brine (300mL), dried over Na_2SO_4, decanted, and concentrated. The crude bright yellow product was subjected to column chromatography; 30% ethyl acetate/hexane to afford **II-7** as a pale-yellow solid (13.4 g, 70% yield).

^{1}H NMR (500 MHz, Chloroform-*d*, 23 ℃) δ 6.40 – 6.34 (m, 2H), 5.16 (dd, *J* = 1.9, 0.9 Hz, 1H), 4.93 (dd, *J* = 3.3, 1.2, 1H), 2.00 – 1.89 (m, 1H), 1.73 – 1.65 (m, 1H), 1.42 (s, 9H).

^{13}C NMR (126 MHz, Chloroform-*d*, 23 ℃) δ 158.49, 134.05, 132.87, 83.48, 81.92, 64.95, 48.06, 28.09.

HRMS: calculated for C_5H_8NO $[M+H\text{-}Boc]^+$ 98.0606, found 98.0606

IR: 2985-2883 cm^{-1},1733 cm^{-1}, 1563 cm^{-1}, 1144 cm^{-1}

M.P.: 43.3-45.2℃

Prepared following literature precedent.[61]

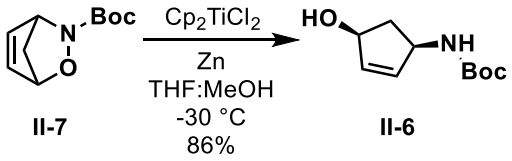

II-7 **II-6**

Under an argon atmosphere, a solution of zinc (4.8 g, 73.7 mmol, 3 equiv) and bis(cyclopentadienyl)titanium(IV) dichloride (9.18 g, 36.8 mmol, 1.5 equiv) in dry THF (60 mL) was stirred at room temperature for 45 min. The solution turned from a dark red to an olive green. The solution was cooled to -30℃ and stirred for 15 min. A solution of the bicycle **II-7** (4.84 g, 24.6 mmol, 1 equiv) in MeOH (50 mL) was added dropwise. The reaction vessel was stirred for 14 h at -30℃. After evaporation under nitrogen of the solvent, the crude product was placed in an ice bath and diluted with 100 mL of ethyl acetate and 100 mL of saturated solution of K_2CO_3 and stirred for 15 min. The solution was suction filtered through a pad of celite, transferred to a separatory funnel, partitioned, and the residual organics were extracted from the aqueous layer with ethyl acetate (3 x 100 mL). The combined organics were washed with brine (100 mL), dried over Na_2SO_4, decanted and concentrated under vacuum to give a pale-yellow solid. The crude product is subjected to column chromatography 30% ethyl acetate/hexane to afford **II-6** as a pale-yellow solid (4.2 g, 86% yield).

^{1}H NMR (500 MHz, Chloroform-*d*, 23℃) δ 5.99 (dd, *J* = 5.7, 2.0 Hz, 1H), 5.85 (ddd, *J* = 5.5, 2.3, 1.0 Hz, 1H), 4.80 (s, 1H), 4.70 (dd, *J* = 6.4, 2.7 Hz, 1H), 4.42 (ddd, *J* = 8.1, 3.8, 1.9 Hz, 1H), 2.79 – 2.70 (m, 1H), 1.55 (m, 1H), 1.44 (s, 9H).

^{13}C NMR (126 MHz, Chloroform-*d*, 23℃) δ 155.25, 136.07, 134.15, 79.58, 75.18, 54.85, 41.38, 28.39.

HRMS: calculated for $C_{10}H_{18}NO_3$ $[M+H]^+$ 200.1287, found 200.1278

IR: 3365 cm^{-1}, 2979-2814 cm^{-1}, 1680 cm^{-1}, 1519 cm^{-1}, 1160 cm^{-1}

M.P.: 44.5-46.8℃

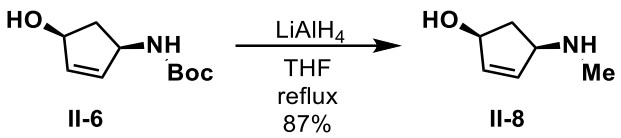

II-6 II-8

Lithium aluminum hydride (4.1 g, 98 mmol, 4 equiv) was placed in a round bottom flask with dry THF (120 mL) and a condenser was attached. A yellow solution of the hydroxyl amine **II-6** (4.86 g, 24.5 mmol, 1 equiv) in dry THF (10 mL) was added dropwise via syringe over 10 min under argon. The reaction mixture was then refluxed for 12 h. The gray solution was placed in an ice bath, diluted with ethyl ether (100 mL), and excess lithium aluminum hydride was quenched by the sequential dropwise addition of water (4 mL), aqueous NaOH (15%, 4 mL), and water (12 mL). After stirring for 5 min, solid Na_2SO_4 was added, and the mixture was allowed to stir for an additional 15 min. The cold bath was removed and the heterogenous mixture was suction filtered over a pad of Na_2SO_4 and concentrated to reveal the methyl amine **II-8** as a dark red oil (2.41 g, 87% yield). The crude product was used directly in the next reaction with no further purification.

^{1}H NMR (500 MHz, Chloroform-*d*, 23℃) δ 6.02 (ddd, *J* = 5.7, 2.0, 1.1 Hz, 1H), 5.97 (ddd, *J* = 5.7, 1.8 Hz, 1.7 Hz, 1H), 4.71 (m, 1H), 3.59 (m, 1H), 2.59 (ddd, *J* = 13.7, 7.2, 6.5 Hz, 1H), 2.46 (s, 3H), 1.44 (ddd, *J* = 13.8, 4.4, 4.3 Hz, 1H).

^{13}C NMR (126 MHz, Chloroform-*d*, 23℃) δ 136.20, 134.82, 75.22, 63.80, 40.61, 34.05.

HRMS: calculated for $C_6H_{11}N$ $[M+H-OH]^+$ 97.0891, found 97.0890

IR: 3972 cm^{-1}, 2854-2745 cm^{-1}, 1663 cm^{-1}, 1011 cm^{-1}

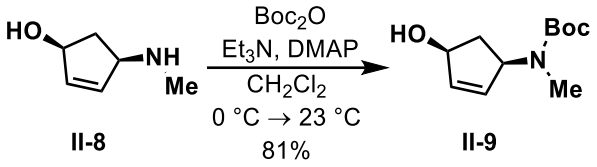

To a flame dried 250 mL round bottom flask was added di-*tert*-butyl-dicarbonate (4.5 g, 20.64 mmol, 1.1 equiv) and DMAP (cat.) in dry dichloromethane (160 mL) and was placed in an ice water bath cooled to 0 ℃ and stirred for 30 min. In a separate pear-shaped flask was added triethylamine (2.86 mL, 20.64 mmol, 1.1 equiv) and precooled to 0 ℃ for 30 min. Separately, in a 25 mL round bottom flask the methyl amine **II-8** (2.12 g, 18.76 mmol, 1 equiv) was dissolved in dichloromethane (10 mL) and cooled to 0 ℃. After 30 min, a solution of **9** was added dropwise to the 250 mL round bottom flask; the transfer was quantified with dry dichloromethane (10 mL), followed by the precooled triethylamine. The dark red solution was warmed to room temperature and stirred for 12 h. The reaction mixture was diluted with dichloromethane (50 mL) and saturated ammonium chloride (100 mL). The biphasic mixture was poured into a separatory funnel and partitioned. The residual organics were extracted from the aqueous layer with dichloromethane (3 x 100 mL). The combined organics were washed brine (100 mL), dried over solid Na_2SO_4, decanted, and concentrated under vacuum. The crude product was subjected to column chromatography 10% ethyl acetate/hexanes → 30% ethyl acetate/hexanes to afford **II-9** as a light brown solid (3.25 g, 81% yield). NMR indicated product as a mixture of rotomeric isomers at room temperature.

^{1}H NMR (500 MHz, DMSO-d_6, 80 ℃) δ 5.92 (dd, *J* = 5.6, 2.1 Hz, 1H), 5.68 (dd, *J* = 5.6, 1.6 Hz, 1H), 4.97 (dd, *J* = 6.2, 1.9 Hz, 1H), 4.65 (d, *J* = 5.3 Hz, 1H), 4.58 (m, 1H), 2.64 (s, 3H), 2.49 (dd, *J* = 13.6, 7.8, 5.6 Hz, 1H), 1.44 (s, 9H), 1.37 (ddd, *J* = 13.6, 5.5, 5.3 Hz, 1H).

^{1}H NMR (500 MHz, Chloroform-*d*, 23℃) δ 5.83 (dd, *J* = 5.7, 2.1 Hz, 1H), 5.60 (dd, *J* = 5.9, 1.5 Hz, 1H), 4.89 (m, 1H), 4.60 (m, 1H), 2.58 (s, 3H), 2.51 (ddd, *J* = 13.9, 7.9, 5.6 Hz, 1H), 1.38 (m, 1H), 1.33 (s, 9H).

^{13}C NMR (126 MHz, DMSO-d_6, 80℃) δ 160.06,142.80, 137.30, 83.80, 78.60, 64.49, 43.05, 33.63 33.44.

HRMS: calculated for $C_{11}H_{20}NO_3$ $[M+H]^+$ 214.1437, found 214.1443

IR: 3260cm^{-1}, 2975-2868 cm^{-1}, 1684 cm^{-1}, 1140 cm^{-1}

M.P.: 44.5-46.5℃

Prepared following literature precedent.[13]

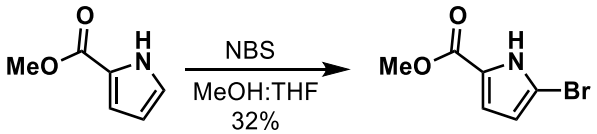

I-47

A solution of the pyrrole-2-carboxylate methyl ester (3.0 g, 24 mmol, 1 equiv) was dissolved in THF (225 mL) and MeOH (120 mL) and placed in an ice bath cooled to 0 ℃ and stirred for 30 min. Recrystallized NBS from water (4.3 g, 24 mmol, 1 equiv) was added in portions. The first portion of NBS (0.76 g) was added and stirred for 30 min, a second portion of NBS (0.94 g) was added and after 40 min, a third portion of NBS (0.774 g) and after 40 min, the fourth and last portion of NBS (1.8 g) was added. After stirring for 2 h at 0 ℃, the solvent was removed under vacuum to give a gray solid. The crude product was subjected to column chromatography 10% ether in hexanes to give the brominated pyrrole as a white solid (1.59 g, 32% yield).

^{1}H NMR (500 MHz, Chloroform-*d*, 23 ℃) δ 9.99 (s, 1H), 6.83 (dd, *J* = 3.9, 2.6 Hz, 1H), 6.21 (dd, *J* = 3.9, 2.5 Hz, 1H), 3.89 (s, 3H).

^{13}C NMR (126 MHz, Chloroform-*d*, 23 ℃) δ 161.01, 123.73, 116.84, 112.71, 105.41, 51.84.

HRMS: calculated for $C_6H_6NO_2$ $[M+H-Br]^+$ 125.0476, found 125.0474

IR: 3231 cm^{-1}, 1684 cm^{-1}, 1550 cm^{-1}, 742 cm^{-1}

M.P.: 102.3-104.7 ℃

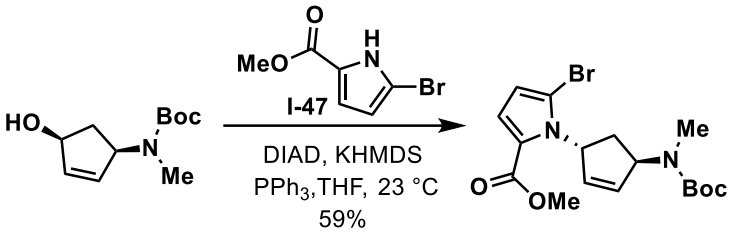

II-9 **II-10**

A clear solution of the pyrrole (2.3 g, 11.27 mmol, 1 equiv) and triphenylphosphine (3.5 g, 17.35 mmol, 1.54 equiv) in freshly distilled THF (90 mL) was placed in an ice water bath cooled to 0℃ and stirred for 20 min under argon. Diisopropyl azodicarboxylate (4.4 mL, 17.35 mmol, 1.54 equiv) was added dropwise via syringe and the reaction mixture turned a milky yellow. A solution of the hydroxy amine **II-9** (2.4 g, 11.27 mmol, 1 equiv) in THF (5 mL) was added dropwise to the solution; the transfer was quantitated with dry THF (5 mL). KHMDS (35 mL, 0.5 M in toluene, 17.35 mmol, 1 equiv) was added *directly* after the addition of **II-9.** After 10 min the milky yellow solution turned a deep red, the ice bath was removed and allowed to stir at room temperature for 13 h. The reaction mixture was diluted with ethyl acetate (100 mL) and saturated ammonium chloride (100 mL), the biphasic solution was poured into a separatory funnel and partitioned. The organics were extracted from the aqueous layer with ethyl acetate (3 x 100 mL), combined, washed with brine (100 mL), dried over solid Na_2SO_4, decanted, and concentrated. The crude red liquid was purified by silica gel chromatography; 10% ether in hexanes to afford **II-10** as a clear oil (2.68 g, 59%). NMR indicated product as a mixture of rotomeric isomers at room temperature.

^{1}H NMR (500 MHz, DMSO-d_6, 80℃) δ 6.93 (d, J = 4.1 Hz, 1H), 6.69 (ddd, J = 9.1, 6.0, 2.8 Hz, 1H), 6.31 (d, J = 4.1 Hz, 1H), 5.97 (m, 1H), 5.87 (m, 1H), 5.49 (m, 1H), 3.77 (s, 3H), 2.69 (s, 3H), 2.41 (m, 1H), 2.23 (m, 1H), 1.45 (s, 9H).

^{1}H NMR (500 MHz, Chloroform-*d*, 23℃) δ 6.95 (d, *J* = 4.1, 1H), 6.92 (br s, 1H), 6.21 (d, *J* = 4.1 Hz, 1H), 5.93 (ddd, *J* = 5.7, 2.1, 2.0 Hz, 1H), 5.81 (ddd, *J* = 5.4, 2.8, 2.6 Hz, 1H), 5,49 (br s, 1H), 3.80 (s, 3H), 2.72 (s, 3H), 2.50 (m, 1H), 2.24 (m, 1H), 1.48 (s, 9H).

^{13}C NMR (126 MHz, DMSO-d_6, 80℃) δ 160.58, 155.33, 134.21, 124.69, 119.35, 113.66, 109.13, 79.39, 63.51, 62.48, 51.67, 34.60, 29.72, 28.64, 21.94.

HRMS: calculated for $C_{12}H_{12}BrN_2O_2$ $[M+H\text{-}Boc]^+$ 299.0395, found 299.0475

IR: 2979-2925 cm^{-1}, 1693 cm^{-1}, 1677 cm^{-1}, 1142 cm^{-1}, 736 cm^{-1}

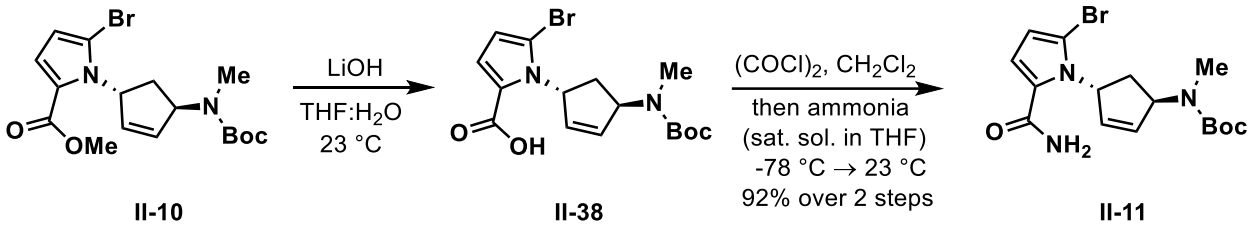

II-10 **II-38** **II-11**

To a solution of the ester **II-10** (0.141 g, 0.35 mmol, 1 equiv) in THF (4 mL) and water (10 mL) was added LiOH (0.44 g, 10 mmol, 30 equiv). After the clear solution was stirring for 12 h, it was acidified to pH = 2 using 1M HCl and diluted with ethyl acetate (4 mL). The biphasic mixture was poured into a separatory funnel, partitioned, and the residual organics were extracted from the aqueous layer using ethyl acetate (3 x 20 mL). The combined organics were washed with brine (20 mL), dried over Na_2SO_4, decanted and concentrated. The crude product **II-38** was purified by silica gel chromatography; 30% ethyl acetate in hexanes to afford the acid as a white solid. NMR indicated product as a mixture of rotomeric isomers at room temperature.

^{1}H NMR (500 MHz, DMSO-*d*$_6$, 80℃) δ 6.89 (d, *J* = 4.1 Hz, 1H), 6.82 (ddd, *J* = 8.5, 5.4, 2.7 Hz, 1H), 6.27 (d, *J* = 4.1 Hz, 1H), 5.97 (m, 1H), 5.85 (m, 1H), 5.49 (dd, *J* = 8.4, 2.8 Hz, 1H), 2.69 (s, 3H), 2.41 (ddd, *J* = 15.0, 9.3, 6.0 Hz, 1H), 2.21 (ddd, *J* = 14.6, 9.5, 3.2 Hz, 1H), 1.45 (s, 9H).

^{1}H NMR (500 MHz, Chloroform-*d*, 23℃) δ 10.84 (br s, 1H), 7.10 (d, *J* = 4.1 Hz, 1H), 6.87 (br s, 1H), 6.24 (d, *J* = 4.2 Hz, 1H), 5.92 (m, 1H), 5.82 (m, 1H), 5.5 (br s, 1H), 2.72 (s, 3H), 2.52 (br s, 1H), 2.24 (br s, 1H), 1.48 (s, 9H).

^{13}C NMR (126 MHz, DMSO-*d*$_6$, 80℃) δ 161.53, 155.39, 134.37, 134.00, 125.94, 119.02, 113.35, 108.09, 79.39, 63.21, 62.63, 34.65, 29.77, 28.67.

HRMS: calculated for $C_{11}H_{14}BrN_2O_2$ $[M+H\text{-}Boc]^+$ 285.0238, found 285.0256

IR: 3136cm^{-1}, 2975-2879 cm^{-1}, 1691 cm^{-1}, 1662 cm^{-1}, 915 cm^{-1}, 739 cm^{-1}

M.P.: 189.7-194.9℃

The carboxylic acid **II-38** (0.125 g, 0.32 mmol, 1 equiv) in dichloromethane (7 mL) was placed in an ice bath cooled to 0℃ and stirred for 20 min under an argon atmosphere. Oxalyl chloride (55 µL, 0.64 mmol, 2 equiv) was added dropwise, followed by three drops of DMF. The ice bath was removed, and the solution was allowed to warm to room temperature. The reaction was monitored by NMR for full conversion to the acid chloride, approximately 1 hour, and the solution was concentrated under nitrogen. Fresh anhydrous ammonia was condensed at -78℃ in THF (2 mL) and the newly prepped acid chloride in THF (1 mL) was added dropwise; the transfer was quantitated with dry THF (1 mL). The reaction vessel was stirred for 2 h at -78℃ under argon and warmed to room temperature. Afterwards, the solution was diluted with ethyl acetate (4 mL) and water (5 mL), the biphasic mixture was transferred to a separatory funnel and washed with water (3 x 5 mL). The combined organics were washed with brine (5 mL), dried over solid Na_2SO_4, decanted, and concentrated under nitrogen. The resulting crude product was subjected to silica gel chromatography; 30% → 50% ethyl acetate in hexanes to afford the amide **II-11** as a light brown oil (0.115 g, 92% yield). NMR indicated product as a mixture of rotomeric isomers at room temperature.

^{1}H NMR (500 MHz, DMSO-d_6, 80℃) δ 7.08 (br s, 2H), 6.87 (m, 1H), 6.80 (d, J = 4.2 Hz, 1H), 6.21 (d, J = 4.0 Hz, 1H), 5.95 (ddd, J = 5.7, 2.2, 2.1 Hz, 1H), 5.81 (ddd, J = 5.5, 3.0, 2.6 Hz, 1H), 5.48 (m, 1H), 2.66 (s, 3H), 2.39 (m, 1H), 2.17 (m, 1H), 1.44 (s, 9H).

^{1}H NMR (500 MHz, Chloroform-*d*, 23℃) δ 6.93-6.73 (br s, 1H), 6.60 (d, *J* = 4.1 Hz, 1H), 6.19 (d, *J* = 4.1 Hz, 1H), 5.93 (m, 1H), 5.80 (m, 1H), 5.67-5.46 (br s, 1H), 2.69 (s, 3H), 2.54 (m, 1H), 2.25 (m, 1H), 1.47 (s, 9H).

^{13}C NMR (126 MHz, DMSO-d_6, 80℃) δ 167.90, 160.10, 139.60, 138.37, 133.87, 119.29, 117.25, 110.26, 84.07, 67.60, 67.17, 39.52, 34.38, 33.41.

HRMS: calculated for $C_{11}H_{14}BrN_3O$ $[M+H\text{-}Boc]^+$ 283.0320, found 283.0325

IR: 3344 cm^{-1}, 2977-2927 cm^{-1}, 1652 cm^{-1}, 1603 cm^{-1}, 1142 cm^{-1}, 742 cm^{-1}

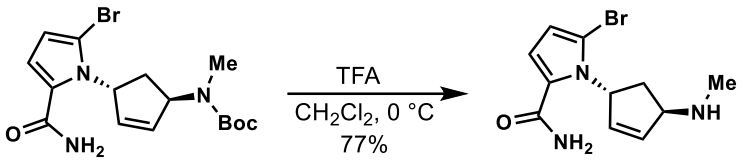

II-11 **II-12**

A solution of the amide **II-11** (48.6 mg, 0.13 mmol, 1 equiv) in dry dichloromethane (6 mL) was placed in an ice bath and cooled to 0 ℃ and stirred for 20 min under argon. TFA (2 mL) was added dropwise over 2 min. The ice bath was removed and was stirred at room temperature for 10 h. Excess TFA was slowly neutralized with aqueous $NaHCO_3$ (10 mL). The biphasic mixture was poured into a separatory funnel, partitioned, washed with brine (20 mL), dried over Na_2SO_4, decanted and concentrated. The crude product was subjected to column chromatography 10% methanol in dichloromethane + 1% triethylamine to afford the pure product as a light brown oil (27.7 mg, 77%).

^{1}H NMR (500 MHz, Chloroform-*d*, 23 ℃) δ 6.72 (m, 1H), 6.58 (d, *J* = 4.1 Hz, 1H), 6.17 (d, *J* = 4.0 Hz, 1H), 6.03 (m, 1H), 5.88 (m, 1H), 5.64-5.44 (br s, 1H), 4.18 (m, 1H), 2.49 (m, 1H), 2.47 (s, 3H), 2.34 (ddd, *J* = 14.3, 9.1, 2.5 Hz, 1H).

^{13}C NMR (126 MHz, Chloroform-*d*, 23 ℃) δ 162.91, 135.10, 133.42, 127.01, 114.16, 112.51, 107.79, 65.40, 63.04, 36.43, 33.57.

IR: 3330 cm^{-1}, 2918-2879 cm^{-1}, 1668 cm^{-1}, 1604 cm^{-1}, 724 cm^{-1}

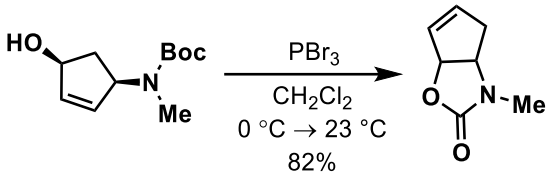

II-9 **II-14**

A solution of the alcohol **II-9** (73 mg, 0.34 mmol, 1 equiv) in dry dichloromethane (2 mL) was placed in an ice bath and cooled to 0 ℃ under argon and stirred for 20 min. PBr_3 (34 µL, 34 mmol, 1 M in DCM, 1 equiv) was added dropwise and the solution was allowed to warm to room temperature. The clear solution was stirred at room temperature for 1 hour and then diluted with dichloromethane (2 mL) and then HBr was slowly neutralized with aqueous $NaHCO_3$ (5 mL). The biphasic mixture was poured into a separatory funnel and partitioned. The residual organics were extracted from the aqueous layer using dichloromethane (3 x 10 mL), washed with brine (15 mL), dried over Na_2SO_4, decanted and concentrated. The crude material was subjected to silica chromatography 20% ethyl acetate/hexanes to yield the clear oil (39 mg, 82% yield).

^{1}H NMR (500 MHz, Chloroform-*d*, 23 ℃) δ 6.05 (m, 1H), 5.85 (m, 1H), 5.40 (ddd, *J* = 7.0, 2.3, 1.2 Hz, 1H), 4.24 (ddd, *J* = 7.7, 5.2, 2.6 Hz, 1H), 2.85 (s, 3H), 2.57 (m, 2H).

^{13}C NMR (126 MHz, Chloroform-*d*, 23 ℃) δ 157.38, 135.00, 128.65, 82.36, 58.89, 36.89, 29.54.

HRMS: calculated for $C_7H_{10}NO_2$ $[M+H]^+$ 140.0711, found 140.0746

IR: 2920-2875 cm^{-1}, 1735 cm^{-1}, 1026 cm^{-1}

Prepared following literature precedent.[13]

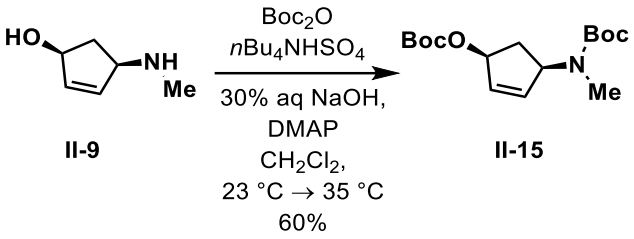

To a flame dried 500 mL round bottom flask was added di-*tert*-butyl-dicarbonate (8.2 g, 38 mmol, 2.5 equiv), *n*Bu_4NHSO_4 (0.5 g, 1.5 mmol, 0.1 equiv), and **II-9** (1.7 g, 1 5mmol, 1 equiv) in dry dichloromethane (150 mL) and the reaction flask was placed in an ice water bath cooled to 0℃ and stirred for 30 min. 30% aqueous sodium hydroxide (15 mL) was added dropwise, and the reaction was warmed to room temperature and stirred overnight, and then heated in an oil bath to 35℃ for 5 h. The dark red solution was warmed to room temperature and stirred for 12 h. The reaction mixture was diluted with dichloromethane (50 mL) and saturated sodium chloride (100 mL). The biphasic mixture was poured into a separatory funnel and partitioned. The residual organics were extracted from the aqueous layer with dichloromethane (3 x 100 mL). The combined organics were dried over solid Na_2SO_4, decanted, and concentrated under vacuum. The crude product was subjected to column chromatography 10% ethyl acetate/hexanes → 20% ethyl acetate/hexanes to afford **II-15** as a clear oil (2.82 g, 60% yield). NMR indicated product as a mixture of rotomeric isomers at room temperature.

^{1}H NMR (500 MHz, DMSO-d_6, 80℃) δ 6.03 – 5.94 (m, 2H), 5.37 (ddd, *J* = 6.3, 5.1, 1.4 Hz, 1H), 5.06 (dd, *J* = 6.8, 6.4 Hz, 1H), 2.69 (m, *J* = 14.3, 8.0, 1.1 Hz, 1H), 2.62 (s, 3H), 1.52 (m, 1H), 1.45 (s, 9H), 1.44 (s, 9H).

^{1}H NMR (500 MHz, Chloroform-*d*, 23℃) δ 5.98 (br s, 1H), 5.90 (br s, 1H), 5.39 (br s, 1H), 5.28 (br s, 0.5H), 5.05 (br s, 0.3H), 4.65 (br s, 0.2H), 2.76 (m, 1H), 2.64 (s, 3H), 1.59 (m, 1H), 1.48 (s, 9H), 1.45 (s, 9H).

^{13}C NMR (126 MHz, DMSO-d_6, 80℃) δ 155.20, 153.00, 137.12, 132.35, 81.94, 80.08, 79.39, 59.52, 34.86, 28.96, 28.64, 28.01.

IR: 2981-2950 cm^{-1}, 1739 cm^{-1}, 1690 cm^{-1}, 1144 cm^{-1}

Prepared following literature precedent.[13]

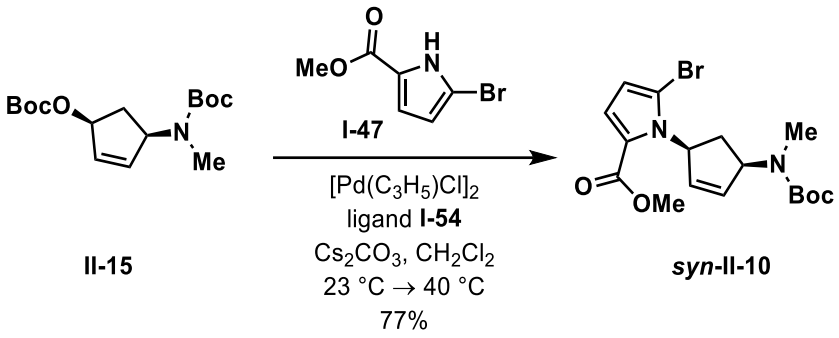

A solution of the ligand **I-54** (17 mg, 6 mol%) and $[Pd(C_3H_5)Cl]_2$ (3 mg, 2 mol%) in dichloromethane (2 mL) which had been stirring for 10 min at room temperature under an argon atmosphere was added to a solution of the Boc protected amino alcohol **II-15** (0.13 g, 0.415 mmol, 1 equiv), pyrrole **I-47** (85 mg, 0.415 mmol, 1 equiv) and Cs_2CO_3 (0.135 g, 0.415 mmol, 1 equiv) in dichloromethane (2 mL) under argon, the resulting solution turned a golden yellow. The reaction vessel was equipped with a condenser and the mixture was heated to 40℃ for 13 h. The reaction was monitored by NMR. The reaction mixture was filtered through a celite cake and concentrated. The crude product was subjected to column chromatography 10% ether in hexanes to afford the pure product *syn*-**II-10** as a yellow oil (0.128 g, 77% yield). NMR indicated product as a mixture of rotomeric isomers at room temperature.

^{1}H NMR (500 MHz, DMSO-d_6, 80℃) δ 6.93 (d, J = 4.1 Hz, 1H), 6.36 – 6.26 (m, 2H), 6.09 (dd, J = 5.8, 2.1 Hz, 1H), 5.90 (ddd, J = 5.8, 2.8, 1.9 Hz, 1H), 5.17 (m, 1H), 3.78 (s, 3H), 2.83 (s, 3H), 2.70 (m, 1H), 2.03 (m, 1H), 1.45 (s, 9H).

^{1}H NMR (500 MHz, Chloroform-d, 23℃) δ 6.94 (d, J = 4.1 Hz, 1H), 6.50 (br s, 1H), 6.20 (d, J = 4.1 Hz, 1H), 6.04 (dd, J = 5.1, 2.2 Hz, 1H), 5.81 (br s, 1H), 5.41-5.10 (br s, 1H), 3.80 (s, 3H), 2.86 (s, 3H), 2.78 (m, 1H), 2.07 (m, 1H), 1.47 (s, 9H).

^{13}C NMR (126 MHz, DMSO-d_6, 80℃) δ 160.55, 155.32, 133.87, 132.36, 124.77, 119.33, 113.80, 109.11, 79.38, 61.54, 59.97, 51.64, 36.85, 29.76, 28.67.

HRMS: calculated for $C_{12}H_{12}BrN_2O_2$ $[M+H\text{-}Boc]^+$ 299.0395, found 299.0403

IR: 2983-2868 cm^{-1}, 1705 cm^{-1}, 1686 cm^{-1}, 1126 cm^{-1}, 744 cm^{-1}

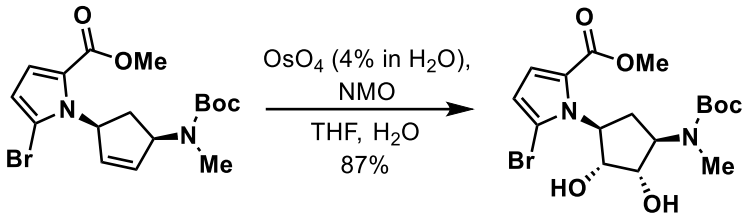

***syn*-II-10** **II-17**

To a stirring solution of the *cis* methyl ester ***syn*-II-10** (9 mg, 23 µmol, 1 equiv) and NMO (5.3 mg, 45 µmol, 2 equiv) in THF (1 mL) was added OsO_4 (26 µL, 4% in H_2O). The reaction vessel was stirred at room temperature for 5 days. After the 5 days, saturated $Na_2S_2O_3$ (5 mL) was added. The biphasic mixture was poured into a separatory funnel and the residual organics were extracted from the aqueous layer with ethyl acetate (3 x 5 mL). The combined organics were washed with brine (10 mL), dried over Na_2SO_4, decanted and concentrated. The crude product was subjected to column chromatography 50% ethyl acetate in hexanes to yield pure product **II-17** as a yellow oil (7.9 mg, 87% yield). NMR indicated product as a mixture of rotomeric isomers at room temperature.

^{1}H NMR (500 MHz, DMSO-d_6, 80℃) δ 7.01 (d, J = 4.2, 1H), 6.34 (d, J = 4.3, 1H), 5.17 (br s, 1H), 4.67 (d, J = 4.0 Hz, 1H), 4.42 (d, J = 5.3 Hz, 1H) 4.43 – 4.23 (m, 4H), 3.78 (s, 3H), 2.85 (s, 3H), 2.26 (dd, J = 11.6, 1.8 Hz, 1H), 1.89 (m, 1H), 1.45 (s, 9H).

^{1}H NMR (500 MHz, Chloroform-d, 23℃) δ 7.04 (d, J = 4.2 Hz, 1H), 6.24 (d, J = 4.2 Hz, 1H), 5.22 (br s, 1H), 4.57-4.44 (m, 3H), 3.95 (br s, 1H), 3.79 (s, 3H), 2.91 (s, 3H), 2.51 (m, 1H), 2.04 (m, 1H), 1.48 (s, 9H).

^{13}C NMR (126 MHz, DMSO-d_6, 80℃) δ 165.41, 160.50, 128.84, 125.09, 117.53, 116.46, 83.87, 77.47, 74.90, 68.76, 65.11, 56.50, 33.92, 33.74, 33.45.

HRMS: calculated for $C_{12}H_{18}BrN_2O_4$ $[M+H\text{-}Boc]^+$ 333.0449, found 333.0525

IR: 3426 cm^{-1}, 2947-2814 cm^{-1}, 1707 cm^{-1}, 1668 cm^{-1}, 1028 cm^{-1}, 1004 cm^{-1}, 752 cm^{-1}

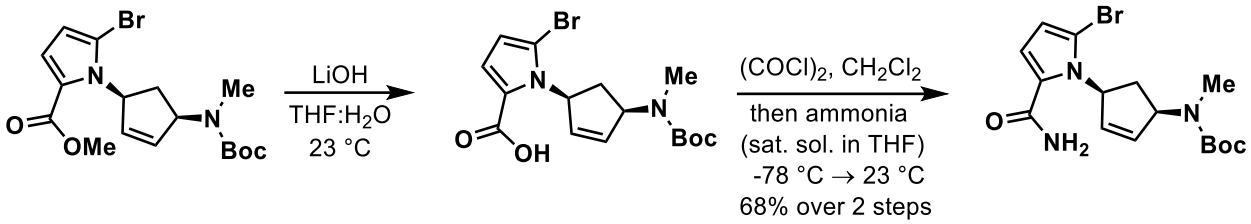

***syn*-II-10** ***syn*-II-38** ***syn*-II-11**

To a solution of the ester *syn*-**II-10** (68 mg, 0.17 mmol, 1 equiv) in THF (3 mL) and water (6 mL) was added LiOH (0.24 g, 5.11 mmol, 30 equiv). After the clear solution was stirring for 12 h, it was acidified to pH = 2 using 1M HCl and diluted with ethyl acetate (4 mL). The biphasic mixture was poured into a separatory funnel, partitioned, and the residual organics were extracted from the aqueous layer using ethyl acetate (3 x 10 mL). The combined organics were washed with brine (10 mL), dried over Na_2SO_4, decanted and concentrated. The crude product was purified by silica gel chromatography; 30% ethyl acetate in hexanes to afford the acid *syn*-**II-11** as a white solid (48.5 mg, 71% yield). NMR indicated product as a mixture of rotomeric isomers at room temperature.

^{1}H NMR (500 MHz, DMSO-d_6, 80℃) δ 6.90 (d, J = 4.1 Hz, 1H), 6.44 (m, 1H), 6.28 (d, J = 4.2 Hz, 1H), 6.09 (m, 1H), 5.88 (m,1H), 5.15 (m, 1H), 2.82 (s, 3H), 2.67 (dd, J = 11.9, 7.6 Hz, 1H), 2.04 (dd, J = 11.9, 9.2 Hz, 1H), 1.45 (s, 9H).

^{1}H NMR (500 MHz, Chloroform-d, 23℃) δ 7.08 (br s, 1H), 6.47 (br s, 1H), 6.25 (br s, 1H), 6.05 (br s, 1H), 5.82 (br s, 1H), 2.86 (br s, 4H), 2.07 (br s, 1H), 1.48 (s, 9H).

^{13}C NMR (126 MHz, DMSO-d_6, 80℃) δ 161.57, 155.30, 134.21, 132.09, 125.75, 119.06, 113.33, 108.28, 79.35, 61.17, 59.92, 36.83, 29.77, 28.66.

HRMS: calculated for $C_{11}H_{14}BrN_2O_2$ $[M+H\text{-}Boc]^+$ 285.0238, found 285.0238

IR: 3176 cm^{-1}, 2983-2897 cm^{-1}, 1698 cm^{-1}, 1661 cm^{-1}, 1519 cm^{-1}, 1105 cm^{-1}, 744 cm^{-1}

M.P.:191.5-196.7℃

The acid (0.119 g, 0.31 mmol, 1 equiv) in dichloromethane (6 mL) was placed in an ice bath cooled to 0℃ and stirred for 20 min. Oxalyl chloride (53 µL, 0.62 mmol, 2 equiv) was added dropwise, followed by thee drops of dry DMF under an argon atmosphere. The ice bath was removed, and the solution was allowed to warm to room temperature. The reaction was monitored by NMR for full conversion to the acid chloride, approximately 1 hour, and the solution was concentrated under nitrogen. Fresh anhydrous ammonia was condensed at -78℃ in THF (2 mL) in a separate round bottom flask, and the newly prepared acid chloride in THF (1 mL) was added dropwise; the transfer was quantitated with dry THF (1 mL). The reaction vessel was stirred for 2 h at -78℃ and warmed to room temperature. Afterwards, the solution was diluted with ethyl acetate (4 mL) and water (5 mL), the biphasic mixture was transferred to a separatory funnel and washed with water (3 x 5 mL). The combined organics were washed with brine (5 mL), dried over solid Na_2SO_4, decanted, and concentrated under nitrogen. The resulting crude product was subjected to silica gel chromatography; 30% → 50% ethyl acetate in hexanes to afford the amide **II-11** as a light brown oil (70 mg, 59% yield). NMR indicated product as a mixture of rotomeric isomers at room temperature.

^{1}H NMR (500 MHz, DMSO-d_6, 80℃) δ 7.10 (br s, 2H), 6.80 (br s, 1H), 6.45 (br s, 1H), 6.21 (br s, 1H), 6.05 (br s, 1H), 5.84 (br s, 1H), 5.12 (br s, 1H), 2.82 (s, 3H), 2.64 (m, 1H), 2.05 (m, 1H), 1.44 (s, 9H).

^{1}H NMR (500 MHz, Chloroform-*d*, 23℃) δ 6.59 (d, *J* = 4.0 Hz, 1H), 6.48-6.27 (br s, 1H), 6.19 (d, *J* = 4.0 Hz, 1H), 6.03 (m, 1H), 5.80 (br s, 1H), 5.64 – 5.42 (br s, 1H), 2.87 (s, 3H), 2.80 (br s, 1H), 2.12 (dd, *J* = 11.9, 9.3 Hz, 1H), 1.47(s, 9H).

^{13}C NMR (126 MHz, DMSO-d_6, 80℃) δ 163.08, 155.30, 134.46, 131.83, 129.02, 114.61, 112.52, 105.77, 79.30, 60.89, 59.93, 37.05, 29.75, 28.67.

HRMS: calculated for $C_{11}H_{14}BrN_3O$ $[M+H\text{-}Boc]^+$ 283.0320, found 283.0322

IR: 3336 cm^{-1}, 3184 cm^{-1} 2968-2810 cm^{-1}, 1660 cm^{-1}, 1603 cm^{-1}, 1437 cm^{-1}, 742 cm^{-1}

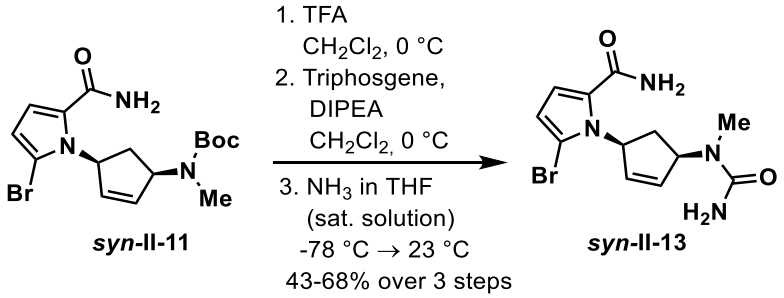

The amide *syn*-**II-11** (70 mg, 0.183 mmol, 1 equiv) was dissolved in dry dichloromethane (10 mL) and cooled to 0℃ under argon. TFA (3 mL) was added dropwise, and the reaction was warmed to room temperature. The reaction was monitored by NMR for full deprotection, approximately 1 hour, and the solution was concentrated under nitrogen. The deprotected product was dissolved in dichloromethane (4 mL) and added dropwise to a cooled solution (0℃) of triphosgene (27 mg, 0.09 mmol, 0.5 equiv) in dichloromethane (5 mL). The transfer of the deprotected amine was quantitated with dichloromethane (1 mL). Diisopropylethylamine (70 µL, 0.4 mmol, 2.2 equiv) was added directly afterwards, and the reaction flask was stirred at 0℃ for 1 h. Reaction was monitored via NMR and concentrated under nitrogen upon completion. Fresh anhydrous ammonia was condensed at -78℃ in THF (2 mL) in a separate round bottom flask. The acylated product was taken up in THF (4 mL) and added dropwise to the anhydrous ammonia. The reaction flask was stirred at -78℃ for 2 h, and then slowly warmed to room temperature under an argon atmosphere. The reaction was stirred at room temperature for 12 h. Concentrated under nitrogen flow and subjected to silica gel chromatography, 3% MeOH in $CHCl_3$ + 1% NH_4OH → 5% MeOH in $CHCl_3$ + 1% NH_4OH → 9% MeOH in $CHCl_3$ + 1% NH_4OH to provide the pure product as an amorphous pale-yellow foam (36 mg, 61% yield over three steps). NMR indicates product with minor impurities.

^{1}H NMR (500 MHz, Methanol-*d*, 23℃) δ 6.76 (d, *J* = 4.0 Hz, 1H), 6.38 (ddd, *J* = 12.5, 9.9, 2.7 Hz, 1H), 6.20 (d, *J* = 4.1 Hz, 1H), 6.08 (dd, *J* = 5.6, 2.2 Hz, 1H), 5.82 (dd, *J* = 5.8, 2.8, 1H), 5.28 (br s, 1H), 2.93 (s, 3H), 2.76 (dd, *J* = 12.0, 7.5 Hz, 1H), 2.11 (dd , *J* = 12.0, 9.4 Hz, 1H).

^{13}C NMR (126 MHz, Methanol-*d*, 23℃) δ 164.46, 160.45, 134.19, 131.37, 127.75, 114.51, 112.23, 106.49, 61.00, 36.29, 29.05.

HRMS: calculated for $C_{12}H_{16}BrN_4O_2$ $[M+H]^+$ 327.0456, found 327.0461

IR: 3391 cm^{-1}, 3191 cm^{-1}, 1671 cm^{-1}, 1636 cm^{-1}, 1581 cm^{-1}

2.10.3. Experimental Procedure for Route 2 Synthesis

Prepared following literature precedent. [20]

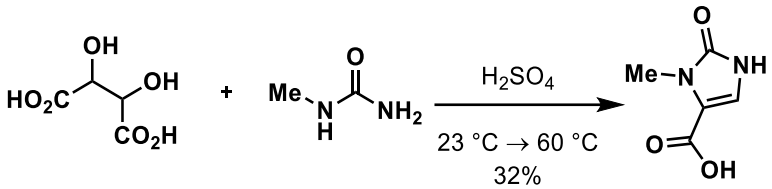

II-21

Tartaric acid (10 g, 66.7 mmol, 1 equiv) and *N*-methylurea (5.43 g, 73 mmol, 1.1 equiv) were added in 6 portions over the course of 1 h to a stirring solution of sulfuric acid (45 mL). After the last portion was added, the solution was heated to 80℃ and stirred for 3 h, and the solution turned a brown/yellow color. After 3 h, the reaction was poured into a 500 mL beaker with ice. The solution was left until the ice had completely melted (approx. 30 min), and then filtered over a frit funnel. The solid was transferred from the frit funnel using the methanol to a round bottom flask and concentrated under vacuum to afford **II-21** as a cream powder (3 g, 32 %). The crude product was used directly in the next reaction with no further purification.

^{1}H NMR (500 MHz, DMSO-d_6, 23℃) δ 10.82 (s, 1H), 7.26 (d, J = 2.6 Hz, 1H), 3.27 (*s*, 3H).

^{13}C NMR (126 MHz, DMSO-d_6, 23℃) δ 161.29, 154.11, 118.81, 115.36, 28.83.

HRMS: calculated for $C_5H_7N_2O_3$ $[M+H]^+$ 143.0456, found 143.0462

IR: 3153 cm^{-1}, 3096 cm^{-1}, 1678 cm^{-1}, 1636 cm^{-1}, 1572 cm^{-1}

M.P.: 222.2 - 230.1℃

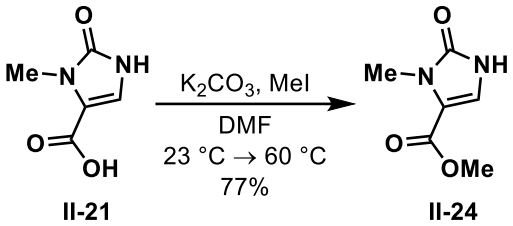

II-21 **II-24**

Under an argon atmosphere, to 50 mL dry round bottom flask was added potassium carbonate (0.138 g, 1 mmol, 1 equiv), carboxylic acid **II-21** (0.15 g, 1 mmol, 1 equiv) and dry DMF (10 mL). The reaction was stirred at room temperature for 10 min. Methyl iodide (65 µL, 1 mmol, 1 equiv) was added dropwise to the reaction and allowed to stir for 2 h at room temperature. After 2 h, it was heated to 60℃ and stirred for 1 h. Upon completion, the reaction was concentrated under nitrogen, taken up in ethyl acetate and filtered over celite, and then transferred to a round bottom flask and concentrated under vacuum. The brown crude mixture was taken to the next step without further purification and yielded the product as a pale-yellow solid (0.127 g, 77%).

^{1}H NMR (500 MHz, Chloroform-*d*, 23℃) δ 11.63 (br s, 1H), 7.12 (d, *J* = 2.4 Hz, 1H), 3.81 (s, 3H), 3.52 (s, 3H).

^{13}C NMR (126 MHz, Chloroform-*d*, 23℃) δ 160.11, 155.21, 118.22, 115.48, 51.50, 29.05.

HRMS: calculated for $C_6H_9N_2O_3$ $[M+H]^+$ 157.0613, found 157.0675

IR: 3517 cm^{-1}, 3138 cm^{-1}, 1700 cm^{-1}, 1658 cm^{-1}, 1581 cm^{-1}

M.P.: 192.3-193.1℃

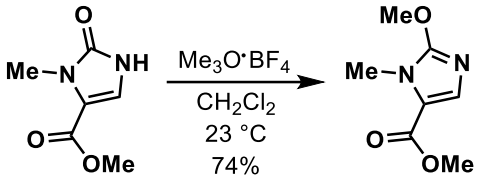

II-24 **II-25**

To a stirring solution of methyl ester **II-24** (0.328 g, 2.1 mmol, 1 equiv) in dry dichloromethane (21 mL) under an argon atmosphere and at room temperature was added trimethyloxonium tetrafluoroborate (1.24 g, 8.4 mmol, 4 equiv). The reaction was stirred at room temperature for 24 h and turned a light pink. Monitoring the reaction was done by performing a mini workup on the aliquot, and analysis *via* NMR. Once the reaction was complete, dichloromethane was added (20 mL), followed by sodium bicarbonate till a pH = 7 is achieved. The biphasic mixture was poured into a separatory funnel and partitioned. The residual organics were extracted from the aqueous layer with dichloromethane (3 x 50 mL). The combined organics were dried over solid Na_2SO_4, decanted, and concentrated under vacuum. The crude product was taken directly to the next reaction without further purification and provided **II-25** as a white solid (0.264 g, 74% yield).

^{1}H NMR (500 MHz, Chloroform-*d*, 23℃) δ 7.43 (s, 1H), 4.10 (s, 3H), 3.83 (s, 3H), 3.66 (s, 3H).

^{13}C NMR (126 MHz, Chloroform-*d*, 23℃) δ 160.89, 156.07, 133.32, 119.17, 56.98, 51.10, 30.06.

HRMS: calculated for $C_7H_{10}N_2O_3$ $[M+H]^+$ 171.0769, found 171.0872

IR: 2915 cm^{-1}, 2851 cm^{-1}, 1698 cm^{-1}, 1675 cm^{-1}, 1583 cm^{-1}

M.P.: 62.3-63.1℃

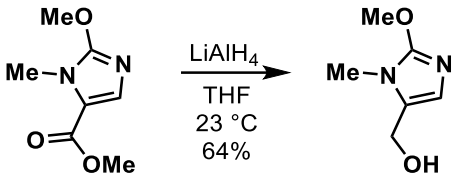

II-25 **II-26**

Under an argon atmosphere, with dry THF (30 mL) and methyl ether **II-25** (0.5 g, 2.98 mmol, 1 equiv) at 0℃ was added powder lithium aluminum hydride (0.23 g, 5,96 mmol, 2 equiv) slowly in portions over the course of ten min. The reaction was then warmed to room temperature and stirred for 4 h. TLC was used to monitor the reaction, and upon completion the gray solution was placed in an ice bath, diluted with ethyl ether (20 mL), and excess lithium aluminum hydride was quenched by the sequential dropwise addition of water (2 mL), aqueous NaOH (15%, 2 mL), and water (4 mL) at 0℃. After stirring for 5 min, solid Na_2SO_4 was added, and the mixture was allowed to stir for an additional 15 min. The cold bath was removed and the heterogenous mixture was suction filtered over a pad of Na_2SO_4 and concentrated to reveal the alcohol **II-26** as cream colored solid (0.27 g, 64% yield). The crude product was used directly in the next reaction with no further purification.

^{1}H NMR (500 MHz, Chloroform-*d*, 23℃) δ 6.56 (s, 1H), 4.51 (s, 2H), 4.01 (s, 3H), 3.42 (s, 3H).

^{13}C NMR (126 MHz, Chloroform-*d*, 23℃) δ 154.21, 127.18, 121.89, 56.43, 55.04, 28.29.

HRMS: calculated for $C_6H_{11}N_2O_2$ $[M+H]^+$ 143.0820, found 143.0914

IR: 3215 cm^{-1}, 2930 cm^{-1}, 1583 cm^{-1}, 1554 cm^{-1}

M.P.: 224.7-226.2℃

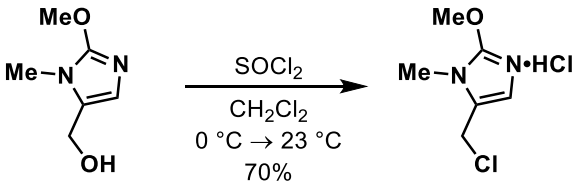

II-26 **II-27**

Alcohol **II-26** (0.242 g, 1.7 mmol, 1 equiv) in dry dichloromethane (25 mL) was cooled to 0℃ in an ice bath under an argon atmosphere. Thionyl chloride (0.2 mL, 2.6 mmol, 1.5 equiv) was added dropwise to the solution, and the resulting reaction turned a bright pink upon initial addition. The ice bath was removed, and the reaction was allowed to warm to room temperature and turned a pale yellow/brown color. Monitored *via* NMR, after 1 h the reaction was complete, and concentrated under a flow of nitrogen. Diethyl ether was added to the flask (3 x 5 mL) and pipetted out to remove byproducts, and leaving the product behind, which is only soluble in dichloromethane and chloroform. The crude product was isolated as a dark purple/black solid (0.231 g, 70%) and used without further purification. Upon exposure to base or sonication the product decomposes.

^{1}H NMR (500 MHz, Chloroform-*d*, 23℃) δ 7.08 (s, 1H) 4.59 (s, 2H), 4.53 (s, 3H), 3.59 (s, 3H).

^{13}C NMR (126 MHz, Chloroform-*d*, 23℃) δ 149.89, 124.75, 113.53, 62.97, 33.82, 29.63.

IR: 3096 cm^{-1}, 1709 cm^{-1}, 1629 cm^{-1}, 1603 cm^{-1}

M.P.: 90.8-93.3℃

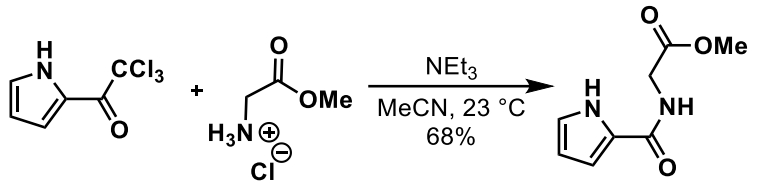

II-23

The pyrrole (2.12 g, 10 mmol, 1 equiv) and amino methyl ester (1.88 g, 15 mmol,1.5 equiv) was added to a flame dried 500 mL round bottom flask under an argon atmosphere. Dry acetonitrile (150 mL) was added, followed directly by dry triethylamine (2.8 mL, 20 mmol, 2 equiv). The reaction was stirred at room temperature for 24 h. Reaction was monitored via NMR. Upon completion, the solution was filter over a fritted funnel and then concentrated. The solid was dissolved in ethyl acetate (100 mL), washed with 1M HCl (3 x 50 mL). The organics were dried over Na_2SO_4, decanted, and concentrated. The crude product was subjected to silica gel chromatography 50% ethyl acetate in hexanes to afford the pure product as a white crystalline solid (1.32 g, 68% yield).

^{1}H NMR (500 MHz, Chloroform-*d,* 23℃) δ 9.63 (br s, 1H), 6.93 (dd, *J* = 2.7, 1.2 Hz, 1H), 6.65 (ddd, *J* = 3.8, 2.5, 1.3 Hz, 1H), 6.44 (br s, 1H), 6.24 (dd, *J* = 3.8, 2.6 Hz, 1H), 4.21 (d, *J* = 5.3 Hz, 2H), 3.79 (s, 3H).

^{13}C NMR (126 MHz, Chloroform-*d,* 23℃) δ 170.60, 161.09, 125.17, 121.94, 109.97, 109.72, 52.47, 41.12.

HRMS: calculated for $C_8H_{11}N_2O_3$ $[M+H]^+$ 183.0769, found 183.0114

IR: 3384 cm^{-1}, 3217 cm^{-1}, 1733 cm^{-1}, 1633 cm^{-1}, 1556 cm^{-1}, 1517 cm^{-1}

M.P.: 142.9-146.4℃

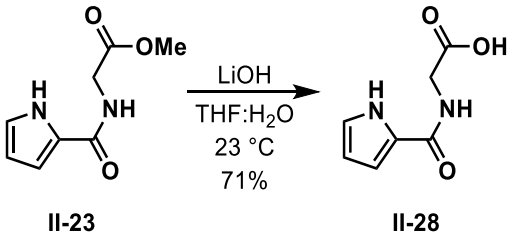

II-23 **II-28**

The methyl ester **II-23** (2.48 g, 13.6 mmol, 1 equiv) was dissolved in THF (68 mL) at room temperature, and to the stirring solution was added water (270 mL) and lithium hydroxide (11.4 g, 272 mmol, 20 equiv). The reaction turned a pink color upon initial addition of lithium hydroxide. The solution was stirred overnight, and TLC confirmed conversion of starting material. 1M HCl was added to pH = 2, and the biphasic mixture was poured into a separatory funnel and partitioned. The residual organics were extracted from the aqueous layer with ethyl acetate (3 x 150 mL). The combined organics were dried over solid Na_2SO_4, decanted, and concentrated under vacuum. The crude product was subjected to silica gel chromatography, 100% ethyl acetate + 1% AcOH, to provide pure **II-28** as a white powder solid (1.64 g, 71% yield).

^{1}H NMR (500 MHz, DMSO-*d*$_6$, 23℃) δ 12.54 (br. s, 1H), 11.46 (s, 1H), 8.31 (dd, *J* = 6.1, 3.5 Hz, 1H), 6.85 (m, 1H), 6.77 (m, 1H), 6.07 (m, 1H), 3.85 (d, *J* = 6.0 Hz, 2H).

^{13}C NMR (126 MHz, DMSO-*d*$_6$, 23℃) δ 172.18, 161.34, 126.30, 122.00, 110.72, 109.08, 40.98.

HRMS: calculated for $C_7H_9N_2O_3$ $[M+H]^+$ 169.0613, found 169.0670

IR: 3383 cm^{-1}, 3239 cm^{-1}, 1735 cm^{-1}, 1702 cm^{-1}, 1638 cm^{-1}, 1596 cm^{-1}

M.P.: 154.3-156.2℃

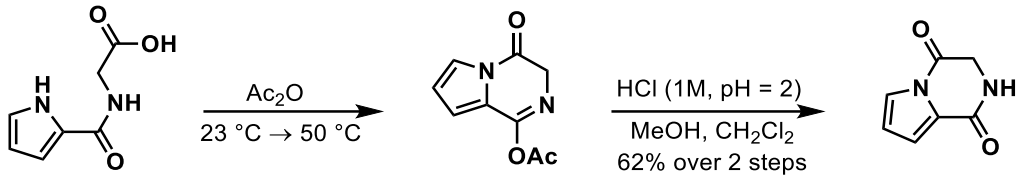

II-28 **II-29** **II-22**

Carboxylic acid **II-28** (0.6 g, 3.57 mmol, 1 equiv) in acetic anhydride (45 mL) was stirred for 30 min at room temperature, and then heated to 50℃ for 3 h. Upon heating, the reaction solution turned a bright golden yellow. Reaction was monitored *via* NMR, and after conversion to **II-29**, the solution was concentrated under nitrogen flow. The resultant product was dissolved in dichloromethane, transferred to a separatory funnel, and washed with sodium bicarbonate. The organic layer was dried over Na_2SO_4, decanted, and concentrated under vacuum. The crude product was taken directly to the next step without further purification.

Compound **II-29** was dissolved in methanol (56 mL) and dichloromethane (20 mL) at room temperature. To the stirring solution was added 1M HCl to a pH = 2, and the resulting solution was stirred for 24 h. Reaction was monitored *via* NMR, upon which the reaction was concentrated under a flow of nitrogen to provide a bright yellow/orange solid. The crude product was subjected to silica gel chromatography, 50% ethyl acetate in hexanes → 100% ethyl acetate, to provide pure **II-22** as a bright red powder solid (0.32 g, 62% yield).

^{1}H NMR (500 MHz, DMSO-d_6, 23℃) δ 8.19 (br s, 1H), 7.57 (dd, J = 3.2, 1.6 Hz, 1H), 6.93 (dd, J = 3.4, 1.5 Hz, 1H), 6.56 (dd, J = 3.3, 3.2 Hz, 1H), 4.38 (d, J = 2.1 Hz, 2H).

^{1}H NMR (500 MHz, Chloroform-d, 23℃) δ 7.56 (dd, J = 3.2, 1.5 Hz, 1H), 7.18 (dd, J = 3.6, 1.5 Hz, 1H), 6.56 (d, J = 3.3 Hz, 1H), 4.47 (d, J = 2.0 Hz, 2H).

^{13}C NMR (126 MHz, DMSO-d_6, 23℃) δ 163.29, 156.38, 126.83, 119.17, 117.05, 115.21, 46.89.

HRMS: calculated for $C_7H_7N_2O_2$ $[M+H]^+$ 151.0507, found 151.0508

IR: 3167 cm^{-1}, 1711 cm^{-1}, 1667 cm^{-1}, 1618 cm^{-1}, 1574 cm^{-1}

M.P.: 231.6-232.2℃

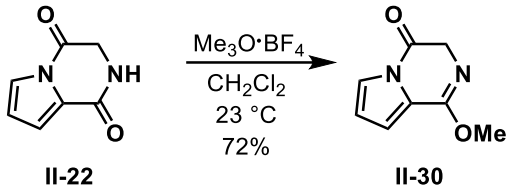

II-22 **II-30**

Compound **II-22** (100 mg, 0.67 mmol, 1 equiv) was dissolved in dry dichloromethane (10 mL) and added to a flame dried round bottom flask under an argon atmosphere. Trimethyloxonium tetrafluoroborate (99 mg, 0.67 mmol) was added in one portion at room temperature. The resulting solution was stirred at room temperature for 48 h. Monitoring the reaction is done by performing a mini workup on the aliquot, and then *via* NMR. Upon completion, the reaction was diluted with dichloromethane (10 mL), saturated sodium bicarbonate was added to a pH = 7 was achieved. The biphasic mixture was poured into a separatory funnel and partitioned. The residual organics were extracted from the aqueous layer with dichloromethane (3 x 20 mL). The combined organics were dried over solid Na_2SO_4, decanted, and concentrated under vacuum. The crude product was subjected to silica gel chomatography,10% ethyl acetate in hexanes to provide **II-30** as a red solid (78 mg, 72% yield).

^{1}H NMR (500 MHz, Chloroform-*d*, 23℃) δ 7.52 (dd, *J* = 3.2, 1.5 Hz, 1H), 6.67 (dd, *J* = 3.3, 1.5 Hz, 1H), 6.47 (dd, *J* = 3.3, 3.2 Hz, 1H), 4.58 (s, 2H), 3.87 (s, 3H).

^{13}C NMR (126 MHz, Chloroform-*d*, 23℃) δ 167.18, 153.47, 122.80, 117.79, 114.71, 112.75, 52.89, 52.78.

HRMS: calculated for $C_8H_9N_2O_2$ $[M+H]^+$ 165.0664, found 165.0964

IR: 3129 cm^{-1}, 1720 cm^{-1}, 1658 cm^{-1}, 1559 cm^{-1}

M.P.: 79.4-82.1℃

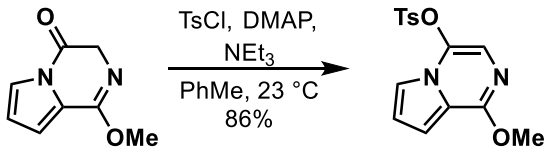

II-30 **II-31**

To a flame dried 50 mL round bottom flask was added methyl ether **II-30** (0.156 g, 0.952 mmol, 1 equiv), and DMAP (0.175 g, 1.43 mmol, 1.5 equiv), and freshly distilled toluene (6 mL). Triethylamine was added (0.2 mL, 1.43 mmol, 1.5 equiv), followed by tosyl chloride (0.273 g, 1.43 mmol, 1.5 equiv) at room temperature. Upon addition of tosyl chloride, the reaction turned a deep blood red. The reaction was stirred at room temperature for 1.5 h. Water (12 mL) was added and the biphasic solution was transferred to a separatory funnel and partitioned. The residual organics were extracted from the aqueous layer with ethyl acetate (3 x 10 mL). The combined organics were dried over solid Na_2SO_4, decanted, and concentrated under vacuum. The crude product was subjected to silica gel chomatography,10% ethyl acetate in hexanes → 30% ethyl acetate in hexanes to provide **II-31** as a blood red solid (0.26 g, 86% yield).

^{1}H NMR (500 MHz, Chloroform-*d*, 23℃) δ 7.85 (d, *J* = 8.5 Hz, 2H), 7.39 (dd, *J* = 2.7, 1.4 Hz, 1H), 7.38 (d, *J* = 7.8 Hz, 2H), 6.81 (dd, *J* = 4.0, 1.4 Hz, 1H), 6.71 (dd, *J* = 4.0, 2.7 Hz, 1H), 6.60 (s, 1H), 4.02 (s, 3H), 2.47 (s, 3H).

^{13}C NMR (126 MHz, Chloroform-*d*, 23℃) δ 155.01, 146.58, 132.47, 131.44, 130.20, 128.71, 121.83, 114.56, 113.87, 113.39, 104.09, 53.64, 21.83.

HRMS: calculated for $C_7H_7N_2O_2$ $[M+H]^+$ 151.0507, found 151.0508

IR: 3096 cm^{-1}, 1636 cm^{-1}, 1591 cm^{-1}, 1519 cm^{-1}

M.P.: 68.4-70.3℃

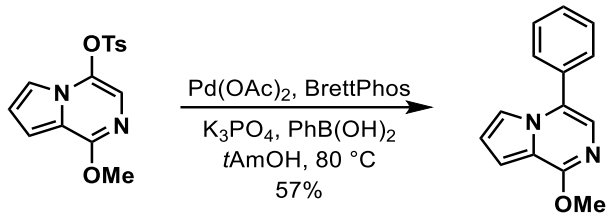

II-31 **II-32**

A flame dried flask equipped with a stir bar was charged with $Pd(OAc)_2$ (4.2 mg, 0.019 mmol, 2 mol%), BrettPhos (20 mg, 0.04 mmol, 4 mol %), K_3PO_4 (60 mg, 0.282 mmol, 3 equiv), $PhB(OH)_2$ (23 mg, 0.188 mmol, 2 equiv), and aryl tosylate **II-31** (30 mg, 0.094 mmol, 1 equiv). The flask was evacuated and back filled with argon three times. Freshly deoxygenated *t*AmOH was added to the flask, and the reaction was added to a preheated oil bath at 80℃ and stirred for 2 h. The reaction was monitored via NMR. Upon completion, the reaction was allowed to cool to room temperature, filtered over celite using dichloromethane as the solvent. Concentrated using rotary vacuum, and subjected to silica gel chromatography, 5% ethyl acetate in hexanes to provide the product as a yellow oil (12 mg, 57% yield).

^{1}H NMR (500 MHz, Chloroform-*d*, 23℃) δ 7.63 – 7.57 (m, 2H), 7.55 – 7.45 (m, 3H), 7.41 (dd, *J* = 2.6, 1.4 Hz, 1H), 7.04 (s, 1H), 6.88 (dd, *J* = 4.0, 1.4 Hz, 1H), 6.72 (dd, *J* = 4.1, 2.6 Hz, 1H), 4.10 (s, 3H).

^{13}C NMR (126 MHz, Chloroform-*d*, 23℃) δ 156.40, 132.68, 129.14, 129.05, 128.79, 126.69, 123.50, 120.56, 114.73, 113.05, 102.91, 53.25.

HRMS: calculated for $C_{14}H_{13}N_2O$ $[M+H]^+$ 225.1028, found 225.1122

IR: 3060 cm^{-1}, 1622 cm^{-1}, 1514 cm^{-1}, 1444 cm^{-1}

M.P.: 30.8-32.2℃

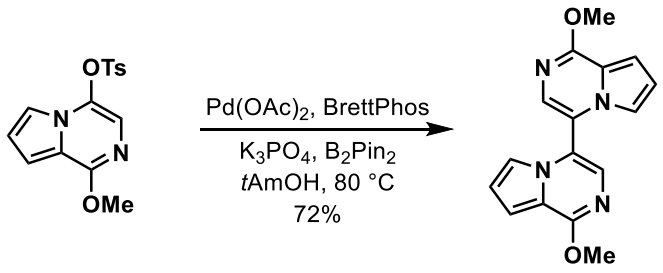

II-31 **II-33**

A flame dried flask equipped with a stir bar was charged with $Pd(OAc)_2$ (4.2 mg, 0.019mmol, 2 mol%), BrettPhos (20 mg, 0.04 mmol, 4 mol%), K_3PO_4 (60 mg, 0.282 mmol, 3 equiv), B_2Pin_2 (48 mg, 0.188 mmol, 2 equiv), and aryl tosylate **II-31** (30 mg, 0.094 mmol, 1 equiv). The flask was evacuated and back filled with argon three times. Freshly deoxygenated *t*AmOH was added to the flask, and the reaction was added to a preheated oil bath and stirred for 2 h. The reaction was monitored via NMR. Upon completion, the reaction was allowed to cool to room temperature, filtered over celite using dichloromethane as the solvent. Concentrated using rotary vacuum, and subjected to silica gel chromatography, 5% ethyl acetate in hexanes → 10% ethyl acetate in hexanes to provide the product as a sticky bright red oil (9.9 mg, 72% yield).

^{1}H NMR (500 MHz, Chloroform-*d*, 23℃) δ 7.36 (s, 1H), 6.95 (dd, *J* = 4.1, 1.4 Hz, 1H), 6.78 (dd, *J* = 2.6, 1.4 Hz, 1H), 6.70 (dd, *J* = 4.1, 2.6 Hz, 1H), 4.14 (s, 3H).

^{13}C NMR (126 MHz, Chloroform-*d*, 23℃) δ 157.78, 126.98, 119.77, 118.25, 115.61, 113.69, 103.76, 53.59.

HRMS: calculated for $C_{16}H_{15}N_4O_2$ $[M+H]^+$ 295.1195, found 295.1415

IR: 3091 cm^{-1}, 3003 cm^{-1}, 2915 cm^{-1}, 1508 cm^{-1}, 1446 cm^{-1}

2.10.4 Confirmation of *syn*-isomer via NOESY studies

NOE for *anti* and *syn* isomers; The protons next to the pyrrole and N-Boc for the *syn*-isomer shows correlation to same CH_2 proton. However, for the *anti*-isomer those protons show correlation to opposite CH_2 protons.

Figure 2.7. NOESY for *syn*-isomer **II-10**

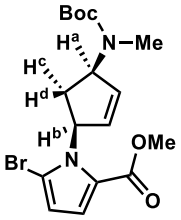

***syn*-II-10**

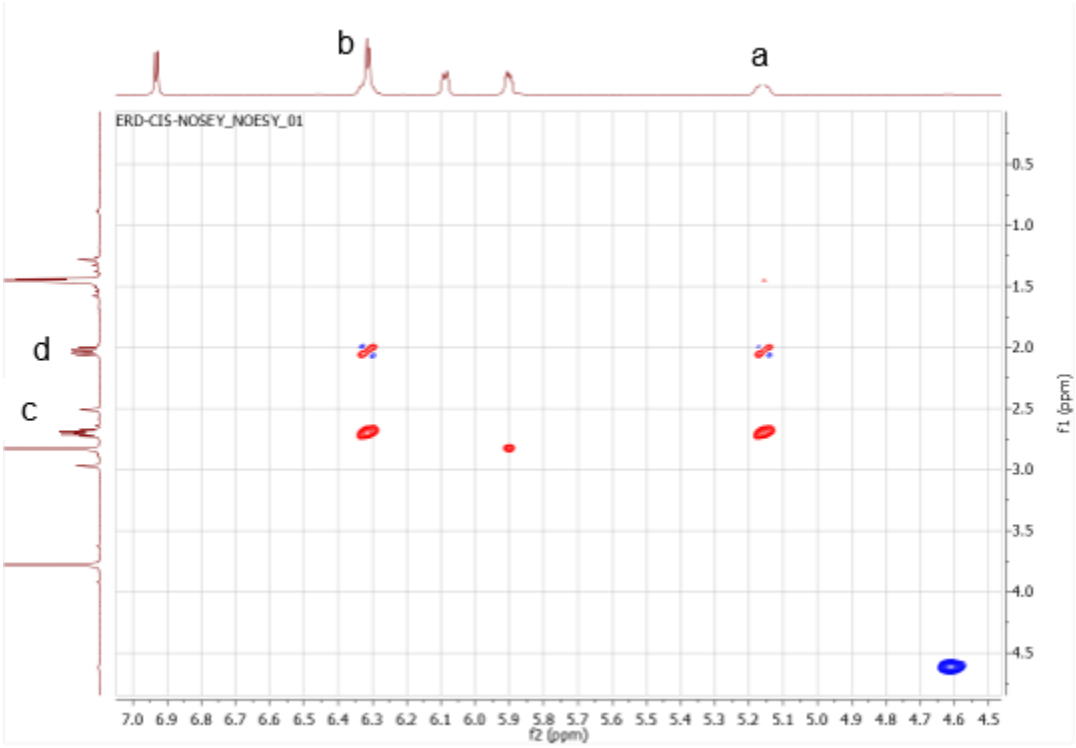

Figure 2.8. NOESY for *anti*-isomer **II-10**

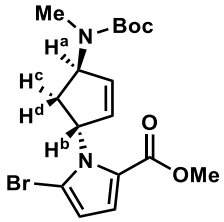

***anti*-II-10**

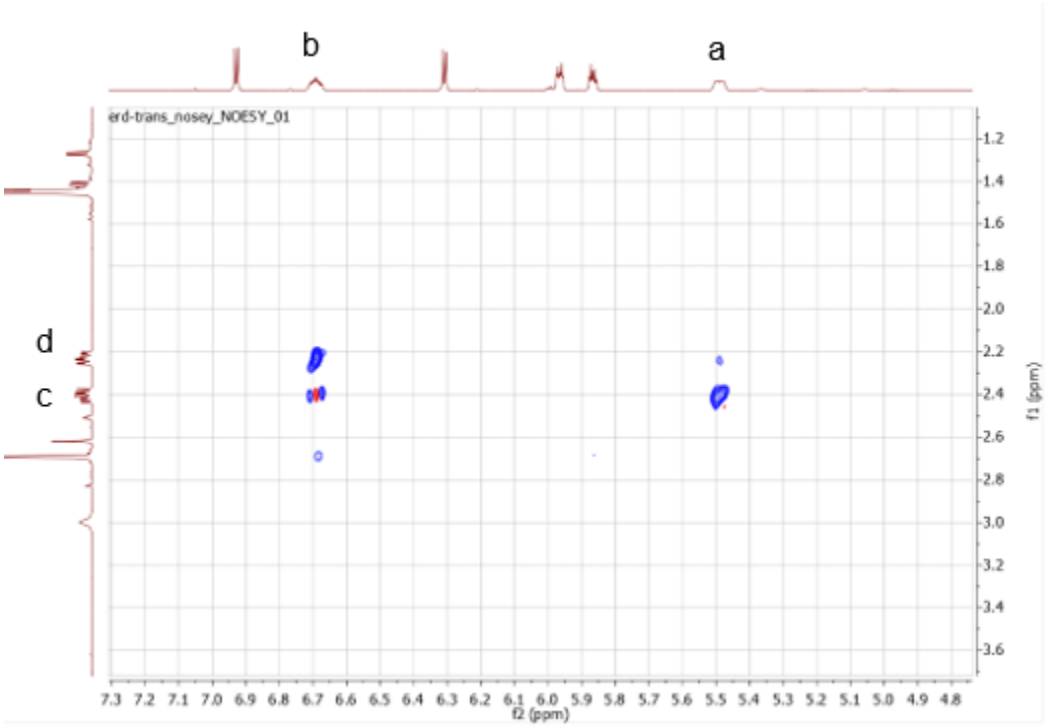

2.10.5. Catalog of Spectra

Figure 2.9. ^{1}H NMR of compound **II-7** (500 MHz, Chloroform-*d*, 23 ℃)

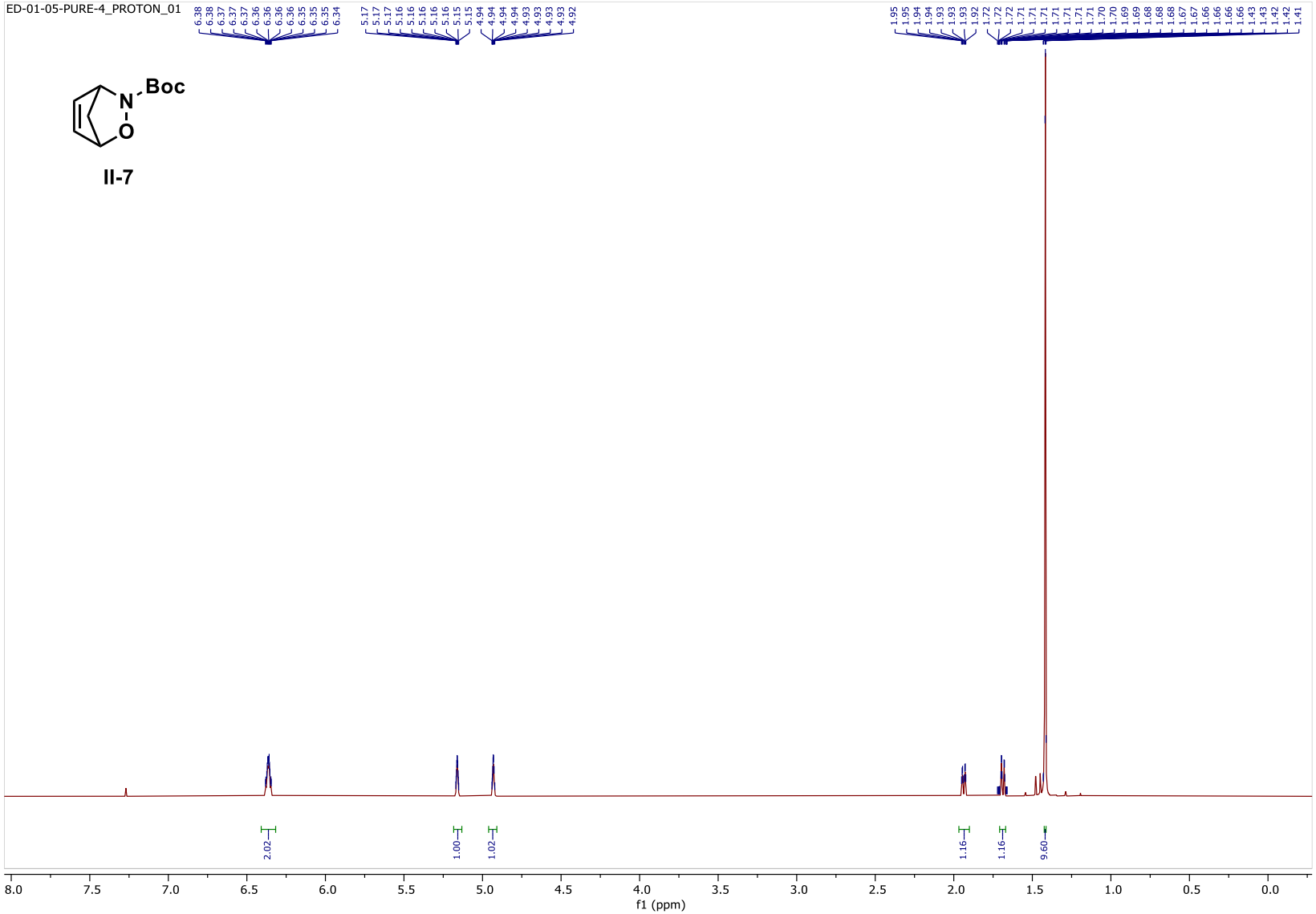

Figure 2.10. ^{13}C NMR of compound **II-7** (126 MHz, Chloroform-*d*, 23 ℃)

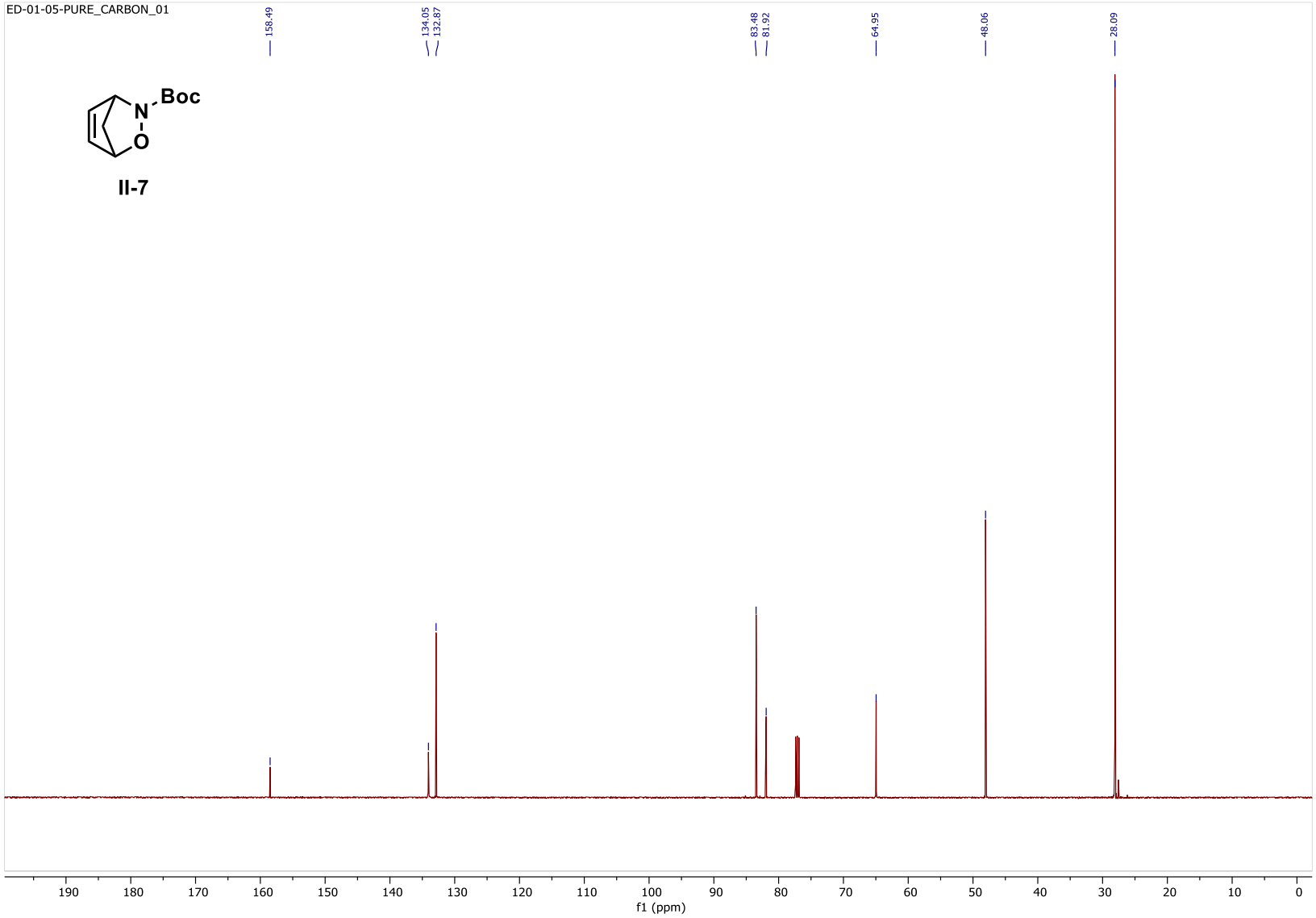

Figure 2.11. ^{1}H NMR of compound **II-6** (500 MHz, Chloroform-*d*, 23 ℃)

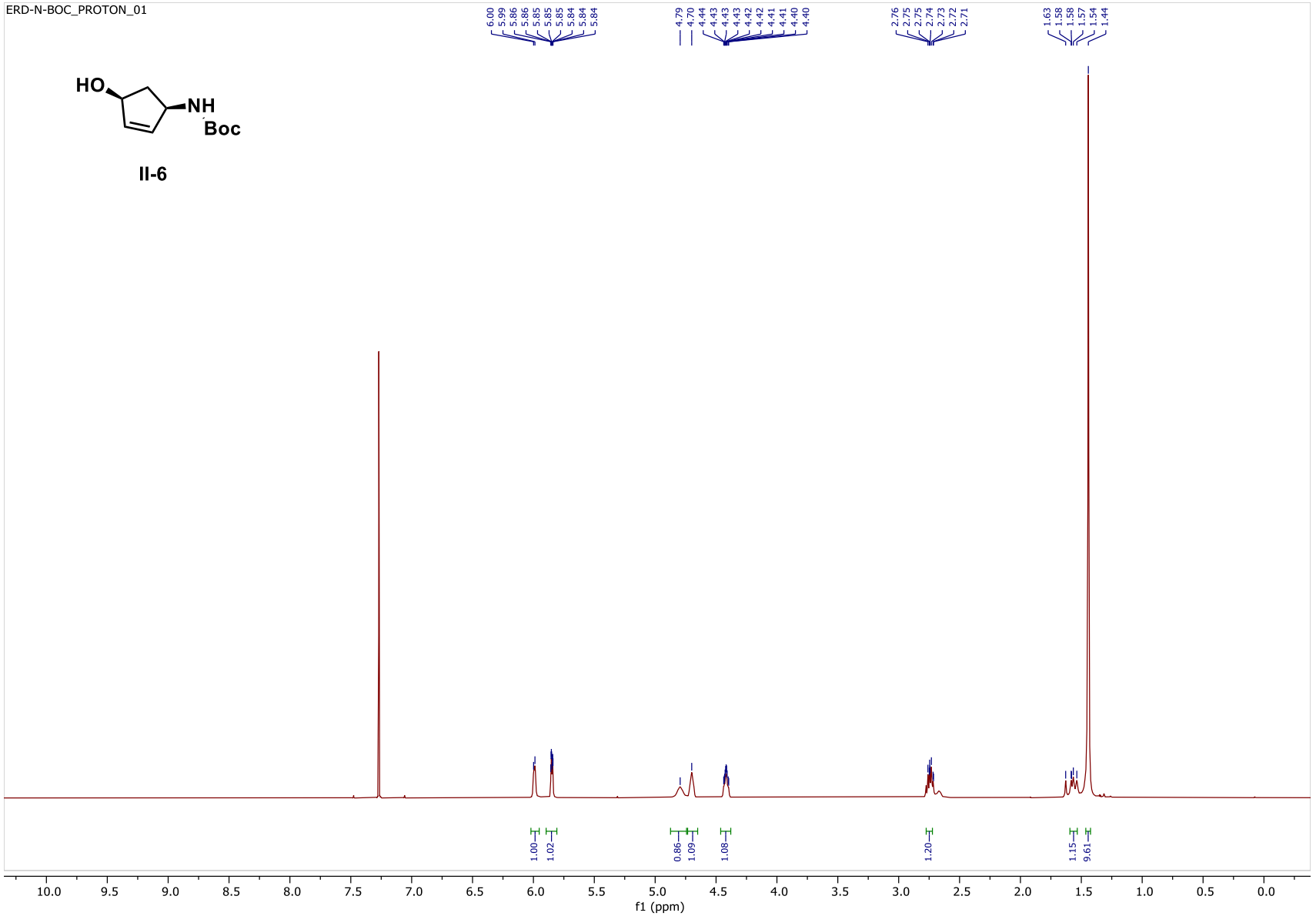

Figure 2.12. ^{13}C NMR of compound **II-6** (126 MHz, Chloroform-*d*, 23 ℃)

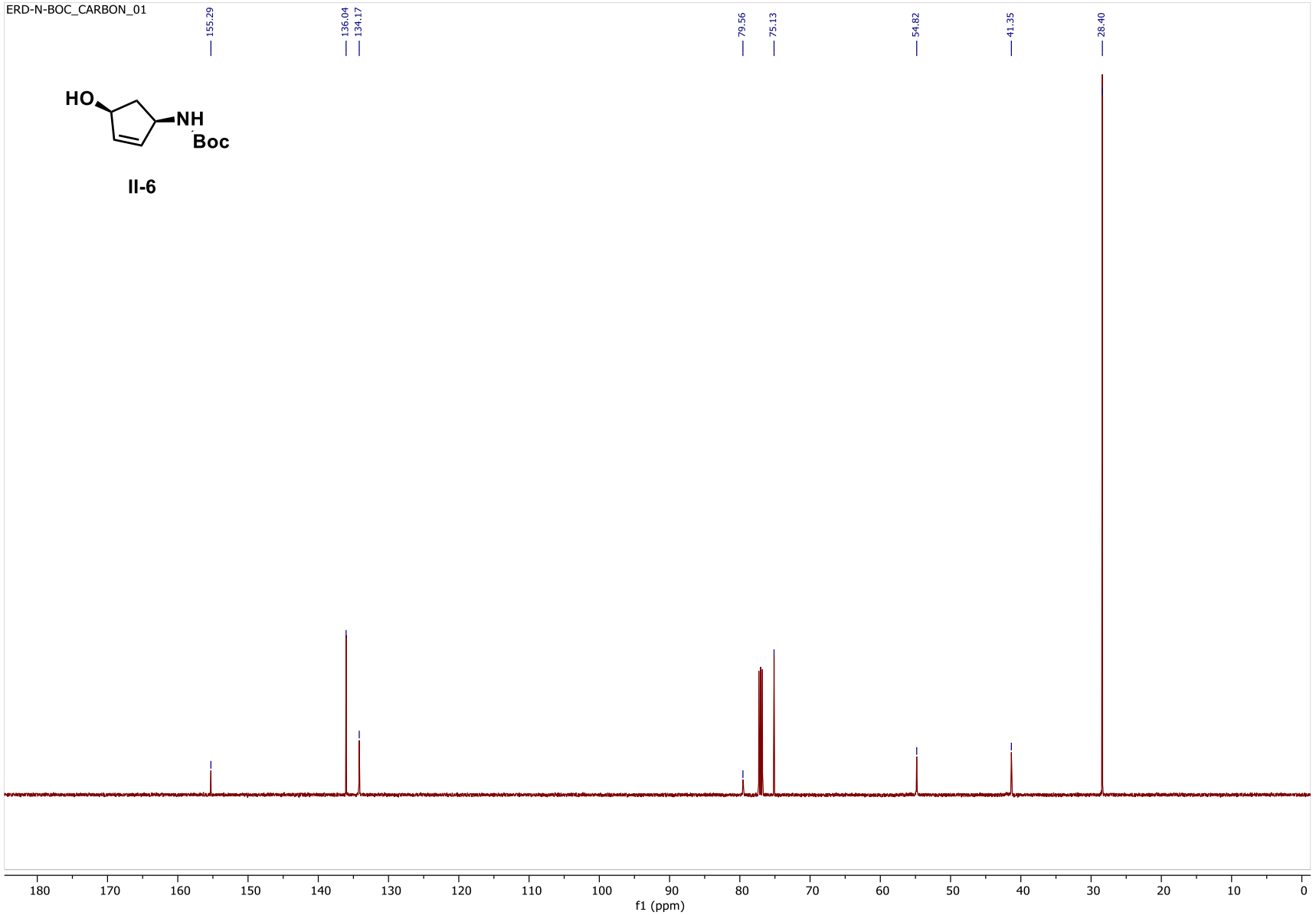

Figure 2.13. ^{1}H NMR of compound **II-8** (500 MHz, Chloroform-*d*, 23 ℃)

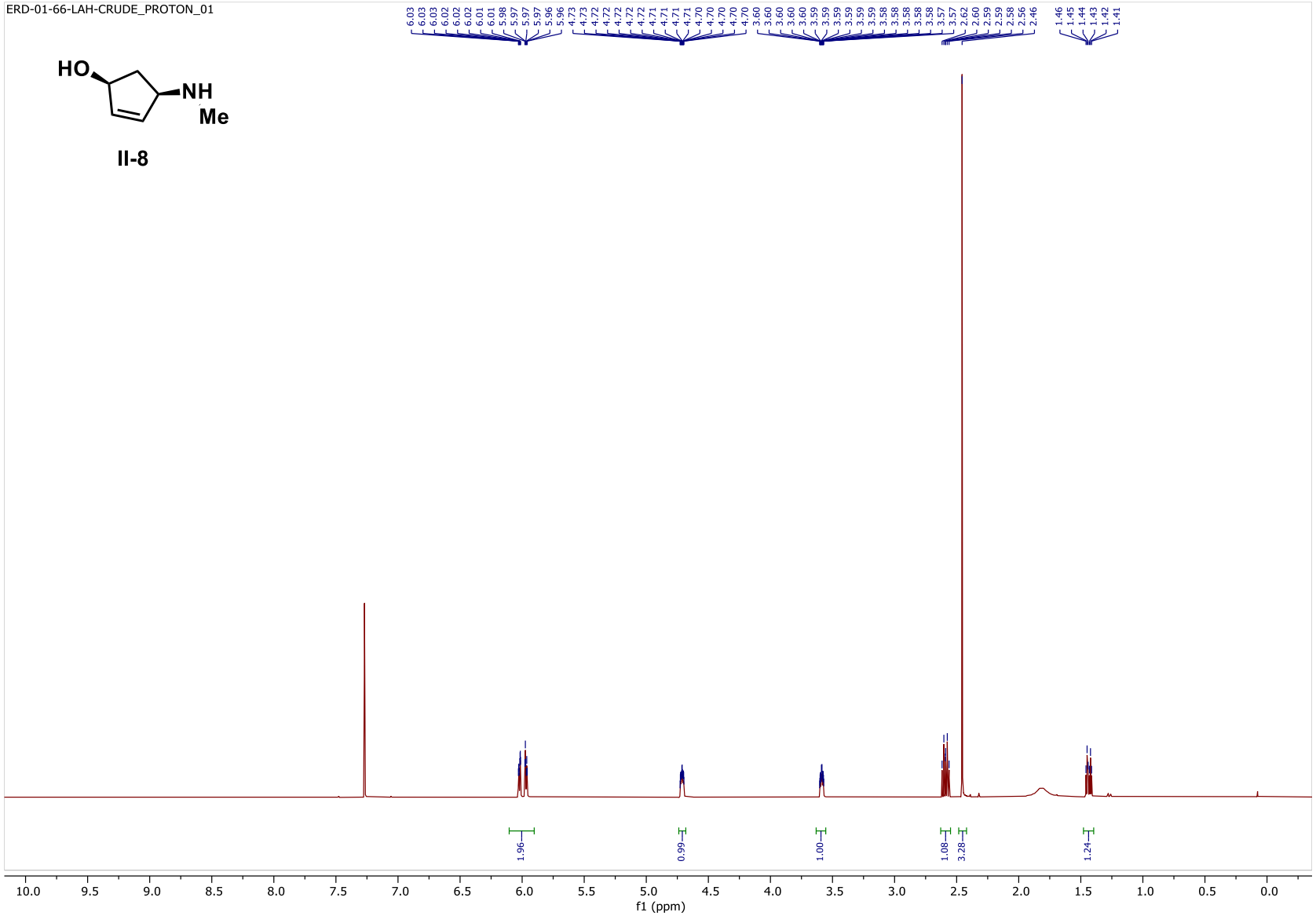

Figure 2.14. ^{13}C NMR of compound **II-8** (126 MHz, Chloroform-*d*, 23 ℃)

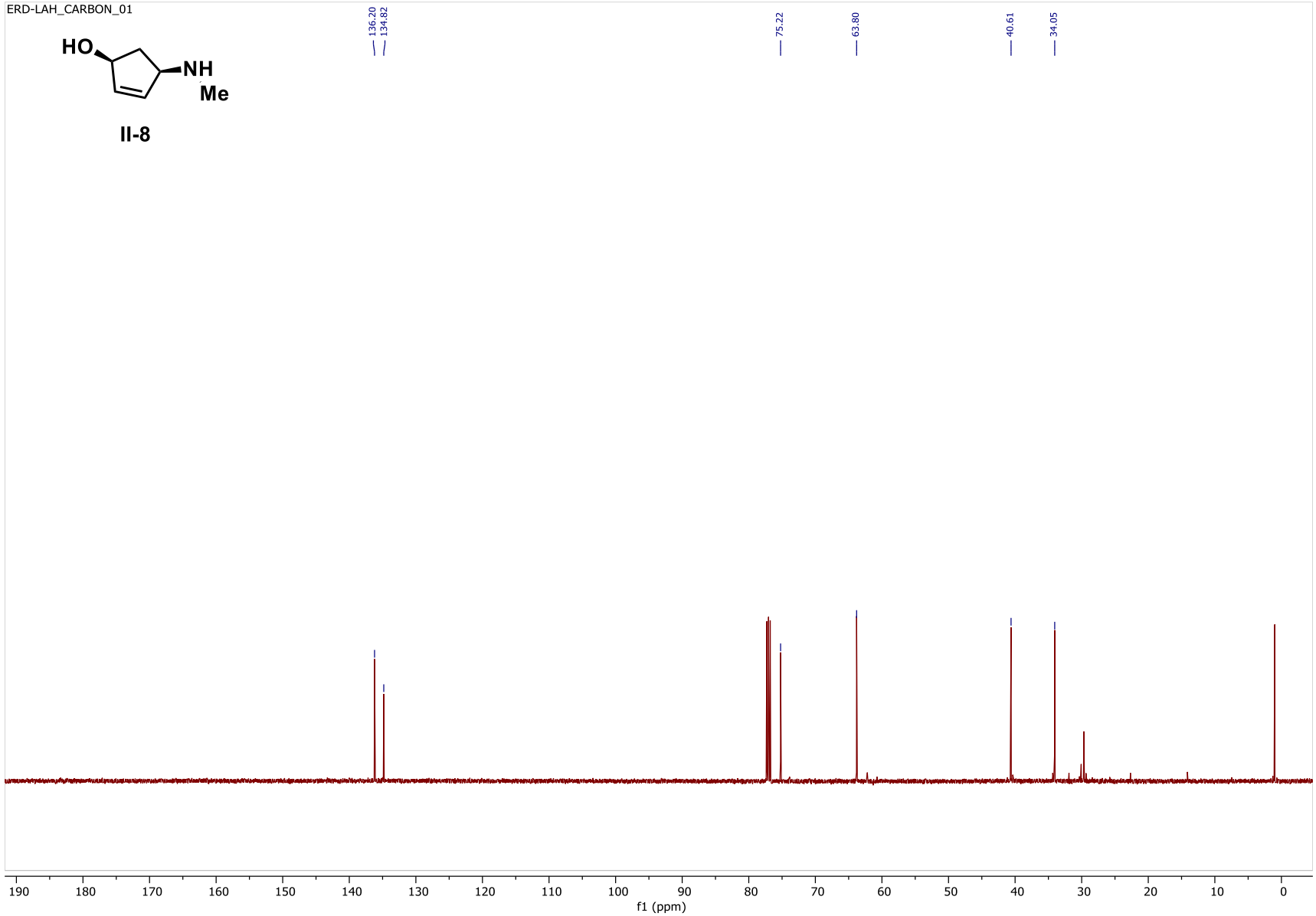

Figure 2.15. ^{1}H NMR of compound **II-9** (500 MHz, DMSO-d_6, 80 ℃)

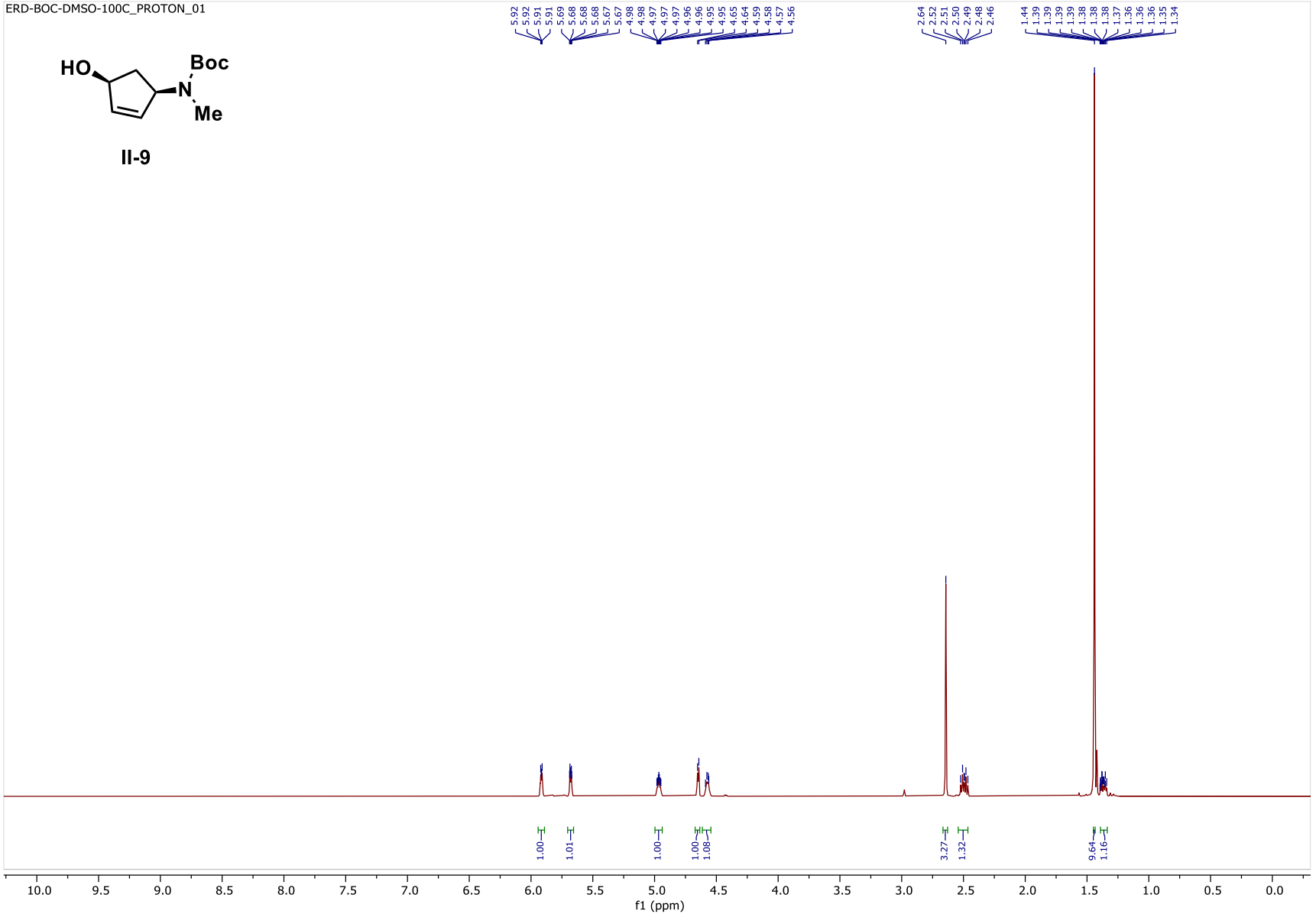

Figure 2.16. ^{13}C NMR of compound **II-9** (126 MHz, DMSO-d_6, 80 ℃)

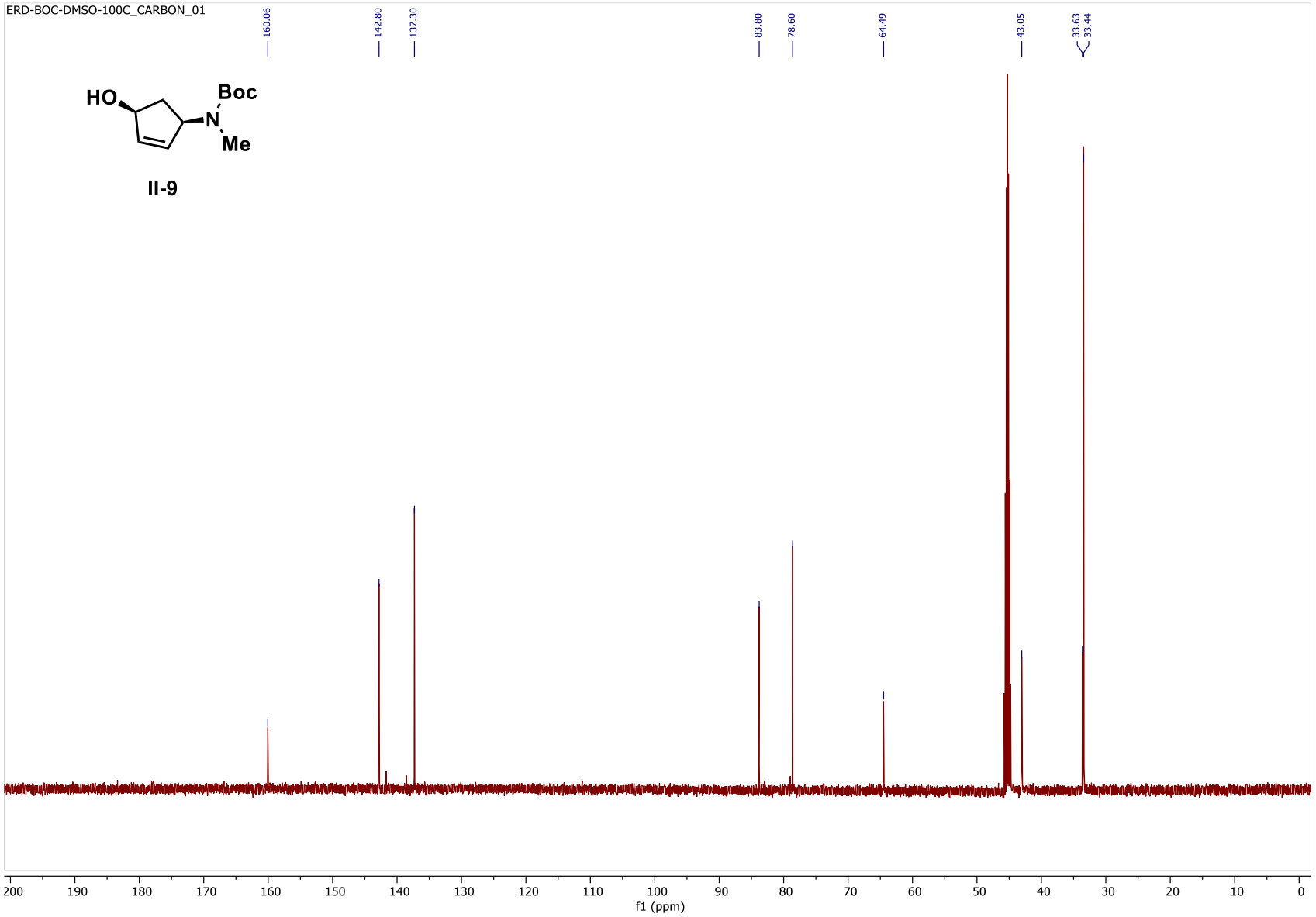

Figure 2.17. ^{1}H NMR of compound *anti*-**II-10** (500 MHz, DMSO-d_6, 80 ℃)

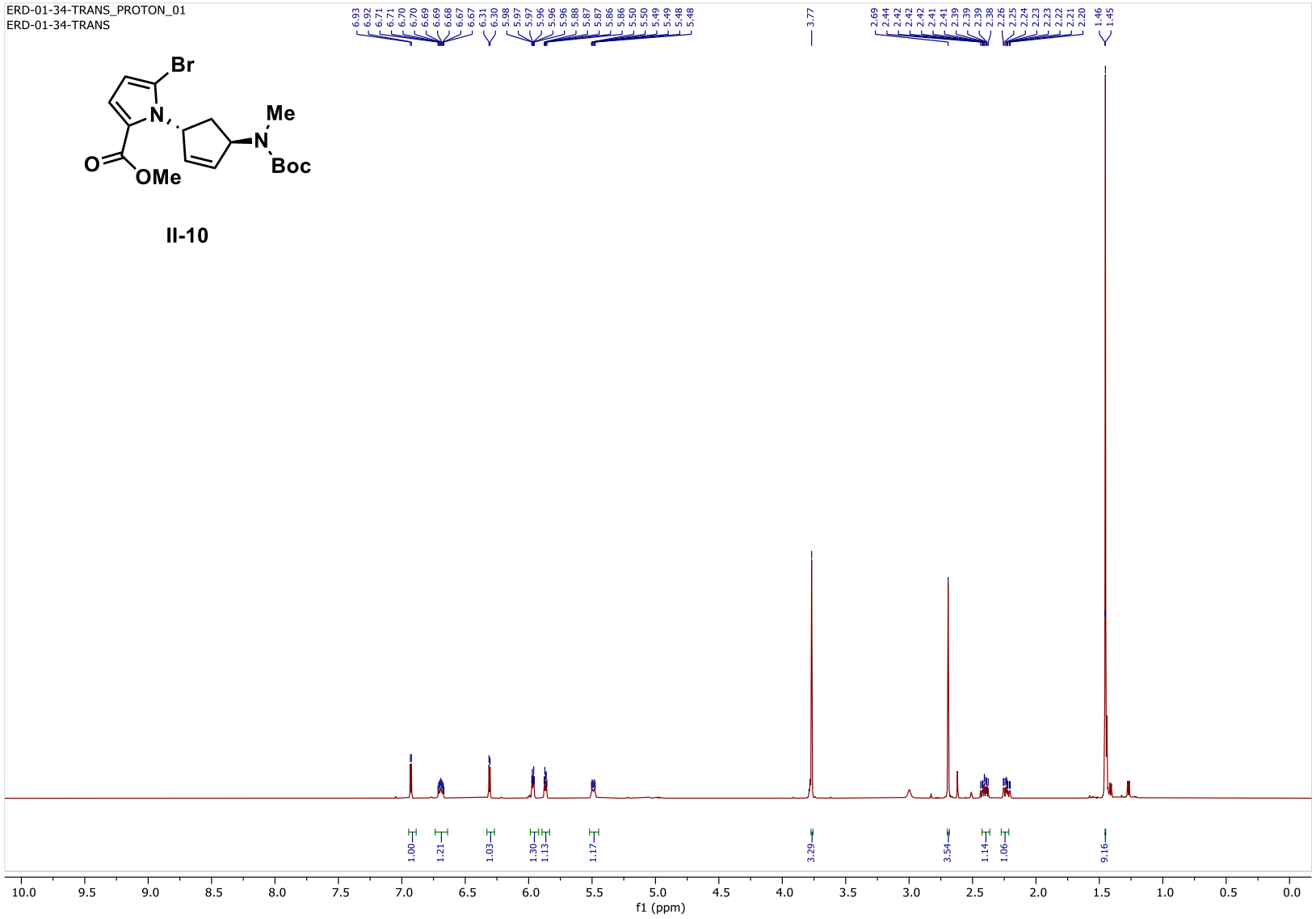

Figure 2.18. ^{13}C NMR of compound *anti*-**II-10** (126 MHz, DMSO-d_6, 80 ℃)

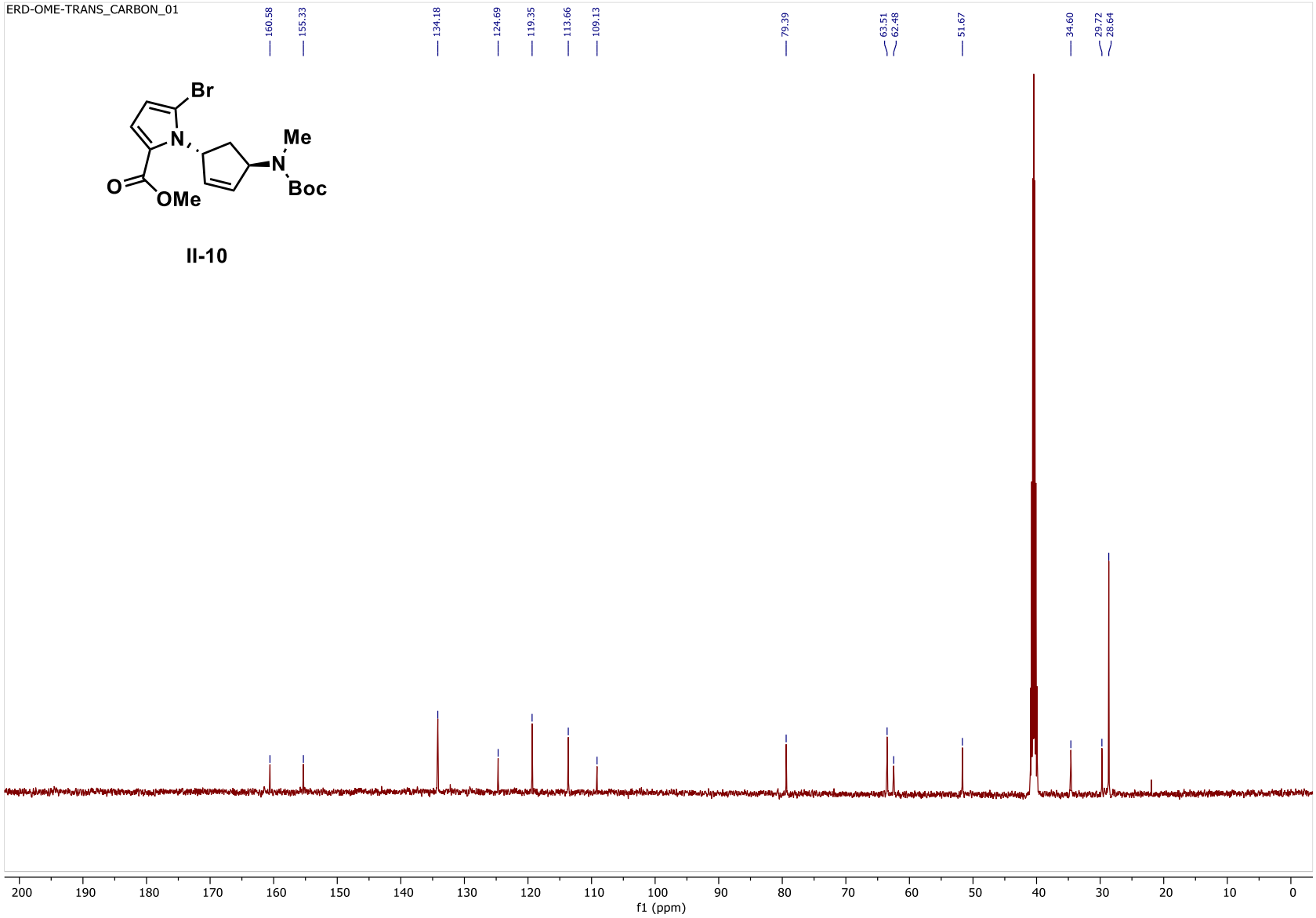

Figure 2.19. NOESY of compound *anti*-**II-10**

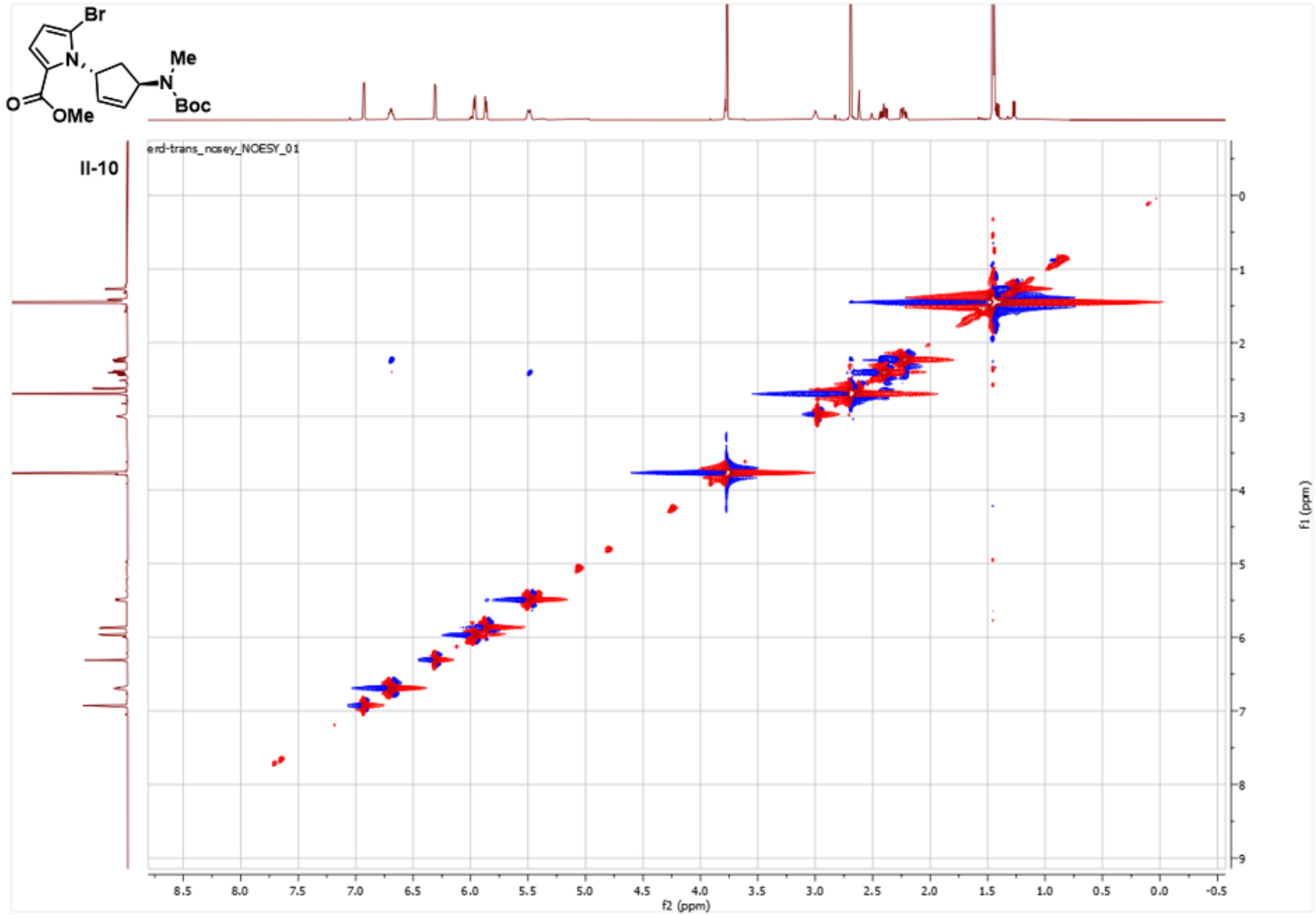

Figure 2.20. ^{1}H NMR of compound **I-47** (500 MHz, Chloroform-*d*, 23℃)

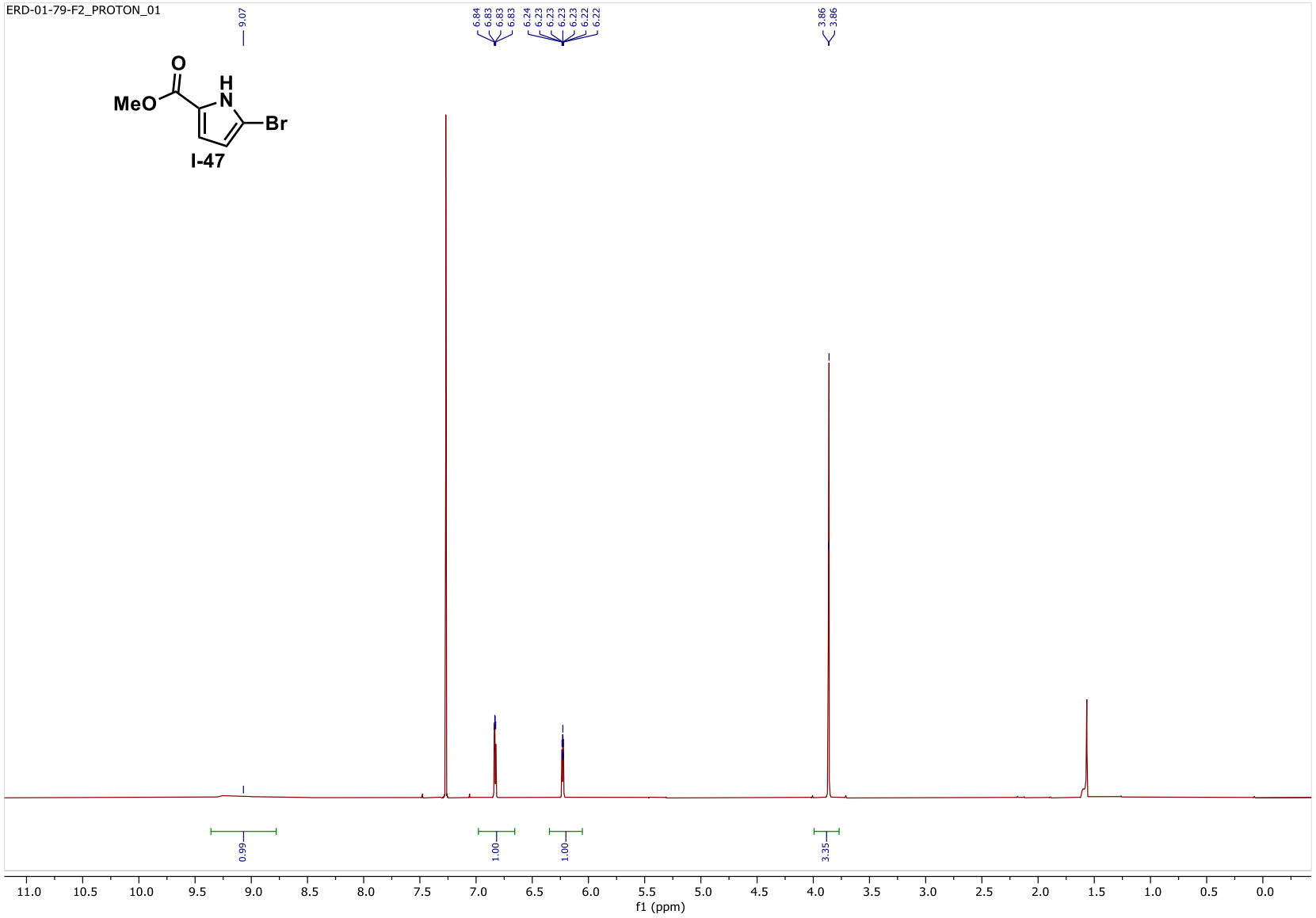

Figure 2.21. ^{13}C NMR of compound **I-47** (126 MHz, Chloroform-*d*, 23 ℃)

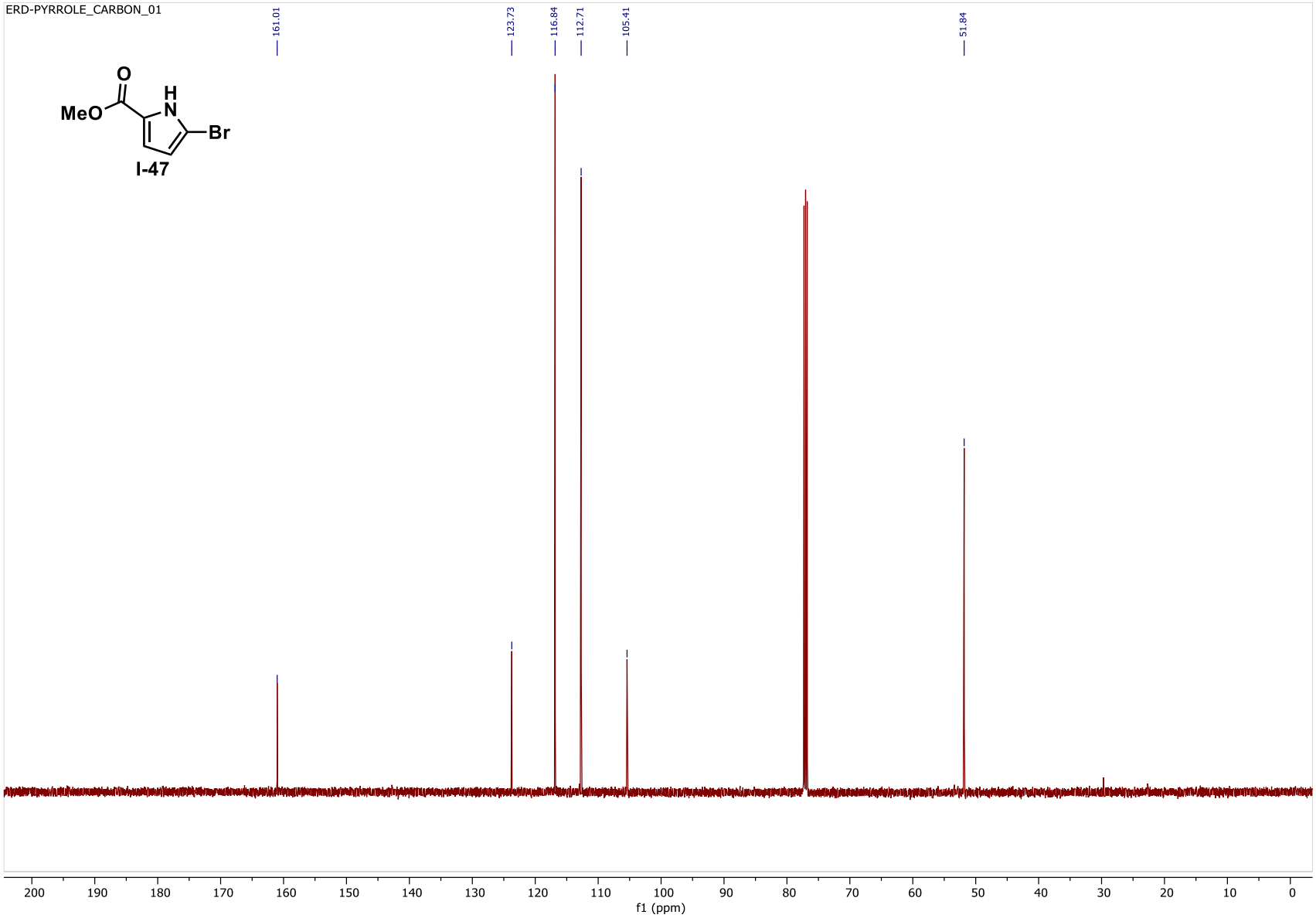

Figure 2.22. ^{1}H NMR of compound *anti*-**II-38** (500 MHz, DMSO-d_6, 80℃)

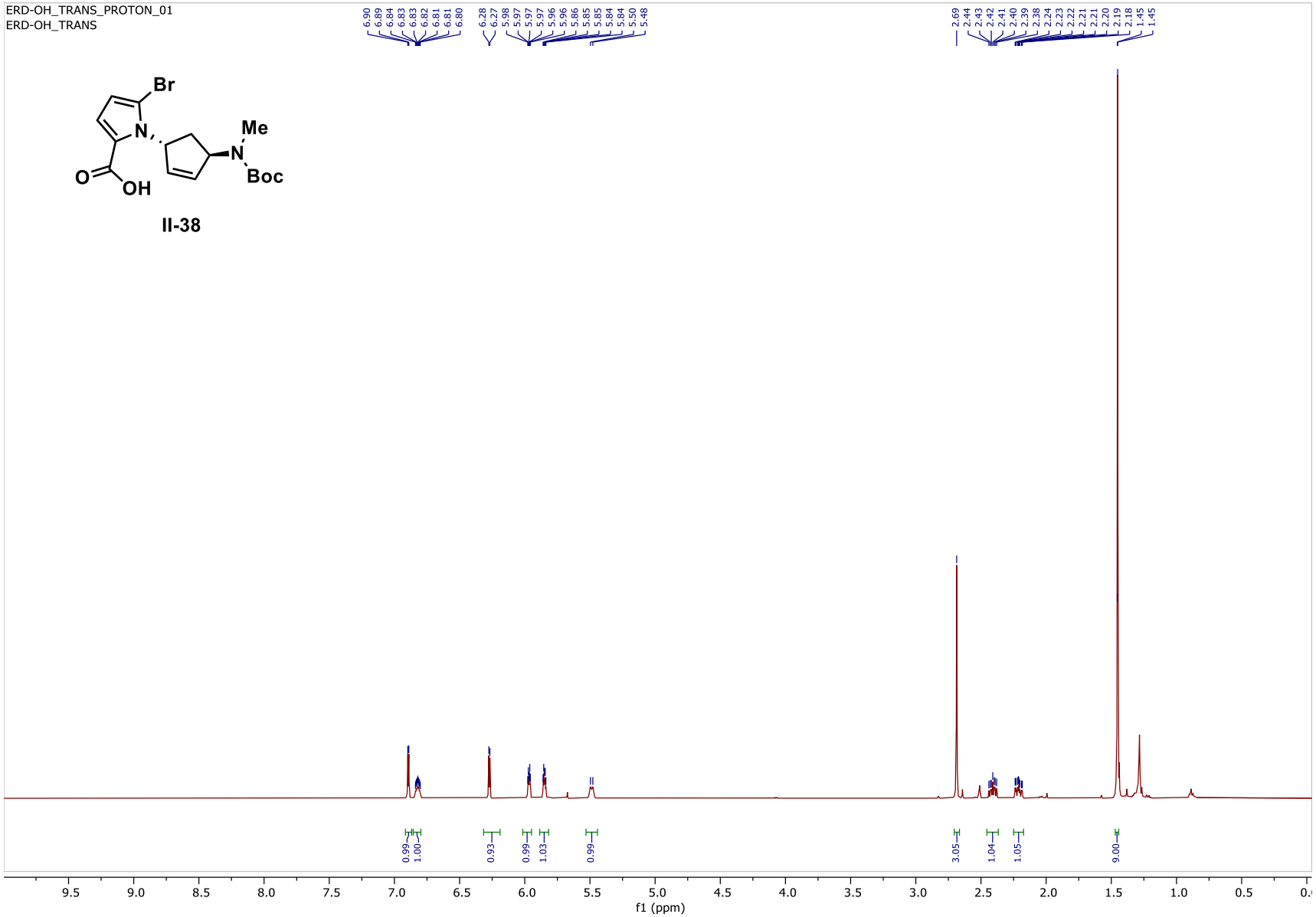

Figure 2.23. ^{13}C NMR of compound *anti*-**II-38** (126 MHz, DMSO-d_6, 80 ℃)

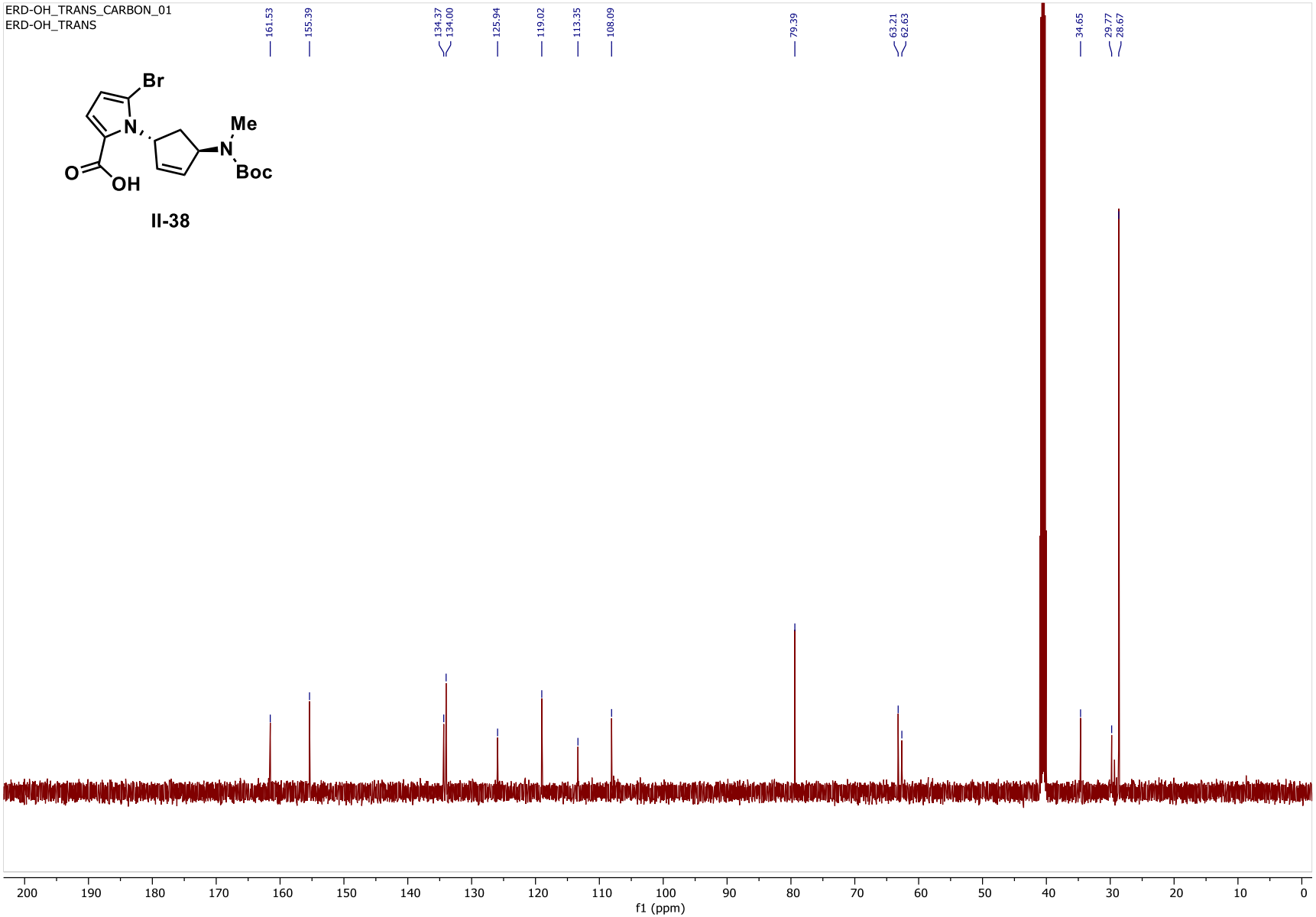

Figure 2.24. ^{1}H NMR of compound *anti*-**II-11** (500 MHz, DMSO-d_6, 80 ℃)

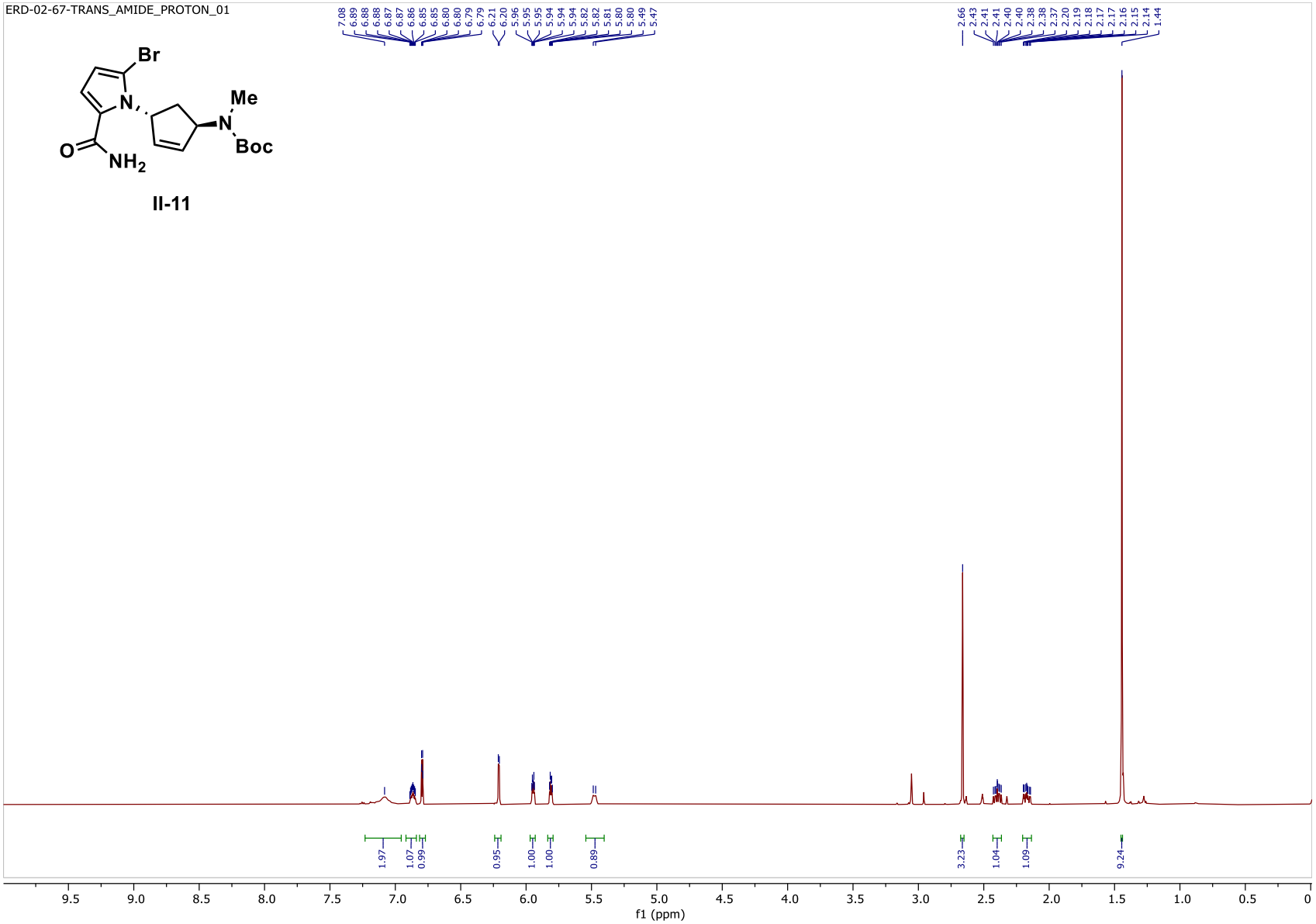

Figure 2.25. ^{13}C NMR of compound *anti*-**II-11** (126 MHz, DMSO-d_6, 80 ℃)

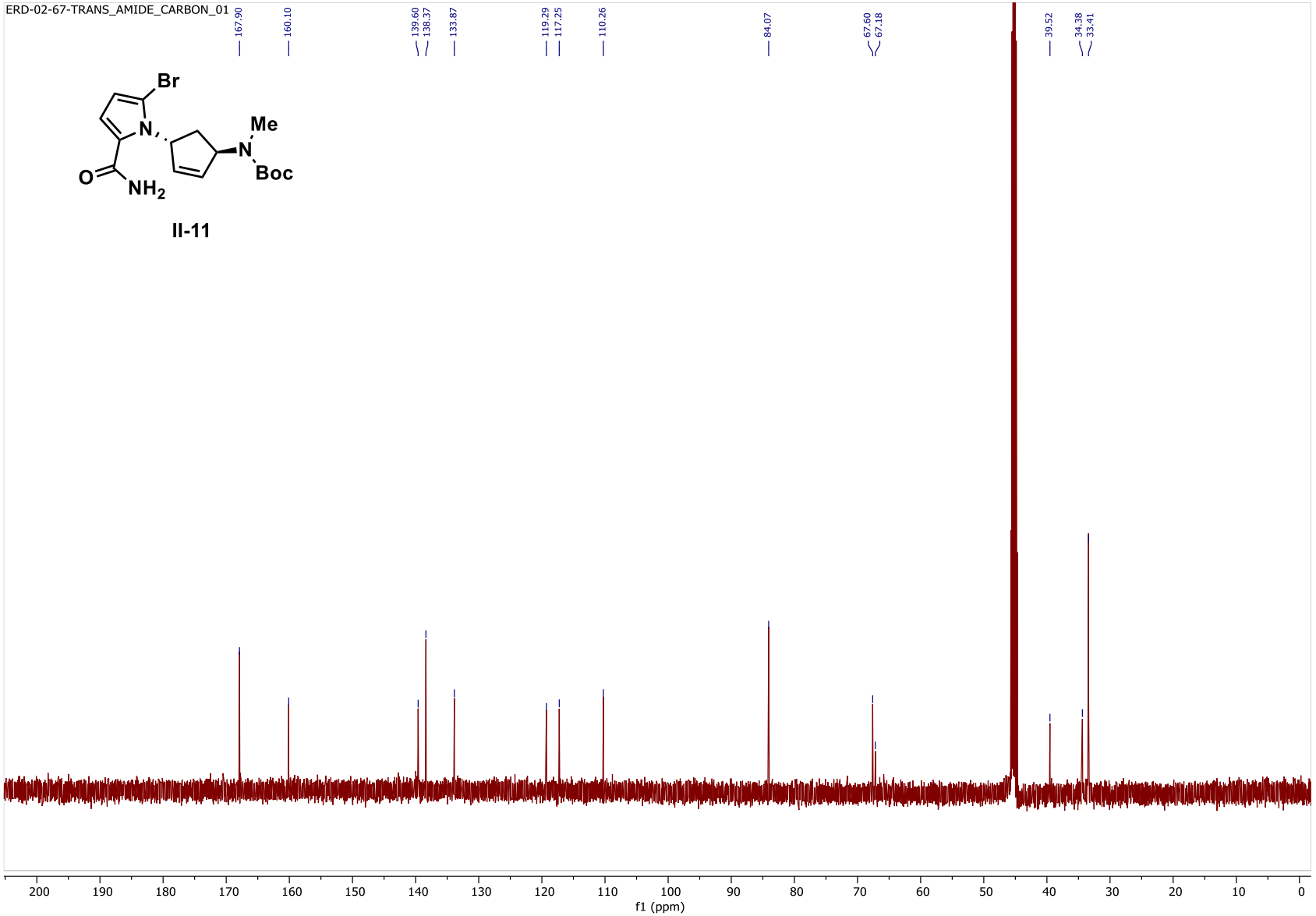

Figure 2.26. ^{1}H NMR of compound *anti*-**II-12** (500 MHz, Chloroform-*d*, 23 ℃)

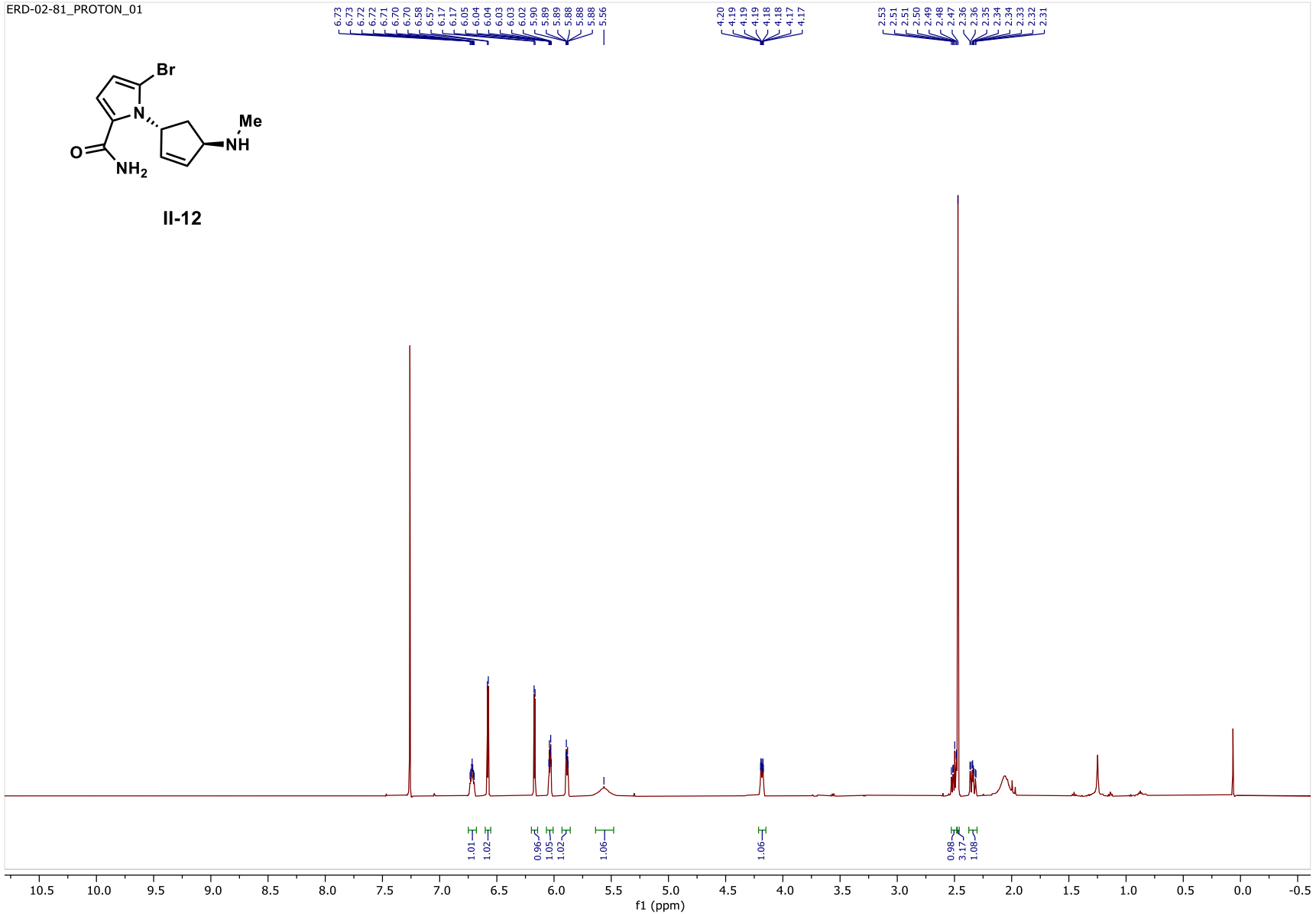

Figure 2.27. ^{13}C NMR of compound *anti*-**II-12** (126 MHz, Chloroform-*d*, 23 ℃)

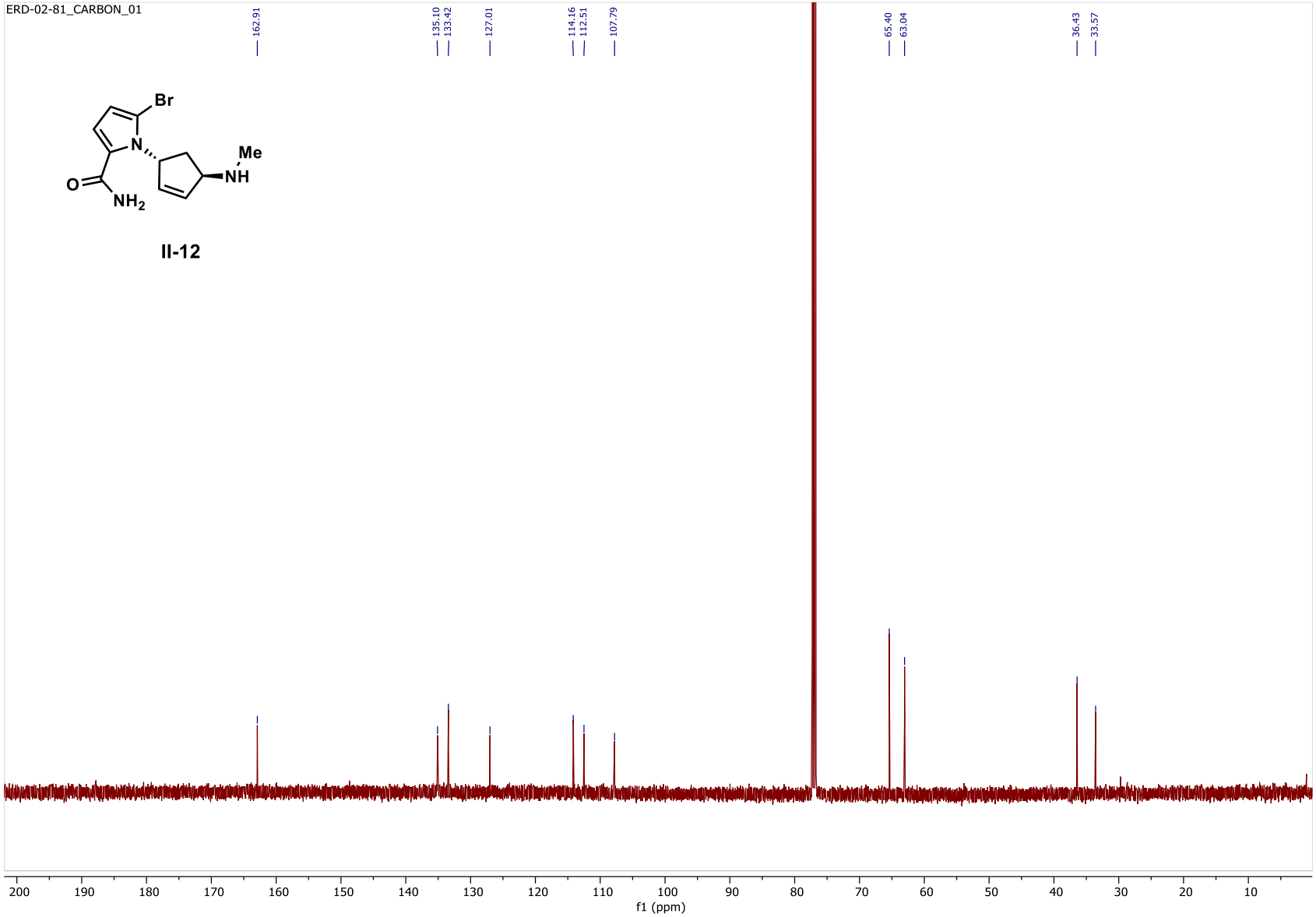

Figure 2.28. ^{1}H NMR of compound **II-14** (500 MHz, Chloroform-*d*, 23 ℃)

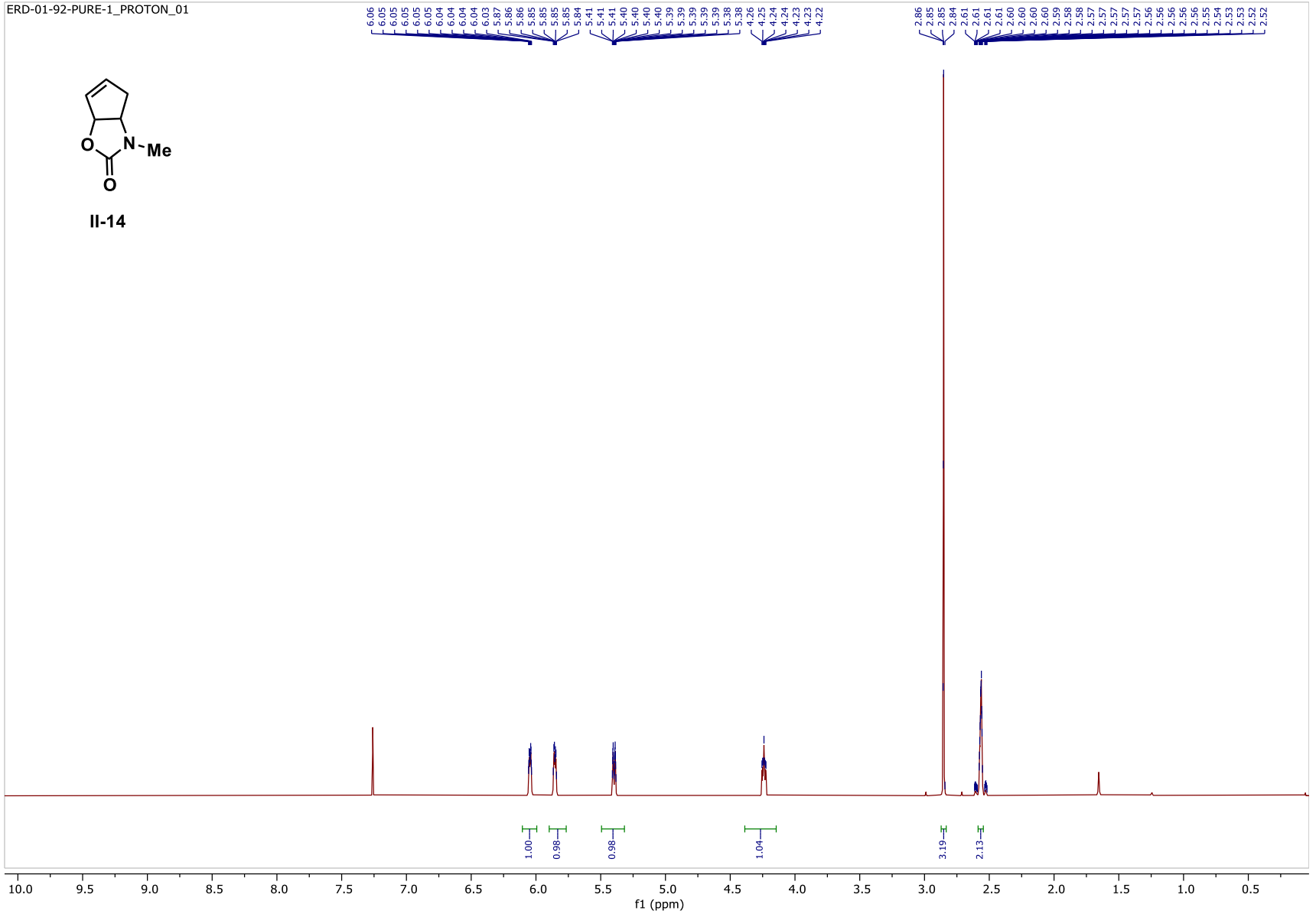

Figure 2.29. ^{13}C NMR of compound **II-14** (126 MHz, Chloroform-*d*, 23 ℃)

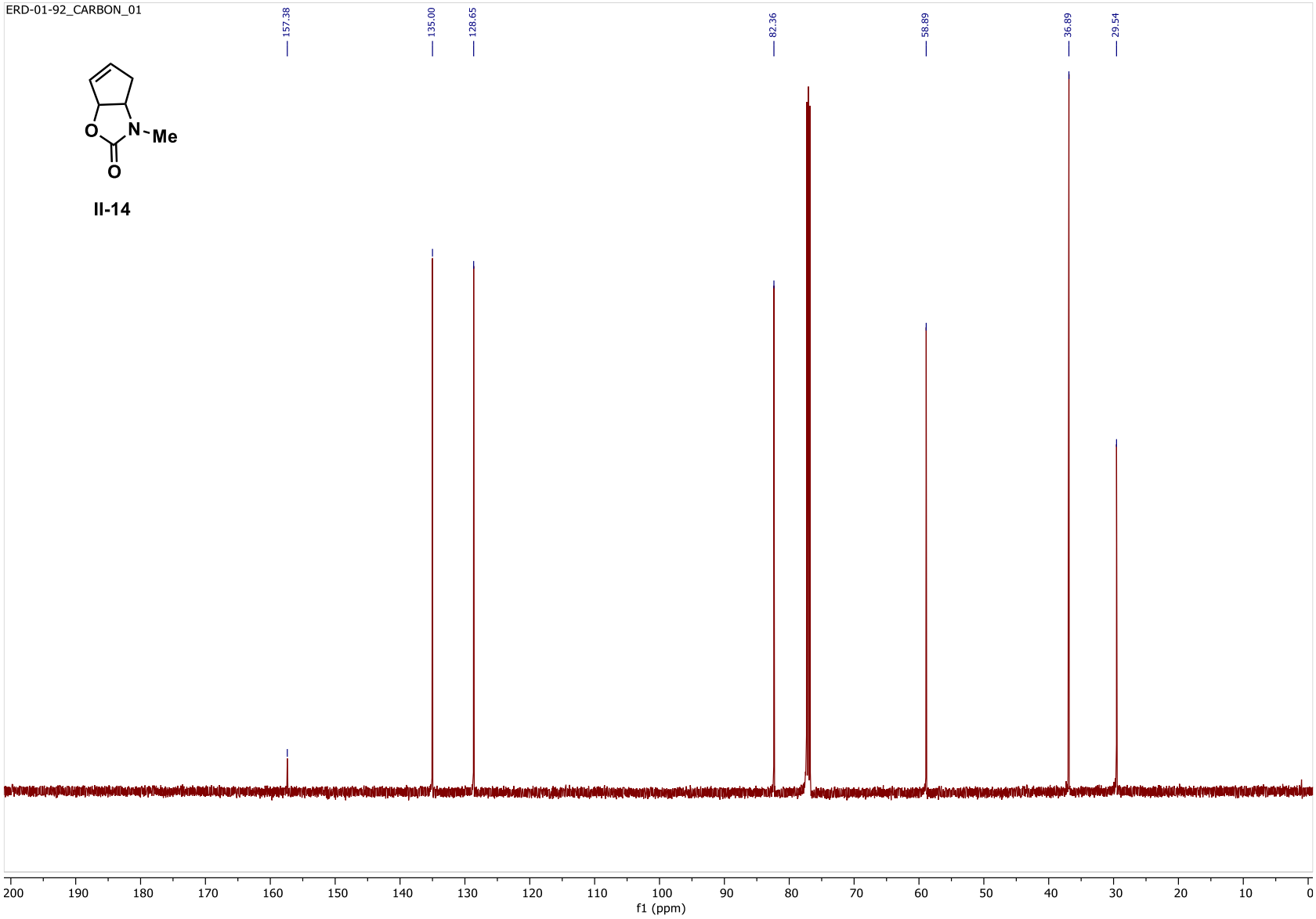

Figure 2.30. ^{1}H NMR of compound **II-15** (500 MHz, DMSO-d_6, 80 ℃)

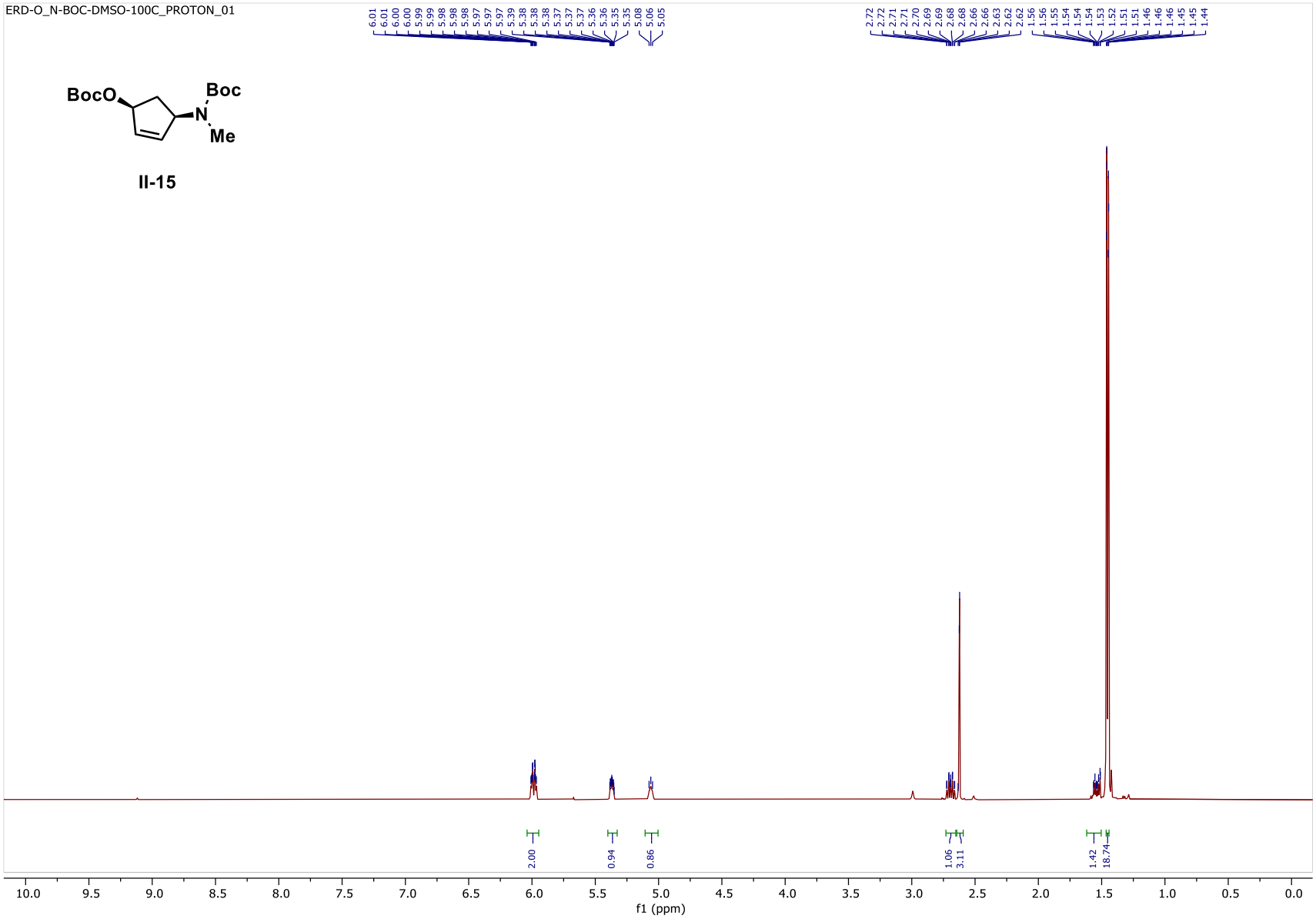

Figure 2.31. ^{13}C NMR of compound **II-15** (126 MHz, DMSO-d_6, 80 ℃)

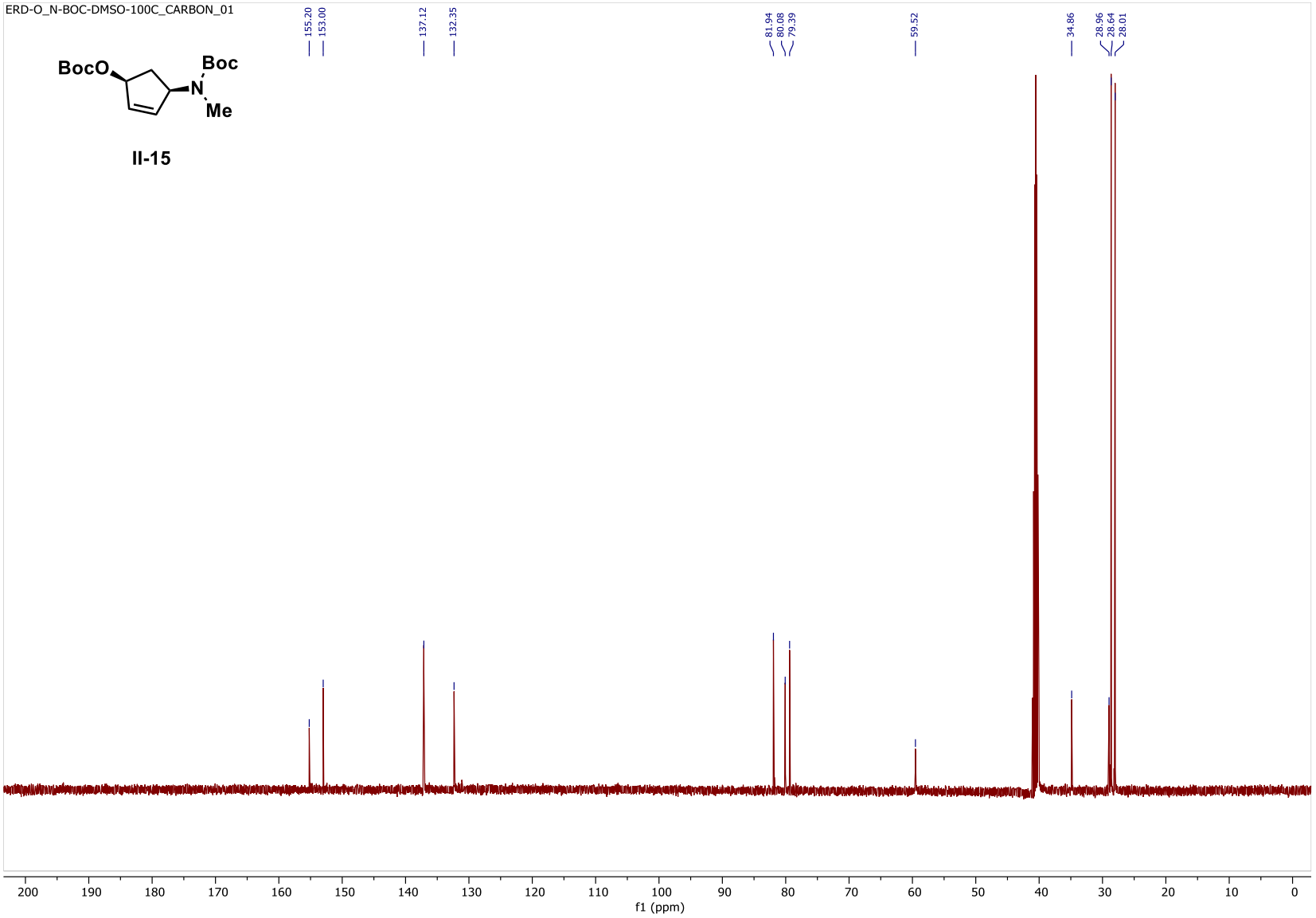

Figure 2.32. ^{1}H NMR of compound *syn*-**II-10** (500 MHz, DMSO-d_6, 80℃)

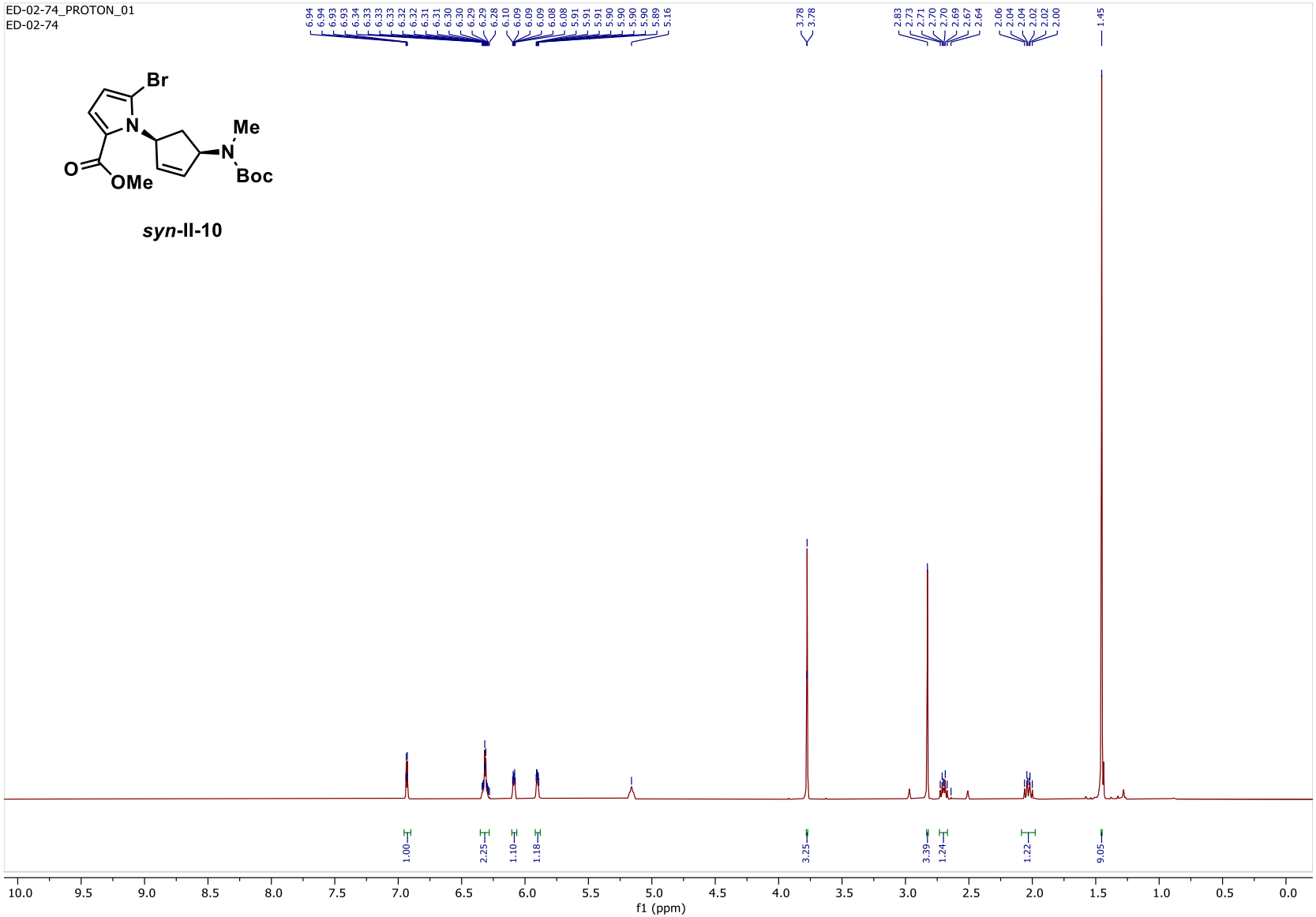

Figure 2.33. ^{13}C NMR of compound *syn*-**II-10** (126 MHz, DMSO-d_6, 80 ℃)

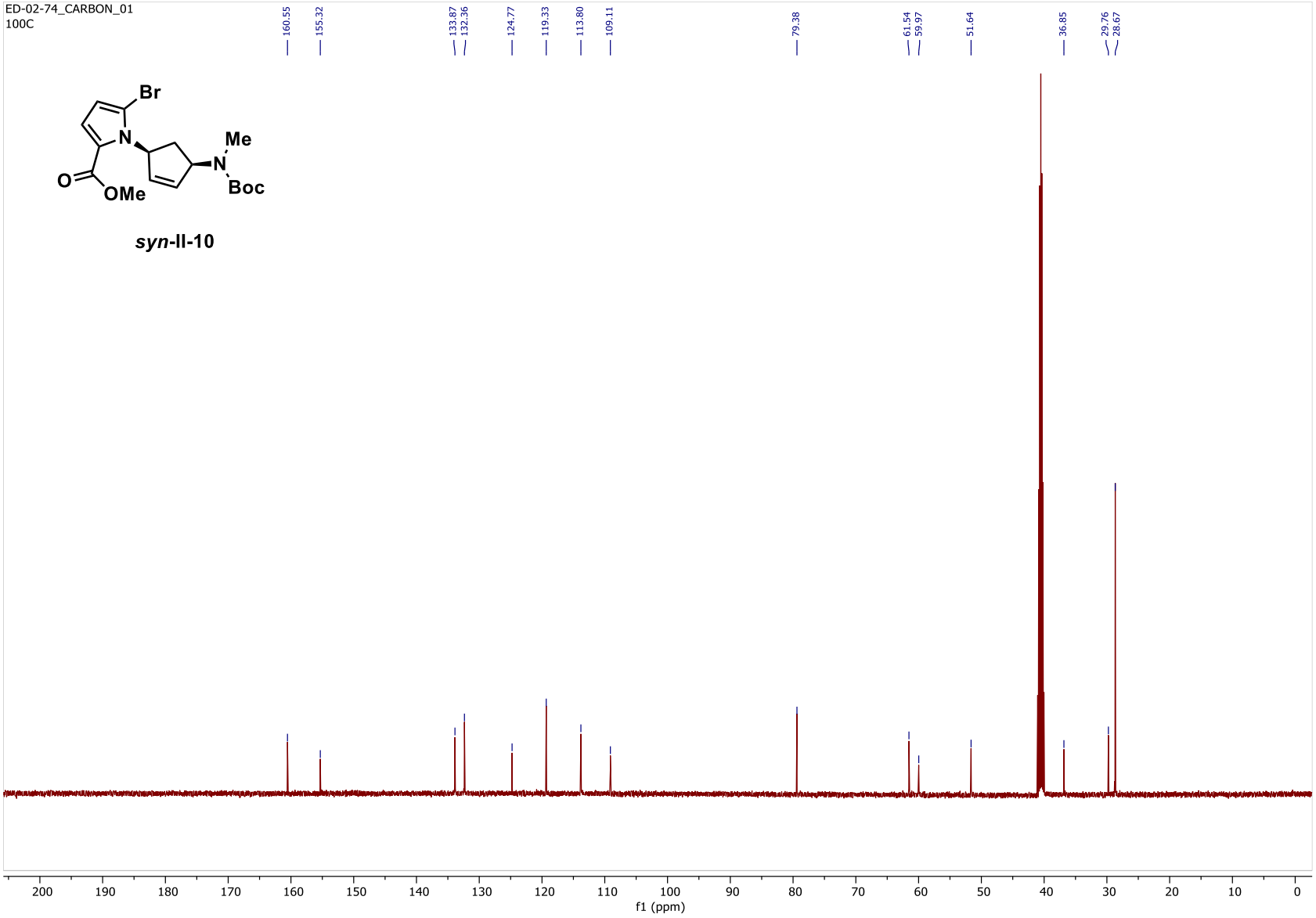

Figure 2.34. NOESY of compound *syn*-**II-10**

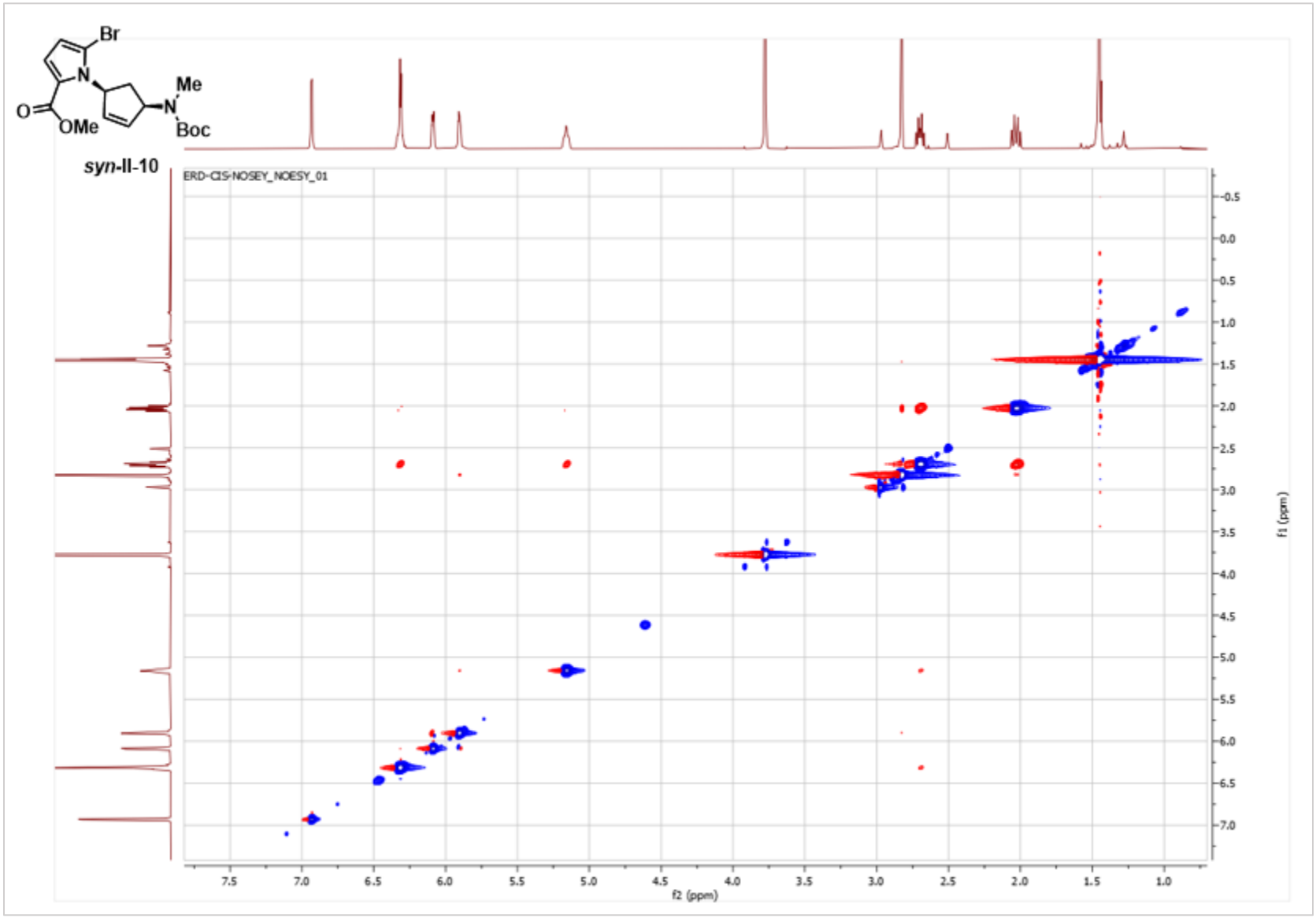

Figure 2.35. ^{1}H NMR of compound *syn*-**II-38** (500 MHz, DMSO-d_6, 80 ℃)

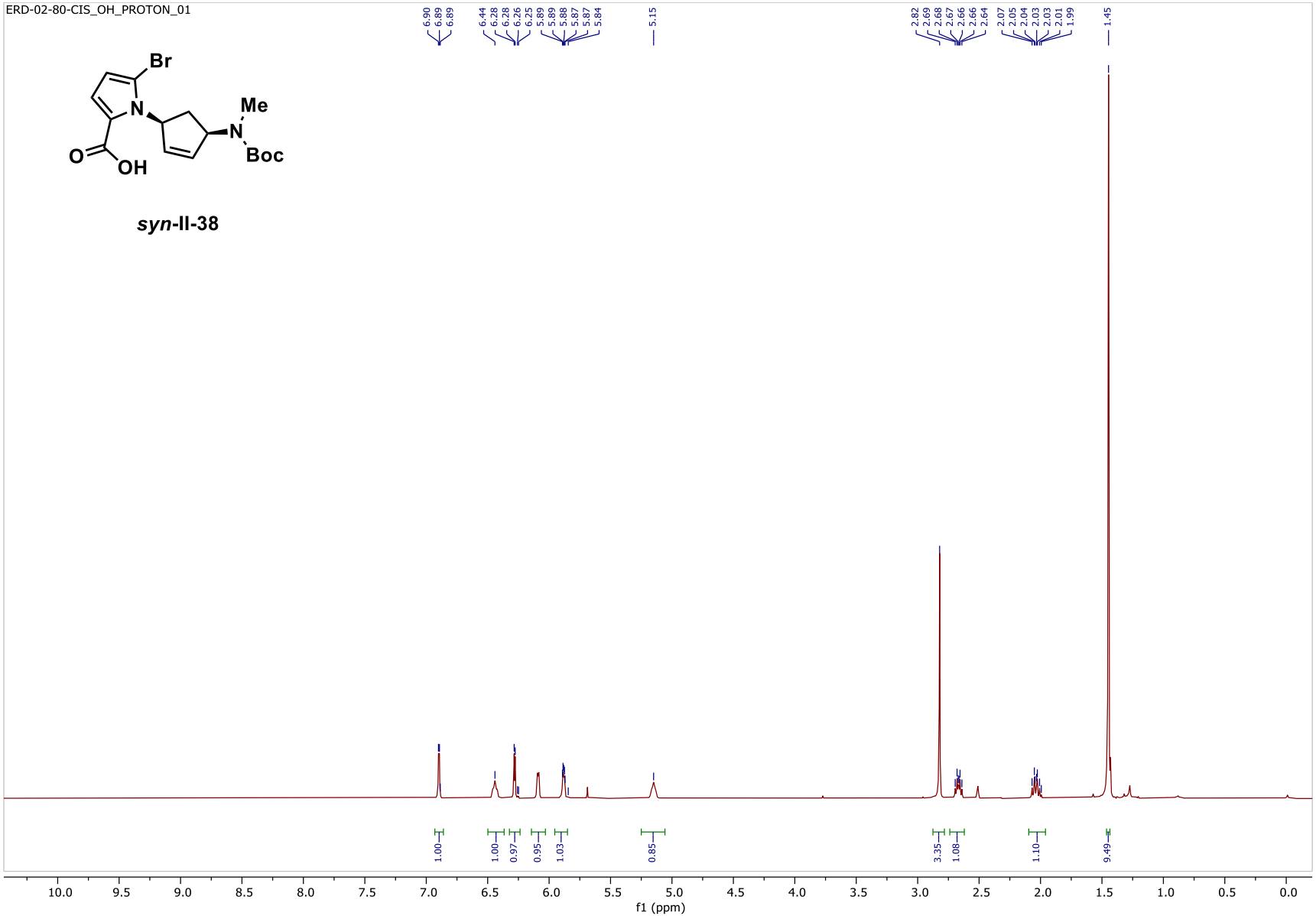

Figure 2.36. ^{13}C NMR of compound *syn*-**II-38** (126 MHz, DMSO-d_6, 80 ℃)

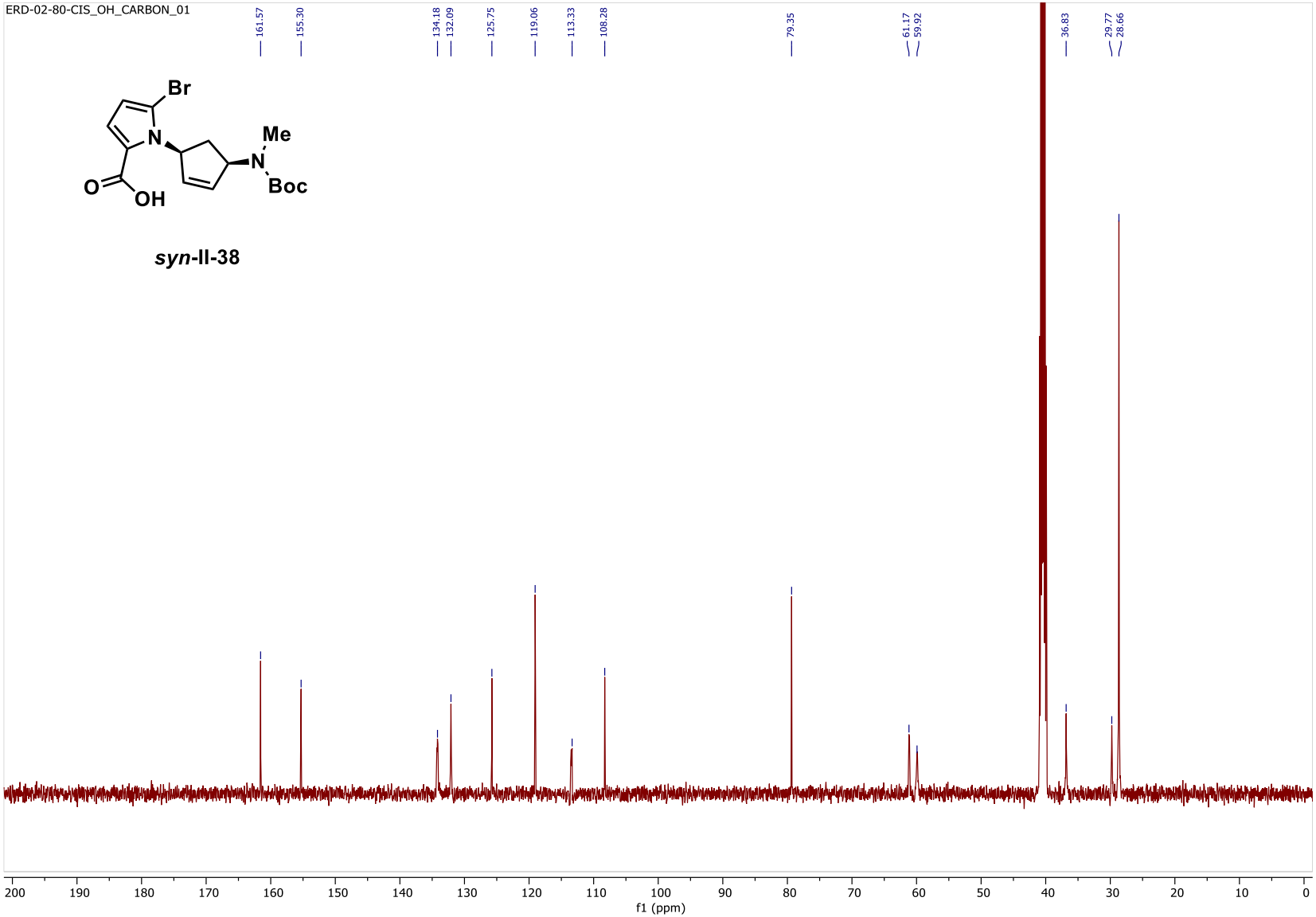

Figure 2.37. ^{1}H NMR of compound **II-17** (500 MHz, DMSO-d_6, 80 ℃)

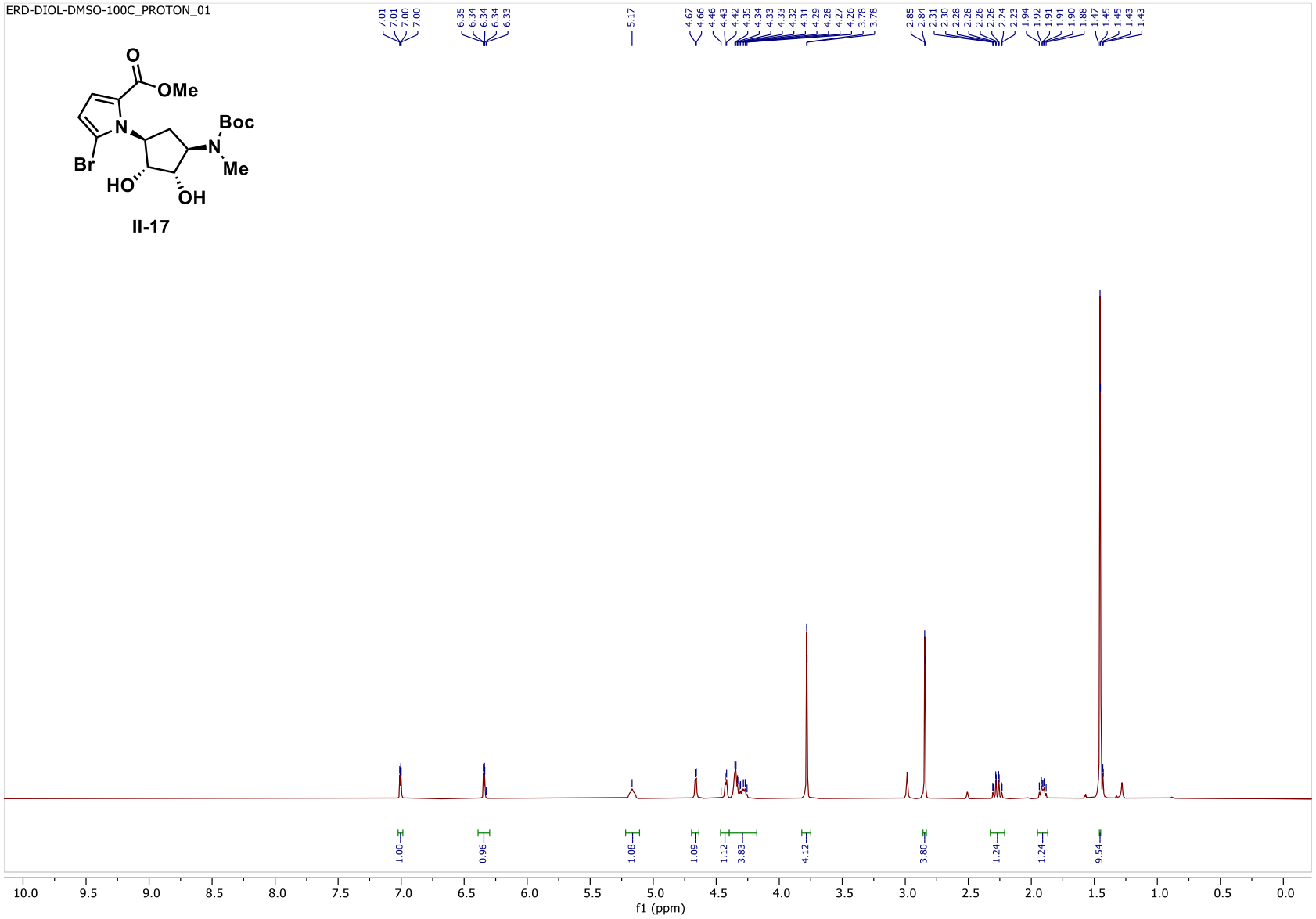

Figure 2.38. ^{13}C NMR of compound **II-17** (126 MHz, DMSO-d_6, 80 ℃)

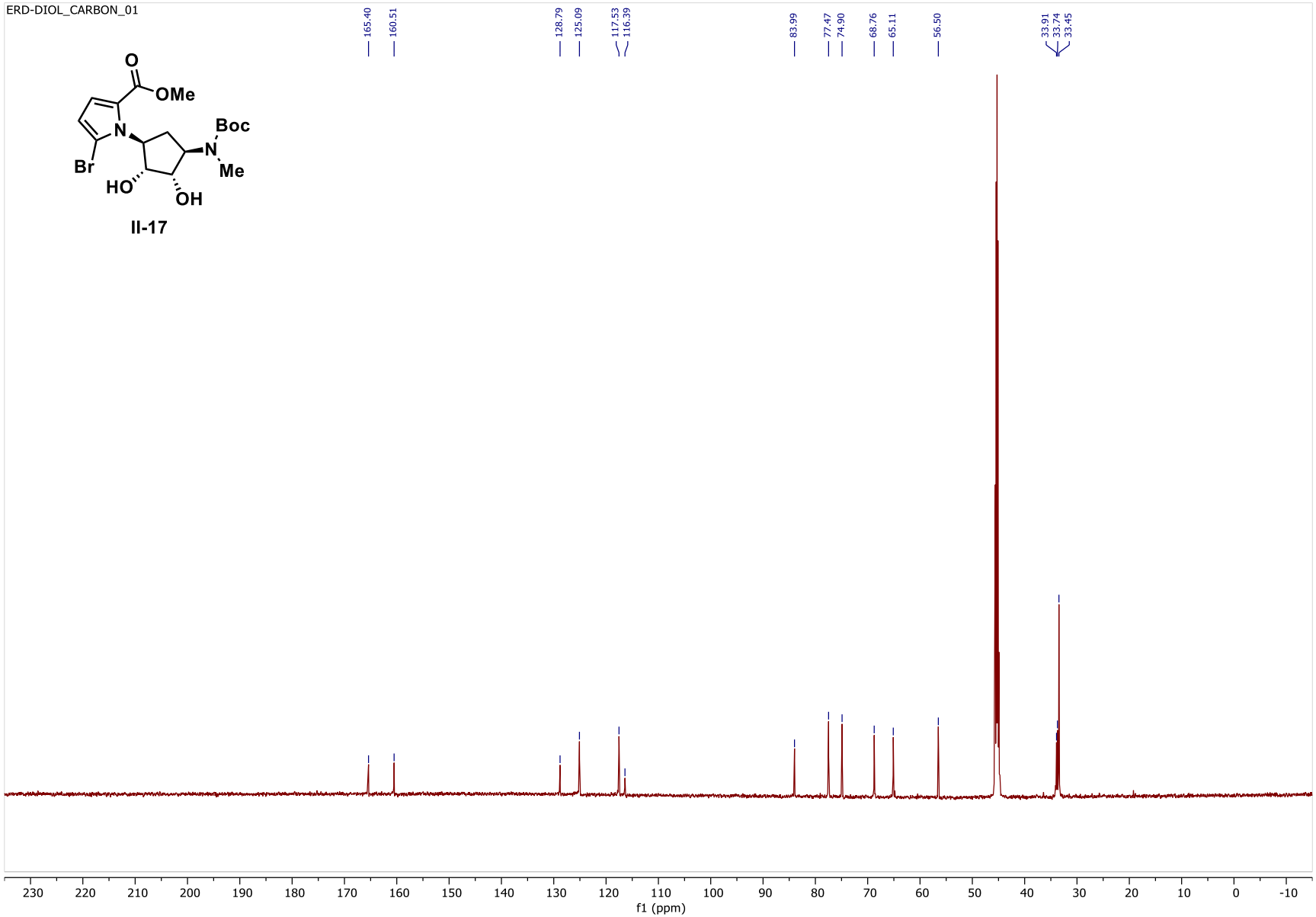

Figure 2.39. ^{1}H NMR of compound *syn*-**II-11** (500 MHz, DMSO-d_6, 80℃)

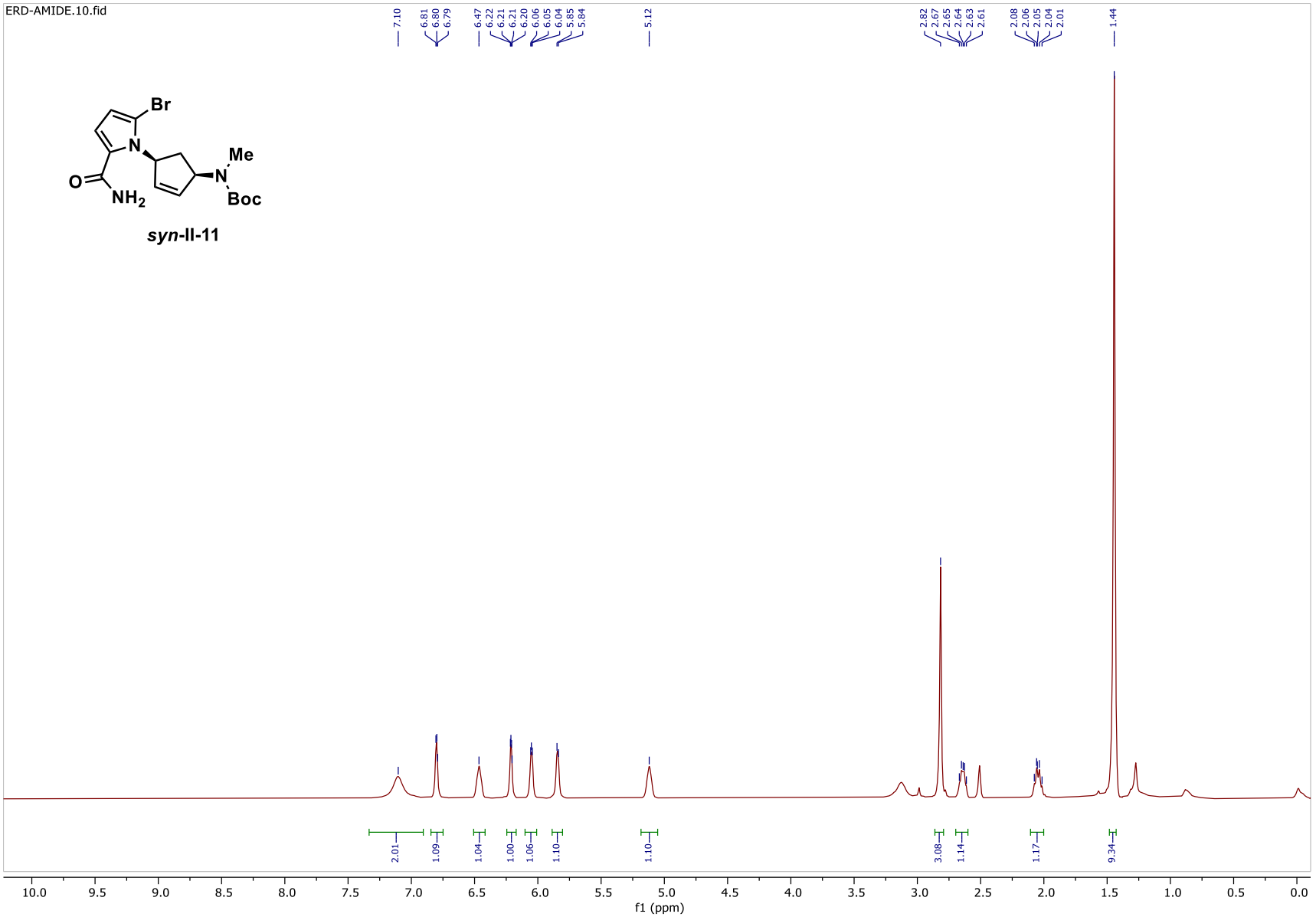

Figure 2.40. ^{13}C NMR of compound *syn*-**II-11** (126 MHz, DMSO-d_6, 80 ℃)

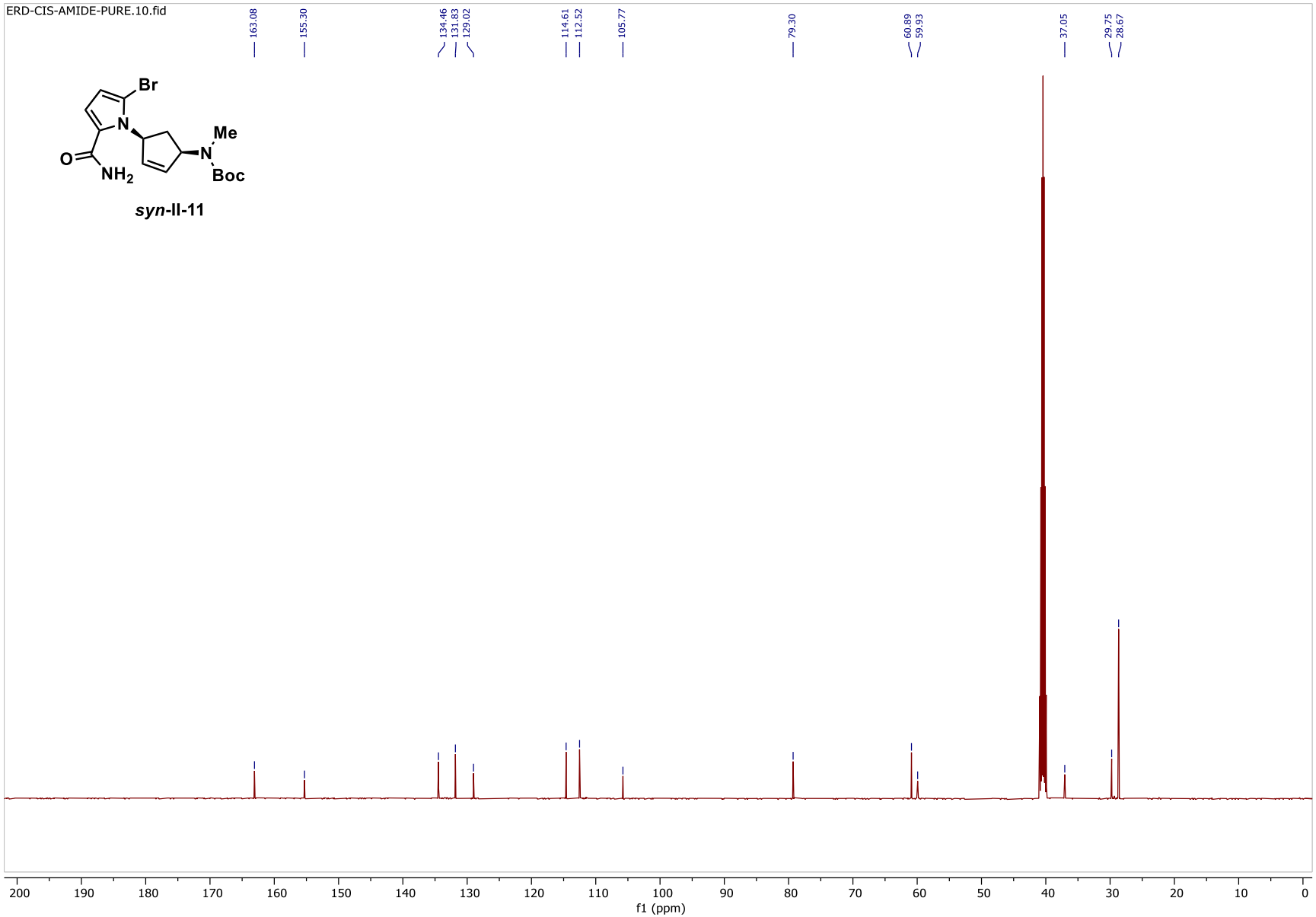

Figure 2.41. ^{1}H NMR of compound *syn*-**II-13** (500 MHz, methanol-*d*, 23 ℃)

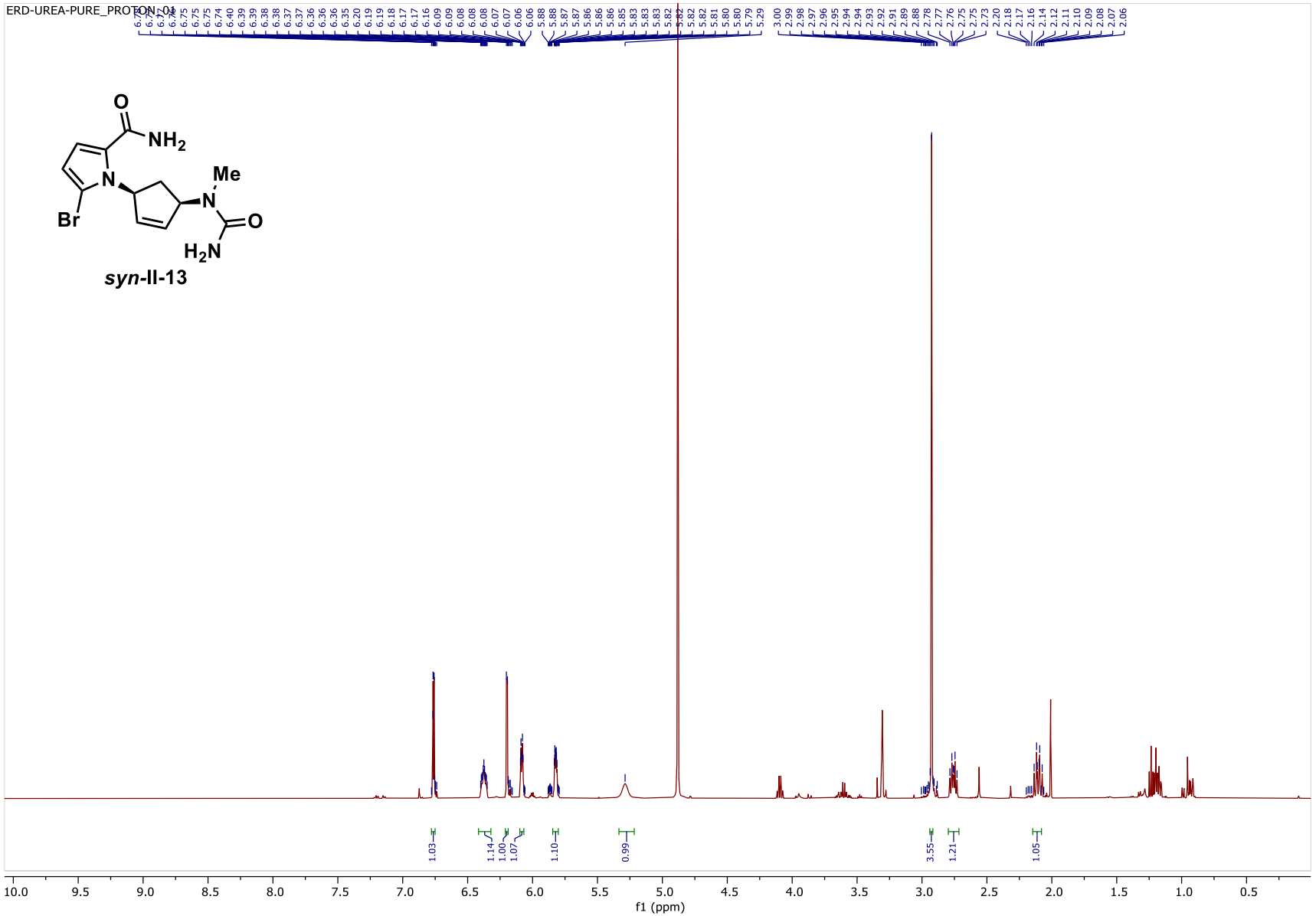

Figure 2.42. ^{13}C NMR of compound *syn*-**II-13** (126 MHz, methanol-*d*, 23℃)

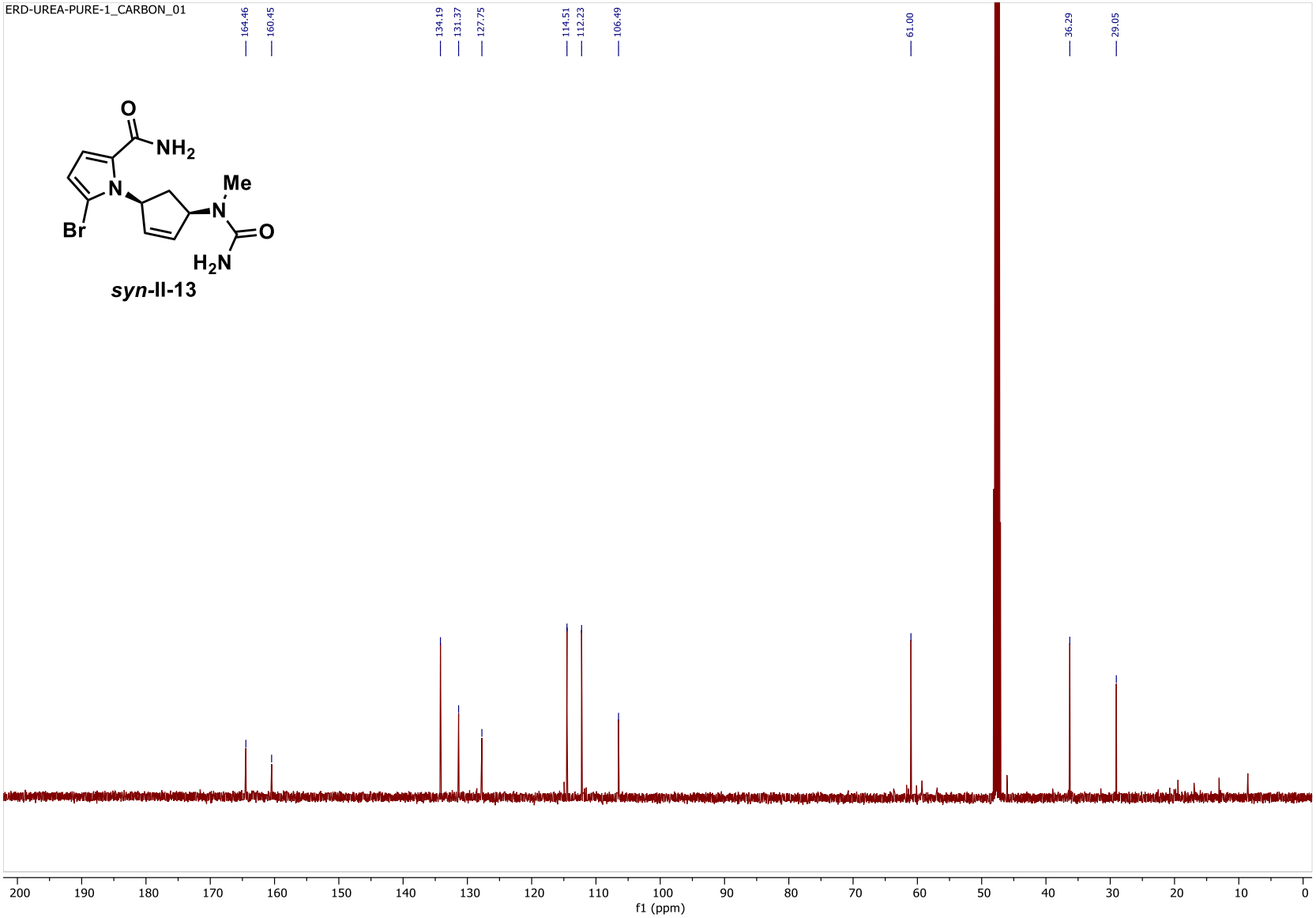

Figure 2.43. ^{1}H NMR of compound **II-21** (500 MHz, DMSO-d_6, 23 ℃)

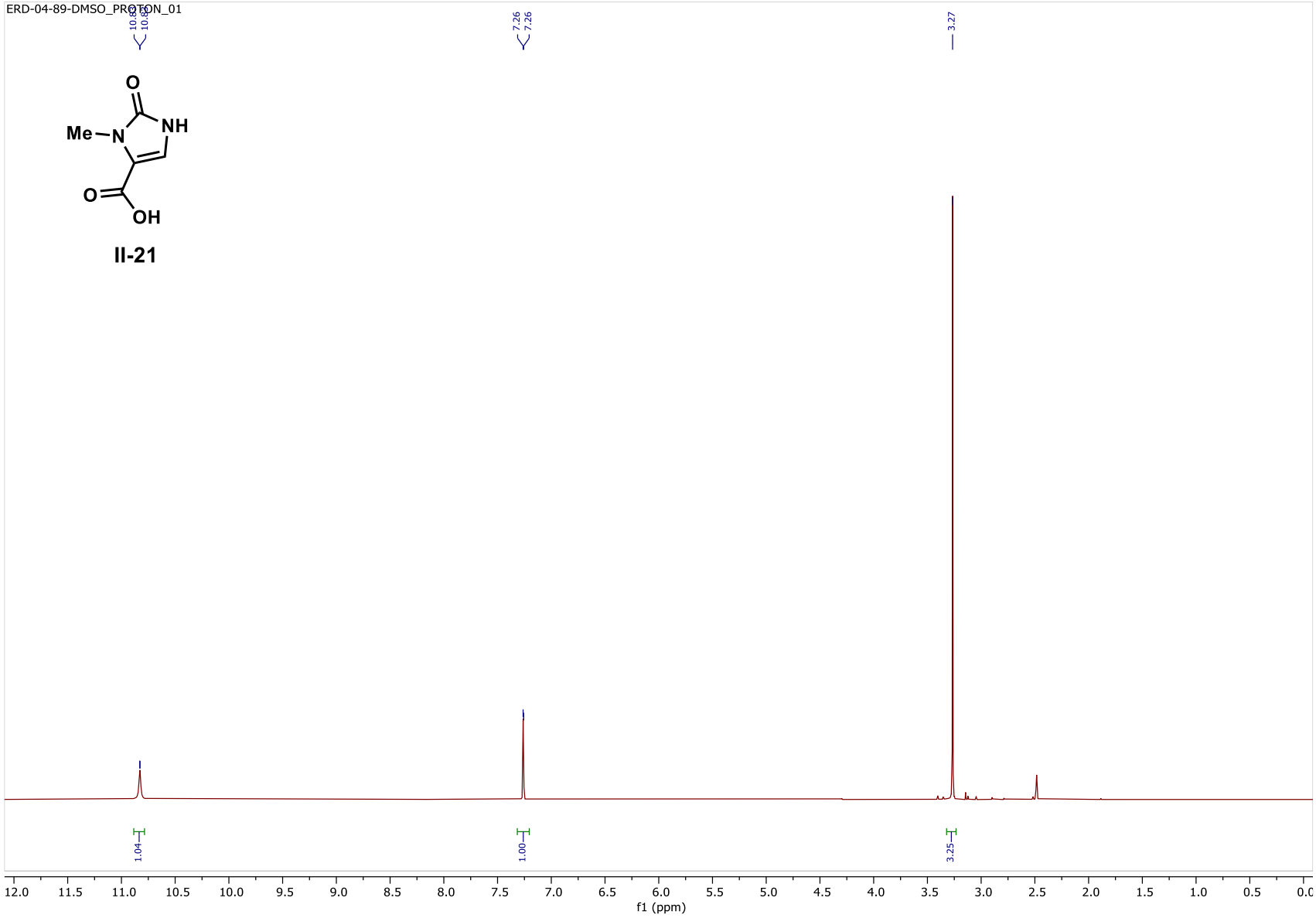

Figure 2.44. ^{13}C NMR of compound **II-21** (126 MHz, DMSO-d_6, 23℃)

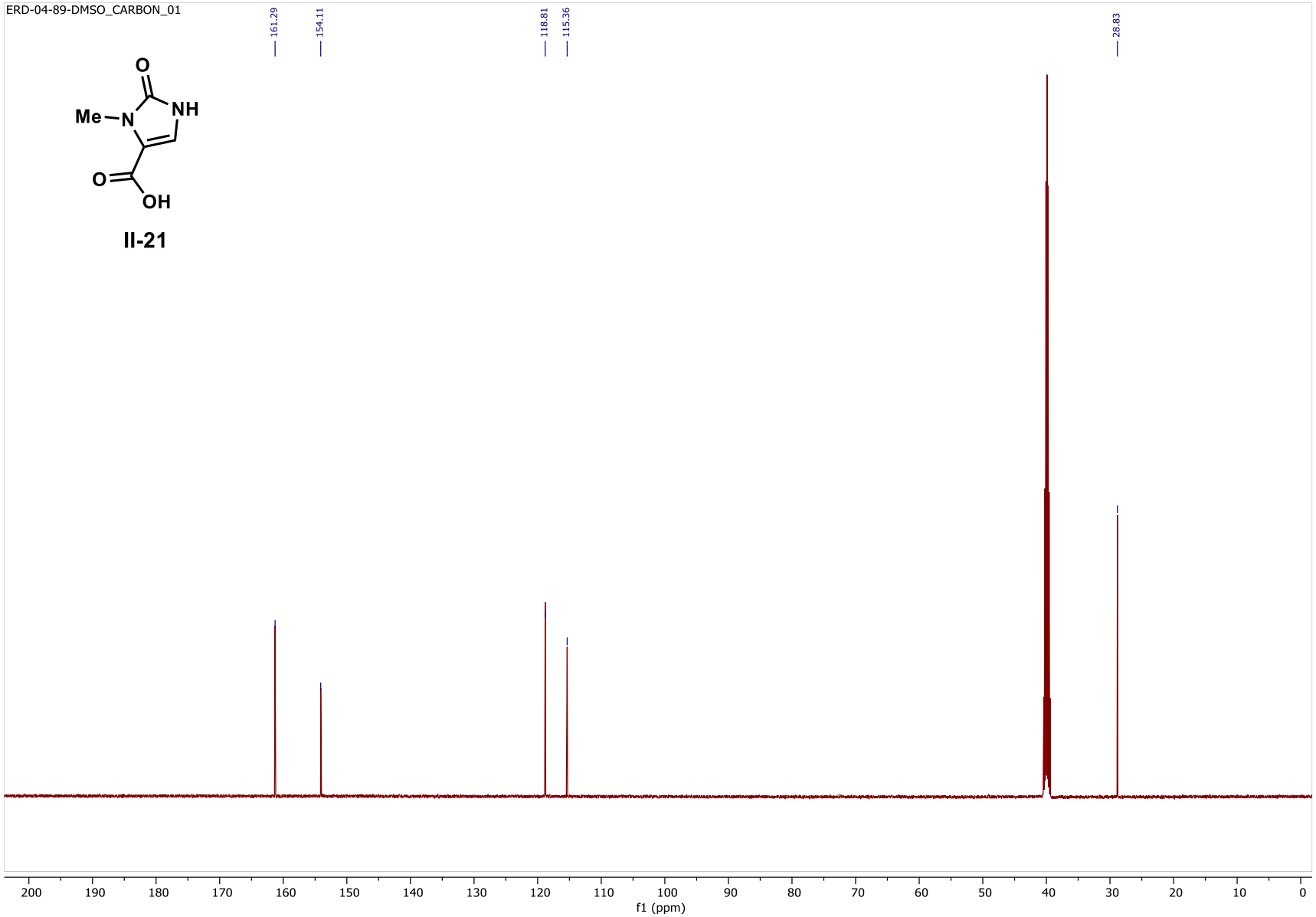

Figure 2.45. ^{1}H NMR of compound **II-24** (500 MHz, Chloroform-*d*, 23℃)

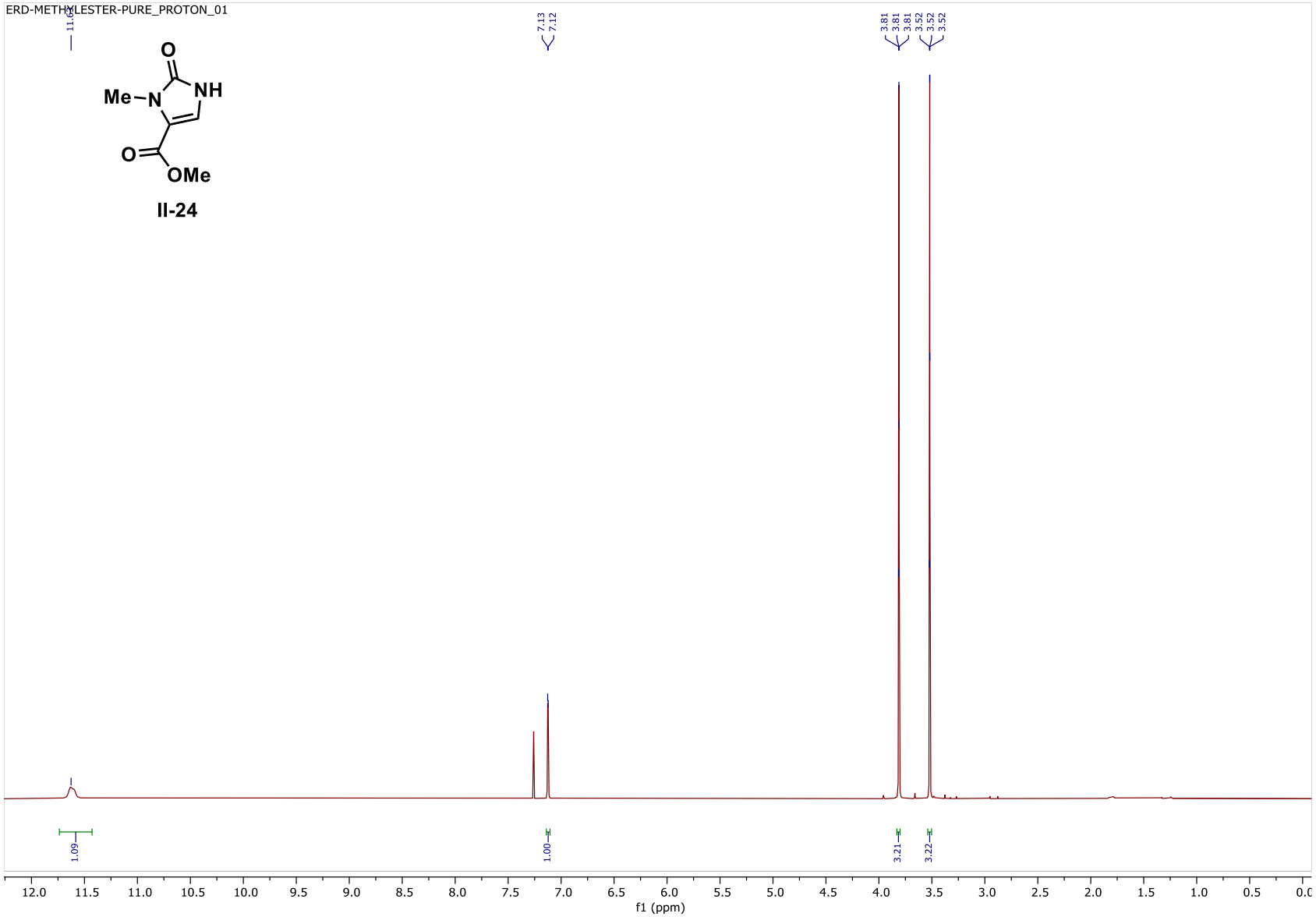

Figure 2.46. ^{13}C NMR of compound **II-24** (126 MHz, Chloroform-*d*, 23 ℃)

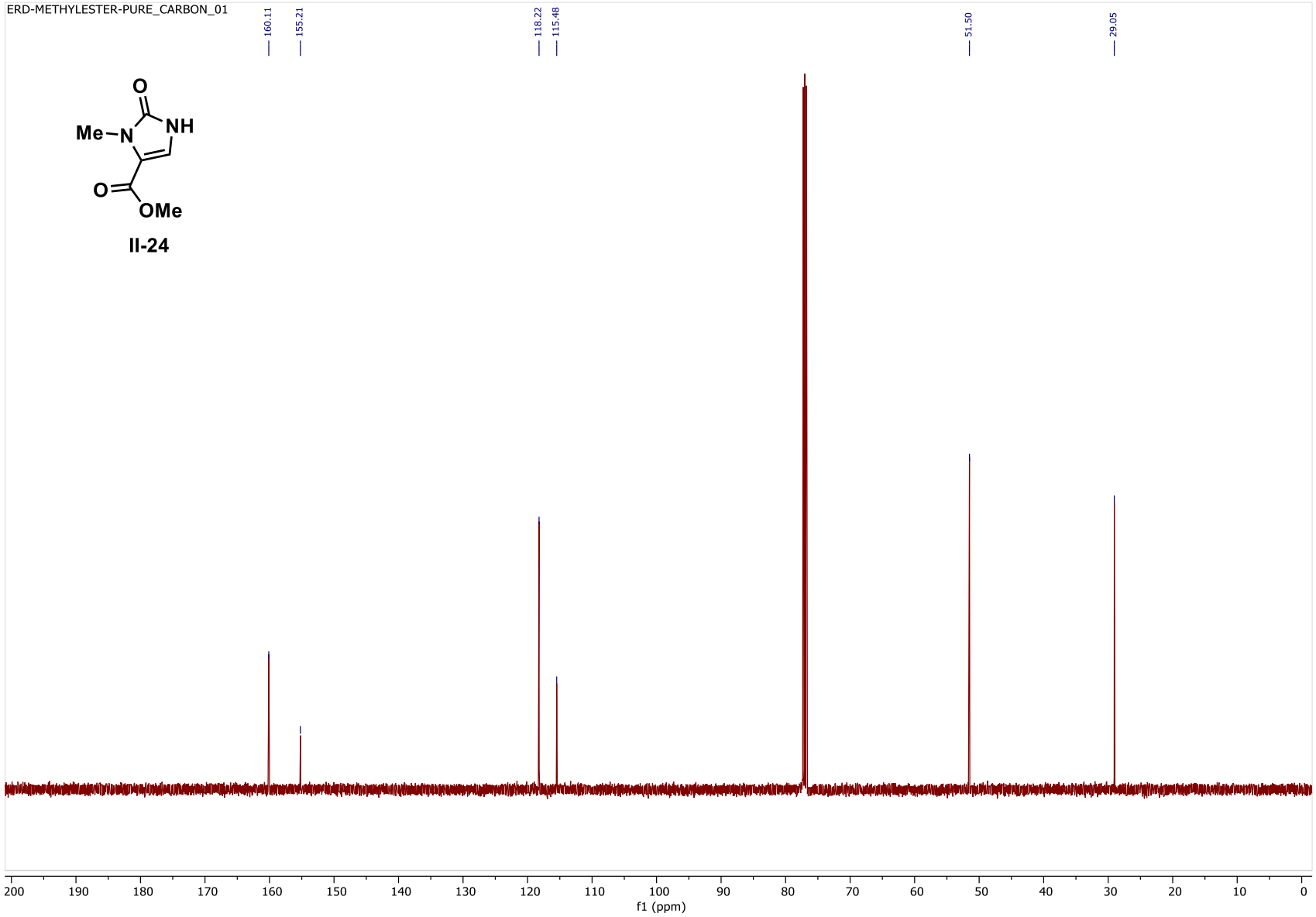

Figure 2.47. ^{1}H NMR of compound **II-25** (500 MHz, Chloroform-*d*, 23 ℃)

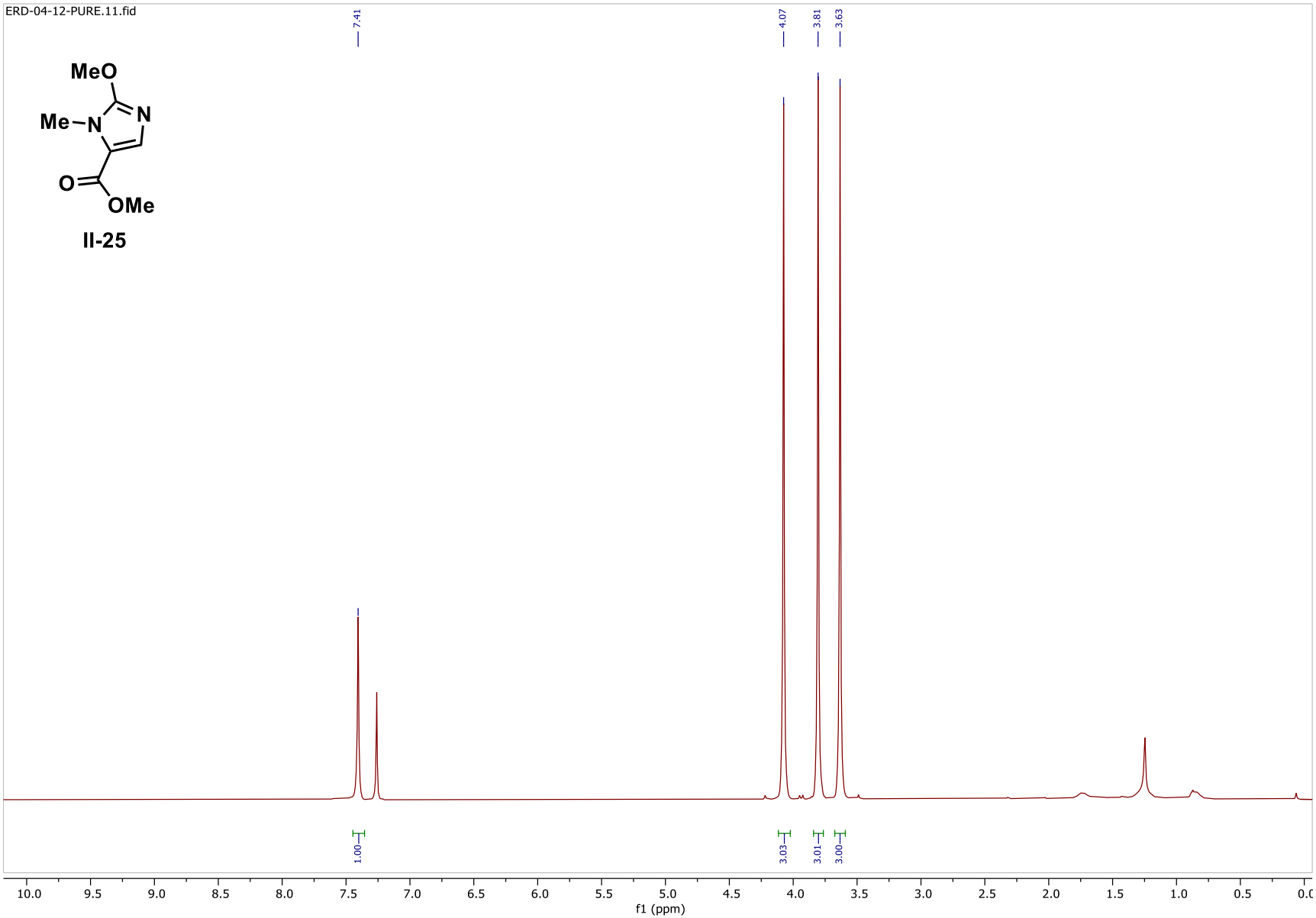

Figure 2.48. ^{13}C NMR of compound **II-25** (126 MHz, Chloroform-*d*, 23 ℃)

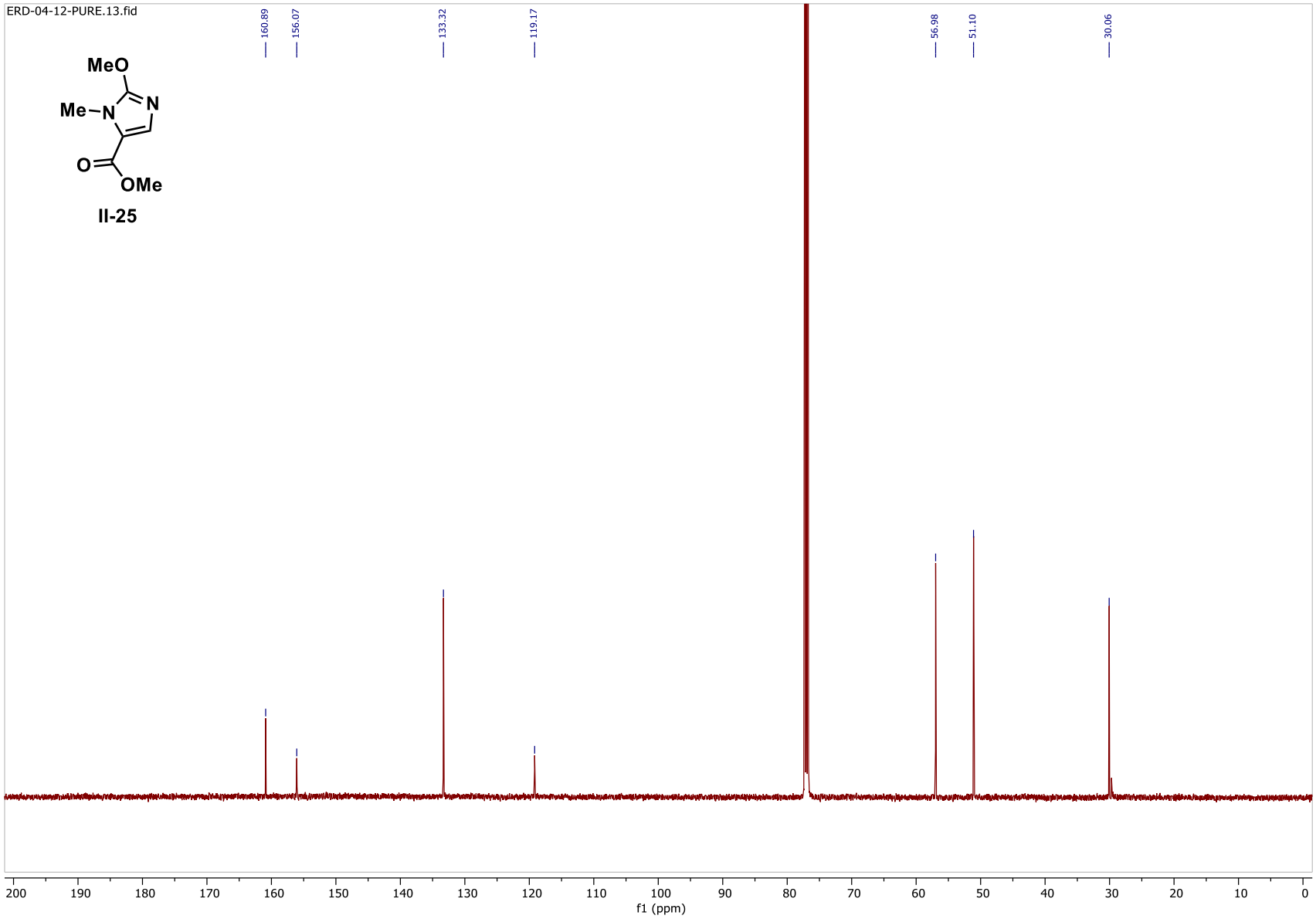

Figure 2.49. ^{1}H NMR of compound **II-26** (500 MHz, Chloroform-*d*, 23 ℃)

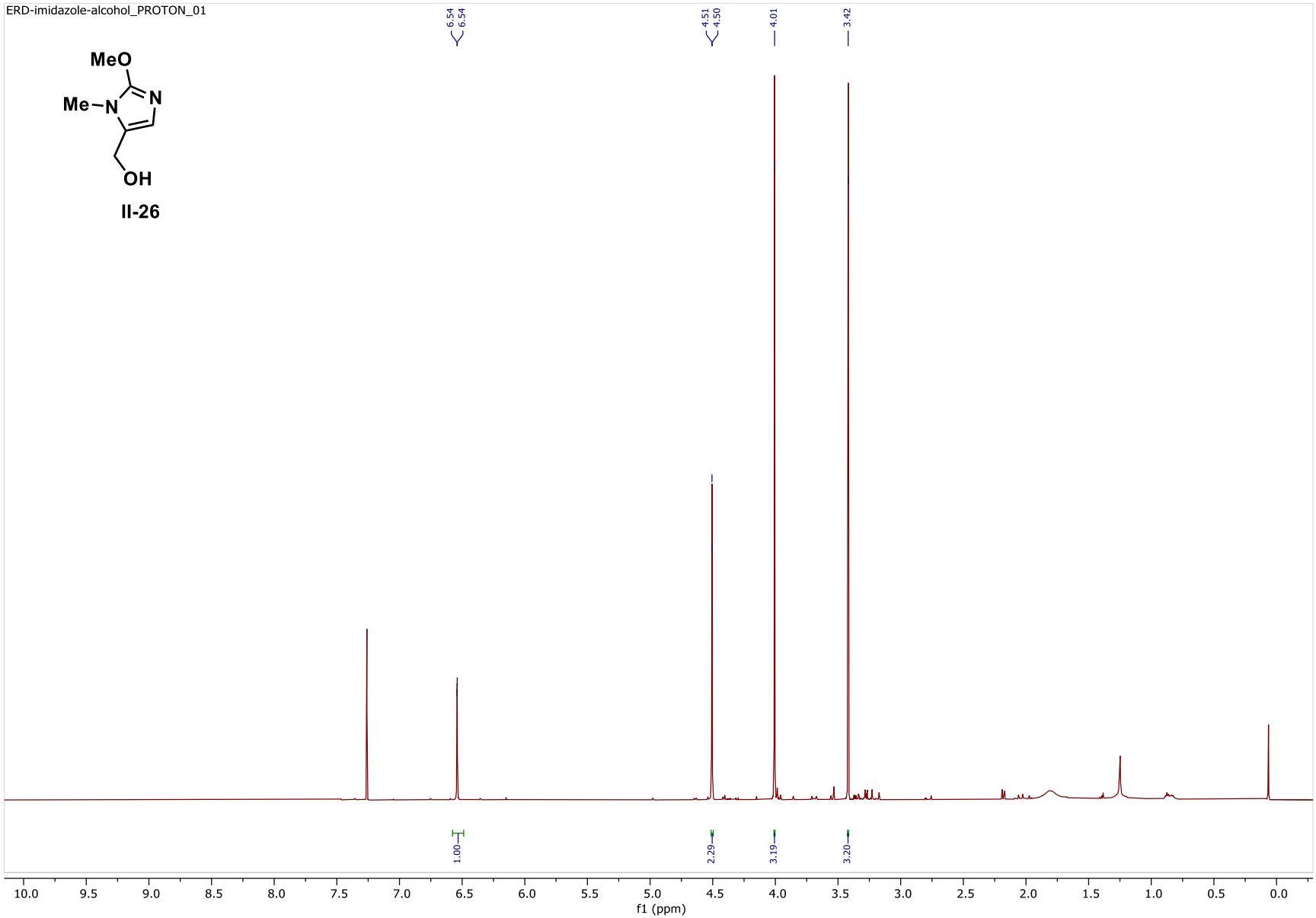

Figure 2.50. ^{13}C NMR of compound **II-26** (126 MHz, Chloroform-*d*, 23 ℃)

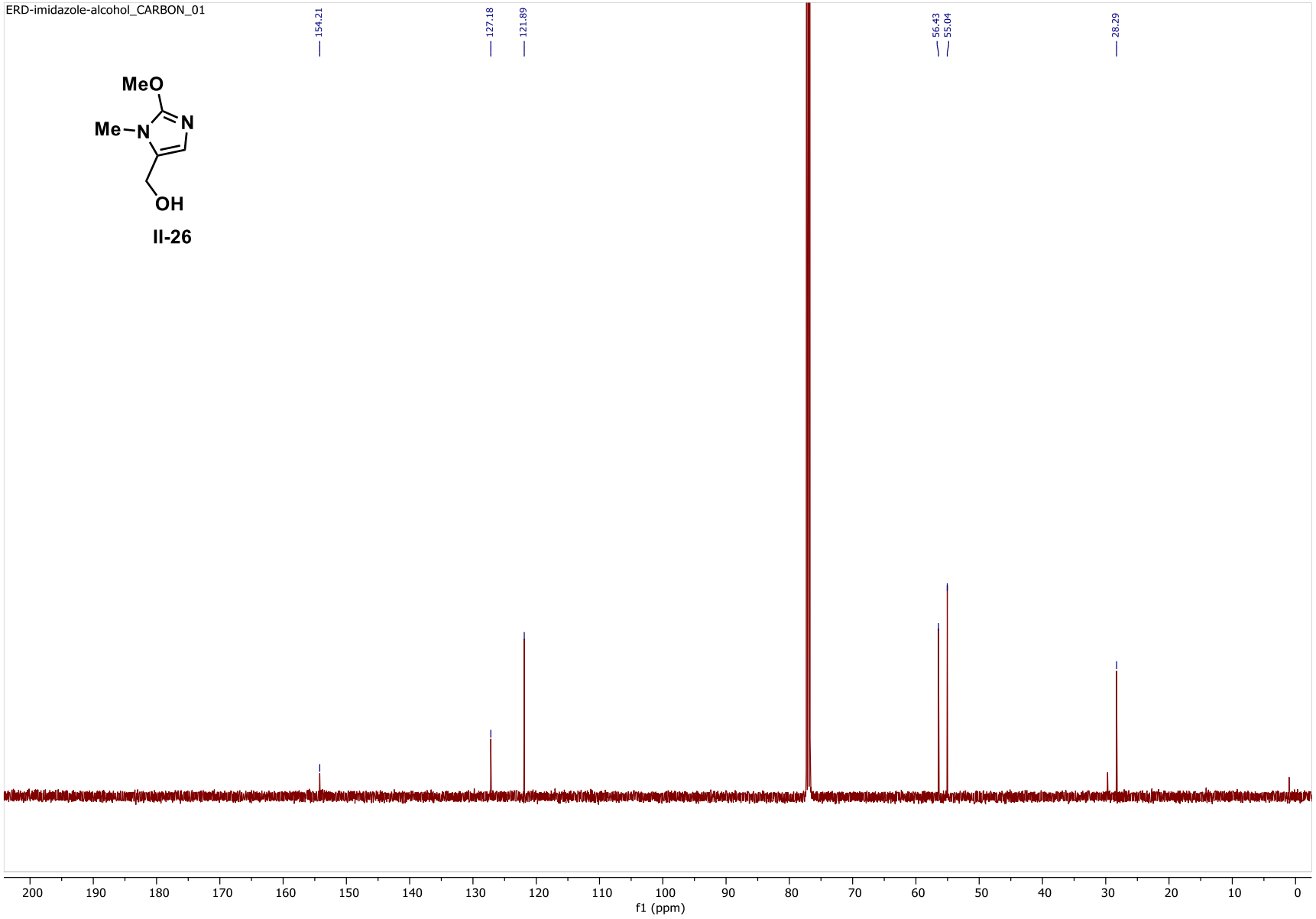

Figure 2.51. ^{1}H NMR of compound **II-27** (500 MHz, Chloroform-*d*, 23 ℃)

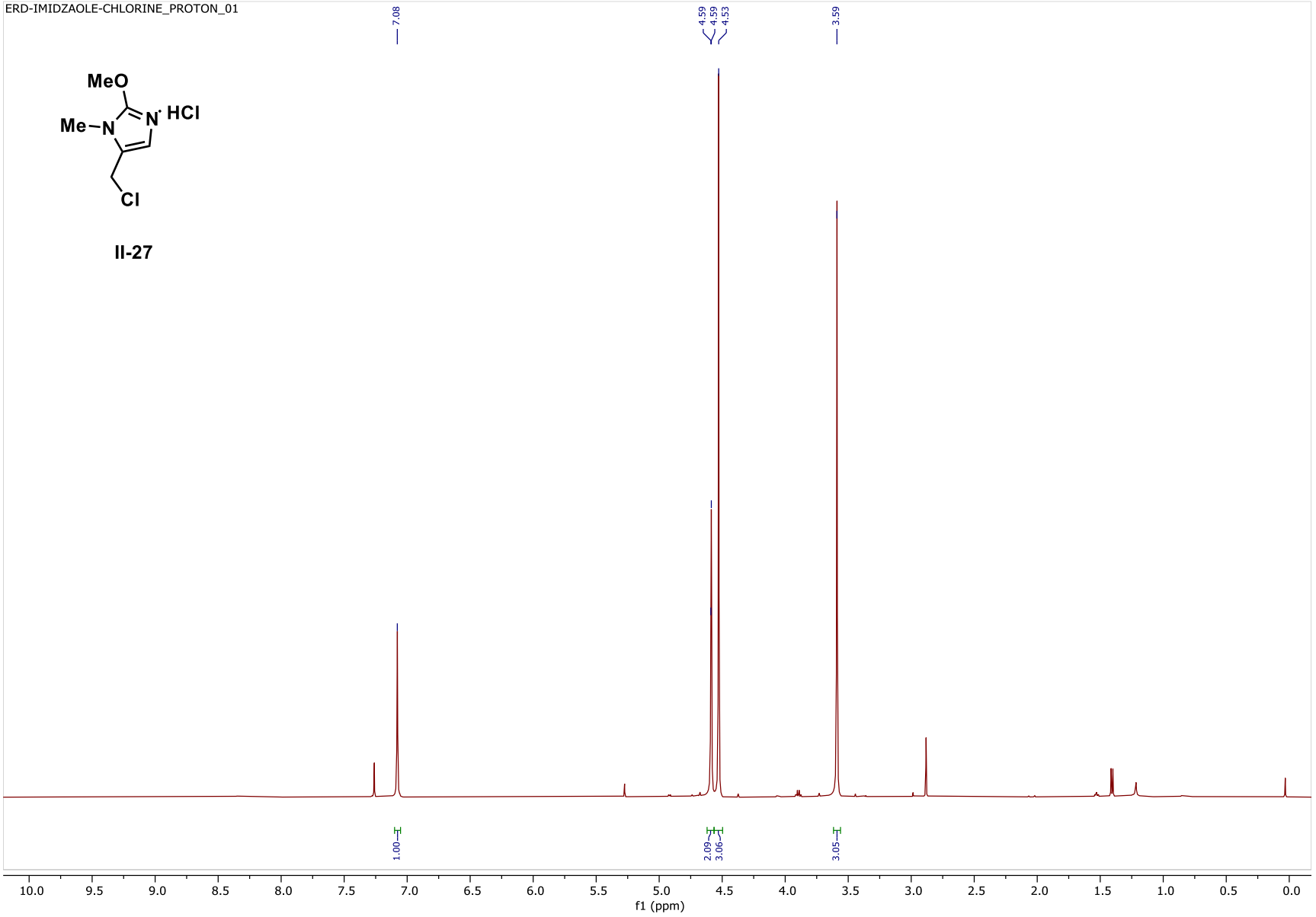

Figure 2.52. ^{13}C NMR of compound **II-27** (126 MHz, Chloroform-*d*, 23 ℃)

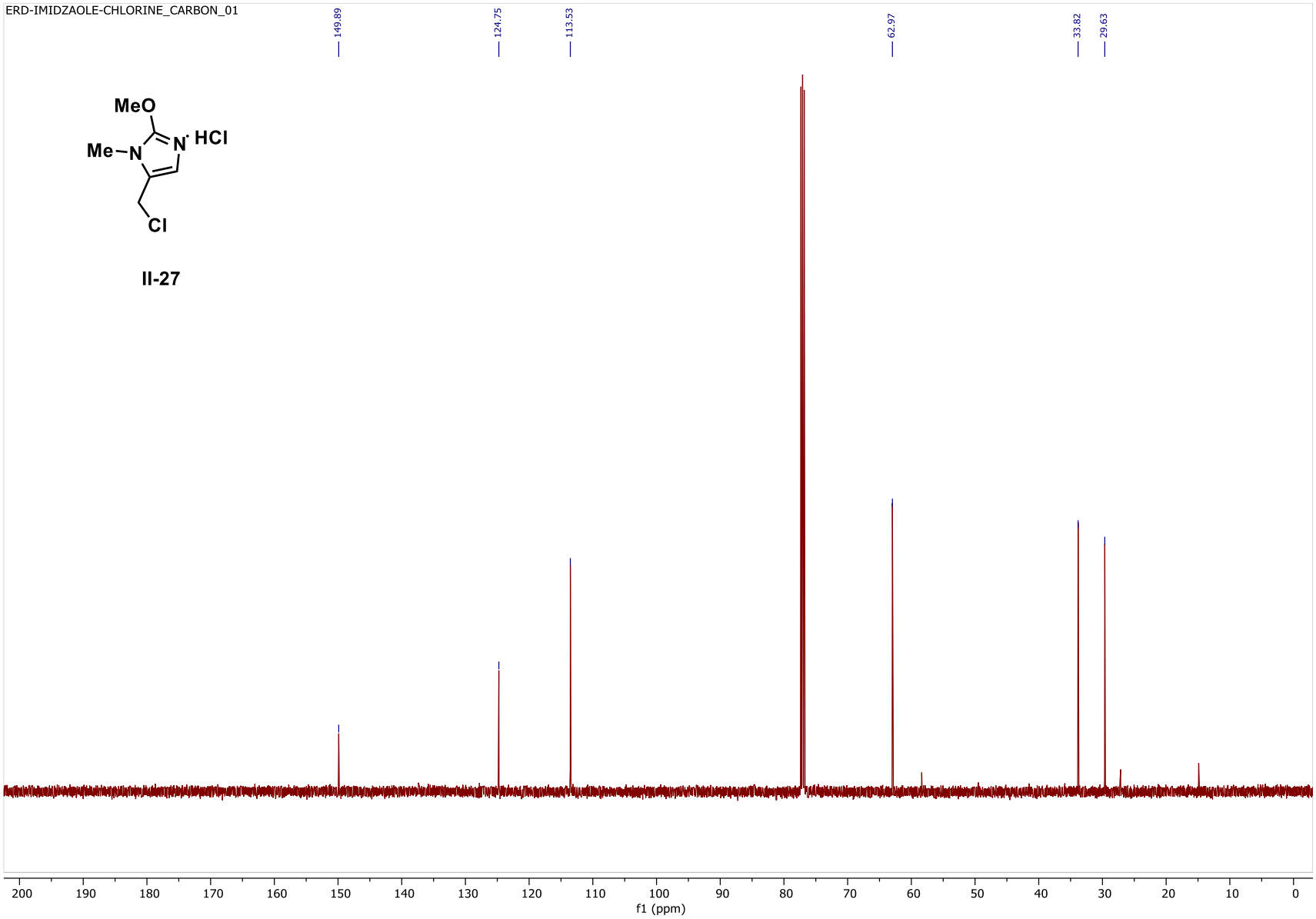

Figure 2.53. ^{1}H NMR of compound **II-23** (500 MHz, Chloroform-*d*, 23 ℃)

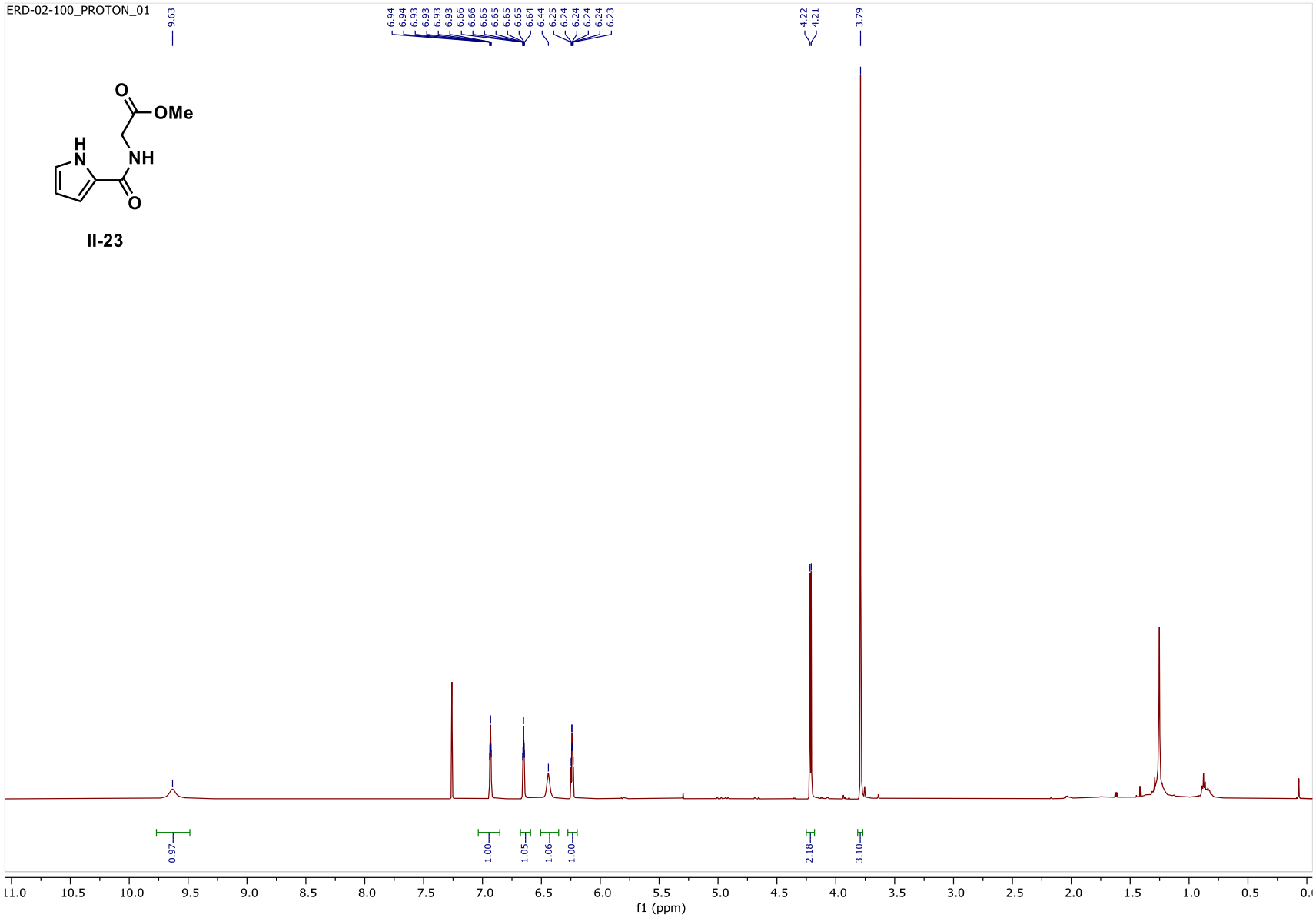

Figure 2.54. ^{13}C NMR of compound **II-23** (126 MHz, Chloroform-*d*, 23 ℃)

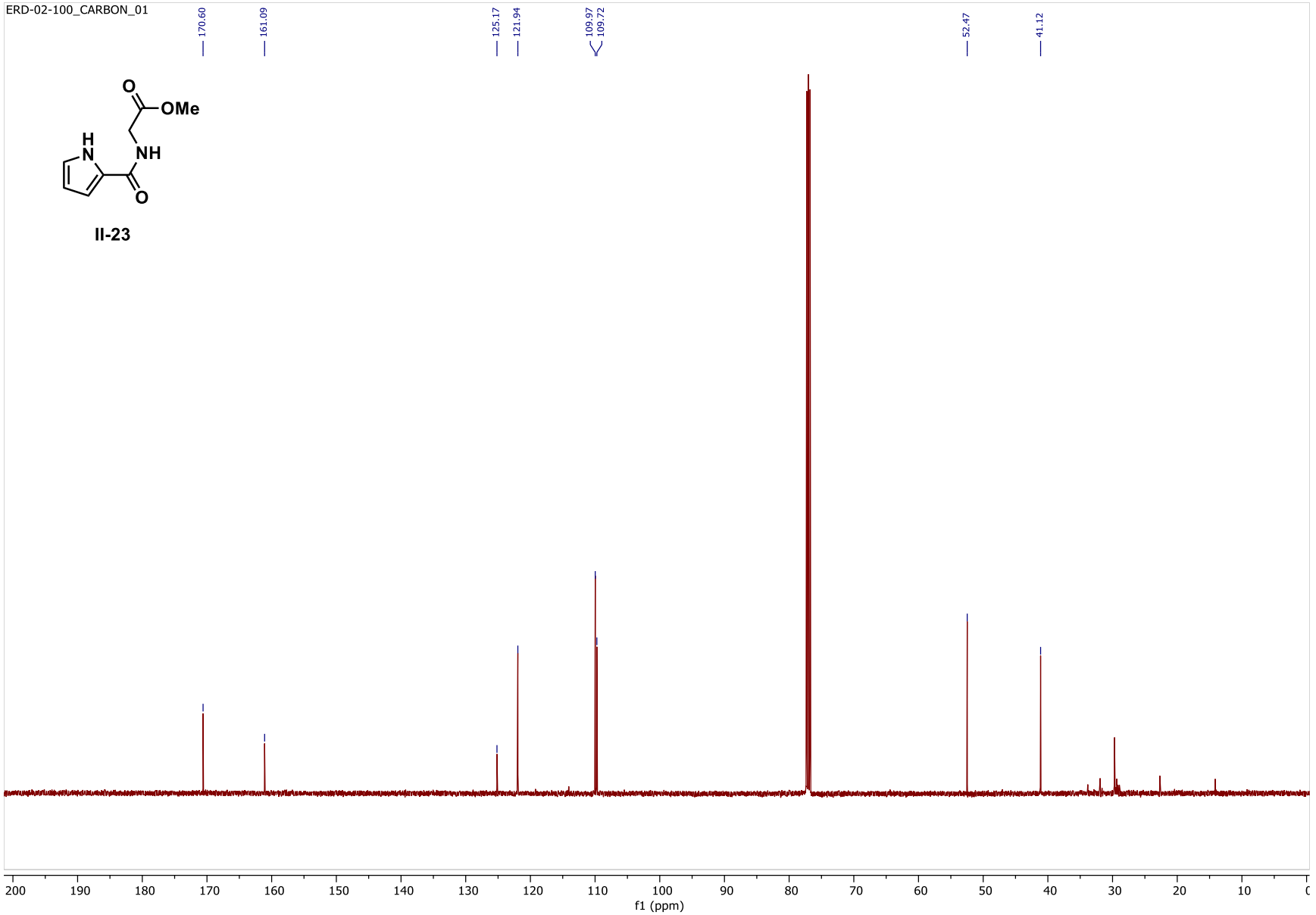

Figure 2.55. ^{1}H NMR of compound **II-28** (500 MHz, DMSO-d_6, 23 ℃)

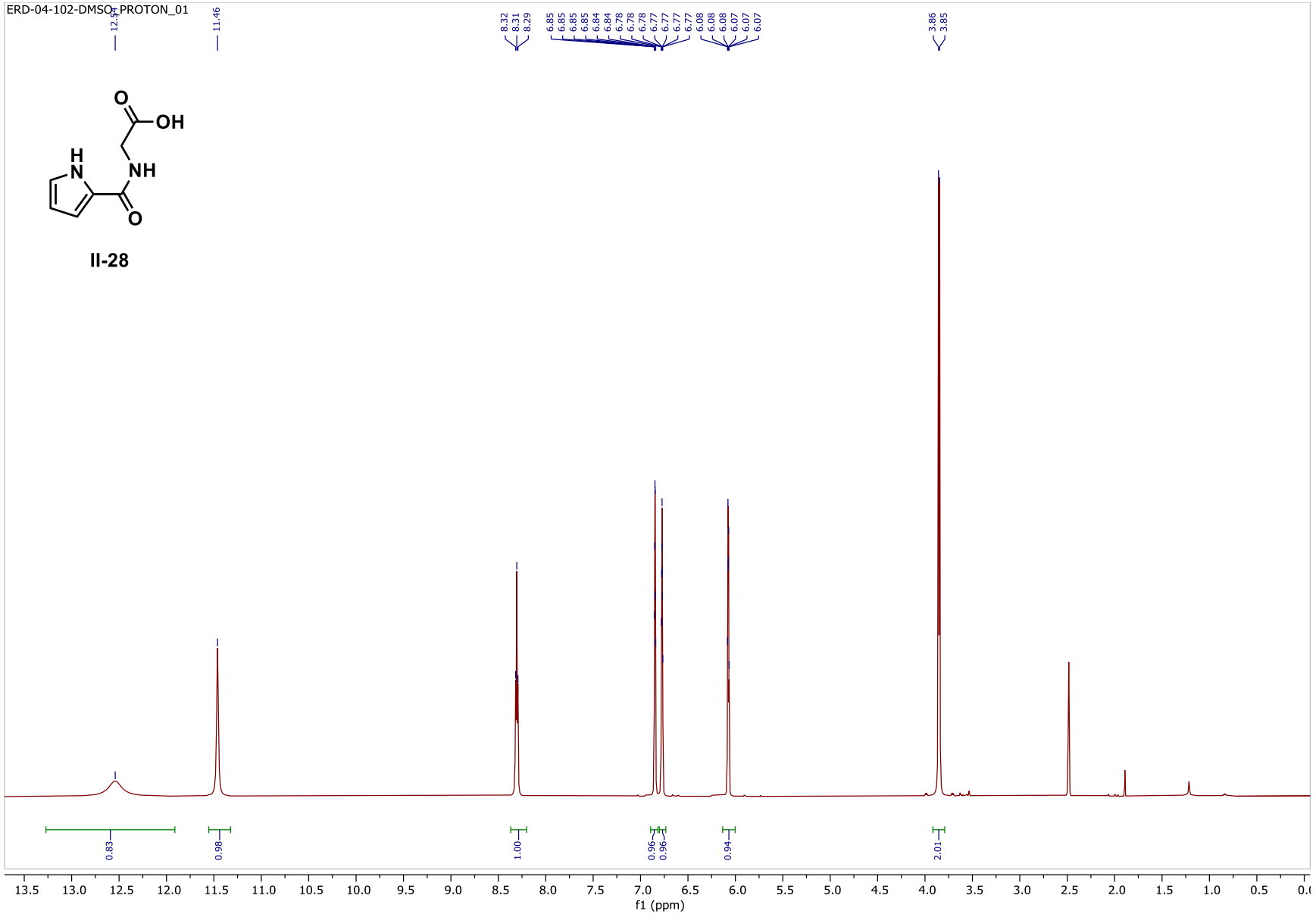

Figure 2.56. ^{13}C NMR of compound **II-28** (126 MHz, DMSO-d_6, 23 ℃)

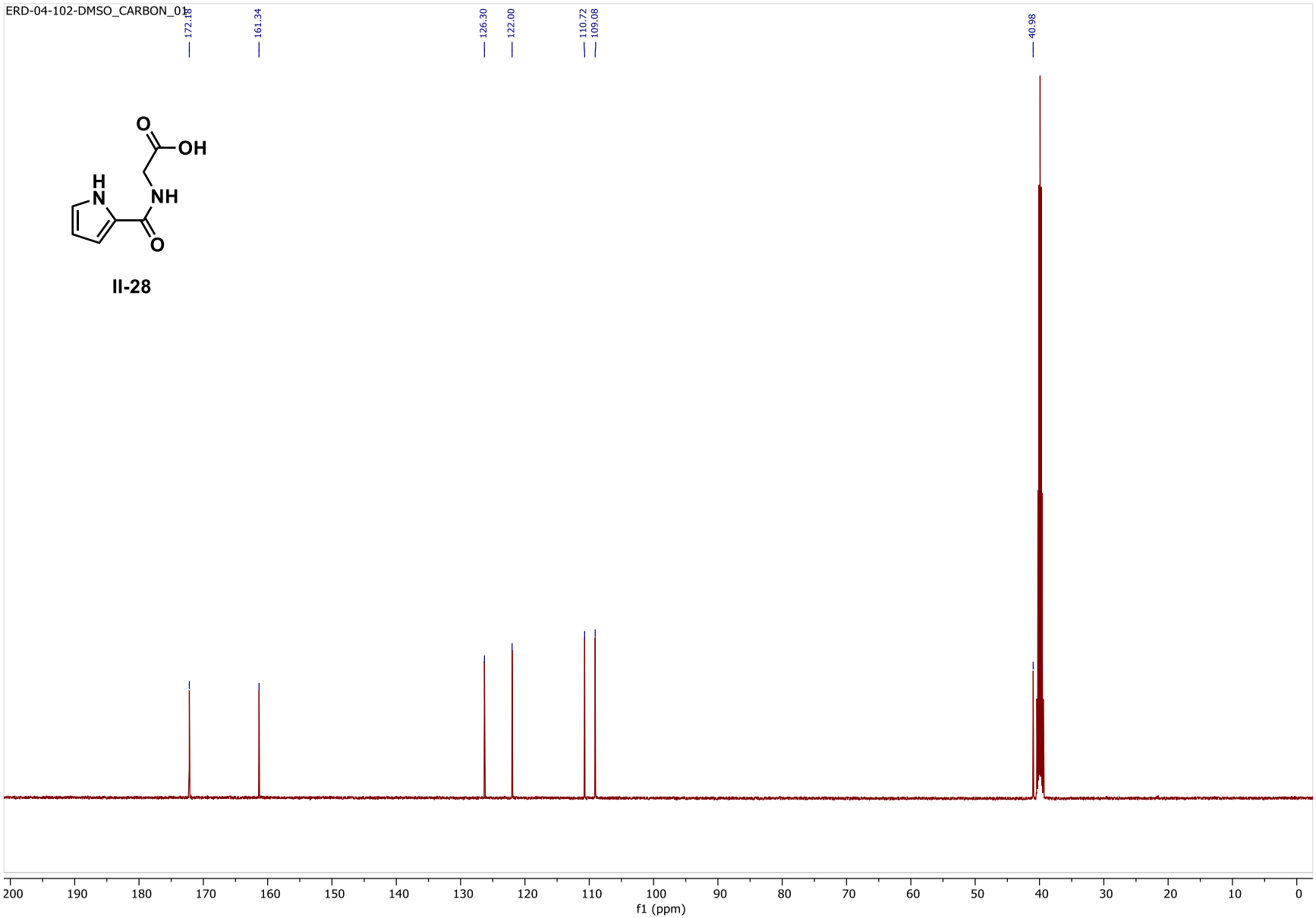

Figure 2.57. ^{1}H NMR of compound **II-22** (500 MHz, DMSO-d_6, 23 ℃)

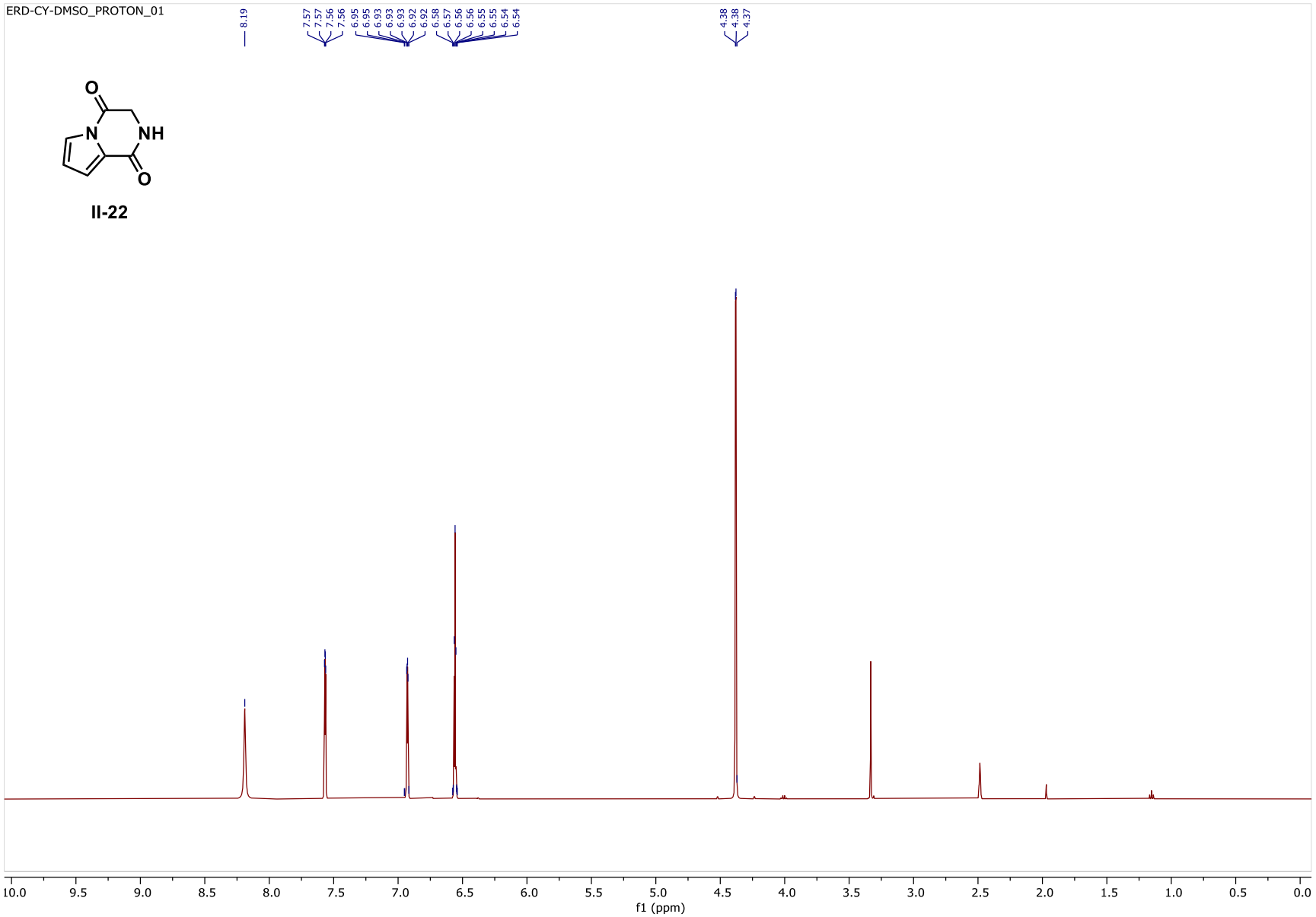

Figure 2.58. ^{13}C NMR of compound **II-22** (126 MHz, DMSO-d_6, 23℃)

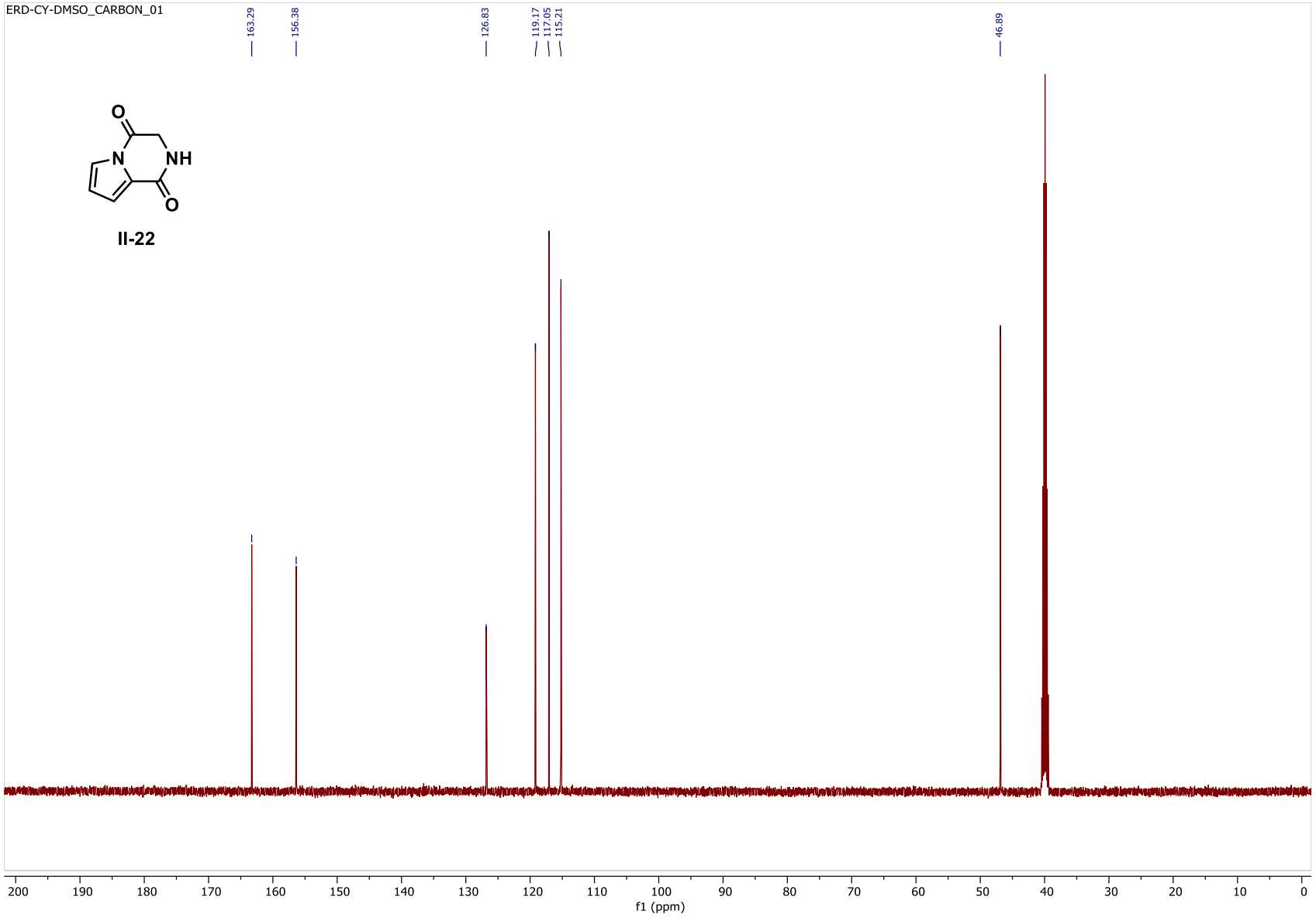

Figure 2.59. ^{1}H NMR of compound **II-30** (500 MHz, Chloroform-*d*, 23 ℃)

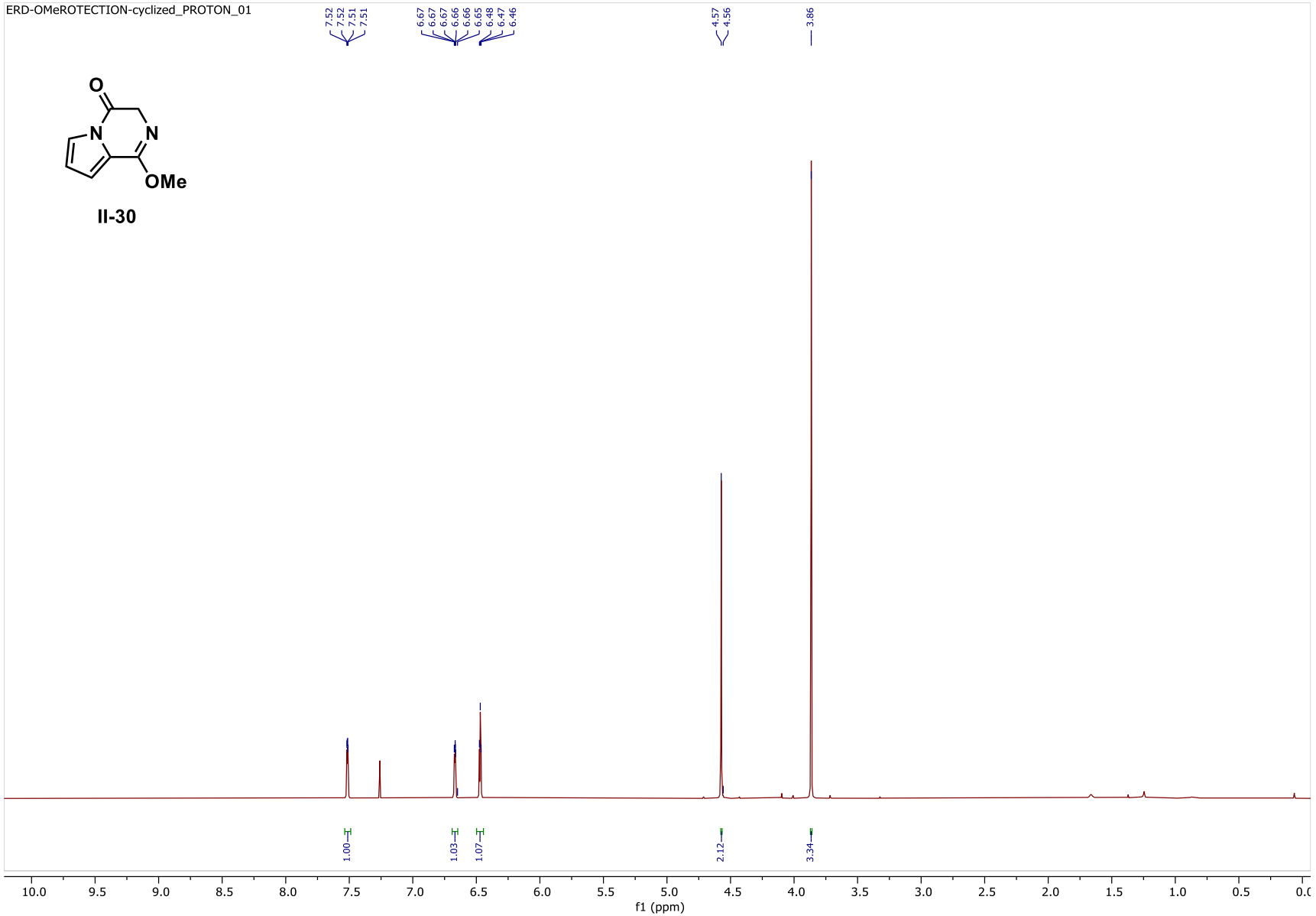

Figure 2.60. ^{13}C NMR of compound **II-30** (126 MHz, Chloroform-*d*, 23 ℃)

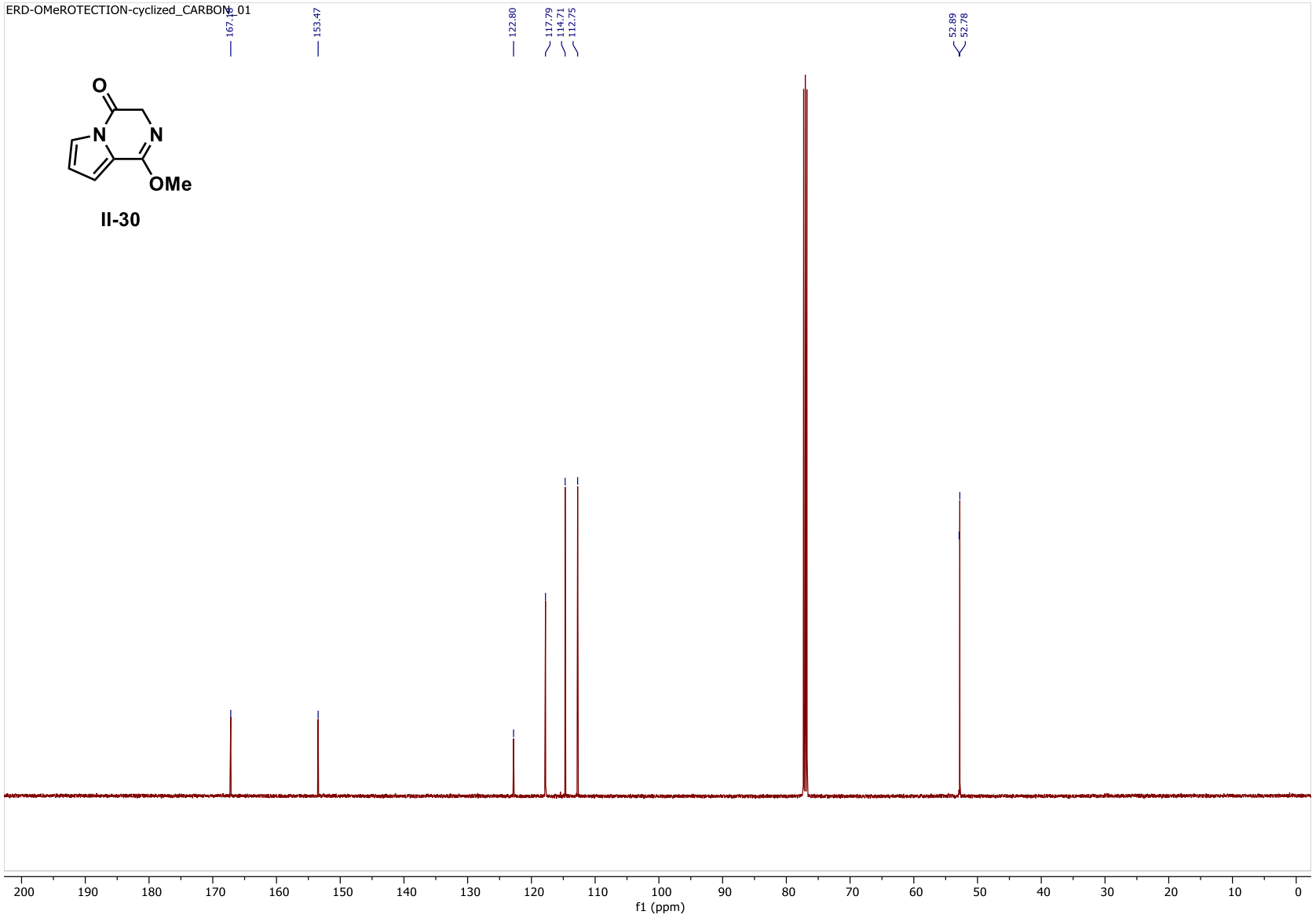

Figure 2.61. ^{1}H NMR of compound **II-31** (500 MHz, Chloroform-*d*, 23 ℃)

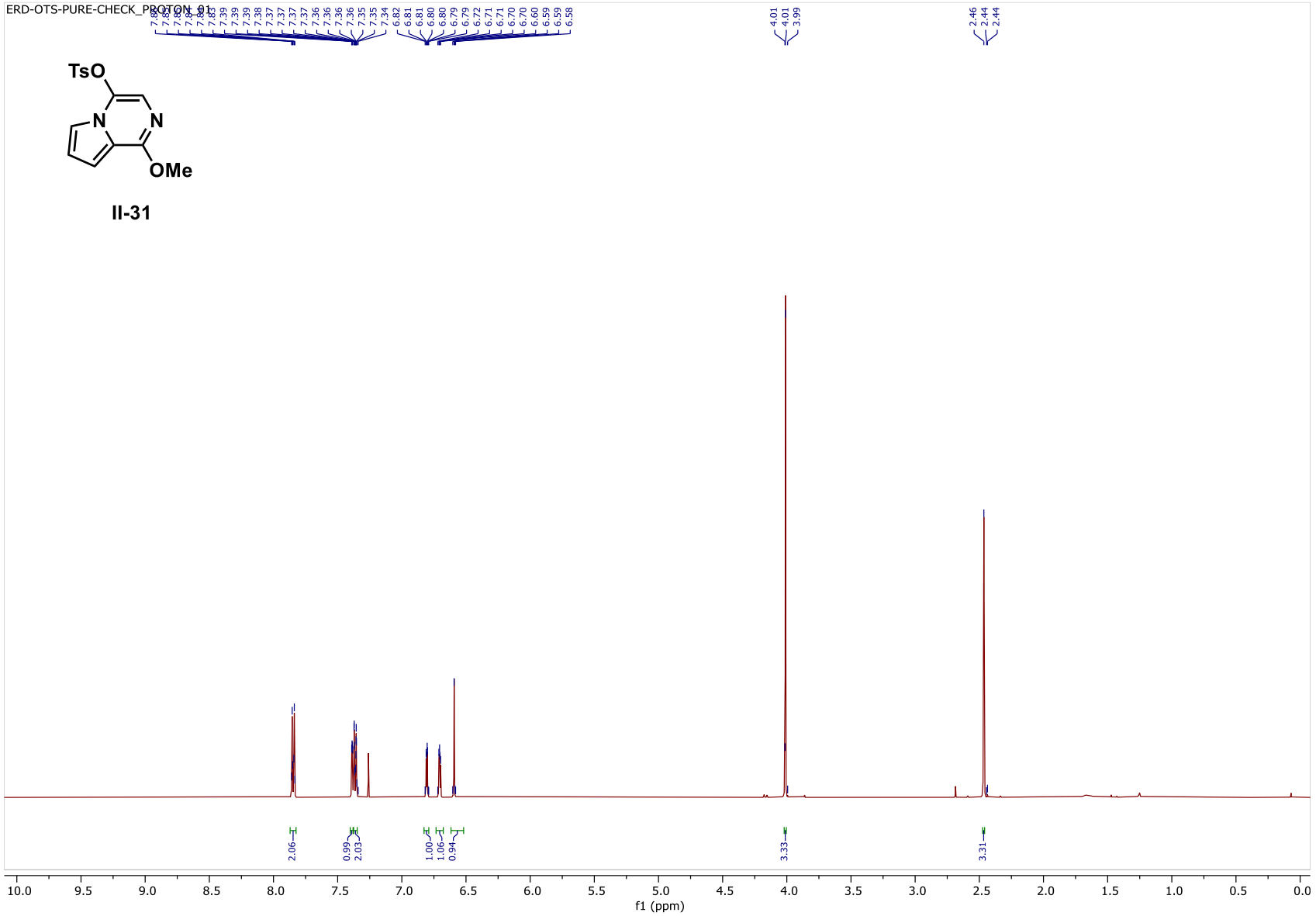

Figure 2.62. ^{13}C NMR of compound **II-31** (126 MHz, Chloroform-*d*, 23 ℃)

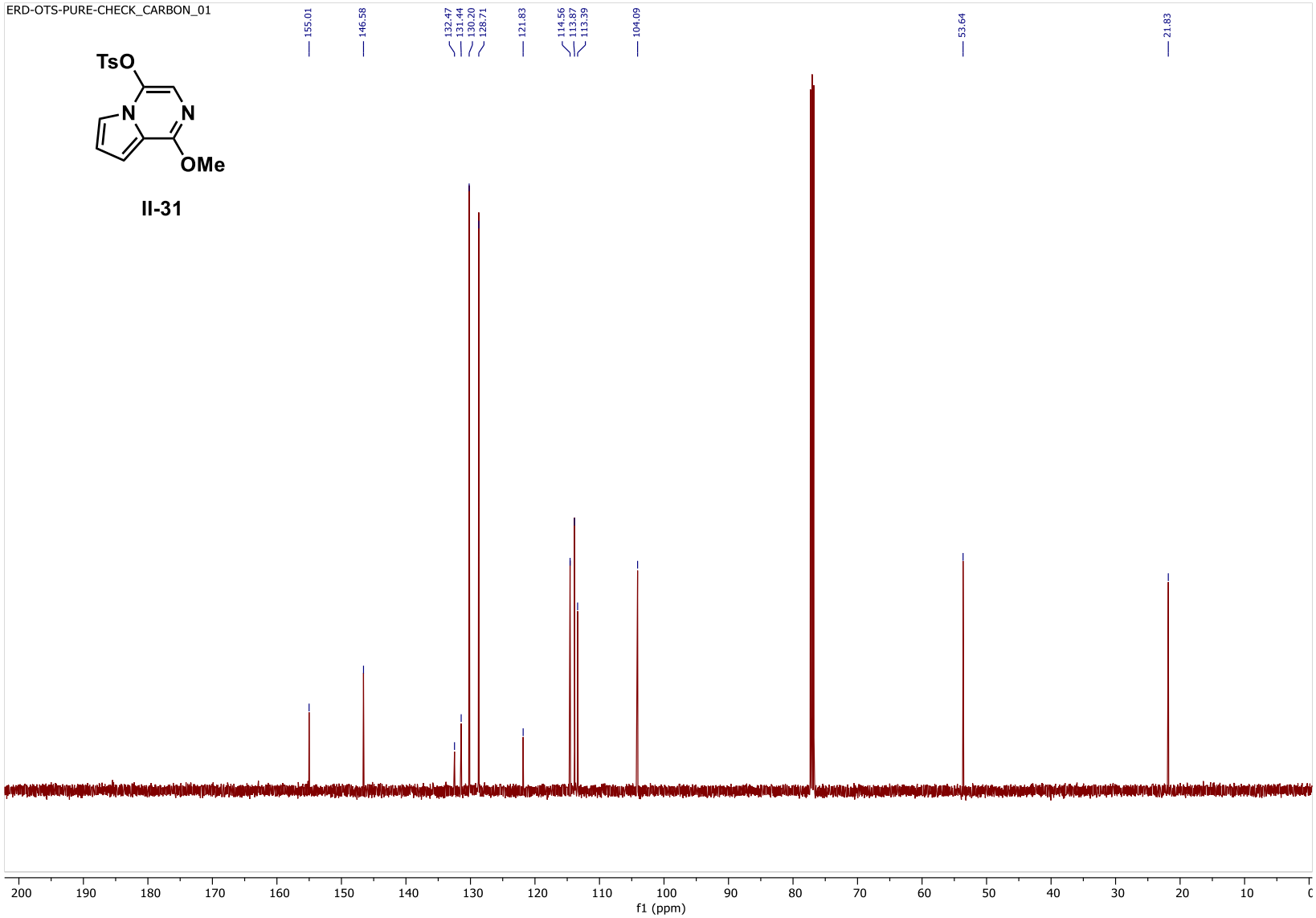

Figure 2.63. ^{1}H NMR of compound **II-33** (500 MHz, Chloroform-*d*, 23 ℃)

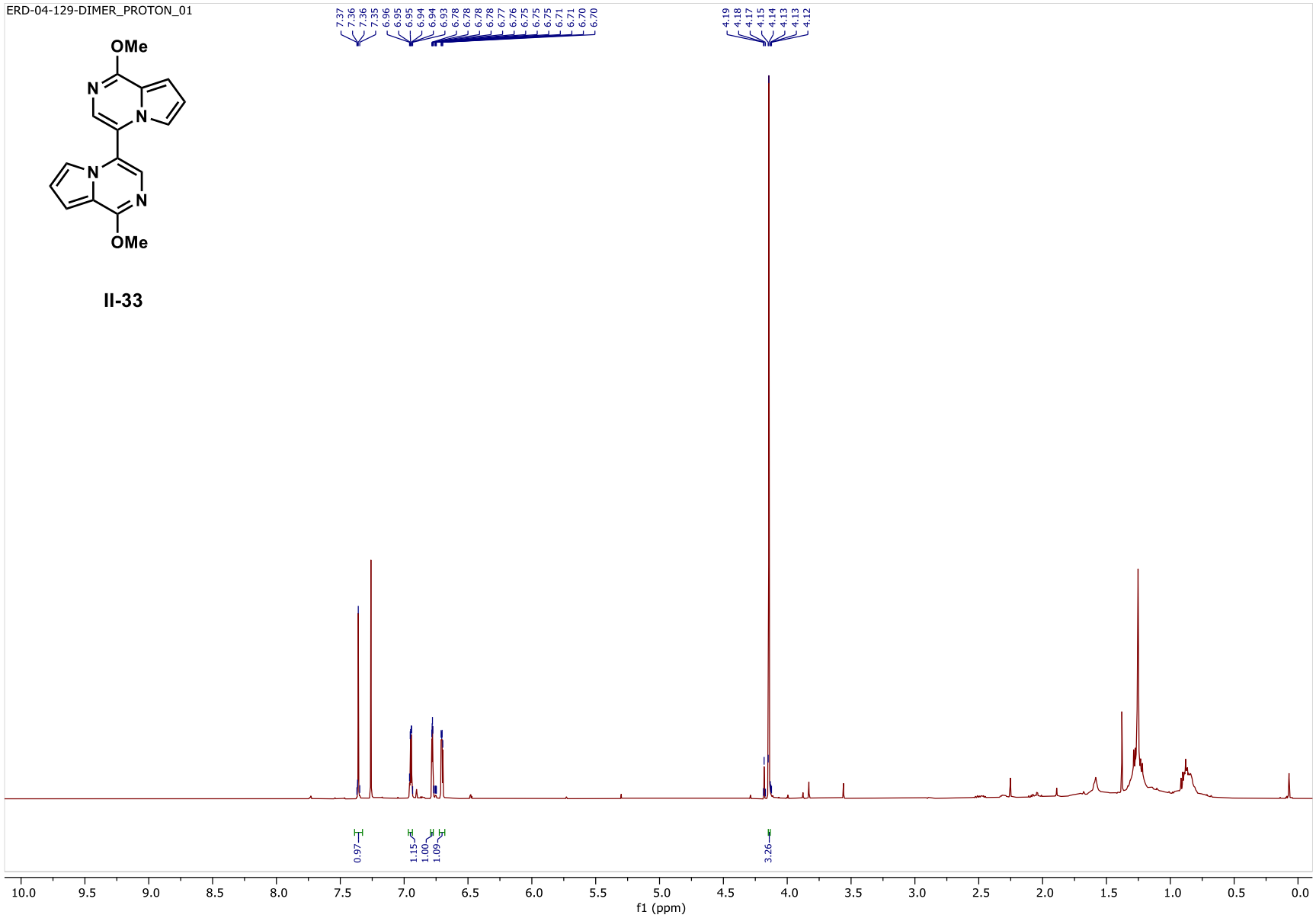

Figure 2.64. ^{13}C NMR of compound **II-33** (126 MHz, Chloroform-*d*, 23 ℃)

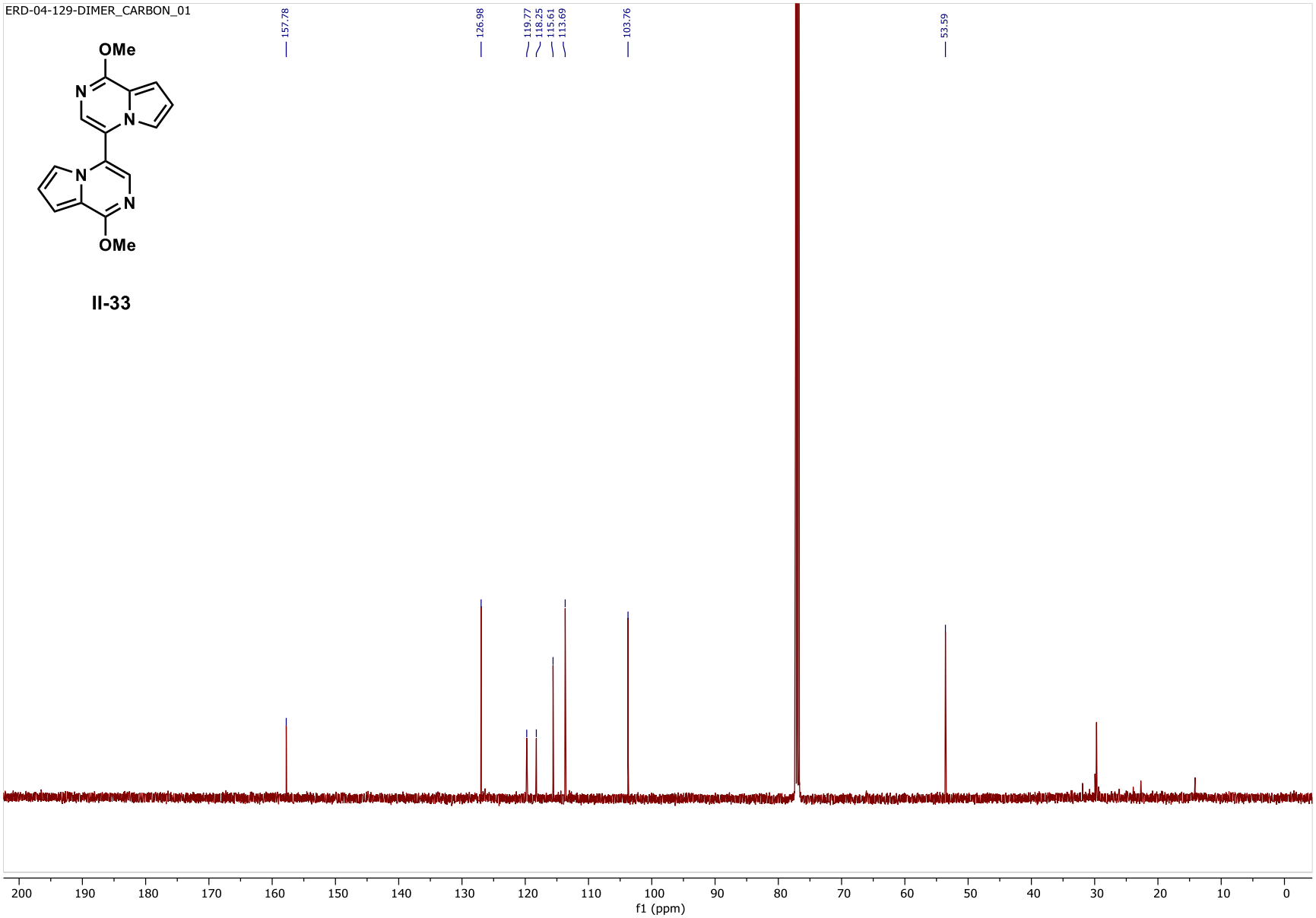

Figure 2.65. ^{1}H NMR of compound **II-32** (500 MHz, Chloroform-*d*, 23 ℃)

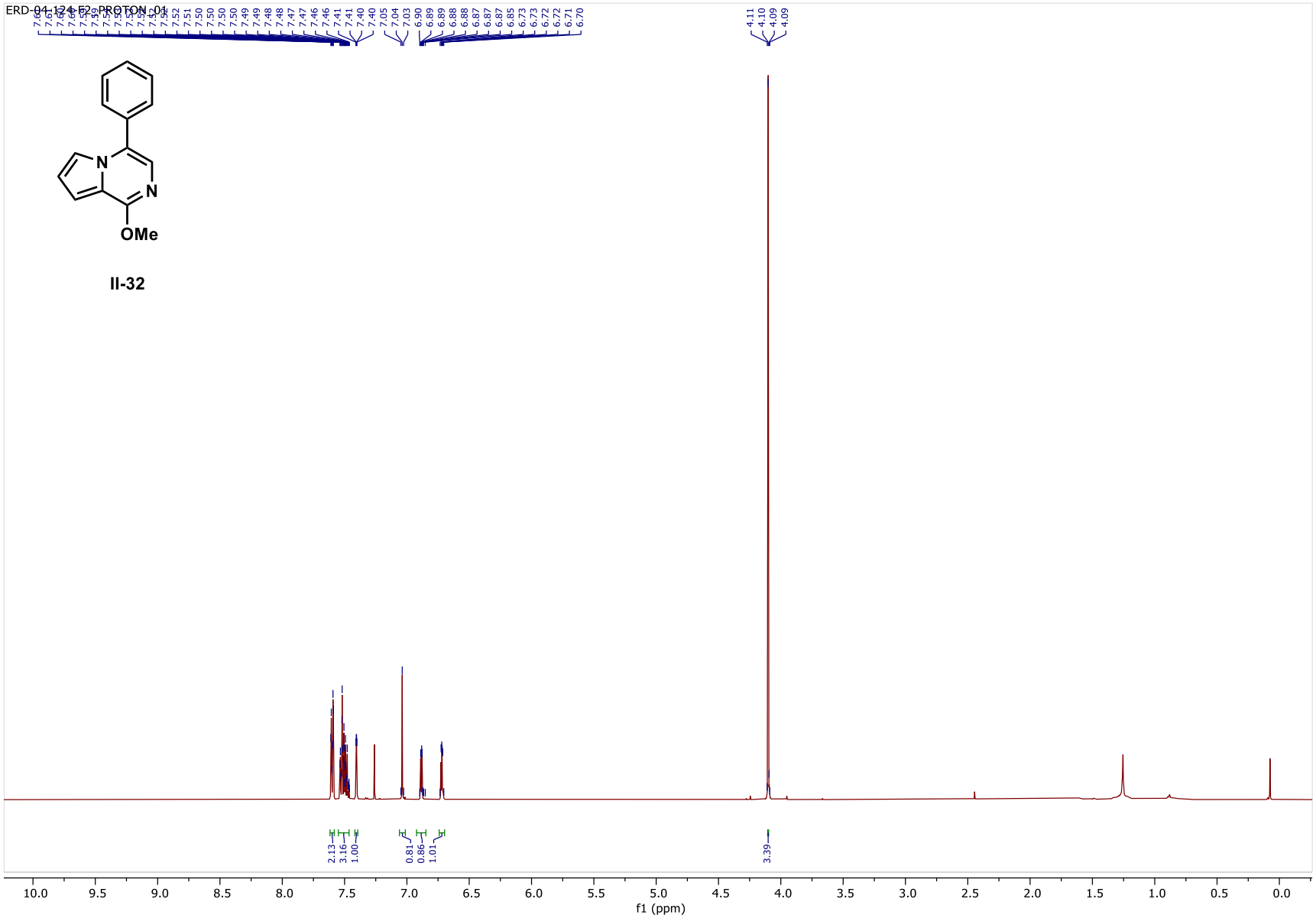

Figure 2.66. ^{13}C NMR of compound **II-32** (126 MHz, Chloroform-*d*, 23 ℃)

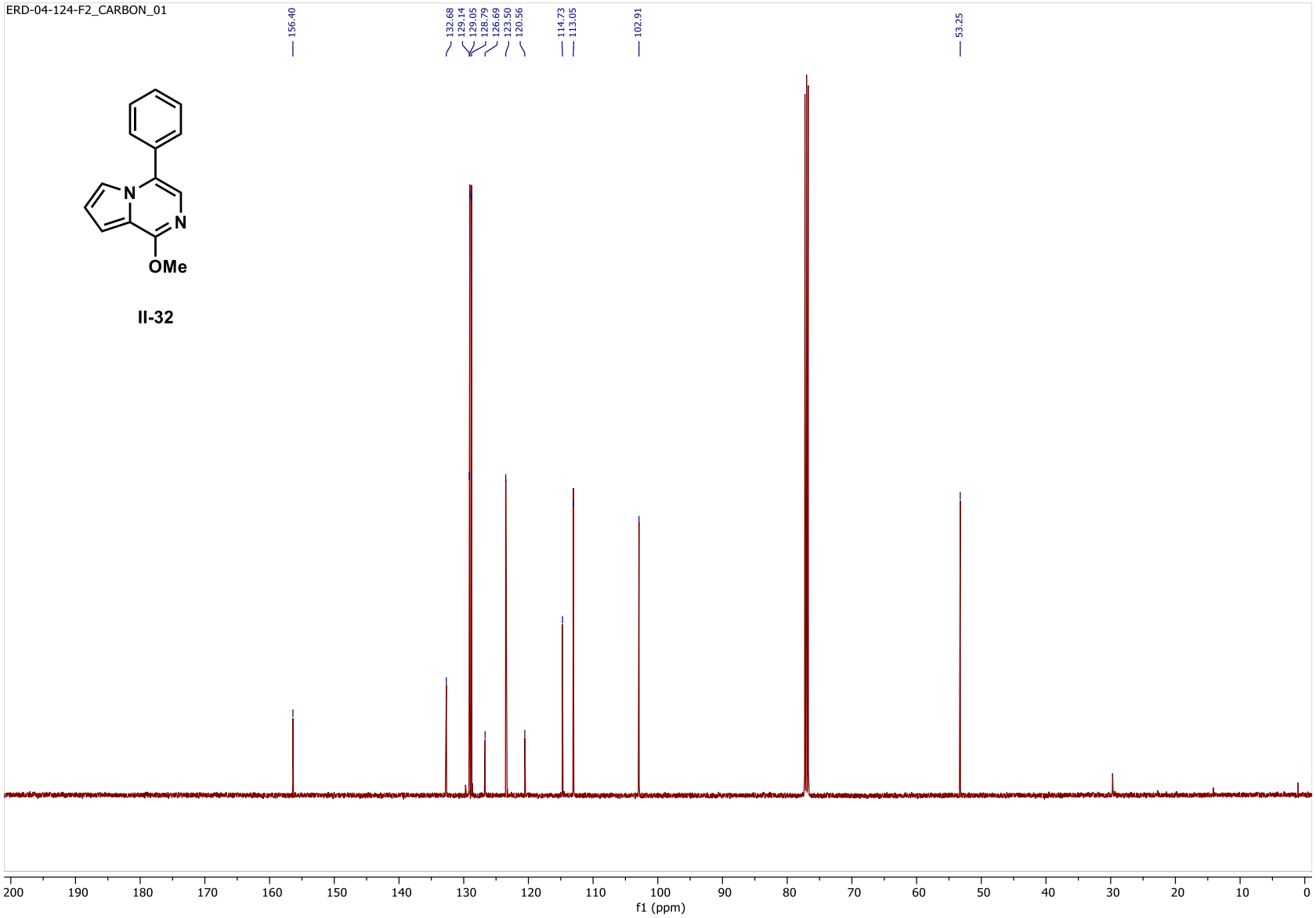

Chapter 3 – Mechanistic Investigations of the Uncatalyzed Chlorocyclization of 4-phenyl-4-pentenoic acid

3.1. Introduction

Electrophilic halofunctionalization reactions are a well-known, long-time researched organic transformation in organic synthesis. Generally, the mechanism that is typically invoked is a stepwise addition reaction , which involves alkene capture of an electrophilic halogen, leading to the bridged, cyclic halirenium intermediate. Nucleophilic attack of the latter intermediate leads to the product (Figure 3.1).[72] The nucleophile in this scenario can be halides, water, alcohols, amines, carboxylates, or other nucleophilic centers.

Figure 3.1. Commonly Depicted Mechanism of Electrophilic Addition to Alkene (Ad_E2)

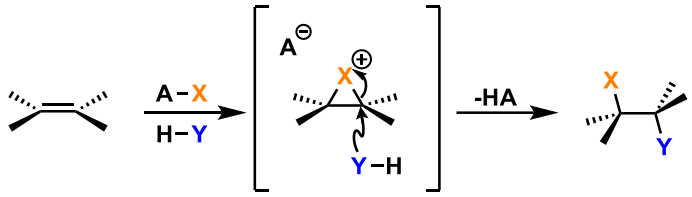

This transformation can introduce multiple, complex functionalities with a single operation showcasing its general utility. Previous reports by our own group, as well as others, have demonstrated the applicability of this versatile tool to provide access to numerous scaffolds, including oxazolidinones, oxazolines, dihydrooxazines, lactones, and a variety of other cyclic and acyclic motifs.[52,73,74] Research from our group has found that the cinchona alkaloid, $(DHQD)_2PHAL$, is particularly effective at catalyzing chlorocyclization of substrates such as unsaturated amides, carbamates, naphthols, and

carboxylic acids in good yields and high enantio- and diastereoselectivity.[48, 75, 76] Despite the growth seen in the halofunctionalization field, mechanistic investigations of these reactions are lacking. A recent mechanistic study from our lab explores how the catalyst guides the enantioselective cyclization by templating the ring closure though hydrogen bonding and van der Waals interactions.[77] However, much less attention has been given to understanding the intrinsic nature and stereopreferences of these reactions in the absence of a catalyst. Having a full analysis of the reaction path and stereochemical control element is essential to providing mechanistic reference points for the analysis and design of stereocontrolled pathways for halofunctionalization reactions of alkenes. Therefore, it is essential to understand the intrinsic diastereoselectivities of the uncatalyzed chlorocylization of carboxylic acid **III-1-D**.

Under the uncatalyzed reaction conditions, the chlorolactonization occurs sluggishly to provide an *anti:syn* product ratio of 64:36 (Scheme 3.1).[78] The formation of both these isomers in appreciable quantities suggests that at least two different mechanistic pathways could be leading to the different isomers.

Scheme 3.1. Uncatalyzed chlorocyclization of **III-1-D**. Enantiomeric pairs were eliminated for clarity

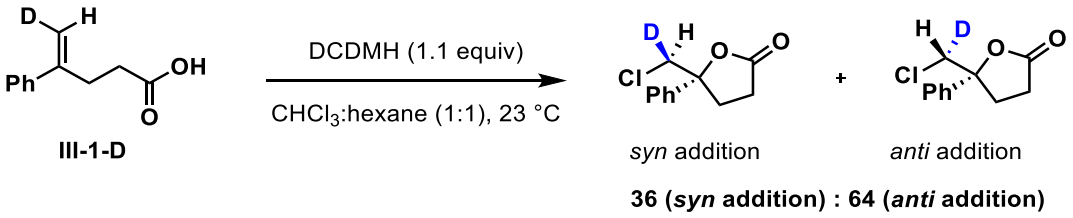

Significant formation of the *syn*-isomer may indicate evidence that these reactions do not simply proceed via the cyclic chloriranium ion, which would solely produce the *anti*-

isomer. For instance, in the *syn*-chlorolactonization product, the oxygen of the carboxylic acid would add to the same face of the olefin as chlorenium ion delivery. This is difficult to explain using the classical mechanistic model of addition *via* a cyclic halonium intermediate, and thus obviates the cyclic halonium ion intermediate. To elucidate the mechanism that leads to the *syn*- and *anti*-isomer, concentration, and solvent studies, as well as a Variable Time Normalization Analysis kinetic study will be utilized.

3.2. Description of Variable Time Normalization Analysis Method (VTNA)

Beforehand, a description of Variable Time Normalization Analysis (VTNA) is discussed. VTNA is a modern method for chemical kinetic analysis. It requires the ability to correlate concentration as a function of time, thus NMR and React-IR are well suited techniques to accomplish this. Ultimately, different reaction concentration profiles on the *same* reaction are measured to determine the order of reaction components.[79,80,81] This method is beneficial because it allows for minimal time for data processing, uses modern reaction monitoring techniques such as NMR, as well as directly analyzing the orders without determining the rate profiles of each reaction. Importantly, the analysis performed under the reaction conditions without the need for exaggerated concentrations, thus enabling analysis of factors at relevant reaction conditions. VTNA also enables use of data throughout the whole reaction as opposed to the small initial rate analysis. Continuing, this method is thought to be of particular value to those who are not experts in kinetics and need to determine the orders of reactions for mechanistic analysis.

For example, let's use the following reaction:

$$A + B \rightarrow C + D$$

From this reaction, the following rate equation can be deduced:

$$rate = -\frac{dA}{dt} = k[A]^{\alpha}[B]^{\beta} \qquad \text{equation 1}$$

Upon rearranging, and taken into the integral form so every variable is in the form of concentration or time leads to the following equation:

$$\int_{A_0}^{A} -\frac{d[A]}{[A]^{\alpha}} = \int_{0}^{t_n} [B]^{\beta} dt \qquad \text{equation 2}$$

While this a relatively complex equation in the integral form, the left side of the equation reveals that the normalized axis for different reaction profiles provides only a function of A, thus the following equation is shown below that sets the right side equal to the function of A :

$$f(A) = \int_0^{t_n} [B]^{\beta} dt \qquad \text{equation 3}$$

Lastly, using the trapezoid approximation to simplify the above equation leads to:

$$f(A) = \int_0^{t_n} [B]^{\beta} dt = \sum \left(\frac{[B]_i + [B]_{i-1}}{2}\right)^{\beta} (t_i - t_{i-1}) \qquad \text{equation 4}$$

This reduces the integral function to a summation and simplifies the equation so that it can be easily used if the concentration of B and time is known. Since the summation expression is rather large, it will be abbreviated as follows:

$$\sum \left(\frac{[B]_i + [B]_{i-1}}{2}\right)^{\beta} (t_i - t_{i-1}) = \sum [B]^{\beta} \Delta t \ \ (abbreviated\ form) \qquad \text{equation 5}$$

This above equation normalizes the time between each set of data points by the average concentration of the points, and therefore the effect of concentration on the reactant being studied has been normalized from the time axis. In order to determine the order of A and B using VTNA at least two experiments with different excess values are studied (Table 3.1). A different excess experiment is when the concentration of one reactant is increased, hence the name of the experiments being “different excess experiments”. The aim of different excess experiments is to elucidate the effect of one of the reactants by comparing the reaction profiles of each, where identical reaction conditions are present except for the concentration of the reactant that is analyzed.

Table 3.1. Set of different excess experiments

Exp	[A] (M)	[B] (M)
1	4	5
2	4	6

For example, in reaction 1 and 2, plotting [A] vs. time leads to a non-overlaying plot due to the change of concentration in B (Figure 3.2a). However, different excess experiments when plotted as [A] vs $\sum [B]^{\beta} \Delta t$ should yield overlaying plots when the B in equation $\sum [B]^{\beta} \Delta t$ is raised to the correct order (β), as a result providing the reaction order of B. This analysis is shown in Figure 3.2b, Figure 3.2c, and Figure 3.2d. As the value of β is changed, this shows an effect on the graphs, and ultimately leads to overlaying plots when β is equal to 2, therefore, indicating that the order of B is 2.

Figure 3.2. Example of VTNA of different excess experiments

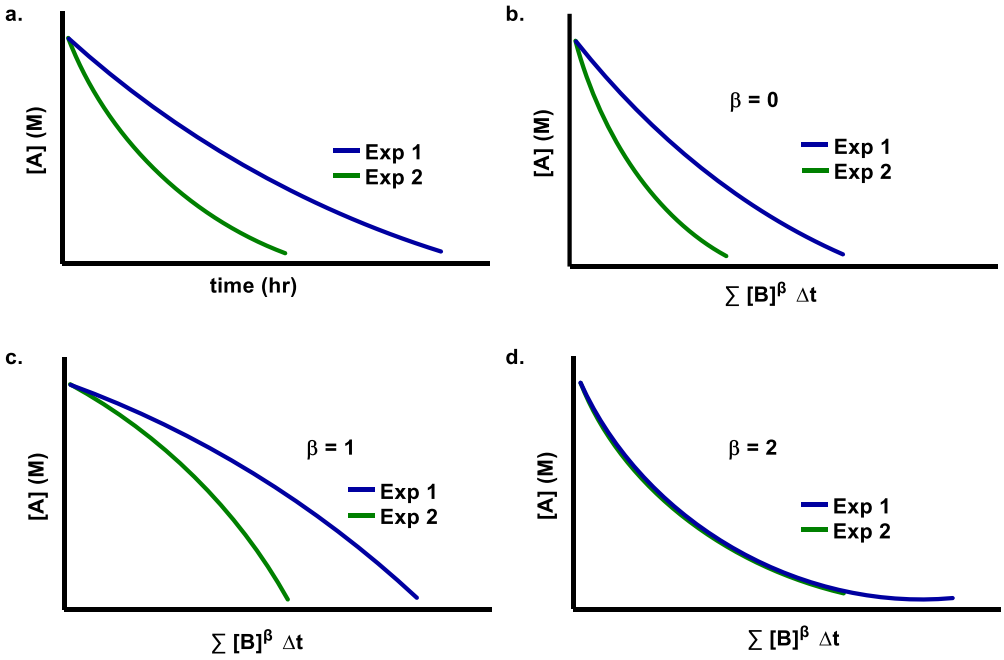

The normalization of the time scale can be applied to as many reaction components that is desired as long as their concentration can be measured, either directly or indirectly. Thus, in the above example, the order of A could be elucidated by plotting $\sum [A]^{\alpha} \Delta t$ against B, or even C or D (products). It is possible to apply time normalization to all of the components in the reaction, and when all of the changing kinetic driving forces are raised to the correct power, this will cause the reaction profiles to become a straight line. VTNA will be used later in this chapter to determine the reaction orders of the reagents in the uncatalyzed chlorocyclization of alkenoic acids.

The reader is referred to a great resource that details all of the different ways to study the kinetics of reactions, as well as a general example of using VTNA to determine the reaction orders of the components in a reaction.[82]

3.3. Background

One of the very first catalytic, asymmetric halofunctionalization reactions was published in 2010 by Borhan and coworkers, which catalyzed a 1,1-disubstitiuted alkene to undergo chlorocyclization to provide a lactone (Figure 3.3a).[75] Using a monodeuterated alkene to generate an asymmetric sp^3 center (CDHC) the absolute and relative facial selectivity of the chlorenium (electrophile) and oxygen (nucleophile) addition across the double bond was revealed (Figure 3.3a). Here, the catalyzed reaction of the deuterated carboxylic acid provided primarily *syn*-selectivity with a *syn:anti* ratio of 89:11, obviating the bridging chloronium mechanism that proceeds via the intermediacy of the textbook 3-membered cyclic halirenium ion, which would follow the commonly depicted mechanism (Figure 3.1).[78] However, recent reports have provided an alternative mechanistic route. Borhan and co-workers, as well as Denmark and co-workers, have shown evidence for a one-step concerted Ad_E3-type addition mechanism (Figure 3.3b).[83,84] In this type of addition mechanism, the nucleophile is poised for attack onto the olefin, followed by subsequent capture of a halonium ion. Our recent work has noted that the reaction rate was directly correlated to the nucleophilicity of the internal nucleophile proximal to the alkene. Here, the ability of the nucleophile to activate the alkene pi system to attack the electrophilic halogenating agent points to a concerted Ad_E3-type addition mechanism that can occur in a *syn* or *anti*-fashion.

Figure 3.3. a) Catalytic asymmetric chlorolactonization of alkenoic acid **III-1-D** by DCDMH and mediated by $(DHQD)_2PHAL$. b) one-step, concerted addition pathway

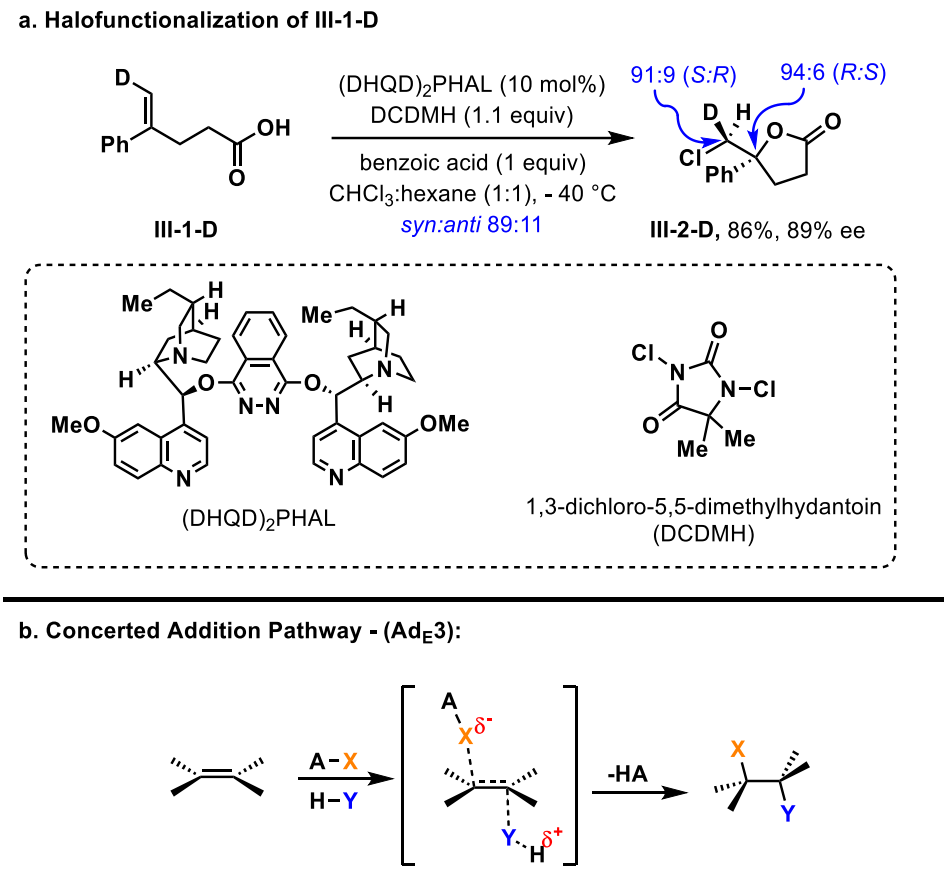

Previously discussed, in Chapter 2, Halenium Ion Affinity (*HalA*) is a parameter that provides a measure of the affinity of a Lewis base species toward binding to a halenium ion (Figure 3.4a). The *HalA* value aids in predictions of regio-, and chemoselectivity of electrophilic alkene halogenation reactions.[55] *HalA* values can be calculated (equation 1, Chapter 2) using density functional models, which relates to the ground state enthalpic difference between the halogenated and de-halogenated species. These values then allow determination of whether the halogenating agent can thermodynamically halogenate an alkene, where the greater *HalA* value is predicted to capture the halenium ion (Figure 3.4b).

Figure 3.4. (a) Halenium Affinities (b) Reactivity prediction based off *HalA* values

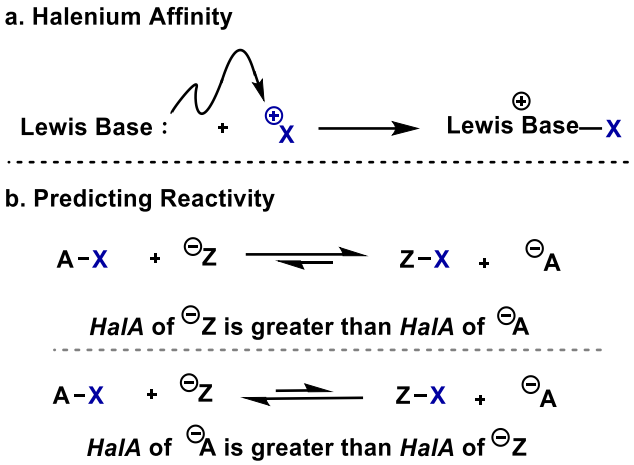

Though calculating *HalA* values and directly applying halenium affinities to assess reactivity, it was predicted that carboxylic acid **III-1** would be unable to undergo chlorocyclization because the byproduct of DCDMH (MCDMH anion) has a higher *HalA* value, and thus the equilibrium of the reaction would lie towards starting material (Figure 3.5a). However, this substrate readily reacted in the presence of DCDMH. This led to revisiting the transition state, leading to the postulate that for the chlorolactonization reaction, the reactive alkene precursor is in a biased conformation with the carboxylic acid (nucleophile) positioned near the alkene, and ready for simultaneous attack of the olefin as it captures the halenium ion (electrophile) (Figure 3.5b).[55]

Figure 3.5. (a) *HalA* values of reported substrates (b) Depiction of the concerted *NAAA* pathway

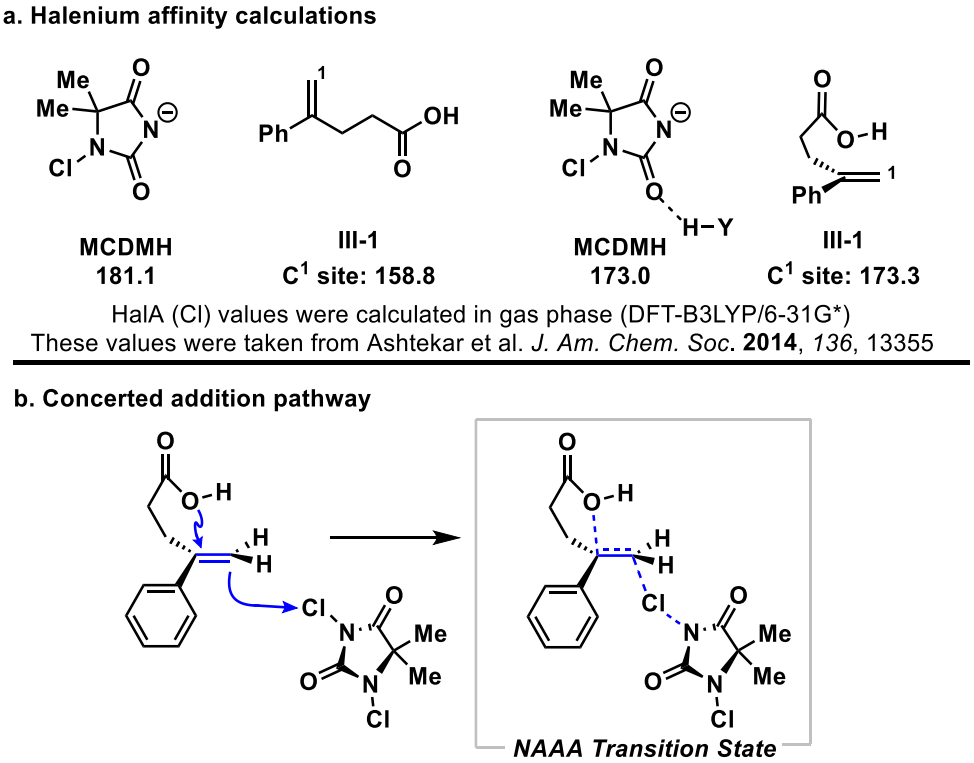

This conformation is now referred to as “nucleophile assisted alkene activation” or *NAAA*, because the otherwise unreactive alkene is now activated to enable halogenation and yield the chlorocyclization product.[83] While this confirmation is slightly higher in energy, it does compensate for the cationic charge development by the nucleophile’s position and thus, prevents the formation of higher energy cationic intermediates.

Due to these prior findings, it was hypothesized that these different transition states could potentially lead to either the *syn*- or *anti*-addition product. Based on the reactive conformation of **III-1** required for reactivity (*NAAA*), the *syn*-addition product is thought to arise from a bimolecular transition state, where the olefin is activated by the proximal oxygen on the carboxylic acid, and this then engages the chlorenium donor. The *syn*-

stereochemistry arises from H-bonding of DCDMH with the carboxylic acid, and the concerted transfer of the chlorenium to the same face (Figure 3.6). For the *anti*-transition state, it was hypothesized that a termolecular transition state, at a *minimum*, exists to lead to the *anti*-selectivity. The carboxylic acid moiety participates in hydrogen bonding to promote the carboxylate (nucleophile) to activate the olefin, while a chlorenium (electrophile) from DCDMH is transferred to the opposite face (Figure 3.6). The hydrogen bonding partner with the carboxylic acid is hypothesized to be the acid dimer, chlorenium donor, or the byproduct of the halogenating species, which is MCDMH in this scenario.

Figure 3.6. Transition states leading to *syn*- and *anti*-addition for chlorolactonization

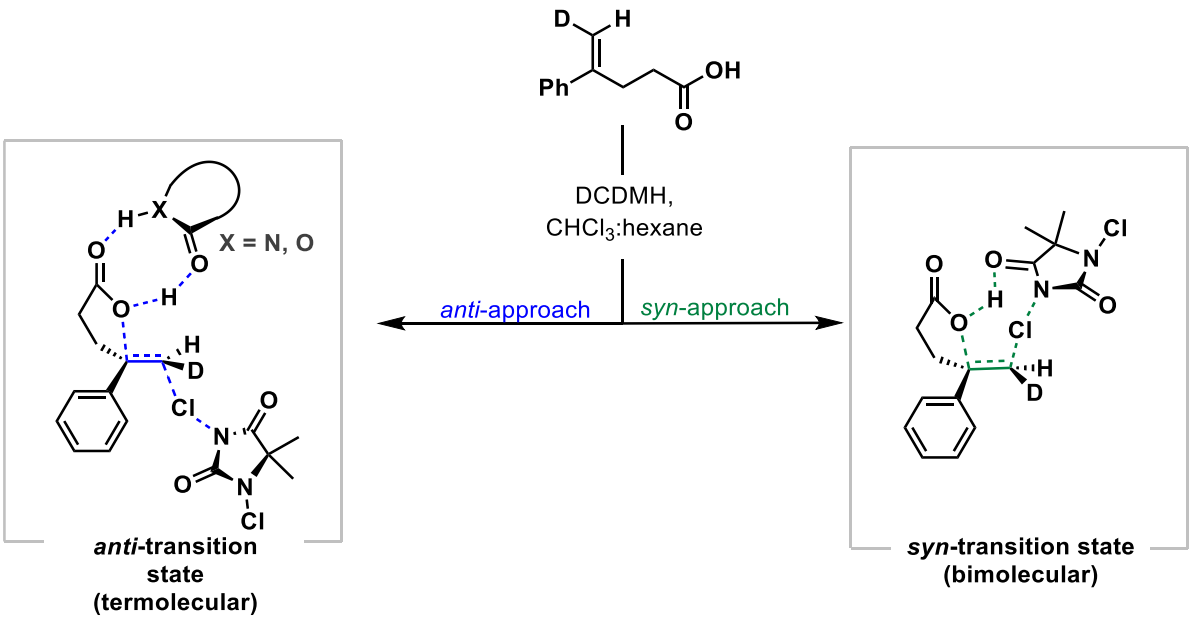

In order to determine the transition states that lead to *syn*- and *anti*-product, as well as determine the validity of the above hypotheses, different variables of this transformation were evaluated systematically. A full kinetic investigation could aid in determining the plausible mechanistic pathways. Specifically, the reaction order of each component within the rate determining step, elucidated with VTNA, is necessary to address mechanistic questions and propose potential pathways.[79,80,81]

3.4. Synthesis of Carboxylic Acid III-1-D and Determination of Stereochemistry

To probe the factors that determine the formation of the *syn*- and *anti*-product, we required a labeled substrate to determine the stereochemical outcome of the newly formed sp^3 carbon center. The deuterated substrate **III-1-D** was accessed in a 4-step synthesis starting with the silylation of alcohol **III-3**, followed by a Pd-catalyzed deutero-hydroarylation,[85] and then subsequent deprotection and oxidation (Scheme 3.2).[78] Silylation of the alcohol was necessary otherwise over deuteration occurred at the terminal sp^2 carbon. The deutero-hydroarylation successfully afforded a high level of deuterium incorporation (88%) and good *Z:E* selectivity (95:5). It is important to note that the stereochemical impurity of the substrate was mathematically considered when conducting the final analysis of the *anti*:*syn* ratio (see Experimental Section).

Scheme 3.2. Synthesis of deuterated substrate **III-1-D**

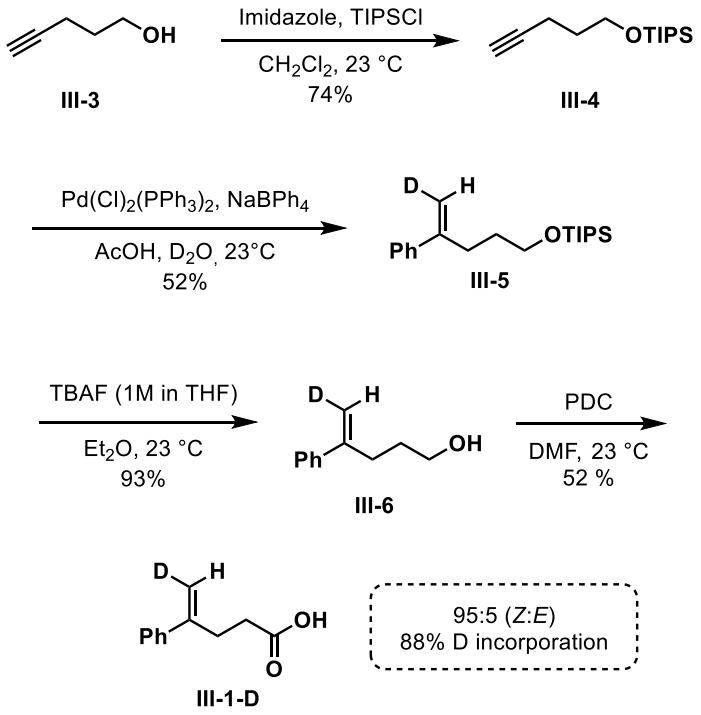

Absolute stereochemistry of the newly formed CDHCl stereocenter was determined *via* NOESY analysis of the epoxide **III-7-D** though a previously reported procedure (Scheme 3.3).[78] **III-1-D** underwent $(DHQD)_2PHAL$ catalyzed chlorocyclization to form **III-2-D**. The absolute configuration of **III-2-D** at C5 is the *R* configuration, which was also previously elucidated.[75] Lithium borohydride reduction, followed by base mediated epoxide formation returned the epoxy alcohol **III-7-D**. The non-deuterated epoxy alcohol **III-7** was synthesized similarly from **III-2**. NOSEY studies of **III-7** shows that H_a (2.73 ppm) has a *syn* orientation to the phenyl group and H_b (2.98 ppm) has an *anti*-orientation to the phenyl group.[78] ^{1}H-NMR analysis of the resulting epoxy alcohol **III-7-D** shows only a peak at 2.73 ppm, establishing that the deuterium has an *anti*-orientation with respect to the phenyl group. Therefore, this leads to the assignment of the *R*-configuration for the carbon bearing the deuterium in the epoxy alcohol **III-7-D**, implying that the stereochemistry at C6 for **III-2-D** is the *S*-configuration because the epoxy alcohol is formed though S_N2 displacement of the chloride.

Scheme 3.3. Absolute stereochemical assignment of the deuterated center (C6)

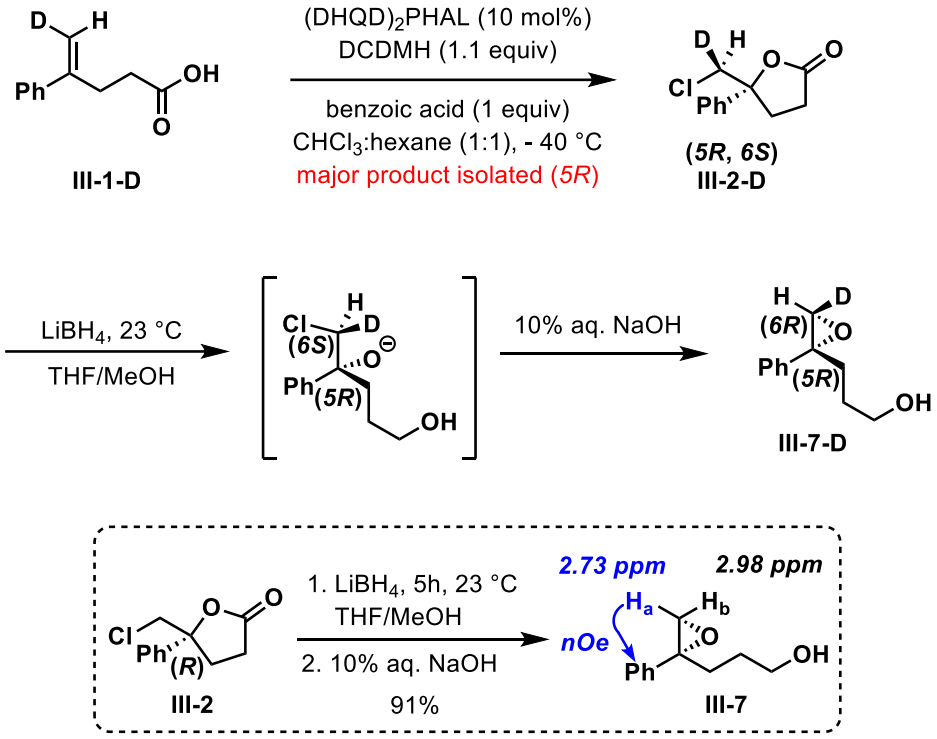

3.5. Chlorenium Ion, Solvent, and Concentration Studies

To investigate the intrinsic factors that determine *anti:syn* ratios in the absence of a catalyst, systematic reaction conditions were studied for chlorocyclization of **III-1-D**. First, the chlorenium source was evaluated (Table 3.2, entries 1-5). Each chlorenium source was screened to determine if the associated *HalA* value with each chlorenium source will have an influence on the outcome. *HalA* values are defined as a parameter to help predict the ability and ease of electrophilic halogenation occurring in the reaction where **III-1-D** is present and undergoes chlorocyclization in the presence of a chlorenium source.[55] It was envisioned that *syn:anti* ratios could be correlated with *HalA* values, and the ease to which the chlorenium donor will halogenate the alkene. The results from these studies indicate

that changes in the chlorenium source do have a significant impact on the resulting *syn:anti* ratio, which range from 13:87 to 36:64. However, the *syn:anti* ratios in this study could not be correlated to the chlorerium ion donor ability, and therefore, no conclusion about *HalA* relating to the *syn:anti* ratio could be determined.

The results appear to indicate that the chlorenium donor must be involved in the step that drives diastereoselectivitiy causing differences in the *syn*- or *anti*-addition.[86] For example, in Figure 3.6, the species participating in the hydrogen bond with the carboxylic acid that leads to the *anti*-product could be the residual chlorenium donor. The greater the ability of the byproduct to participate in hydrogen bonding, the more likely the *anti*-transition state would predominate.

The effects of different solvents on the *anti:syn* ratios were screened (Table 3.2, entries 6-10). The observed diastereoselectivities indicate significant solvent dependance. Generally, solvents with low polarity, such as toluene or dichloromethane, yielded a higher amount of the *syn*-product (56:44 and 45:55, respectively). This is in stark contrast to solvents with high polarity, such as acetonitrile, which afford increased *anti*-product (23:77 *syn:anti*). This solvent effect that leads to different *syn:anti* ratios, contributes to the hypothesis that two different mechanisms arise to provide either the *syn* or *anti* product independently. Each pathway, *syn*-addition and *anti*-addition is affected differently by the solvent polarity and hydrogen bonding capability of a solvent. For instance, in a solvent with higher polarity, a transition state that involves additional buildup of charge as well as hydrogen bonding networks associated with that transition state would be more stable. The proposed *anti*-transition state would have an overall higher dipole moment and an increase in hydrogen bonds as compared to the *syn*-

transition state. Therefore, the more polar solvent might favor this transition state, and enable the structurally defined, concerted pathway, to proceed, delivering increased *anti*-product. However, a nonpolar solvent would be less likely to support a larger dipole moment and the multitude of hydrogen bond donors and acceptors associated with the *anti*-transition state. This would promote the 1:1 reaction complex, facilitating a bimolecular transition state that favors the *syn*-product formation.

.

Table 3.2. Screen of chlorinating reagents, solvents, and concentration effects on *anti:syn* ratios of **III-1-D**

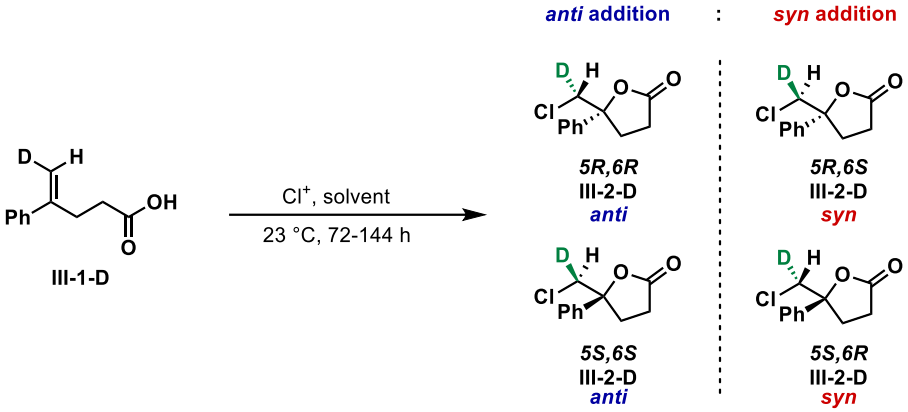

Entry	Cl^+ Source	*HalA* or Solvent ε	Solvent	[Sub] M	[Cl^+] M	*syn : anti*
1	Di.Ch.T	273.3	$CHCl_3$:Hex (1:1)	0.05	0.055	13 : 87
2	TCCA	252.1	$CHCl_3$:Hex (1:1)	0.05	0.055	22 : 78
3	NcSac	265.0	$CHCl_3$:Hex (1:1)	0.05	0.055	21 : 79
4	DCDPH	270.1	$CHCl_3$:Hex (1:1)	0.05	0.055	36 : 64
5	DCDMH	275.7	$CHCl_3$:Hex (1:1)	0.05	0.055	36 : 64
6	DCDMH	37.5	CH_3CN	0.05	0.055	23 : 77
7	DCDMH	2.38	PhMe	0.05	0.055	56 : 44
8	DCDMH	9.0	DCM	0.05	0.055	45 : 55
9	DCDMH	26.1	TFE	0.05	0.055	26 : 74
10	DCDMH	4.8	$CHCl_3$	0.05	0.055	49 : 51
11	DCDMH	3.35	$CHCl_3$:Hex (1:1)	0.05	0.0125	33 : 67
12	DCDMH	-	$CHCl_3$:Hex (1:1)	0.05	0.025	34 : 66
13	DCDMH	-	$CHCl_3$:Hex (1:1)	0.05	0.05	36 : 64
14	DCDMH	-	$CHCl_3$:Hex (1:1)	0.05	0.1	29 : 71
15	DCDMH	-	$CHCl_3$:Hex (1:1)	0.05	0.25	27 : 73
16	DCDMH	-	$CHCl_3$:Hex (1:1)	0.0125	0.05	27 : 73
17	DCDMH	-	$CHCl_3$:Hex (1:1)	0.025	0.05	28 : 72
(13)	DCDMH	-	$CHCl_3$:Hex (1:1)	0.05	0.05	36 : 64
18	DCDMH	-	$CHCl_3$:Hex (1:1)	0.1	0.05	33 : 67
(13)	DCDMH	-	$CHCl_3$:Hex (1:1)	0.05	0.05	36 : 64
19	DCDMH	-	$CHCl_3$:Hex (1:1)	0.025	0.025	41 : 59
20	DCDMH	-	$CHCl_3$:Hex (1:1)	0.0125	0.0125	52 : 48
21	DCDMH	-	$CHCl_3$:Hex (1:1)	0.00625	0.00625	54 : 46

Next, the effect on concentration of reactants on the selectivity of the reaction was studied, and further mechanistic clues emerged about the molecularities of each transition state. Initially, the concentration of DCDMH was systematically changed while keeping the concentration of the deuterated carboxylic acid **III-1-D** constant at 0.05 M in a 1:1 solvent mixture of chloroform:hexanes (Table 3.2., entries 11-15). This showed little change in the *syn:anti* ratio; only a slight increase in *anti*-product was observed when DCDMH concentration was increased. This data suggests that more than one molecule of DCDMH, or the byproduct, MCDMH, is involved in the transition state for *anti*-cyclization, where one molecule of DCDMH is transferring a chlorenium ion, and another molecule of DCDMH or the byproduct of MCDMH, is participating in H-bonding with the carboxylic acid to promote the *anti*-transition state (Figure 3.6). At high concentrations of DCDMH, the *anti*-forming transition state could be composed of two (or more) molecules of DCDMH and one molecule of alkene substrate **III-1-D.**

Next, the concentration of carboxylic acid **III-1-D** was systematically changed while the concentration of DCDMH was held constant at 0.05 M in 1:1 solvent mixture of chloroform:hexane (Table 3.2, entries 16-18). Changes in the concentration of carboxylic acid **III-1-D** revealed that an increase in *anti*-cyclization product occurred as the concentration of **III-1-D** was lowered to 0.0125 M (entry 16). In this scenario, there was a large excess of DCDMH as compared to alkene substrate **III-1-D**, and an increase in *anti*-product support the above suggestion where more than one molecule of DCDMH, or the byproduct MCDMH, is involved in the transition state leading to the increase in *anti*-product. Interestingly, as the concentration of **III-1-D** was increased to 0.1 M, and the concentration of DCDMH was kept consistent at 0.05 M, again an increase in *anti*-product

was observed (Table 3.2., entry 18), presumably due to dimer formation which could satisfy the H-bond partner of the carboxylate (Figure 3.6). This finding reveals that the moiety participating in hydrogen bonding relay proposed for the *anti*-transition state could be fulfilled by the dimer of the carboxylic acid **III-1-D**, DCDMH, or MCDMH.

Furthermore, the concentration of DCDMH and the substrate were both systematically decreased creating a more dilute solution of each reactant, and this led to an increase in *syn*-product formation (Table 3.2., entries 19-21). At lower concentrations, the proposed 1:1 complex of substrate:DCDMH would be favored (Figure 3.6) over the termolecular proposed transition state that leads to the *anti*-product. Here, the DCDMH would function as both the base and the chlorenium ion source, and delivers the chlorenium to the same face as the nucleophile.

At higher concentrations, the *anti*-forming transition state could be composed of one molecule of carboxylic acid **III-1-D**, one molecule of DCDMH, and another molecule that participates in hydrogen bonding relay. Here, the molecule participating in hydrogen bonding relay will activate the carboxylate for nucleophilic attack onto the olefin, enabling chlorenium ion transfer and ring closure to take place in a concerted mechanism with minimal charge separation.

3.6. Kinetic Studies Using VTNA

With this data in hand, a full kinetic investigation of the reaction was conducted to determine the plausible mechanistic pathways by revealing the order of the individual reactants in the rate-determining step. As discussed earlier in this chapter, the method developed by Bures, Variable Time Normalization Analysis (VTNA) offers key insights into reaction mechanisms.[79,80,81] This method reveals the order of each individual component in the reaction by using modern reaction monitoring methods, such as NMR to determine the concentration and time of the variable in question, and then utilizes the following equation to plot the VTNA profiles.

$$\sum \left(\frac{[B]_i + [B]_{i-1}}{2}\right)^{\beta} (t_i - t_{i-1}) \qquad \text{equation 5}$$

The original uncatalyzed conditions of the reaction for **III-1-D** were used initially (Table 3.2, entry 5). To follow the kinetic parameters of this reaction, NMR analysis proved optimal using $CDCl_3$ instead of $CHCl_3$, which still allowed us to use a 1:1 solvent mixture of chloroform:hexanes.

The proton that is present on the newly formed sp^3 carbon, CDHCl, has a different chemical environment for *syn*-cyclization as compared to *anti*-cyclization, thus allowing quantification of the products. Being able to differentiate between the transition state for *syn*- and *anti*-addition, the reaction orders of **III-1-D**, DCDMH, and MCDMH are elucidated individually.

Shown in Table 3.3 are the different set of conditions that were studied for VTNA. Experiment B is the standard reaction condition, (0.5 M **III-1-D** and 0.55 M DCDMH). Experiment A has a slightly lower concentration of **III-1-D** (0.3 M). The concentration of

DCDMH was kept constant, providing a different excess of the substrate **III-1-D** between experiments A and B. Next, experiment C has the concentration of **III-1-D** constant and while the concentration of DCDMH was changed to 0.1 M to provide a different excess in DCDMH between experiments B and C.

Table 3.3. Set of different excess experiment to find orders using VTNA

Exp	[III-1-D] (M)	[DCDMH] (M)
A	0.03	0.055
B	0.05	0.055
C	0.05	0.1

The *syn*-transition state was first investigated. Comparing the reaction profiles of experiments A and B (different excess in carboxylic acid **III-1-D**) indicates that carboxylic acid **III-1-D** is first order with respect to the *syn*-product (Figure 3.7). The *syn*-transition state was previously hypothesized to go through a bimolecular transition state, where one molecule of **III-1-D** reacts with one molecule of DCDMH to undergo cyclization.

Figure 3.7. VTNA analysis of **III-1-D** leading to the *syn*-product from a set of different excess experiments. The plots correspond to experiments A and B and overlay when **III-1-D** is raised to the power of 0.9, indicating *first order*.

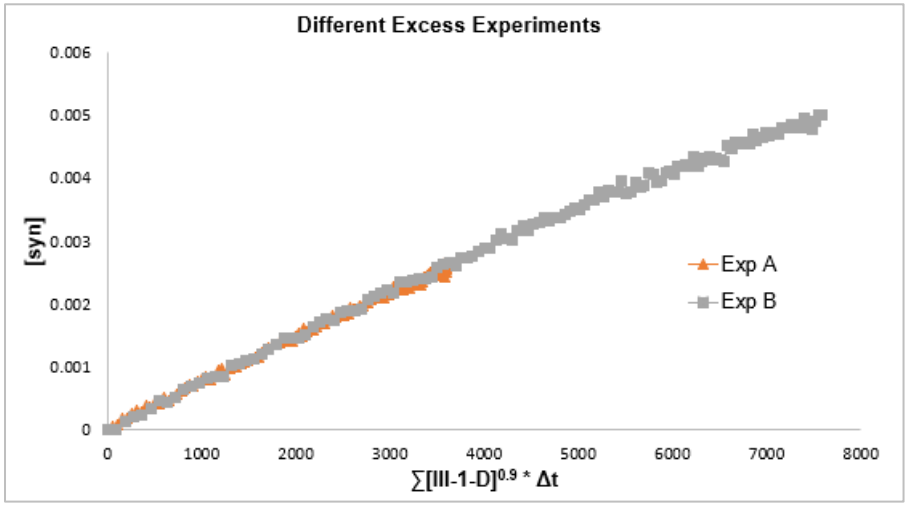

Similarly, the reaction profiles of experiments B and C were next investigated. In experiment B, the conditions are 0.05 M **III-1-D** and 0.055 M DCDMH, and in experiment C the conditions used are 0.05 M **III-1-D** and 0.1 M DCDMH, where a different excess of DCDMH was present to determine the reaction order of DCDMH. As shown in Figure 3.8, the overlay between the two reaction profile occur when the order is raised to 1.2, indicating that DCDMH is first order with respect to the *syn*-transition state.

Figure 3.8. VTNA analysis of DCDMH leading to the *syn*-product from a set of different excess experiments. The plots correspond to experiments B and C and overlay when DCDMH is raised to the power of 0.9, indicating that DCDMH is *first order*.

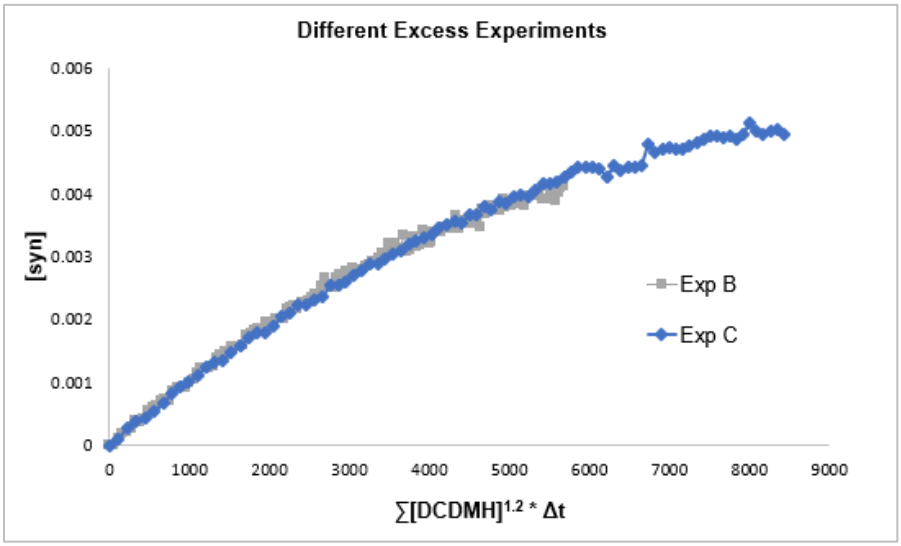

Next, all three experiments, A, B and C, were plotted with all three components present in the reaction, which is **III-1-D**, DCDMH, and the byproduct of DCDMH, MCDMH. In VTNA plots, the reaction profiles will become straight lines when all the driving forces that change during the reaction are raised to the correct order. It is usually beneficial to perform analysis on the orders independently, and then perform the analysis of the combination of orders. Since it was discovered that **III-1-D** and DCDMH are both first order with regard to the *syn*-transition state, the plot of all the variable raised to the correct order should overlay and become a straight line. MCDMH was included in these VTNA plots to determine if there is any effect on the reaction and/or product. The previous equation that is used for VTNA was modified slightly to now include all thee components, shown below:

$$\sum \left(\frac{[III1D]_i + [III1D]_{i-1}}{2}\right)^{\alpha} \left(\frac{[DCDMH]_i + [DCDMH]_{i-1}}{2}\right)^{\alpha} \left(\frac{[MCDMH]_i + [MCDMH]_{i-1}}{2}\right)^{\alpha} (t_i - t_{i-1}) \quad \text{equation 6}$$

Upon plotting all three experiments, A, B, and C, and raising **III-1-D** and DCDMH to the power of 0.9, and MCDMH to a power of 0, an overlay of all three reaction profiles and a straight line is observed (Figure 3.9). Therefore, it can be concluded that the starting carboxylic acid **III-1-D**, and DCDMH indeed are *first order* with respect to the *syn*-cyclized product, while MCDMH has no effect on the *syn*-transition state.

Figure 3.9. VTNA analysis of experiments A, B, and C. The plots overlay when DCDMH and **III-1-D** are raised to the power of 0.9, indicating that *first order*, and when MCDMH is *zero order*

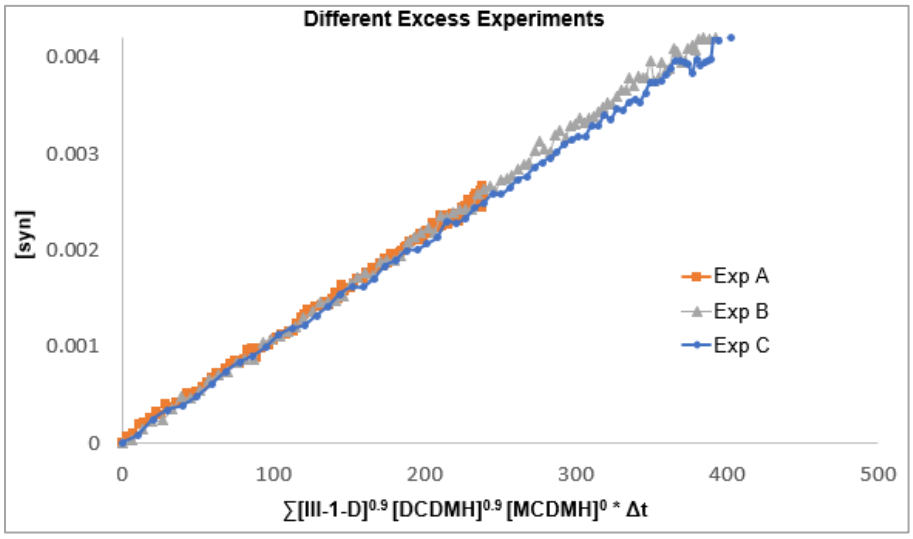

These findings combined with the aforementioned results from the concentration and solvent studies support our initial hypothesis. Evaluation of all the data together, the *syn*-transition state preferentially proceeds though a bimolecular process, yielding the *syn*-cyclized product (Figure 3.10).

Figure 3.10. Transition state leading to the *syn*-cyclized product

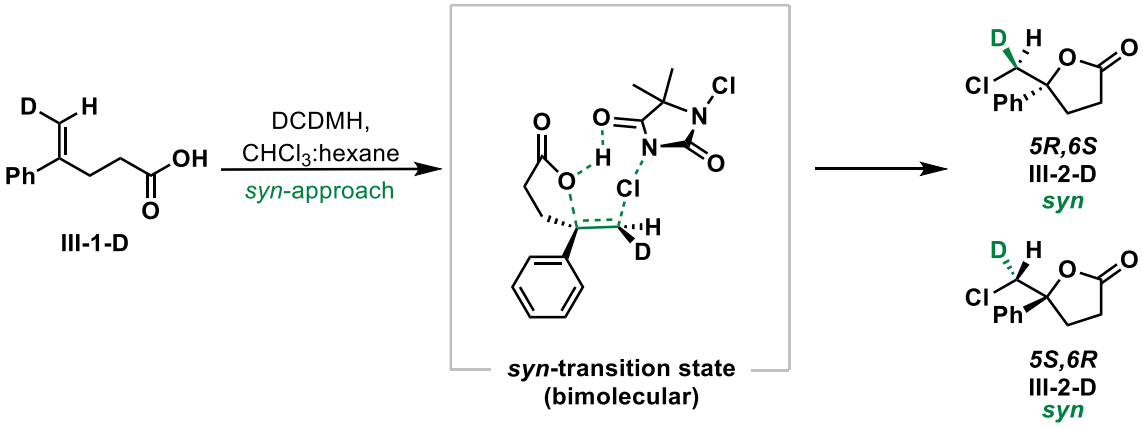

These same VTNA studies were next applied to the *anti*-product to determine the reaction orders. Initially, the order of **III-1-D** and DCDMH were evaluated independently. The reaction profiles of experiments A and B were plotted to determine the order of carboxylic acid for the *anti*-transition state. Interestingly, the carboxylic acid **III-1-D** overlaps when raised to the order of 0.45 (Figure 3.11). It was therefore concluded that **III-1-D** is *half order* dependance with respect to the *anti*-product. This is presumably due to dimer formation of the carboxylic acid.

Figure 3.11. VTNA analysis of **III-1-D** leading to the *anti*-product from a set of different excess experiments. The plots correspond to experiments A and B and overlay when alkene **III-1-D** is raised to the power of 0.45, indicating that **III-1-D** is *half order*.

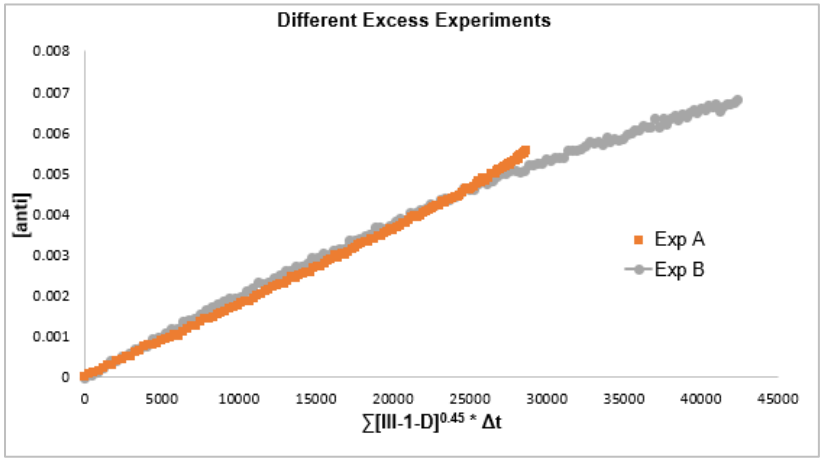

Using experiments B and C, with a different excess in DCDMH, the reaction profiles of these reaction conditions were next investigated. Upon raising DCDMH to the order of 0.9 an overlay occurs, indicating that DCDMH is *first order* with respect to the *anti*-product (Figure 3.12).

Figure 3.12. VTNA analysis of DCDMH leading to the *anti*-product from a set of different excess experiments. The plots correspond to experiments B and C and overlay when DCDMH is raised to the power of 0.9, indicating that DCDMH is *first order*.

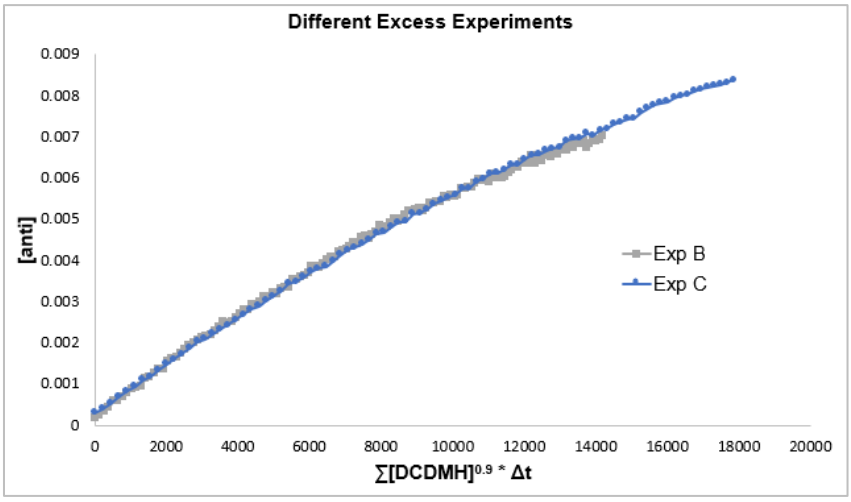

The *anti*-transition state was hypothesized to be termolecular, at minimum, with the starting carboxylic acid participating in hydrogen bonding to promote the oxygen (nucleophile) to activate the olefin, while a chlorine (electrophile) from DCDMH is simultaneously transferred to the opposite face. The VTNA studies elucidated the orders of the *anti*-transition state, where **III-1-D** is *half* order, presumably due to the dimer of the carboxylic acid, and DCDMH was found to be *first* order. Next, all three experiments, A, B and C, were plotted with all three components present in the reaction (**III-1-D**, DCDMH, and the byproduct of DCDMH, MCDMH). MCDMH was also included in these VTNA plots to determine if there is any effect on the reaction and/or product formation. Using the same equation 6 that involved all three components, the three reaction profiles were plotted. Upon raising **III-1-D** to 0.45, DCDMH to 0.95, and MCDMH to 0.2, a straight line with maximum overlap occurs, indicating that, as previously discussed, carboxylic acid **III-1-D** is *half order* dependence, and DCDMH was found to be *first order* dependence for the *anti*-transition state (Figure 3.13).

Figure 3.13. VTNA analysis of experiments A, B, and C. The plots overlay when DCDMH is raised to 0.95 indicating that *first order*, **III-1-D** is raised to 0.45 indicating *half order*, and when MCDMH is raised to an overall order of 0.2.

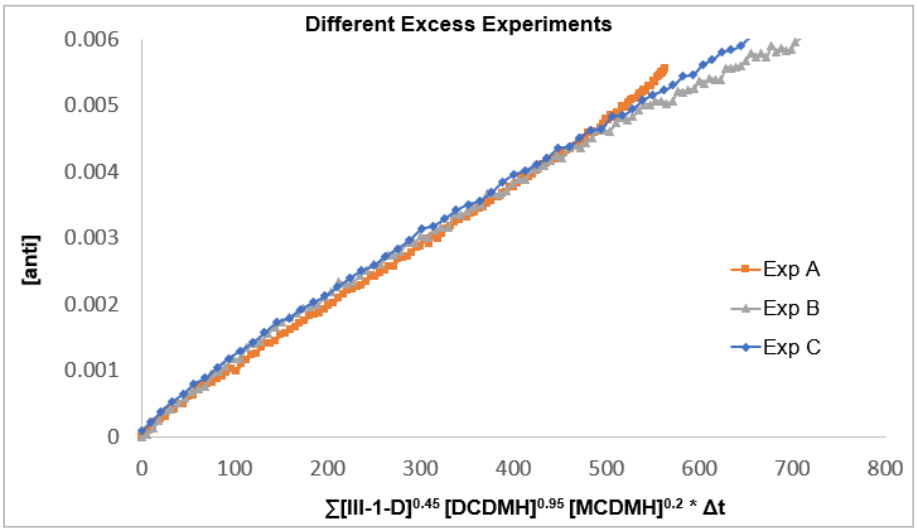

Interestingly, for the *anti*-transition state, it was found that MCDMH has an overall reaction order of 0.2. This is presumably because initially no MCDMH is present within the reaction, however, as the reaction progresses a higher concentration of MCDMH is present which leads to an overall order being a fraction. In order to study the exact order of each reagent at a specific time in the reaction, it is necessary to limit the analysis to the specific time points of the reaction.[79] Since MCDMH does show dependance, and its concentration is zero at the onset of the reaction, an investigation using VTNA at the beginning and at the end of the reaction was done to determine the role of MCDMH.

Upon plotting all three experiments, A, B and C, and limiting the analysis to the beginning of the reaction, it was found that an overlay occurs when **III-1-D** is raised to 0.6, DCDMH is raised to 1, and MCDMH is raised to 0 (Figure 3.14). Indicating that carboxylic acid is *half order*, DCDMH is *first order*, and MCDMH is not involved in the beginning of the reaction.

Figure 3.14. VTNA analysis of experiments A, B, and C in the beginning of *anti*-product formation. The plots overlay when DCDMH is raised to 1 indicating that *first order*, **III-1-D** is raised to 0.6 indicating *half order*, and when MCDMH is raised to an order of 0.

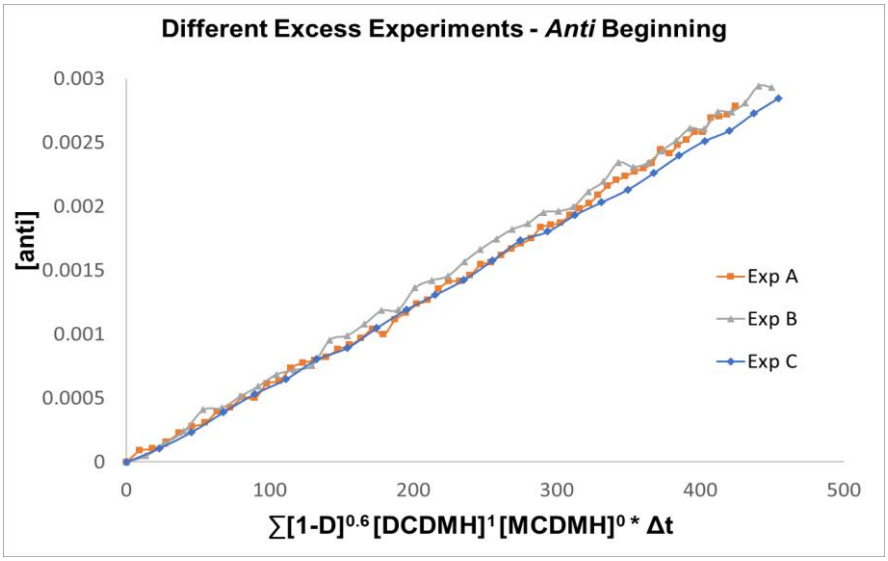

Upon plotting all three experiments, A, B and C, and limiting the analysis to the end of the reaction, there is now a dependance seen with MCDMH (Figure 3.15). Specifically, the plots overlay when carboxylic acid is raised to 0.3, DCDMH is raised to 1 indicating *first order*, and then MCDMH is raised to an order of 0.7. Since MCDMH is now present within the reaction mixture, we see a higher dependance on MCDMH leading to the *anti*-cyclized product.

Figure 3.15. VTNA analysis of experiments A, B, and C at the end of *anti*-product formation. The plots overlay when DCDMH is raised to 1 indicating that *first order*, **III-1-D** is raised to 0.3, and when MCDMH is raised to an order of 0.7.

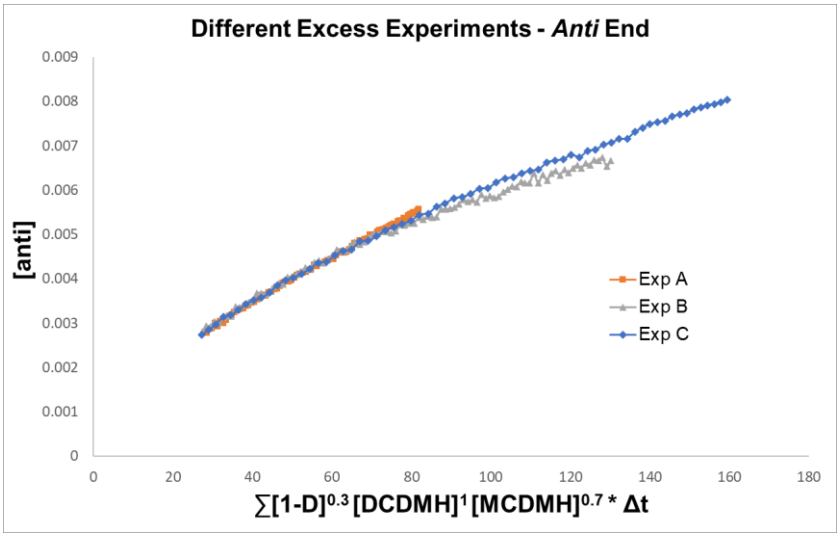

The kinetic studies helped to illuminate the role of the hydrogen bond partner in the termolecular transition state since this could be fulfilled by multiple different species in solution depending on the specific time in the reaction. Predicated on the observed data from the VTNA studies, it was found that the hydrogen bonding partner is primarily the dimer of the carboxylic acid with slight contribution from MCDMH as well (Figure 3.16).

Figure 3.16. Transition state leading to the *anti*-cyclized product

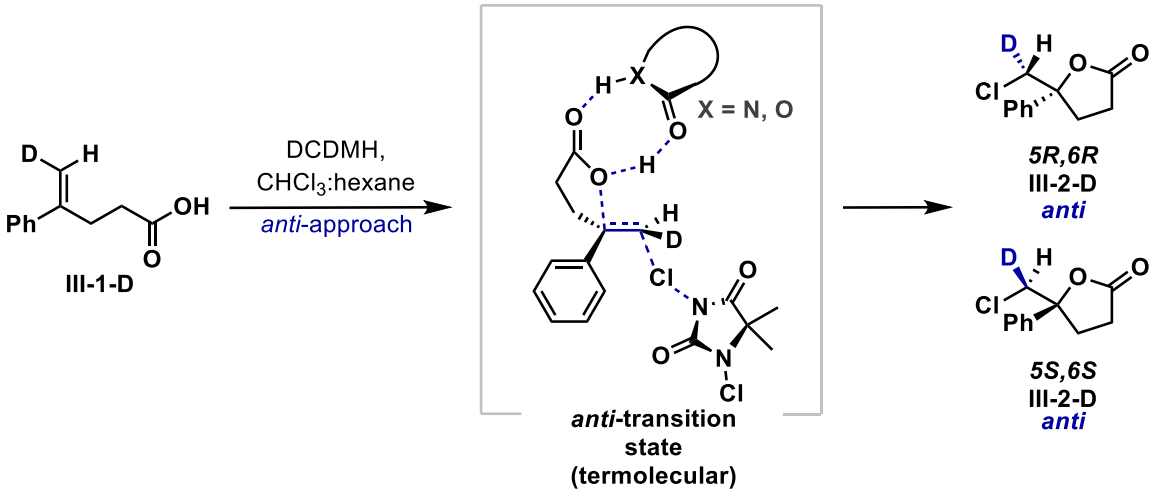

Based off the VTNA results, MCDMH does show dependence on the *anti*-cyclized product. Therefore, this was investigated further to understand the role of MCDMH more accurately. Concentration studies in the presence of MCDMH were performed (Table 3.4). Chloroform was used in these studies because MCDMH is insoluble at higher concentrations in the mixed solvent system of chloroform:hexanes. It is important to note a reaction without MCDMH was also performed in chloroform as well in order to facilitate accurate head-to-head comparisons (Table 3.4, entry 1).

At low concentrations, **III-1-D** and DCDMH showed modest preference for the *syn* product since the 1:1 complex would be favored at lower concentrations (69:31, *syn:anti*). Interestingly, when the concentration of MCDMH was increased to 0.1 M, the selectivity switched to now favor the *anti*-product, with a *syn:anti* ratio of 38:62 (Table 3.4, entry 2). To verify these results, we evaluated another urea-type base, tetramethylurea, which would not be chlorinated in the presence of DCDMH (Table 3.4, Entry 3). The data from these experiments indicate an even stronger preference for the *anti*-product, with a

syn:anti ratio of 11:89. This stronger preference for syn could be due to an electrostatic interaction of the urea, which coordinates to the carboxylic acid to facilitate formation of the termolecular transition state, and promote *anti*-addition product formation (Figure 3.16).

Table 3.4. Screening of MCDMH effects in the *syn*:*anti* ratio of **III-2-D**

Entry	Solvent	[Sub] M	[DCDMH] M	[MCDMH] M	[tetramethylurea] M	*syn : anti*
1	$CHCl_3$	0.00625	0.00625	0	0	69 : 31
2	$CHCl_3$	0.00625	0.00625	0.1	0	38 : 62
3	$CHCl_3$	0.00625	0.00625	0	0.1	11 : 89

The average order of MCDMH in the *anti*-transition state was found to be 0.2. This is consistent with the proposed transition state because in the beginning stages of the reaction, MCDMH is not present or negligible, whereas a higher concentration is present in the later stages of the reaction. Therefore, as MCDMH is produced this acts as the hydrogen bond relay partner for the termolecular transition state. Prior to the formation of MCDMH, or a high enough concentration present in the reaction, it is hypothesized that the dimer of **III-1-D** is fulfilling this role based off the *half order* dependance. To test this hypothesis, benzoic acid was added to the standard conditions, and the *syn:anti* ratio was calculated (Table 3.5).

Table 3.5. Effects of benzoic acid in the *syn*:*anti* ratio of **III-2-D**

Entry	Solvent	[Sub] M	[DCDMH] M	[benzoic acid] M	*syn : anti*
1	$CHCl_3$:Hex (1:1)	0.05	0.055	0	36 : 64
2	$CHCl_3$:Hex (1:1)	0.05	0.055	0.05	27 : 73

The addition of benzoic acid increased the formation of the *anti*-product, providing evidence that the hydrogen bond relay partner in the *anti*-transition state is fulfilled by either the dimer **III-1-D**, MCDMH, or another protic hydrogen bond donor present in solution. Similarly, in the concentration studies using a large excess of **III-1-D** as compared to DCDMH, an increase in *anti*-product was observed (Table 3.2, Entry 19). Based on the VTNA results and concentration studies, it is concluded that the dimer of alkene **III-1-D**, as well as MCDMH, once produced, act as the hydrogen bond relay partner leading to the *anti*-addition transition state.

To verify that the *syn*- and *anti*-cyclized product arise *via* different mechanisms, the orders found for *syn*-addition were input for the *anti*-addition product to yield a plot that does not overlay (Figure 3.17). Since no overlay was observed, this data provides evidence supporting that the *syn*-product arises from a different mechanism than the *anti*-product.

Figure 3.17. Average order of **III-1-D**, DCDMH, and MCDMH for *syn*-addition (top) *anti*-addition product with the same order (bottom)

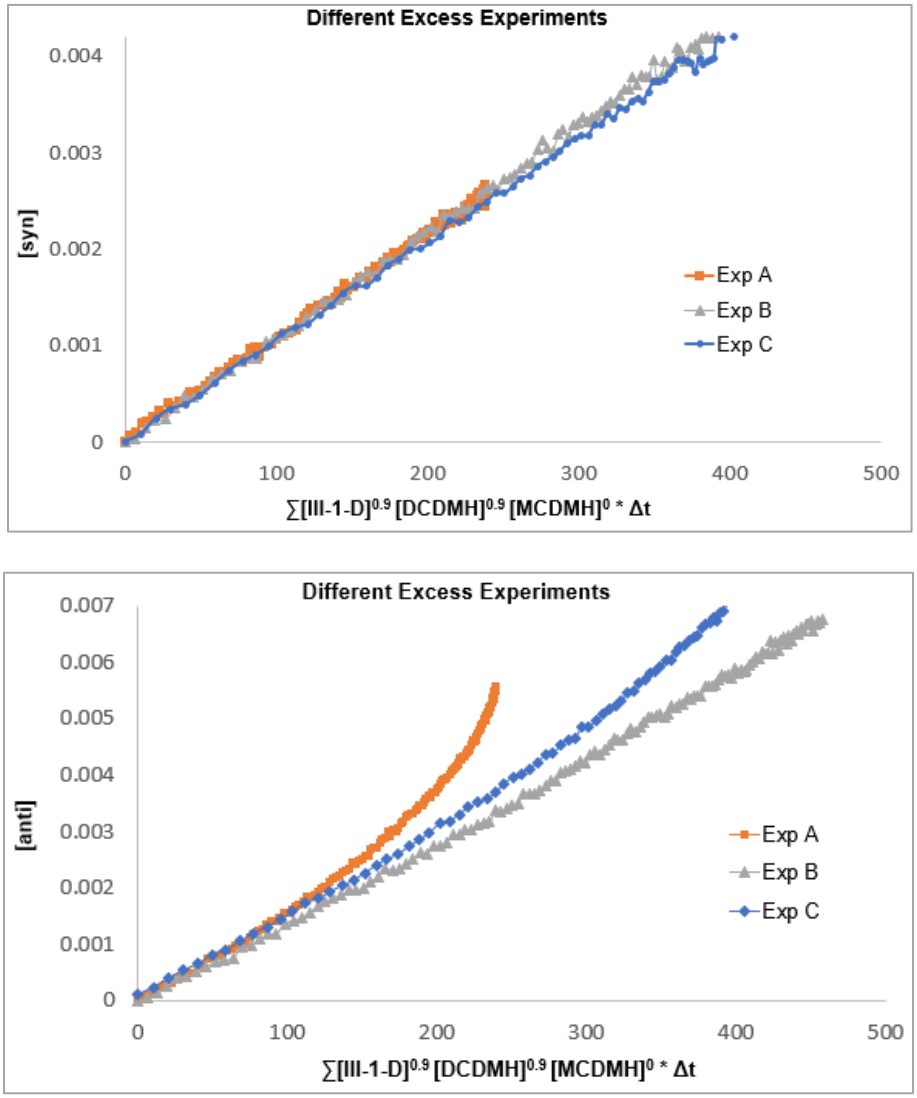

Similarly, the values that were found for *anti*-addition were now input for the *syn*-addition product, and the resulting plot also does not overlay. Again, the lack of an overlay in the plots provides evidence supporting that the *syn*- and *anti*-product are formed *via* different transition states to yield the corresponding products (Figure 3.18).

Figure 3.18. Average order of **III-1-D**, DCDMH, and MCDMH for *anti*-addition (top) *syn*-addition product with the same order (bottom)

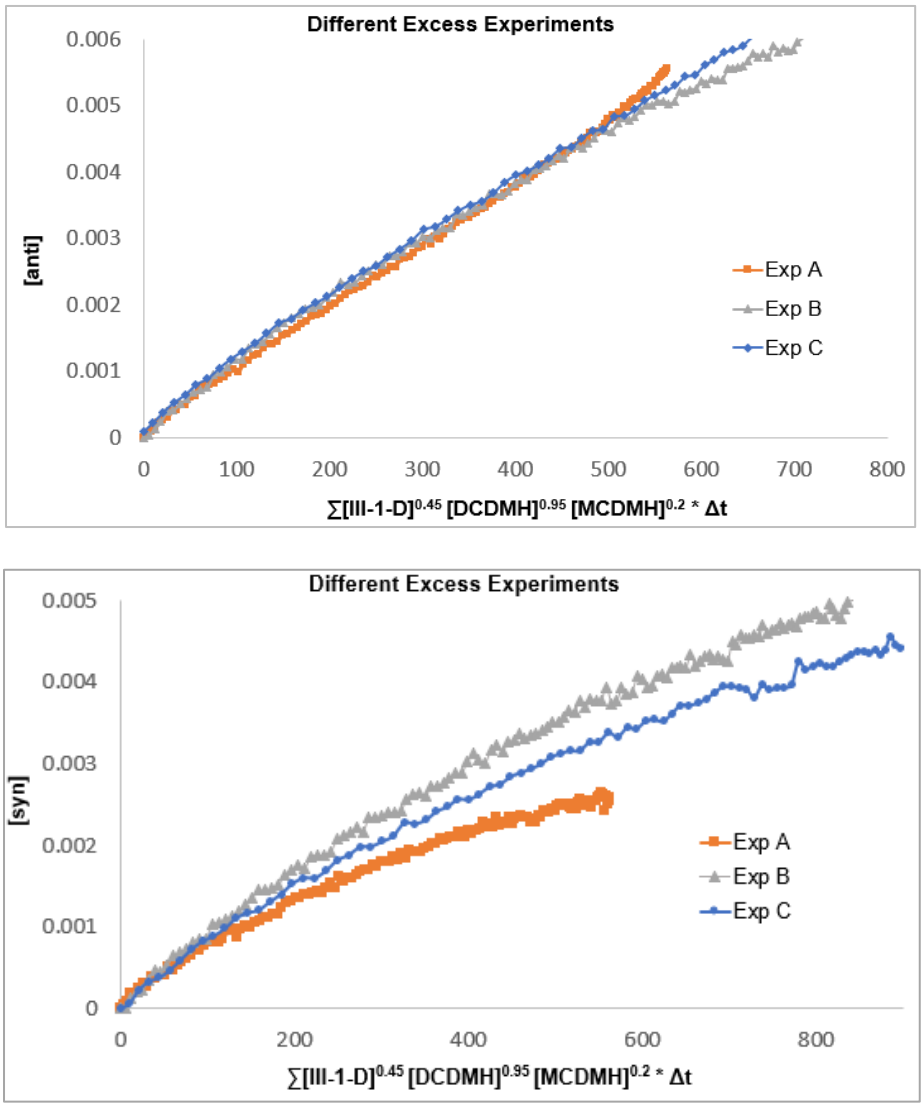

With the results and data from the detailed VTNA analysis of the uncatalyzed chlorolactonization reaction, we can conclude the following observations (See Experimental Section for experimental analysis and data):

a) The *syn*-addition shows *first order* dependence with respect to the carboxylic acid **III-1-D** and the chlorenium ion donor DCDMH.
b) The *anti*-addition product shows *first order* dependence with respect to DCDMH.
c) *Anti*-addition results in average being *half order* dependence with respect to the carboxylic acid **III-1-D** and 0.2 order for MCDMH.
d) Each diastereomer arises from two completely different mechanisms.

3.7. Conclusion

Overall, VTNA and concentration studies have revealed the order of each reagent during the course of the reaction, and provide evidence supporting the plausible differentiated transition states and reaction pathways leading to both the *syn*- and *anti*-addition products, independently. Moreover, it was also found that different cyclization diastereoselectivities are impacted by solvent and chlorenium sources. This information is important for the development of future halofunctionalization reactions. A full analysis and understanding of the reaction pathways and stereochemical control elements are essential to providing mechanistic reference points for the design of selective halofunctionalization of alkenes. More specifically, as more catalytic reactions are developed for halofunctionalization, the intrinsic nature of these reactions should be considered to simplify organocatalysis.

3.8. Experimental Section

3.8.1. General Information

Unless otherwise mentioned, solvents were purified as follows. $CDCl_3$, $CHCl_3$, and hexanes were purchased from Sigma Aldrich and incubated over 4Å MS for 48h prior to use. DCM was dried over CaH_2 and Et_2O was dried over sodium, and freshly distilled prior to use. DMF was freshly distilled over 4Å MS prior to use. NMR spectra were obtained using a 500 MHz Bruker Spectrometer, and referenced using the residual ^1H peak from the deuterated solvent. Column chromatography was performed using SiliCycle silica gel (230-400 mesh). Halofunctionalization reactions were performed in the absence of light. 1,3-Dichloro-5,5-dimethylhydantion (DCDMH) and 3-chloro-5,5-dimethylhydantion (MCDMH) was recrystallized prior to use.

3.8.2. Procedure for synthesis of labeled carboxylic acid III-1-D

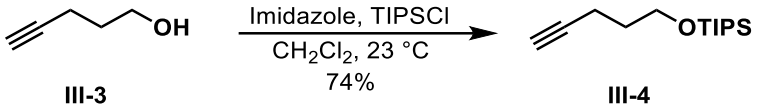

III-3 **III-4**

To a stirring solution of dichloromethane (43 mL) at room temperature was added imidazole (2.93 g, 43 mmol) and TIPSCl (9.2 mL, 43 mmol), and the reaction solution turned a milky white. 4-pentyn-1-ol (0.2 mL, 21.5 mmol) was added dropwise, and stirred overnight under argon. Water (80 mL) was added, partitioned, and the residual organics were extracted from the aqueous layer (3 x 50 mL). The combined organics were dried over Na_2SO_4, decanted, and concentrated under rotovap. The crude oil was subjected to column chromatography; 1% ethyl acetate/hexanes to afford **III-4** as a clear oil (3.8 g, 74% yield).

^{1}H NMR (500 MHz, Chloroform-*d*, 23℃) δ 3.77 (dd, *J* = 6.0, 5.9 Hz, 2H), 2.30 (dd, *J* = 7.1, 2.7 Hz, 2H), 1.91 (t, *J* = 2.7 Hz, 1H), 1.74 (ddd, *J* = 13.2, 7.1, 6.0 Hz, 2H), 1.22 – 0.76 (m, 21H).

^{13}C NMR (126 MHz, Chloroform-*d*, 23℃) δ 84.29, 68.14, 61.65, 31.75, 17.96, 14.84, 11.95.

HRMS: calculated for $C_{11}H_{22}OSi$ $[M+H - iPr]^+$ 198.1439, found 198.1385

IR: 3316 cm^{-1}, 2946 cm^{-1}, 2864 cm^{-1}, 1459 cm^{-1}, 1102 cm^{-1}

Prepared following literature precedent.[85]

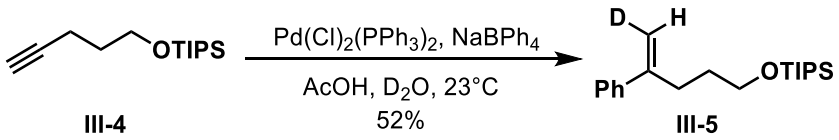

III-4 **III-5**

To a 10 mL flame dried round bottom was added TIPS protected alcohol **III-4** (0.5 g, 2.1 mmol), followed by $NaBPh_4$ (0.72 g, 2.1 mmol) and $Pd(Cl)_2(PPh_3)_2$ (44 mg, 0.0625 mmol) under argon. D_2O (4 mL) was added to the round bottom, followed directly by acetic acid (0.24 mL, 4.2 mmol), the solution turned a cloudy bright yellow, and stirred overnight under argon. Upon completion, which was verified *via* NMR, the reaction solution had turned a deep red color. The solution was filtered over a pad of celite, rinsed with hexanes, and concentrated. The crude product was subjected to column chromatography; 100% hexanes to afford the desired product as a clear oil in 52% yield (0.35 g).

^{1}H NMR for major *Z*-isomer (500 MHz, Chloroform-*d*, 23℃) δ 7.45 (m, 2H), 7.34 (m, 2H), 7.28 (m, 1H), 5.09 (s, 1H), 3.73 (dd, *J* = 6.3, 1.1 Hz, 2H), 2.63 (ddd, *J* = 8.9, 6.2, 1.3 Hz, 2H), 1.72 (ddd, *J* = 9.1, 6.3, 1.2 Hz, 2H), 1.17 – 1.04 (m, 21H).

^{13}C NMR for major *Z*-isomer (126 MHz, Chloroform-*d*, 23℃) δ 148.16, 141.19, 128.28, 127.32, 126.15, 112.16, 111.98 (t), 62.83, 31.70, 31.57, 18.09, 12.06.

HRMS: calculated for $C_{17}H_{27}DOSi$ $[M+H - iPr]^+$ 277.1987, found 277.1840

IR: 2939 cm^{-1}, 2864 cm^{-1}, 1462 cm^{-1}, 1105 cm

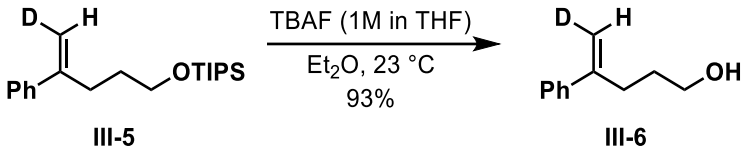

III-5 **III-6**

To a flame dried round bottom flask was added **III-5** (1.00 g, 3.13mmol) followed by Et_2O (33 mL). To the stirring solution was added tetrabutylammonium fluoride (1M in THF, 10 mL) and stirred at room temperature. Upon completion, verified *via* TLC, saturated ammonium chloride was added (20 mL), partitioned, and the residual organics were extracted with ethyl acetate (3 x 20 mL). The combined organics were dried over Na_2SO_4, decanted, and concentrated. The crude product was subjected to column chromatography; 20% ethyl acetate/hexanes to afford the pure product as a clear oil (0.473 g, 93%).

^{1}H NMR for major *Z*-isomer (500 MHz, Chloroform-*d*, 23℃) δ 7.43 (m, 2H), 7.33 (m, *J* = 7.6, 6.8, 1.2 Hz, 2H), 7.28 (m, 1H), 5.09 (dd, *J* = 1.3 Hz, 1H), 3.67 (dd, *J* = 6.4 Hz, 2H), 2.62 (m, 2H), 1.73 (m, 2H).

^{13}C NMR for major *Z*-isomer (126 MHz, Chloroform-*d*, 23℃) δ 147.85, 140.94, 128.33, 127.43, 126.10, 112.51 (t), 62.46, 31.49, 31.13.

HRMS: calculated for $C_{11}H_{13}DO$ $[M+H]^+$ 164.1186, found 164.1184

IR: 3336 cm^{-1}, 2258 cm^{-1}, 1059 cm^{-1}

Prepared following literature precedent.[78]

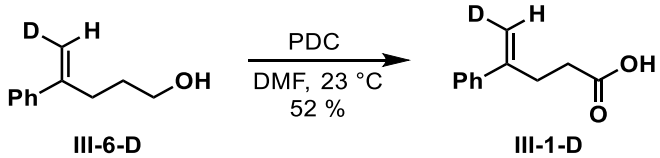

III-6-D **III-1-D**

In a flame dried flask, **III-6-D** (0.473 g, 2.9 mmol) was dissolved in dry DMF (14 mL) and PDC (3.8 g, 10.13 mmol) was added in one portion. The resulting mixture was stirred overnight at room temperature under argon. After completion of the reaction, monitored *via* TLC, a 1:1 mixture of ethyl acetate:hexanes was added (20 mL), and partitioned. The organic layer was washed with water (3 x 10 mL), and residual organics were extracted from the aqueous layer with 1:1 mixture of ethyl acetate:hexanes (2 x 10 mL). The organics were combined, dried over Na_2SO_4, decanted, and concentrated. The crude product was subjected to column chromatography; 30% ethyl acetate/hexanes to afford the pure product as a white crystalline solid [0.268 g, 52% yield, 5% *E* (5.25 ppm), 95% *Z* (5.08 ppm), and 12% 4-phenyl-4-pentenoic acid **III-1** (5.09 and 5.31 ppm)].

^{1}H NMR for major *Z*-isomer (500 MHz, Chloroform-*d*, 23℃) δ 7.43 (m, 2H), 7.38 (m, 2H), 7.30 (m, 1H), 5.12 (dd, *J* = 1.4 Hz, 1H), 2.97 (dd, *J* = 8.6, 6.9 Hz, 2H), 2.56 (dd, *J* = 8.7, 6.9 Hz, 2H).

^{13}C NMR for major *Z*-isomer (126 MHz, Chloroform-*d*, 23℃) δ 179.22, 146.43, 140.37, 128.44, 127.69, 126.08, 112.99, 112.71 (t), 32.93, 30.07.

HRMS: calculated for $C_{11}H_{11}DO_2$ $[M-H]^-$ 176.0822, found 176.0820

IR: 2273 cm^{-1}, 1696 cm^{-1}, 1602 cm^{-1}

3.8.3. Non-catalyzed chlorolactonization of III-1-D

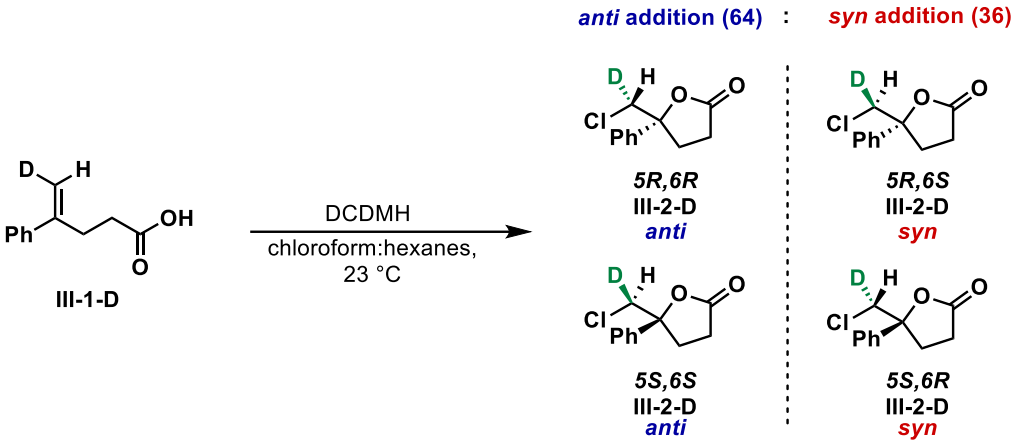

To a flame dried screw-top vial equipped with a stir bar was added DCDMH (21 mg, 0.11 mmol, 1.1 equiv) and deuterated 4-phenyl-4-pentenoic acid **III-1-D** (18 mg, 0.1 mmol, 1 equiv). These reagents were dissolved in a 1:1 mixture of chloroform: hexanes, and stirred at room temperature for 72 h. After completion of the reaction, monitored *via* NMR, the reaction mixture was poured into a separatory funnel chloroform (5 mL) was added. The organic layer was washed with aqueous Na_2SO_3 (2 x 5 mL), and residual organics were extracted from the aqueous layer with chloroform (2 x 10 mL). The combined organics were dried over Na_2SO_4, decanted, and concentrated. The crude product was purified by silica gel chromatography; 20% ethyl acetate/hexanes to afford the desired product as a mixture of two diastereomers in 90% yield (21 mg).

^{1}H NMR (500 MHz, Chloroform-*d*, 23℃) δ 7.54 – 7.34 (m, 5H), 3.83 (s, 0.6H, *anti*-diastereomer), 3.74 (s, 0.3H, *syn*-diastereomer), 2.83 (m, 2H), 2.5 (m, 2H).

^{13}C NMR (126 MHz, Chloroform-*d*, 23℃) δ 175.70, 140.65, 128.86, 128.68, 124.88, 87.04, 51.88 (t) 31.38, 29.01.

3.8.4. Procedure to measure diastereomeric ratio

Following the method published previously in our lab,[78] we are able to calculate the diastereomeric ratio and obtain a *syn*:*anti* ratio. Since there is 12% unlabeled alkenoic acid **III-1**, the integral of each diastereomer was calculated by subtracting the integral of the overlapping non-labeled product as shown in Figure 3.18. Peaks **a**, **b**, **d**, and **e** result in an AB quarter and belong to the non-labeled substrate. Since the integrals of peaks **a** and **e** are equivalent (**a** = **e** = **5.91**) and similarly with integral values for **b** and **d** (**b** = **d** = **11.85**). Peaks **c** and **f** belong to the deuterated product and overlap with **b** and **e**, respectively. Therefore, to obtain the correct values for the deuterated peaks (**c** and **f**), the non-labeled product is subtracted. For example, the correct integral of **c** results from subtracting the integral value of **d** from the overall integral of **c** and **b** (**c** = 100 – **11.85** = **88.15**). Similarly, the correct integral of **f** results from subtracting the integral value of **a** from the overall integral value of **e** and **f** (**f** = 55.18 – **5.91** = **49.27**).

Figure 3.19: ^{1}H NMR spectrum of labeled lactone product with DCDMH

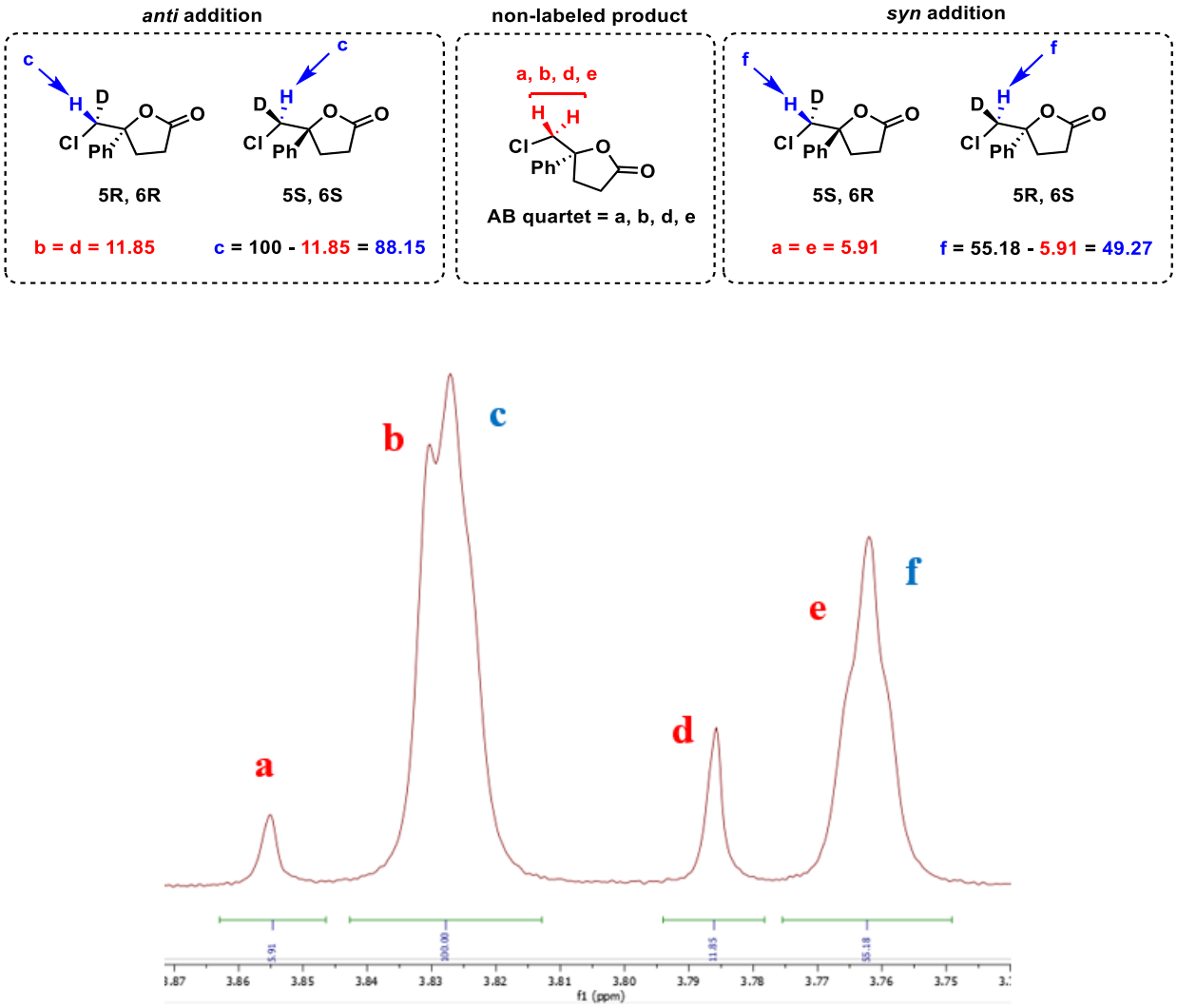

This calculation prior to the 5% correction for the presence of the *E*-isomer, the *syn*:*anti* ratio is 39:61. For correction of the E/Z isomeric mixture, we used the following equations. D_1-*syn* will indicate the diastereomers resulting in *syn*-addition, and D_2-*anti* will indicate the diastereomers resulting in *anti*-addition. Defining the fraction of the product that arises from attack of Cl^+ on the olefin that is *anti* to the nucleophile as A, and that is *syn* to the nucleophile as S, the following equations can be evaluated:

$$D_{1-syn} = E\ \frac{A}{(A+S)} + Z\frac{S}{(A+S)} \qquad (i)$$

$$D_{2-anti} = Z\frac{A}{(A+S)} + E\frac{S}{(A+S)} \qquad (ii)$$

After rearranging and cross-multiplying the above equations, we get equation (*iii*). Since the diastereomeric integral values are available from ^{1}H NMR after correcting for the dihydrogen isomer, integral values of peaks **c** and **f** are 88.15 and 49.27, respectively. Those corresponding values are inserted into equation (*iii*) to determine the ratio of *anti*-addition to *syn*-addition.

$$\frac{D_{1-syn}}{D_{2-anti}} = \frac{(A\ x\ E) - (S\ x\ Z)}{(S\ x\ E) - (A\ x\ Z)} \qquad (iii)$$

Inputting those values will give:

$$\frac{D_{1-syn}}{D_{2-anti}} = \frac{(88.15\ x\ 5) - (49.27\ x\ 95)}{(49.27\ x\ 5) - (88.15\ x\ 95)} = 0.5216 \qquad (iv)$$

Hence, %D_1-*syn* = 34.28 and %D_2-*anti* = 65.72, therefore ***anti*-addition:*syn*-addition = 66:34**

3.8.5. $(DHQD)_2PHAL$ Catalyzed Chlorolactonization of III-1-D

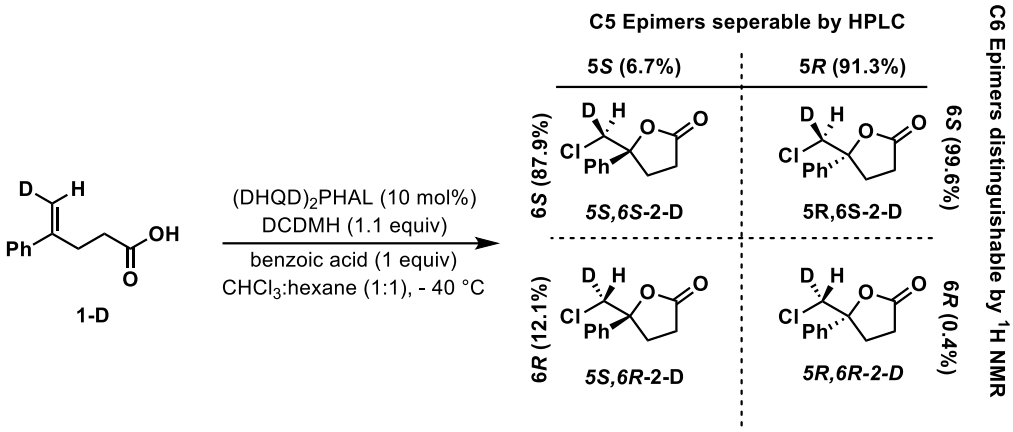

To a flame dried screw-top vial equipped with a stir bar was added $(DHQD)_2PHAL$ (8 mg, 0.01 mmol), DCDMH (22 mg, 0.11 mmol), and benzoic acid (12 mg, 0.1 mmol). A 1:1 solvent mixture of chloroform:hexanes was added (2 mL), and the reaction was cooled to -40℃ using an immersion cooler. The solution was stirred at -40℃ for 20 min. The deuterated carboxylic acid **III-1-D** (18 mg, 0.1 mmol) was added in one portion. The resulting mixture was stirred at -40℃ for 6 h. After completion, the reaction was poured into a separatory funnel, diluted with chloroform (10 mL), and the organic layer was washed with 0.1 M aqueous NaOH (2 x 10 mL). The residual organics were extracted from the aqueous layer using chloroform (2 x 10 mL). The combined organics were dried over Na_2SO_4, decanted, and concentrated. The crude isolate was purified by column chromatography; 20% ethyl acetate/hexanes. Diastereomers at the C6 are not separable using chiral HPLC, however, C5 diastereomers, obtained in a ratio of (5*R*:5*S*) = 93.3:6.7, are separable using a chiralpak OJ-H column (15% *iso*-propanol in hexanes; 0.8 mL/min; 254 nm; RT_1 = 23.15 min (5*R*) and RT_2 = 32.43 min (5*S*)).

The *dr* ratio is obtained *via* chiral HPLC separation, where *R* configuration is favored at C5 position. Since HPLC does not separate deuterated and non-deuterated analogues, we

determined the *syn:anti* ratio for each set of diastereomers after HPLC purification via ^{1}H NMR using the method described above, Section 3.8.3.b. For example, the *R* configuration at C5 is composed of two diastereomers, (5*R*, 6*S*) and (5*R*, 6*R*), which lead to the *syn*- and *anti*-product, respectively. Whereas the *S* configuration at C5 is composed of (5*S*, 6*R*) and (5*S*, 6*S*), which lead to the *syn*- and *anti*-product, respectively (Figure 3.19).

Figure 3.20: Face selectivity in catalyzed chlorolactonization using HPLC and ^{1}H NMR

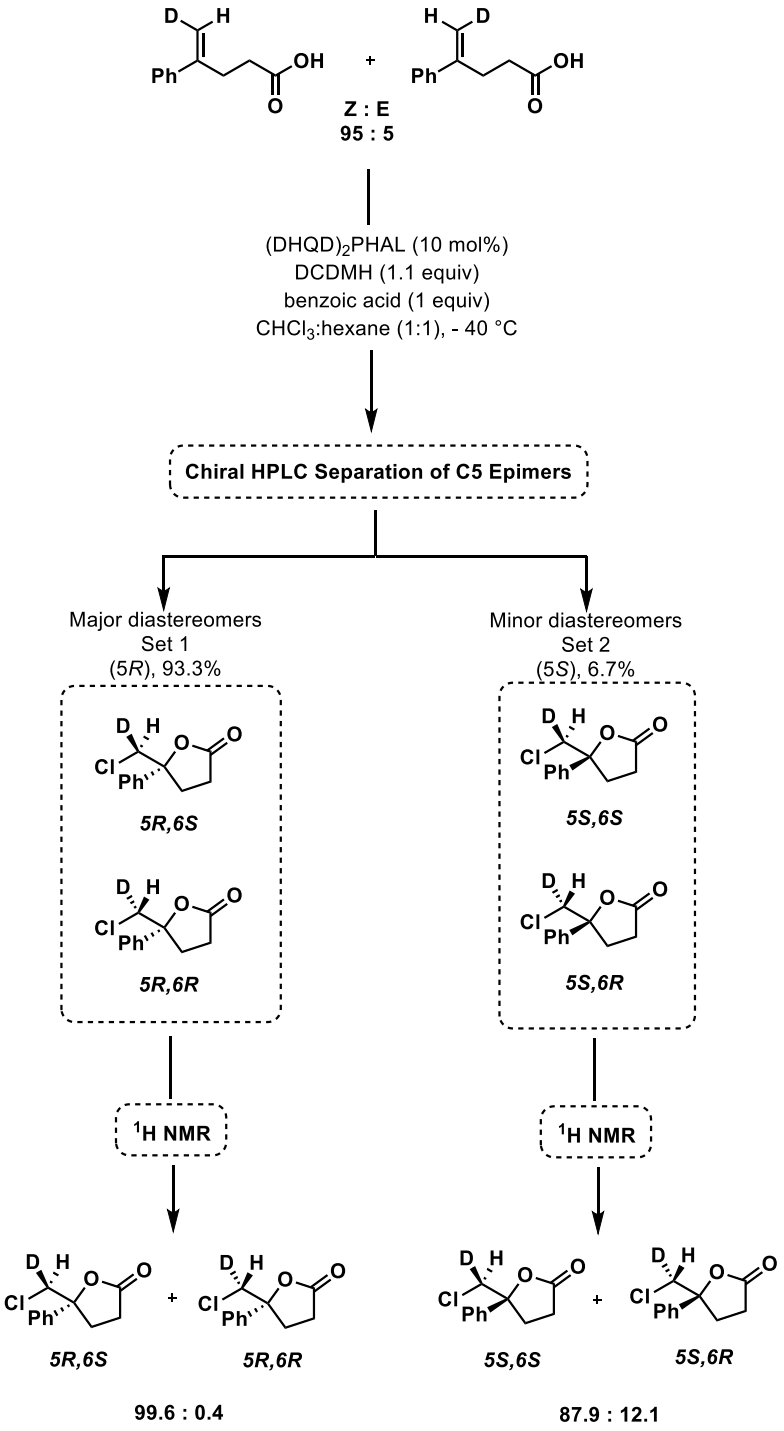

3.8.6. Procedure to measure diastereomeric ratio

In order to obtain the four isomeric products ratios, ^{1}H NMR was implemented after chiral chromatography HPLC. The 5*R*, set 1, contains both (5*R*, 6*S*) and (5*R*, 6*R*), and the 5*S*, set 2, contains both (5*S*, 6*R*) and (5*S*, 6*S*). ^{1}H NMR analysis of both sets revealed a *dr* of *syn:anti* ratio for set 1 to be (>99:1), and a *dr* ratio of *syn:anti* for set 2 to be (12:88). These values are after correction for the non-labeled product and the *Z/E* mixture of the starting material. The corrections are described below.

The steps towards calculating the *dr* of the 5*S* and 5*R* products are as follows. First, the non-labeled product integral values were subtracted from the overall integral values of the diastereomers, as discussed earlier in Section 3.8.3.b and shown in Figure 3.18. As measured from ^{1}H NMR there is a 95:5 mixture of *Z:E* olefin starting material **III-1-D**. Thus, the *E* olefin contributes a fraction to the (*5R,6S)* product via *anti*-addition, whereas (*5R, 6R*) is formed though *syn*-addition. For correction of this isomer, we used the following equations.

Defining the fraction of the product that arises from attack of Cl^+ on the olefin that is *anti* to the nucleophile as A, and that is *syn* to the nucleophile as S, the following equations can be evaluated.

$$(5R, 6S) = Z\,\frac{S}{(A+S)} + E\,\frac{A}{(A+S)} \qquad (v)$$

$$(5R, 6R) = E\,\frac{S}{(A+S)} + Z\,\frac{A}{(A+S)} \qquad (vi)$$

After rearranging and cross-multiplying:

$$\frac{A}{S} = \frac{((5R, 6S)\ x\ E) - ((5R, 6R)\ x\ Z)}{((5R, 6R)\ x\ E) - ((5R, 6S)\ x\ Z)} \qquad (vii)$$

For the 5*R* diastereomer, equation *vii* is used, which is similar to equation *iii.* The diastereomeric ratio is available from ^{1}H NMR by correcting for the dihydrogen isomer as shown in Figure 3.19 and discussed above in Section 3.8.3.b.

syn-addition:*anti*-addition calculation for the 5*R* Isomer (Set 1):

Figure 3.21. ^{1}H NMR spectrum of labeled lactone product (5*R*) catalyzed by $(DHQD)_2PHAL$

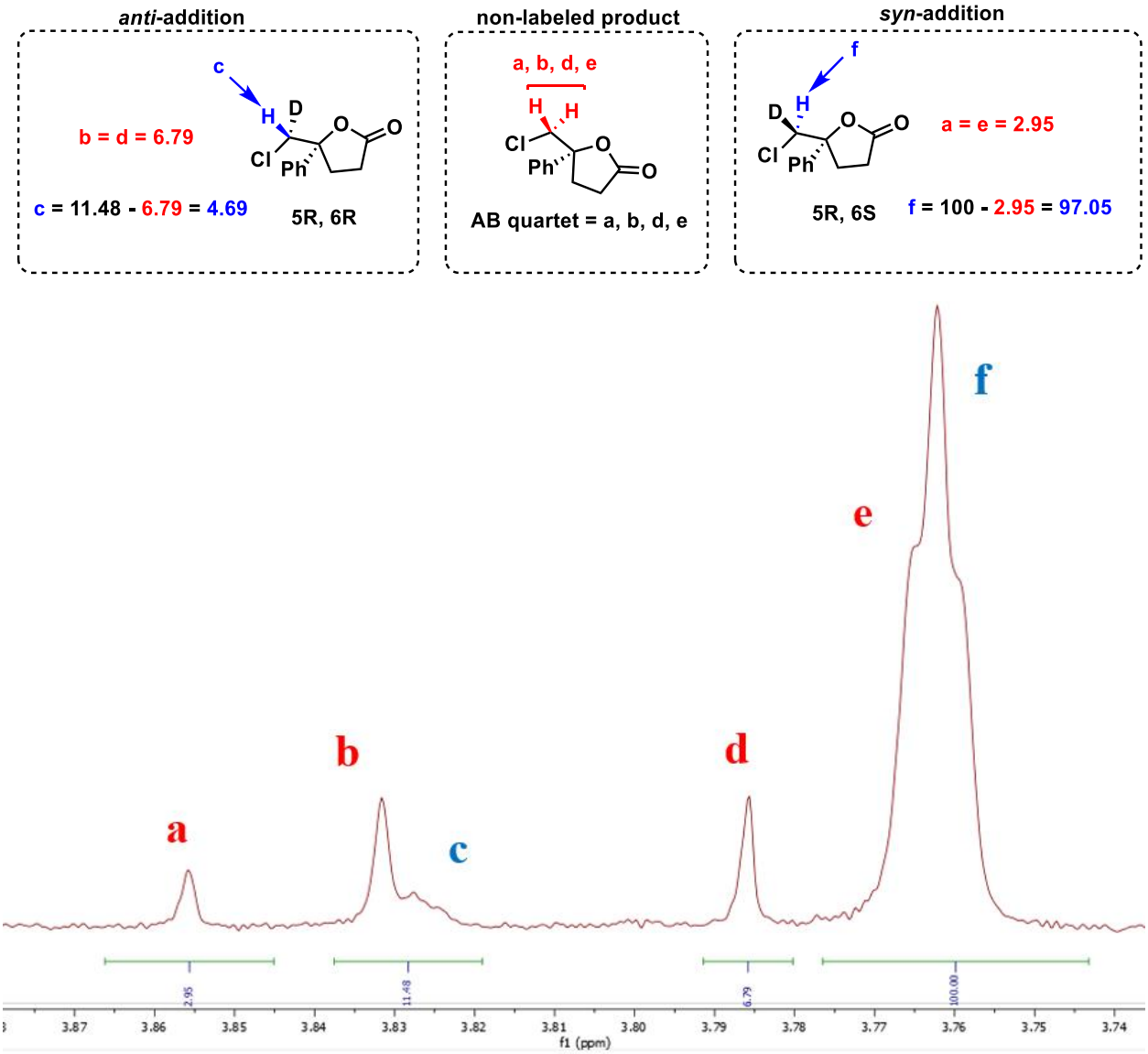

The values of **c** and **f** can be inserted into equation *vii* above. That leads to the following:

$$\frac{A}{S} = \frac{(97.05\ x\ 5) - (4.69\ x\ 95)}{(4.69\ x\ 5) - (97.05\ x\ 95)} = 0.0043 \qquad (viii)$$

Hence, %D_1-*syn* = 99.5 and %D_2-*anti* = 0.5, therefore ***anti*-addition:*syn*-addition = 0.5:99.5**

syn-addition:*anti*-addition calculation for the 5*S* Isomer (Set 2):

Similar to the 5*R* isomer, 5*S* diastereomers *syn:anti* ratio can be determined by the following equation:

$$\frac{S}{A} = \frac{((5S, 6S)\ x\ E) - ((5S, 6R)\ x\ Z)}{((5S, 6R)\ x\ E) - ((5S, 6S)\ x\ Z)} \qquad (x)$$

For the 5*S* diastereomer, equation *x* is used, which is similar to equation v*ii.* The diastereomeric ratio is available from ^{1}H NMR by correcting for the dihydrogen isomer as shown in Figure 3.19 and discussed above in Section 3.8.3.b.

Figure 3.22: ^{1}H NMR spectrum of labeled lactone product (5*S*) catalyzed by $(DHQD)_2PHAL$

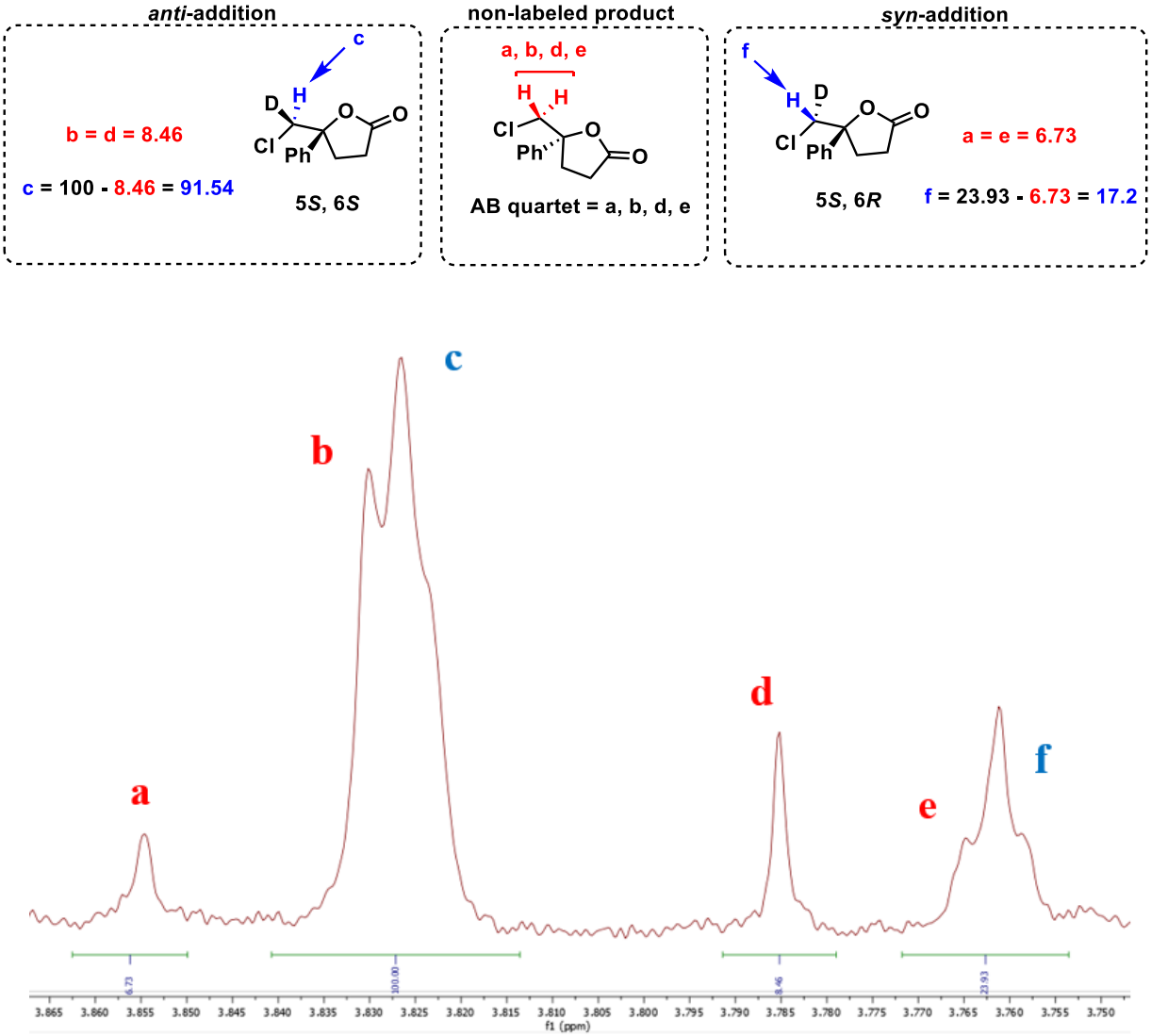

Those values of **c** and **f** can be inserted into equation *x* above. That leads to the following:

$$\frac{S}{E} = \frac{(91.54\ x\ 5) - (17.2\ x\ 95)}{(17.2\ x\ 5) - (91.54\ x\ 95)} = 0.136 \qquad (v)$$

Hence, %D_1-*syn* = 12.1 and %D_2-*anti* = 87.9, therefore ***anti*-addition:*syn*-addition = 88:12**

3.8.7. Absolute Stereochemical Determination at the Deuterated Carbon

Scheme 3.4: Synthesis of Epoxy Alcohol

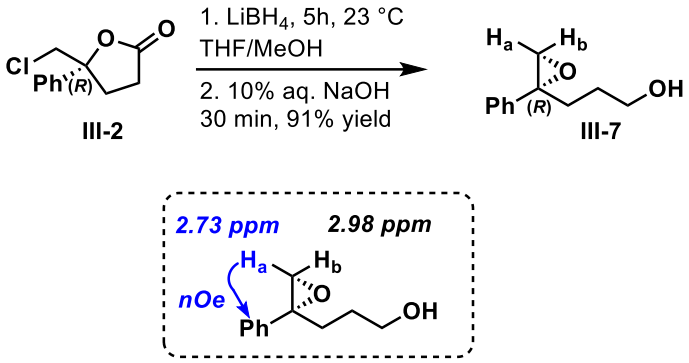

Shown previously in our lab,[78] we are able to convert the lactone **III-2** into epoxy alcohol **III-7**. This is done by a lithium borohydride reduction, followed by a sodium hydroxide mediated cyclization of the resulting chlorohydric intermediate to provide the epoxy alcohol. Performing nOe studies show that H_a, which shows up at 2.73 ppm, has a *syn*-orientation to the phenyl group and H_b, 2.98 ppm, has an *anti*-orientation to the phenyl group. This assignment allowed us to correspond epoxy alcohol **III-7** to the catalyzed lactone labeled product version **III-7-D**.

Scheme 3.5: Absolute stereochemistry determination for the labeled carbon

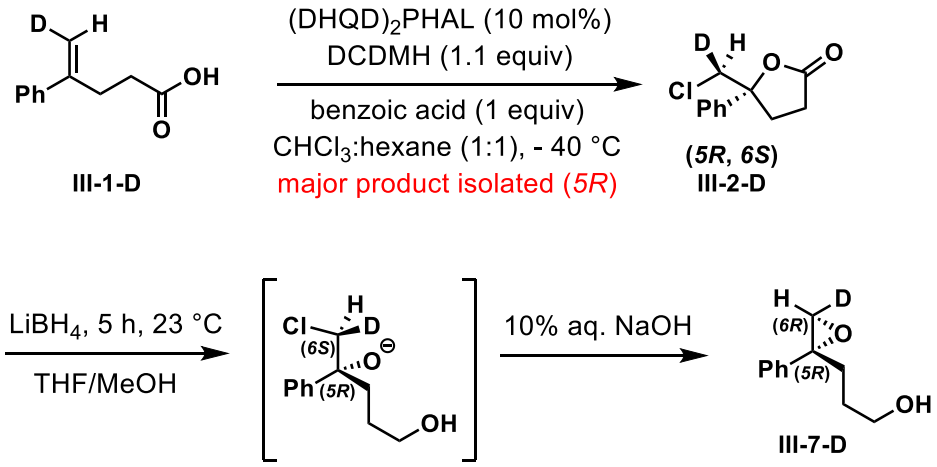

Lactone **III-2-D**, that was synthesized in the presence of $(DHQD)_2PHAL$ was reduced in the presence of lithium borohydride, followed by sodium hydroxide to provide **III-7-D** as the product. ^1H NMR analysis of epoxy alcohol **III-7-D** has a peak at 2.73 ppm, which suggests the deuterium has an *anti*-orientation to the phenyl group. Thus, we can assign an *R* configuration at the carbon bearing the deuterium in **III-7-D**. Since this is formed via S_N2 cyclization from the chlorohydrin intermediate, thus, lactone **III-2-D** is assigned the *S* configuration on the carbon bearing the deuterium.

3.8.8. General Procedure for Synthesis of Epoxy Alcohol III-7-D

Lactone **III-2-D** (25 mg, 0.12 mmol) was dissolved in a 1:1 THF:MeOH mixture (1 mL) and cooled to 0 ℃. Lithium borohydride (8 mg, 0.36 mmol) was added in one portion, and allowed to stir for 5 h at room temperature. To the reaction was then added 10% aqueous NaOH solution (1 mL) and stirred for 30 min at room temperature. The reaction was diluted with dichloromethane (1 mL), placed into a separatory funnel, and partitioned. The

residual organics were extracted from the aqueous layer with DCM (2 x 2 mL). The combined organics were dried over Na_2SO_4, decanted, and concentrated. The crude product was purified via chromatography; 30% ethyl acetate/hexanes with 1% Et_3N to yield **III-7-D** as a colorless oil in 86% yield (10.1 mg).

^{1}H NMR (500 MHz, Chloroform-*d*, 23℃) δ 7.46 – 7.27 (m, 5H), 3.66 (br. m, 2H), 2.73 (s, 1H), 2.43 (m, 1H), 1.78 (m, 1H), 1.65 (m, 2H).

^{13}C NMR (126 MHz, Chloroform-*d*, 23℃) δ 128.42, 127.51, 125.83, 62.32, 60.04, 55.80 (t), 31.62, 27.85.

3.8.9 Kinetic Studies

3.8.10. Sample Preparation for Kinetic Studies

A stock solution of internal standard (*tert*-butyl methyl ether, 0.0667 mmol) was freshly prepared in hexanes (2 mL). In two additional vials, stock solutions of DCDMH (0.11 mmol) in $CDCl_3$ (0.5 mL), and deuterated 4-phenyl-4-pentenoic acid **III-1-D** (0.1 mmol) in $CDCl_3$ (0.5 mL) was freshly prepared each time. Kinetic experiments were performed as follows: To each NMR tube, 0.2 mL of the internal standard stock solution, and 0.2 mL **III-1-D** stock solution was added, followed with 0.2 mL of hexanes to total 0.6 mL of solvent in the NMR tube. The DCDMH stock solution was added, totaling 0.8 mL of solvent, briefly shaken, and quickly inserted into the NMR at room temperature. An initial ^1H NMR was taken, and then the NMR instrument was set up to collect data every 30 mins over the course of 72 h.

3.8.11. Kinetic Experiments and Procedure to Measure *syn* & *anti* Concentration from Isomeric Mixture

Based on the constant concentration of the internal standard (*tert*-butyl methyl ether), concentration of the product **III-2-D** was calculated for the *syn*- and *anti*-product at each data point. The concentration of DCDMH was determined by the amount of product at each data point. The chloromethylene product peaks that is a result of the *Z*-isomer, *E*-isomer, and unlabeled substrate that appears at 3.8 ppm, were used to determine the concentration of the *syn*- and *anti*-product, as well as the DCDMH concentration by

subtracting the concentration of what had reacted from the initial concentration of DCDMH. The peak at 5.12 ppm correspond to the *Z*-isomer, the peak at 5.32 ppm corresponds to the *E*-isomer, and the peaks at 5.14 and 5.34 ppm correspond to the unlabeled starting material, and these peaks were measured to determine the concentration throughout the reaction. The alkene starting material concentration was determined via ^{1}H NMR and solely the *Z*-isomer was measured for VTNA analysis.

To correct for the isomeric mixture of products, the integrals of the unlabeled starting material were subtracted from the overall integral of the labeled diastereomers, as explained earlier in Section 3.8.3.b. Furthermore, as measured earlier by ^{1}H NMR, the deuterated alkenoic acid contains 5% impurity of the *E*-olefin. To account for this and to calculate the correct concentration of the *syn*-product and the *anti*-product we used the following equations. The *syn*-product is a result of *syn*-addition across the *Z*-olefin, and *anti*-addition across the *E*-olefin. Similarly, the *anti*-product is a combination of *anti*-addition to the *Z*-olefin and a fraction of *syn*-addition to the *E*-olefin.

Thus, to calculate the *syn*-product concentration arising solely from the *Z*-olefin, the following equation was used, which is derived from equation *iii*.

$$[syn] = (S\ x\ Z) - (A\ x\ E)$$

The *anti*-product is a result of *anti*-addition to the *Z*-olefin and *syn*-addition to the *E*-olefin, therefore, to calculate the *anti*-product concentration from the *Z*-olefin the following equation was used, which is derived from equation *iii*.

$$[anti] = (A\ x\ Z) - (S\ x\ E)$$

At each data point, those calculations were performed to find the concentration of *syn*-product and *anti*-product independent of one another that is a result of the *Z*-olefin. The experiments designed to determine the order in each reagent is described in Table 3.3.

Table 3.3. VTNA experiment studies

Exp	[III-1-D] (M)	[DCDMH] (M)
A	0.03	0.055
B	0.05	0.055
C	0.05	0.1

The kinetic profile of each experiment is plotted as time (s) vs product concentration (M) after the correction for the Z-isomer. This plot is prior to any VTNA analysis is performed.

Figure 3.23. Kinetic profile of product formation for 0.03 M **III-1-D** and 0.055 M DCDMH

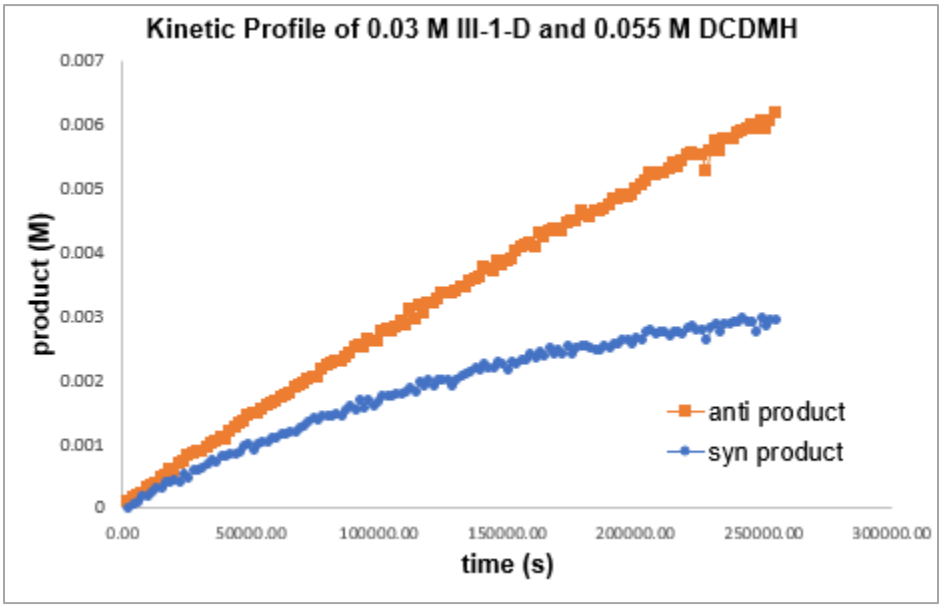

Figure 3.24. Kinetic profile of product formation for 0.05 M **III-1-D** and 0.055 M DCDMH

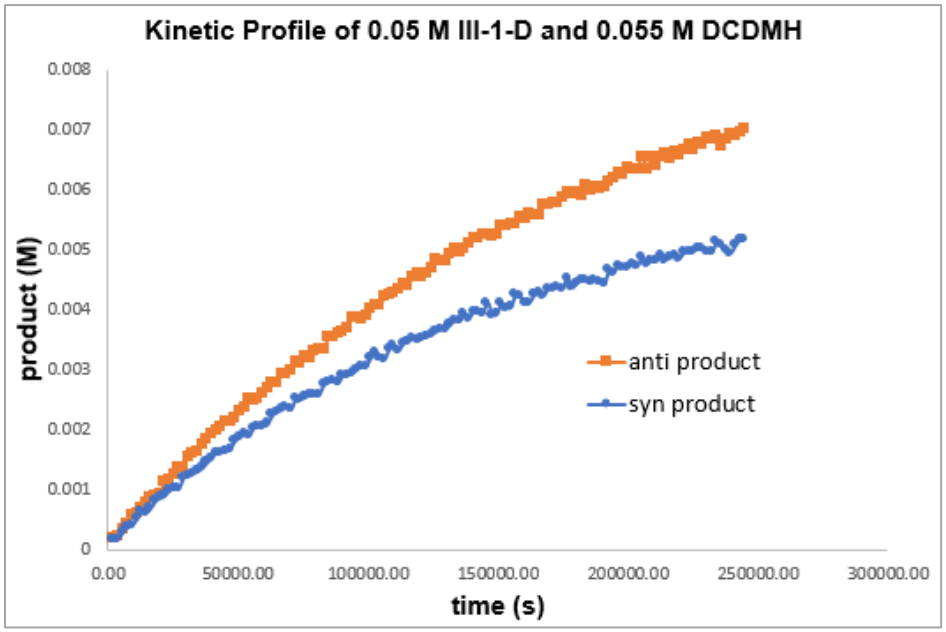

Figure 3.25. Kinetic profile of product formation for 0.05 M **III-1-D** and 0.1 M DCDMH

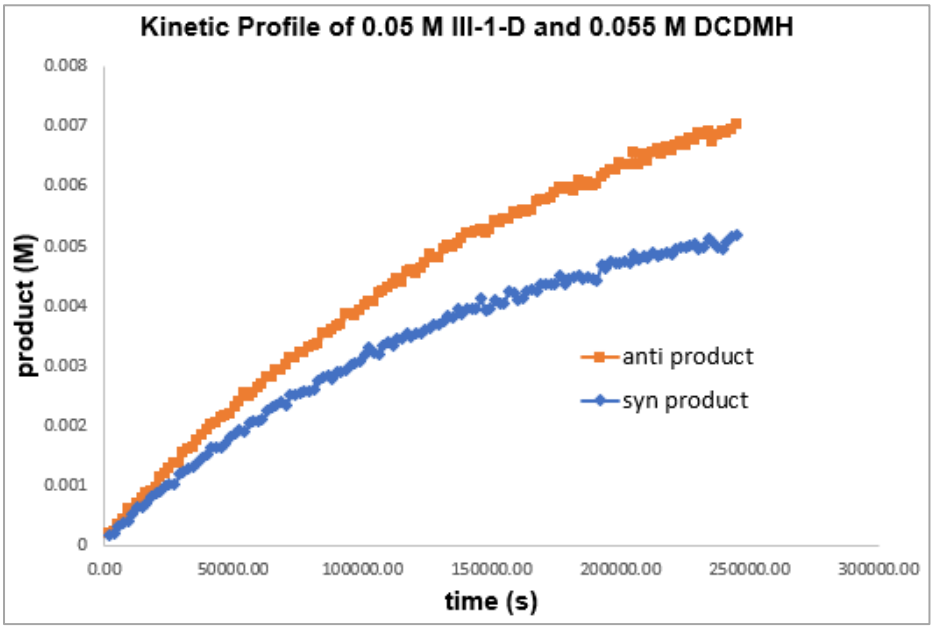

3.9.12. Catalog of Spectra

Figure 3.26. ^{1}H NMR of compound **III-4** (500 MHz, Chloroform-*d*, 23℃)

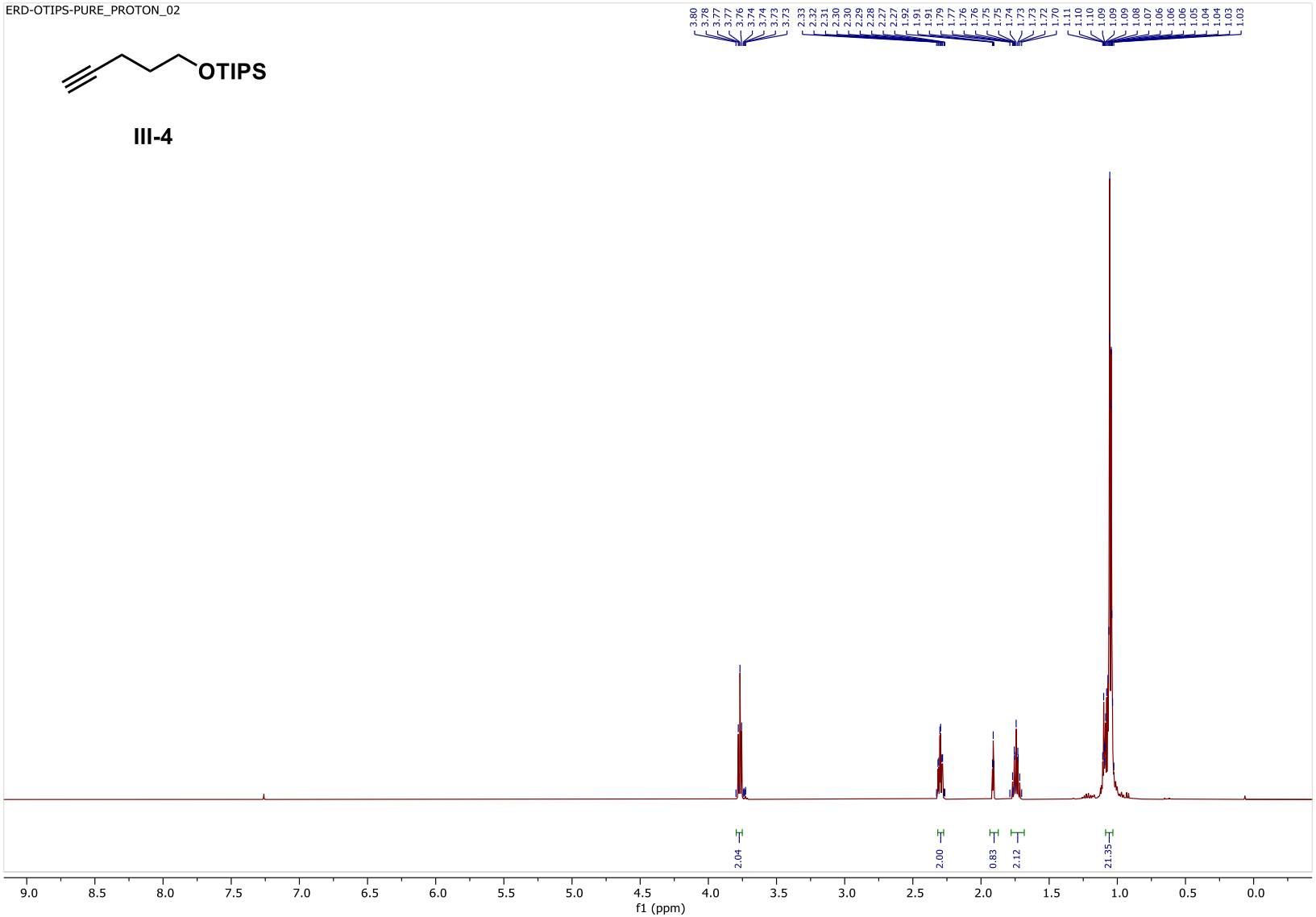

Figure 3.27. ^{13}C NMR of compound **III-4** (126 MHz, Chloroform-*d*, 23 ℃)

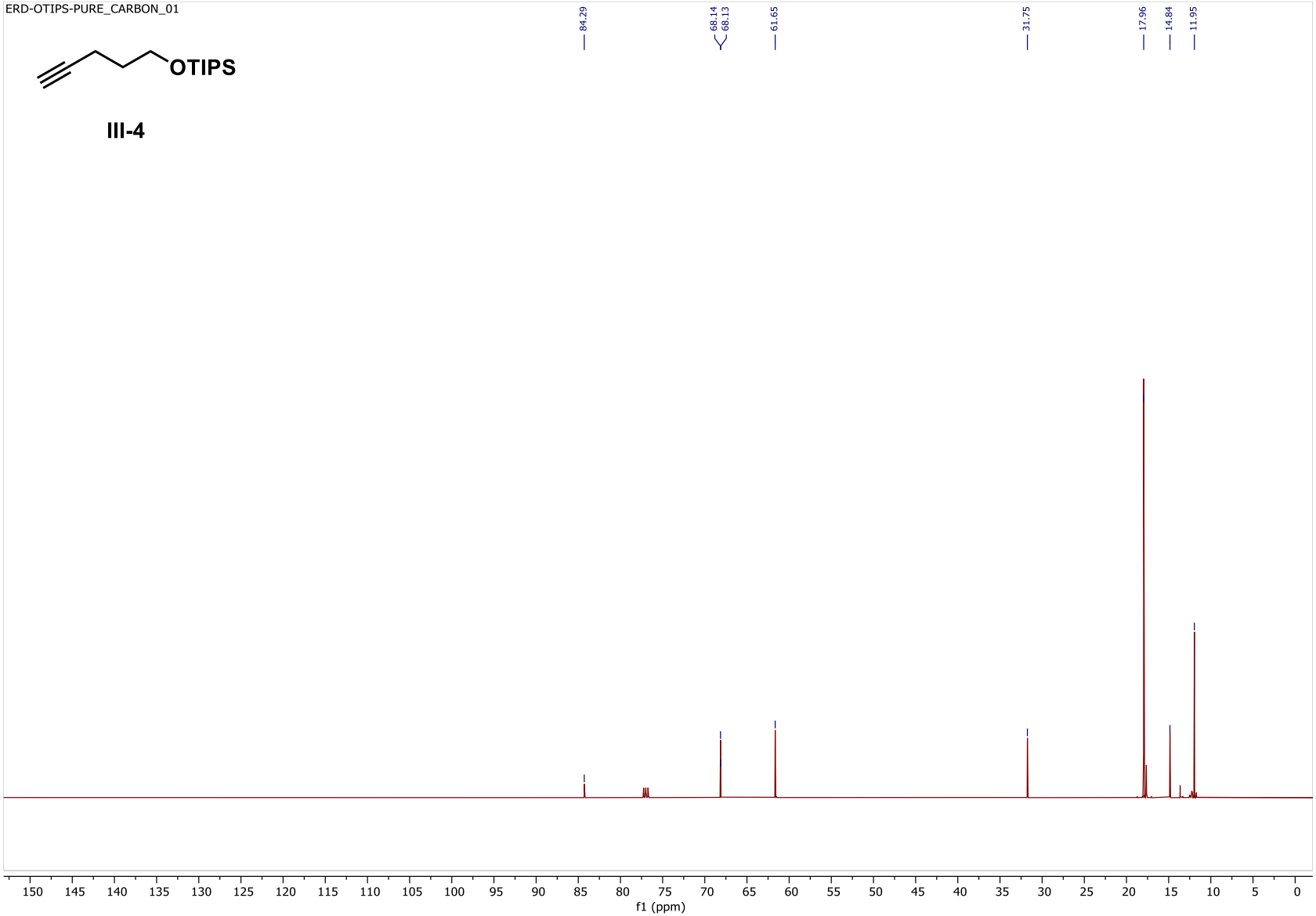

Figure 3.28. ^{1}H NMR of compound **III-5** (500 MHz, Chloroform-*d*, 23℃)

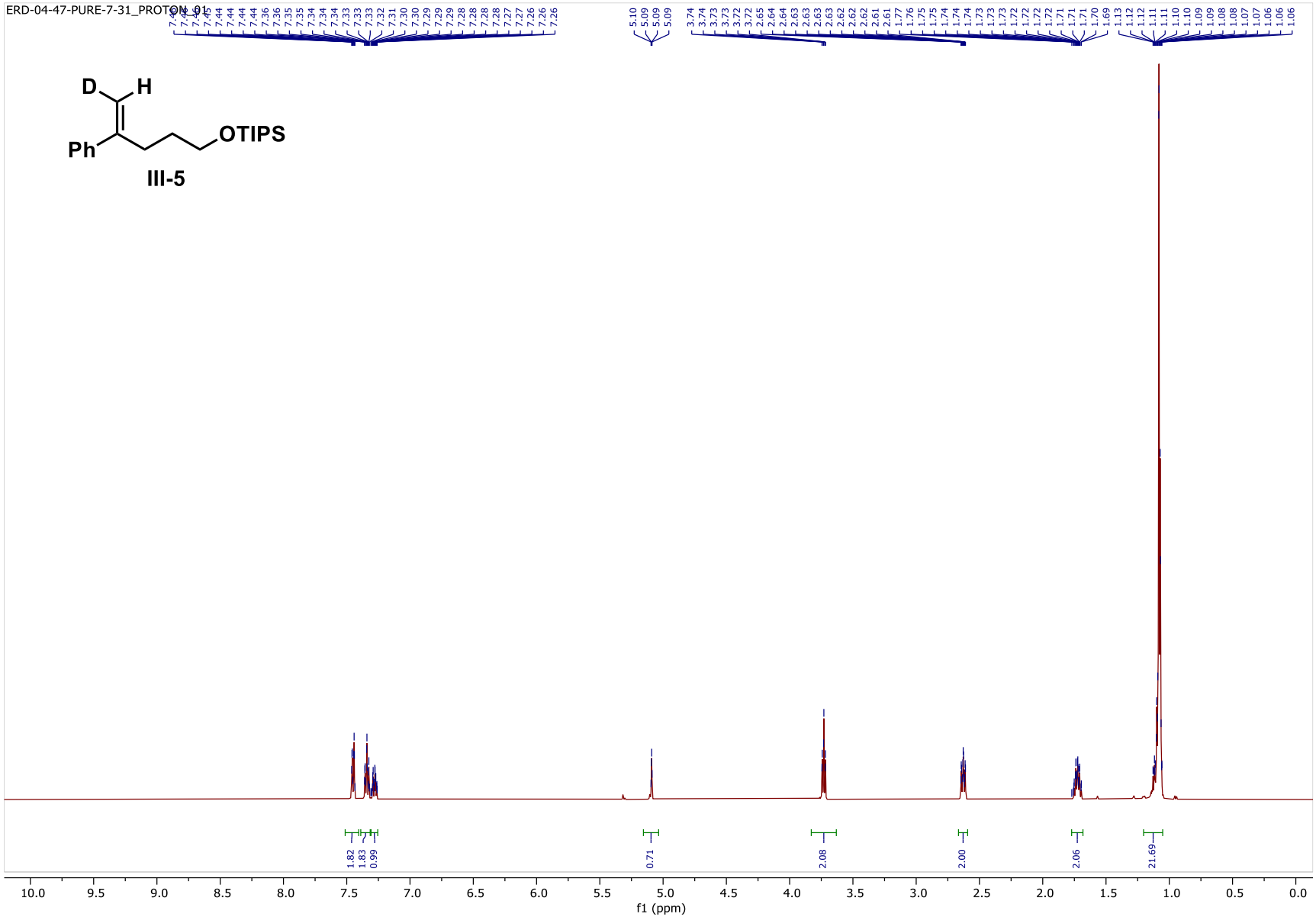

Figure 3.29. ^{13}C NMR of compound **III-5** (126 MHz, Chloroform-*d*, 23 ℃)

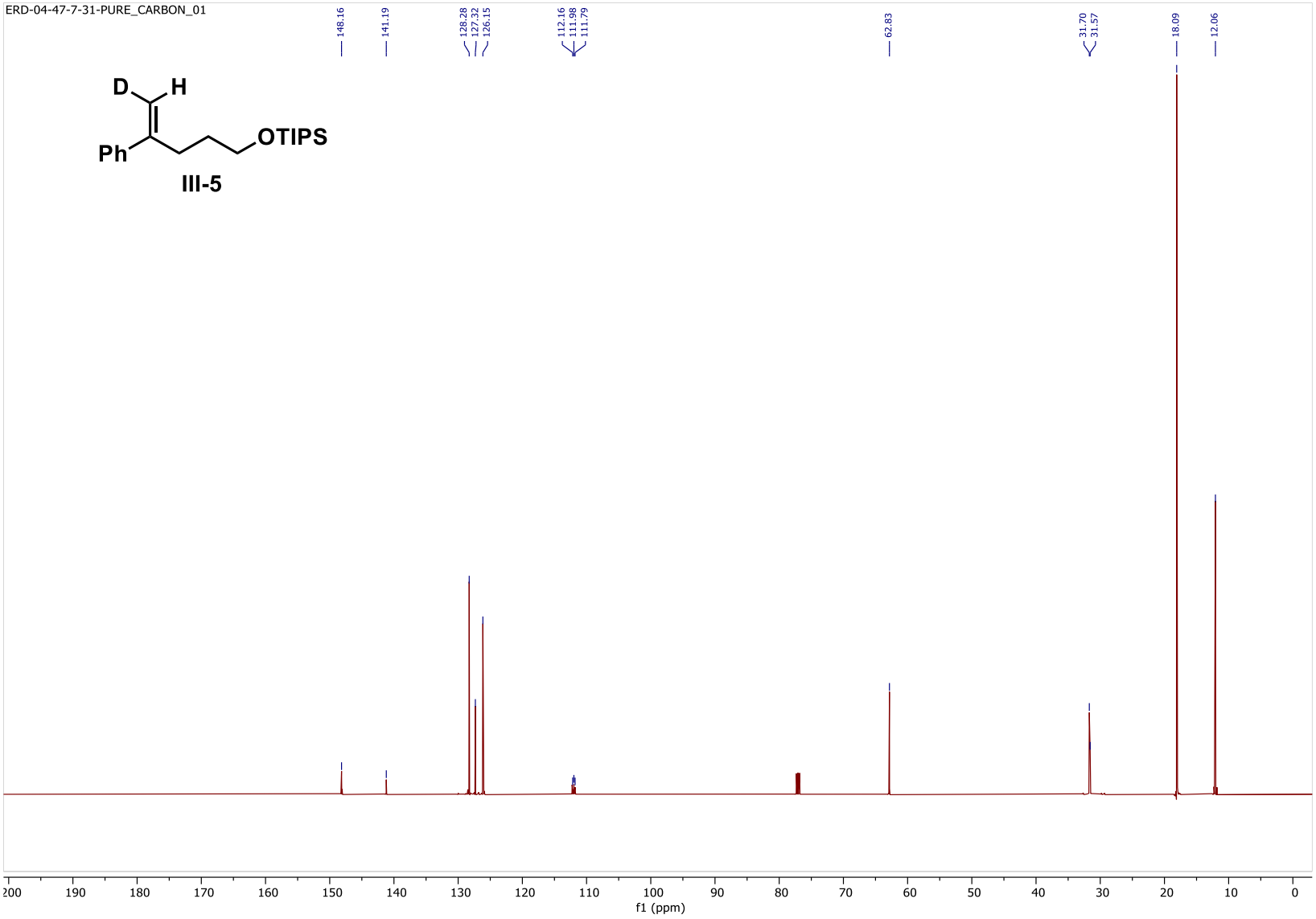

Figure 3.30. ^{1}H NMR of compound **III-6** (500 MHz, Chloroform-*d*, 23℃)

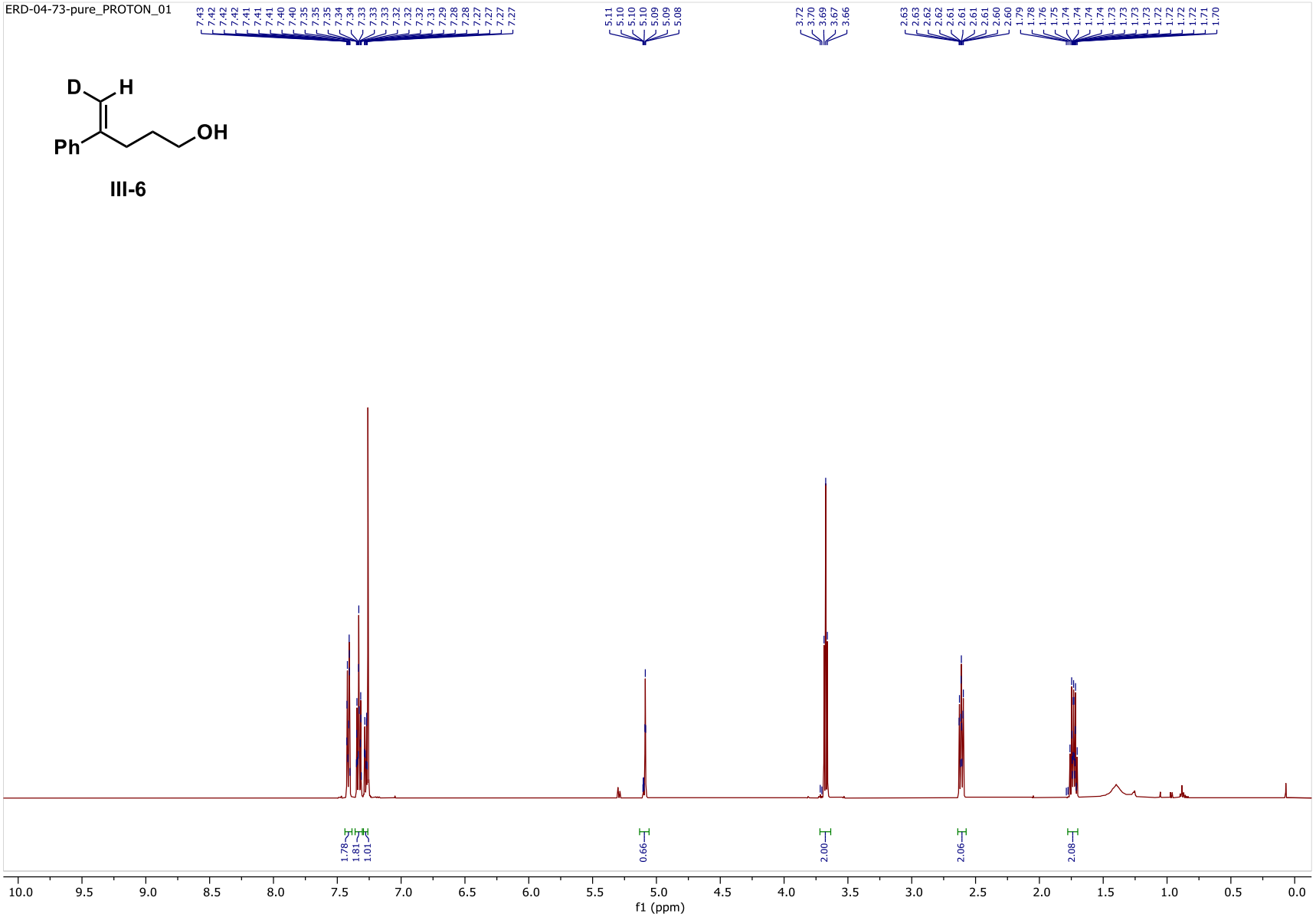

Figure 3.31. ^{13}C NMR of compound **III-6** (126 MHz, Chloroform-*d*, 23 ℃)

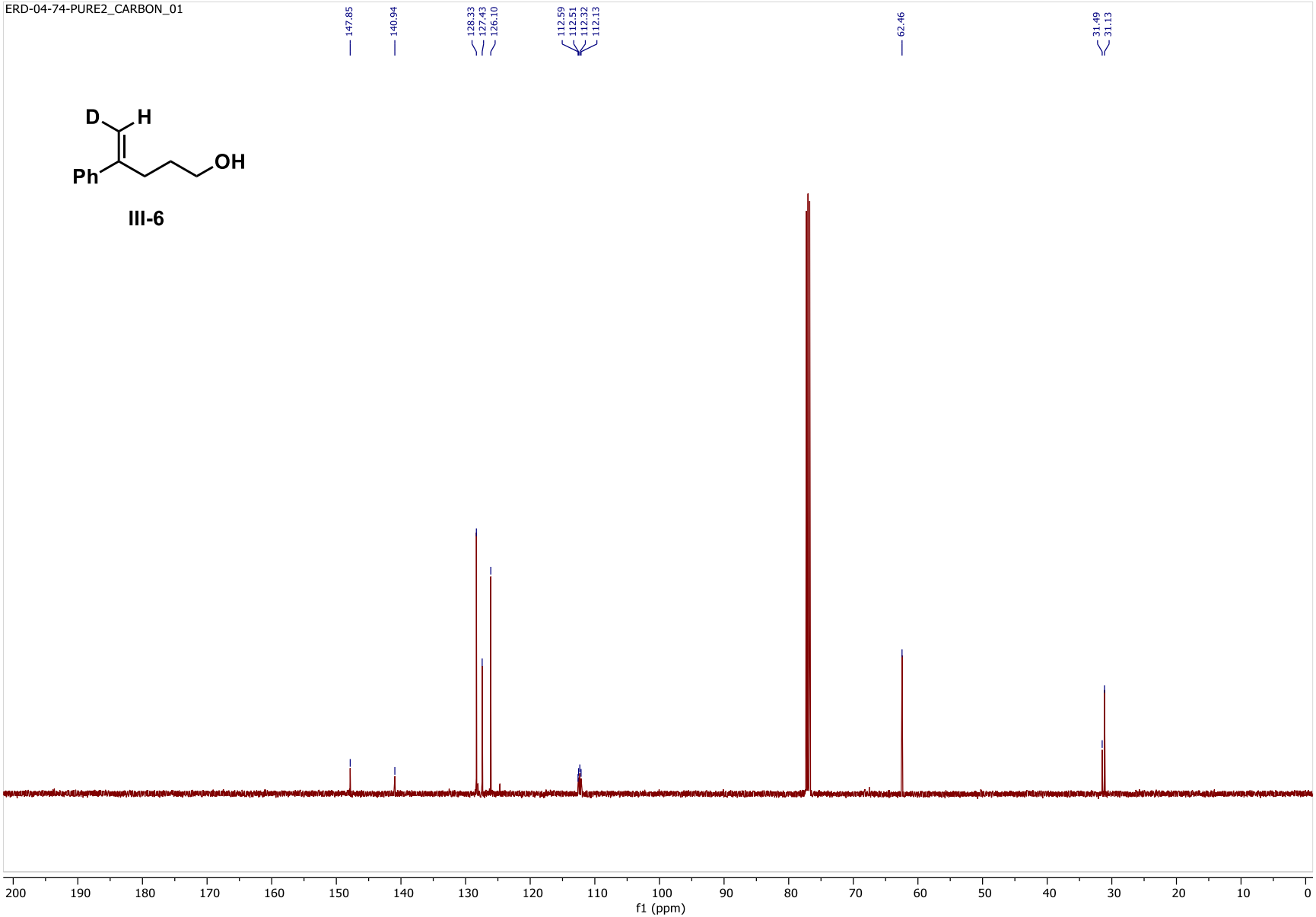

Figure 3.32. ^{1}H NMR of compound **III-1-D** (500 MHz, Chloroform-*d*, 23 ℃)

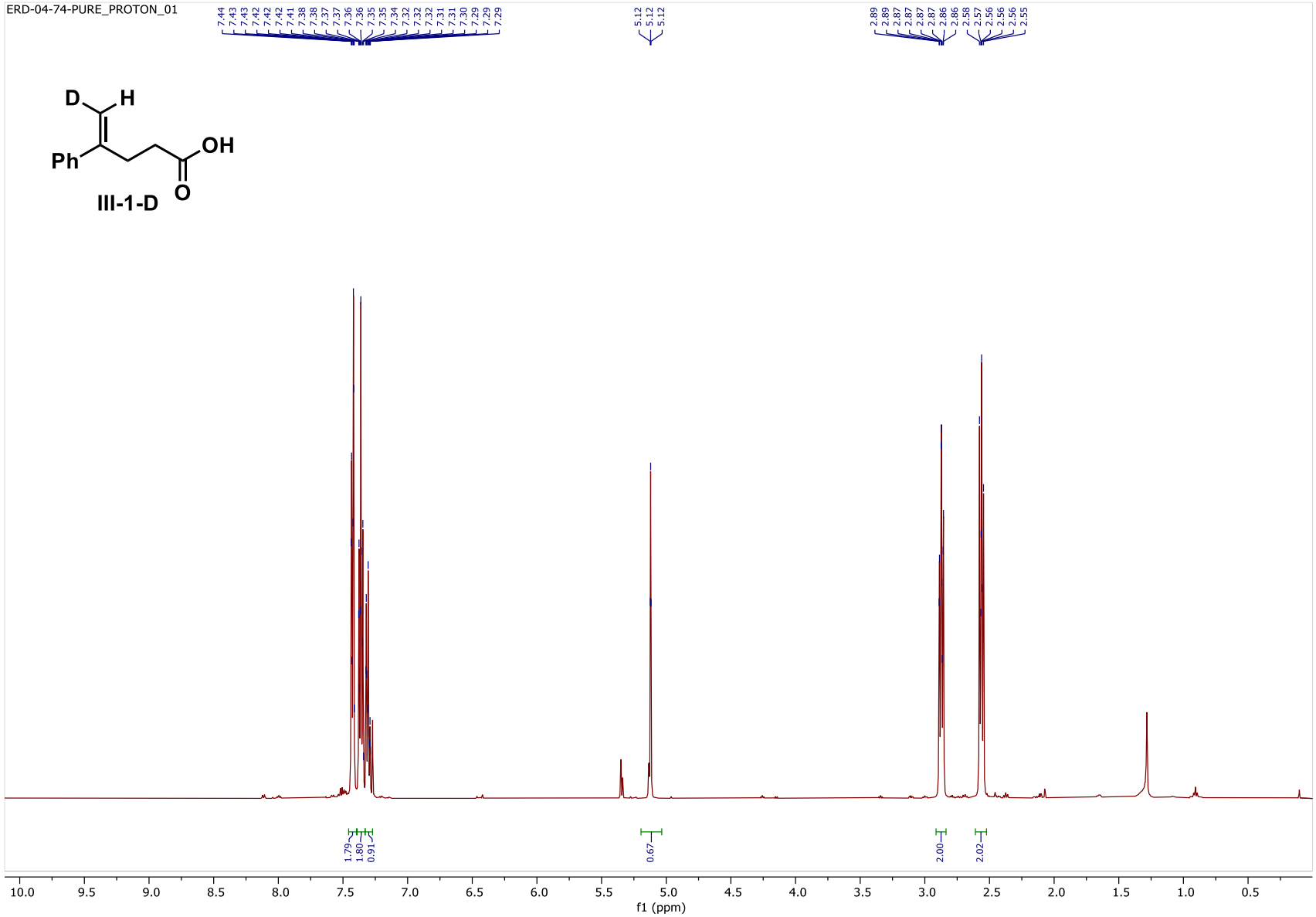

Figure 3.33. ^{13}C NMR of compound **III-1-D** (126 MHz, Chloroform-*d*, 23 ℃)

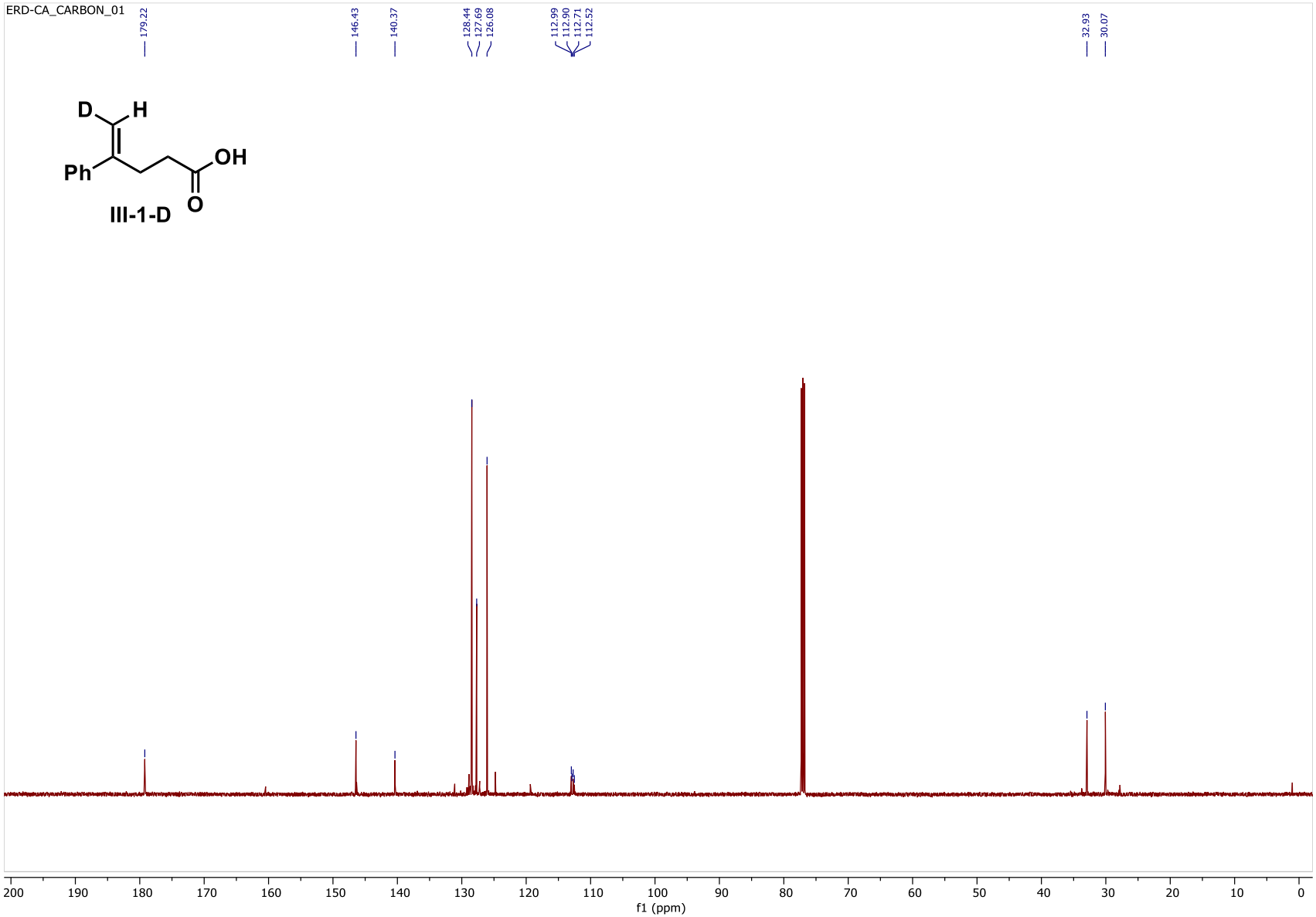

Figure 3.34. ^{1}H NMR of compound **III-2-D** – from uncatalyzed chlorolactonization (500 MHz, Chloroform-*d*, 23℃)

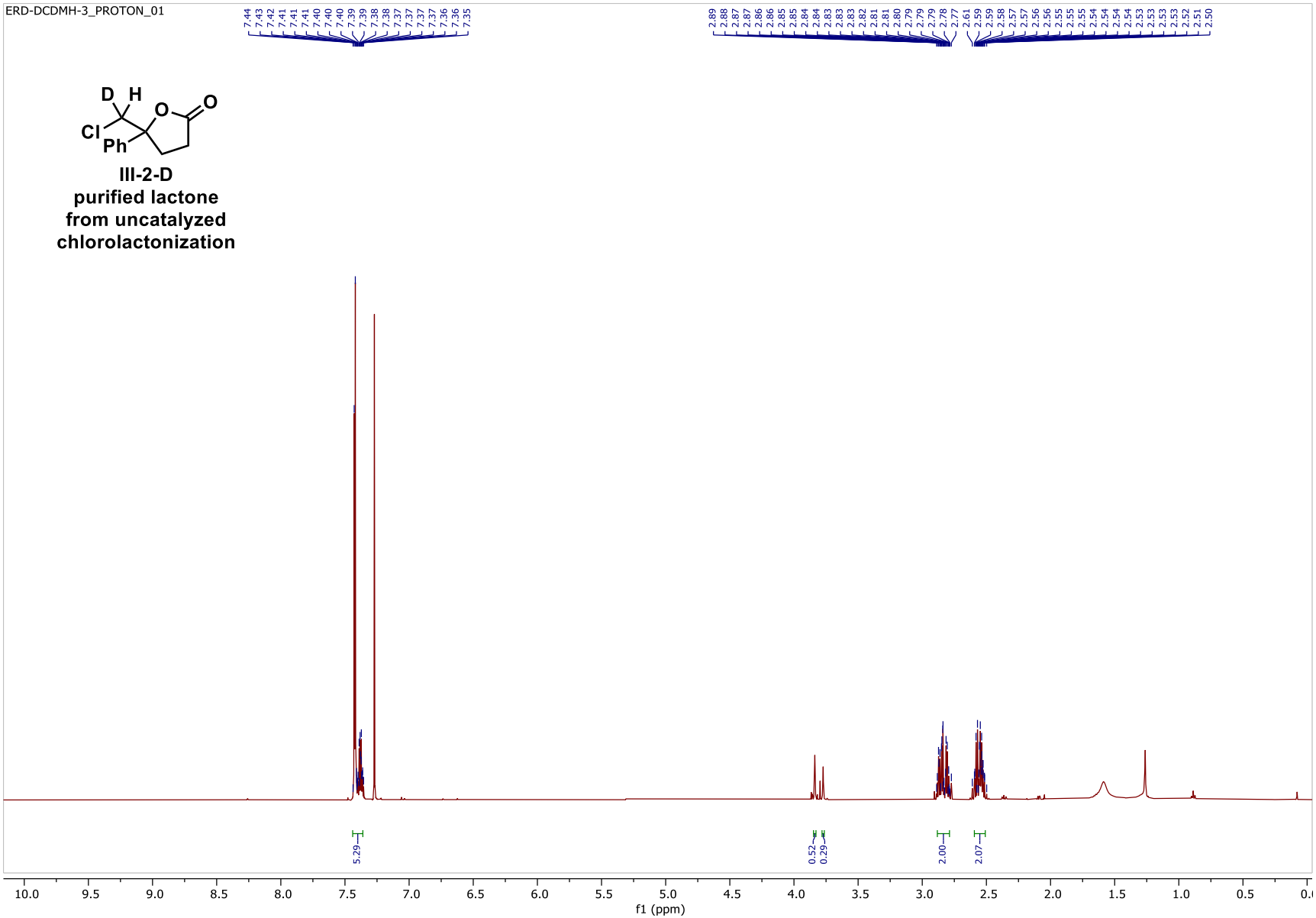

Figure 3.35. ^{1}H NMR of compound **III-2-D** – from catalyzed chlorolactonization (500 MHz, Chloroform-*d*, 23 ℃)

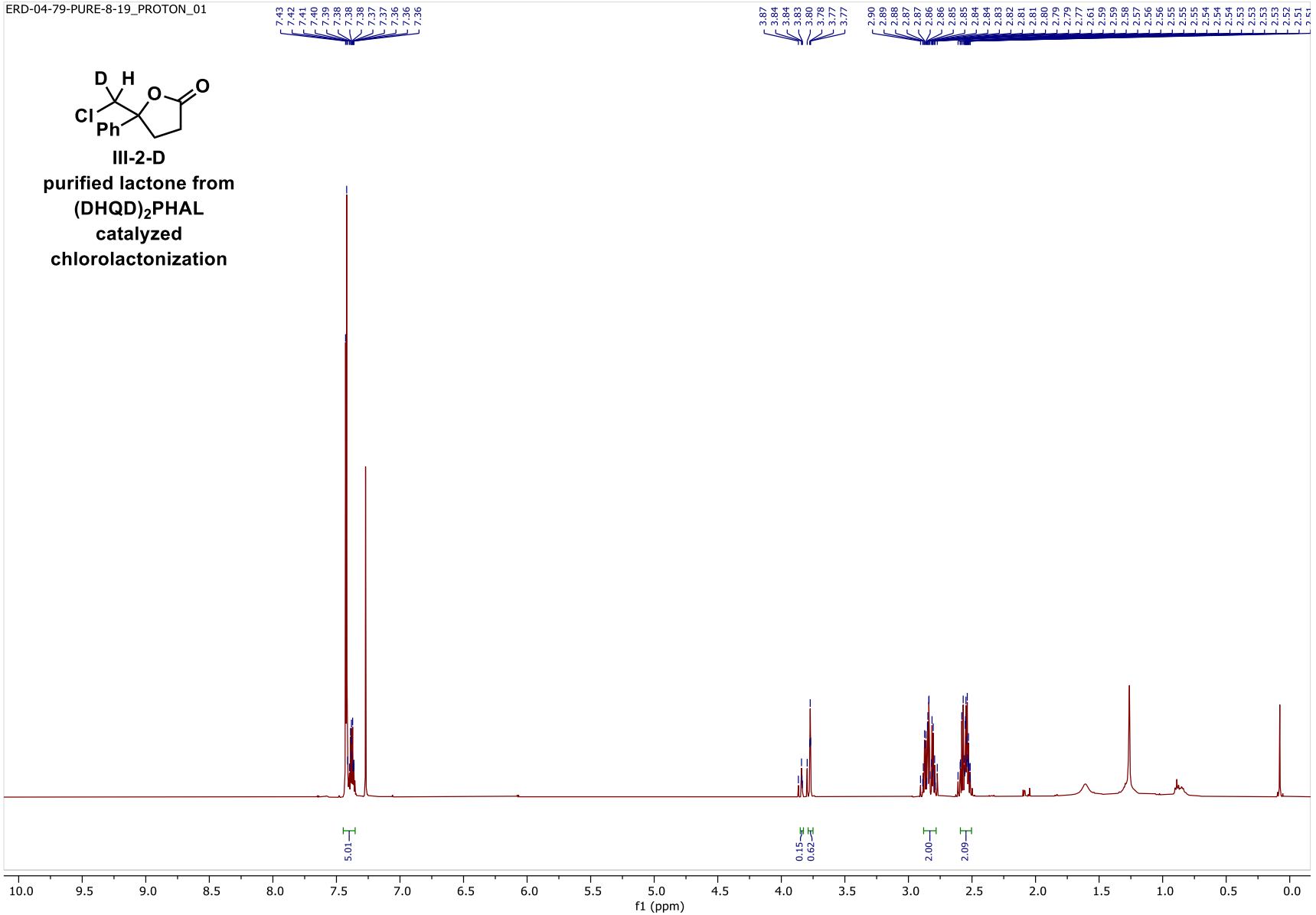

Figure 3.36. ^{13}C NMR of compound **III-2-D** (126 MHz, Chloroform-*d*, 23 ℃)

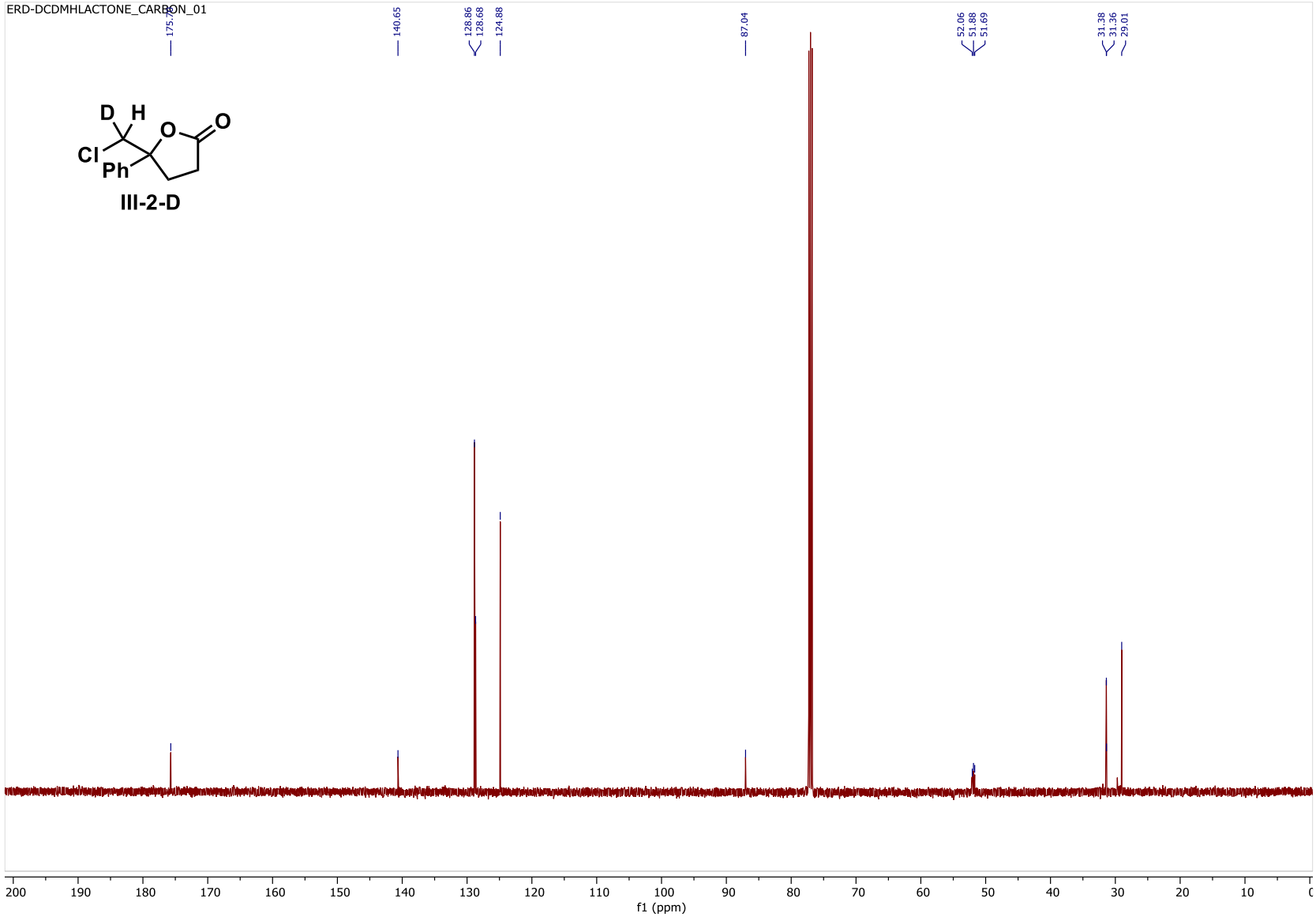

REFERENCES

REFERENCES

(1) D'Ambrosio, M.; Guerriero, A.; Debitus, C.; Ribes, O.; Pusset, J.; Leroy, S.; Pietra, F. Agelastatin a, a New Skeleton Cytotoxic Alkaloid of the Oroidin Family. Isolation from the Axinellid Sponge Agelas Dendromorpha of the Coral Sea. *J. Chem. Soc. Chem. Commun.* **1993**, No. 16, 1305. https://doi.org/10.1039/c39930001305.

(2) Hong, T. W.; Jímenez, D. R.; Molinski, T. F. Agelastatins C and D, New Pentacyclic Bromopyrroles from the Sponge *Cymbastela* Sp., and Potent Arthropod Toxicity of (−)-Agelastatin A. *J. Nat. Prod.* **1998**, *61* (1), 158–161. https://doi.org/10.1021/np9703813.

(3) Tilvi, S.; Moriou, C.; Martin, M.-T.; Gallard, J.-F.; Sorres, J.; Patel, K.; Petek, S.; Debitus, C.; Ermolenko, L.; Al-Mourabit, A. Agelastatin E, Agelastatin F, and Benzosceptrin C from the Marine Sponge *Agelas Dendromorpha*. *J. Nat. Prod.* **2010**, *73* (4), 720–723. https://doi.org/10.1021/np900539j.

(4) Guerriero, A.; D'Ambrosio, M.; Chiasera, G.; Pietra, F. Conformational Preferences and Absolute Configuration of Agelastatin A, a Cytotoxic Alkaloid of the Axinellid Sponge Agelas Dendromorpha from the Coral Sea, via Combined Molecular Modelling, NMR, and Exciton Splitting for Diamide and Hydroxyamide Derivatives. *Helv. Chim. Acta* **1994**, *77* (7), 1895–1902. https://doi.org/10.1002/hlca.19940770720.

(5) Mason, C. K.; McFarlane, S.; Johnston, P. G.; Crowe, P.; Erwin, P. J.; Domostoj, M. M.; Campbell, F. C.; Manaviazar, S.; Hale, K. J.; El-Tanani, M. Agelastatin A: A Novel Inhibitor of Osteopontin-Mediated Adhesion, Invasion, and Colony Formation. *Mol. Cancer Ther.* **2008**, *7* (3), 548–558. https://doi.org/10.1158/1535-7163.MCT-07-2251.

(6) Park, Y.; Liau, B. Uncovering the Cellular Target of Agelastatin A. Cell Chemical Biology, **2017**, 24, 542. https://doi.org/10.1016/j.chembiol.2017.05.002.

(7) Meijer, L.; Thunnissen, A.-M.; White, A.; Garnier, M.; Nikolic, M.; Tsai, L.-H.; Walter, J.; Cleverley, K.; Salinas, P.; Wu, Y.-Z.; Biernat, J.; Mandelkow, E.-M.; Kim, S.-H.; Pettit, G. Inhibition of Cyclin-Dependent Kinases, GSK-3β and CK1 by Hymenialdisine, a Marine Sponge Constituent. *Chem. Biol.* **2000**, *7* (1), 51–63. https://doi.org/10.1016/S1074-5521(00)00063-6.

(8) Harwood, A. J. Regulation of GSK-3: A Cellular Multiprocessor. *Cell* **2001**, *105* (7), 821–824. https://doi.org/10.1016/S0092-8674(01)00412-3.

(9) Stien, D.; Anderson, G. T.; Chase, C. E.; Koh, Y.; Weinreb, S. M. Total Synthesis of the Antitumor Marine Sponge Alkaloid Agelastatin A. *J. Am. Chem. Soc.* **1999**, *121* (41), 9574–9579. https://doi.org/10.1021/ja992487l.

(10) Feldman, K. S.; Saunders, J. C. Alkynyliodonium Salts in Organic Synthesis. Application to the Total Synthesis of (−)-Agelastatin A and (−)-Agelastatin B. *J. Am. Chem. Soc.* **2002**, *124* (31), 9060–9061. https://doi.org/10.1021/ja027121e.

(11) Domostoj, M. M.; Irving, E.; Scheinmann, F.; Hale, K. J. New Total Synthesis of the Marine Antitumor Alkaloid (−)-Agelastatin A. *Org. Lett.* **2004**, *6* (15), 2615–2618. https://doi.org/10.1021/ol0490476.

(12) Davis, F. A.; Deng, J. Asymmetric Total Synthesis of (−)-Agelastatin A Using Sulfinimine (*N* -Sulfinyl Imine) Derived Methodologies. *Org. Lett.* **2005**, *7* (4), 621–623. https://doi.org/10.1021/ol047634l.

(13) Trost, B. M.; Dong, G. A Stereodivergent Strategy to Both Product Enantiomers from the Same Enantiomer of a Stereoinducing Catalyst: Agelastatin A. *Chem. – Eur. J.* **2009**, *15* (28), 6910–6919. https://doi.org/10.1002/chem.200900794.

(14) Ichikawa, Y.; Yamaoka, T.; Nakano, K.; Kotsuki, H. Synthesis of (−)-Agelastatin A by [3.3] Sigmatropic Rearrangement of Allyl Cyanate. *Org. Lett.* **2007**, *9* (16), 2989–2992. https://doi.org/10.1021/ol0709735.

(15) Yoshimitsu, T.; Ino, T.; Tanaka, T. Total Synthesis of (−)-Agelastatin A. *Org. Lett.* **2008**, *10* (23), 5457–5460. https://doi.org/10.1021/ol802225g.

(16) Dickson, D. P.; Wardrop, D. J. Total Synthesis of (±)-Agelastatin A, A Potent Inhibitor of Osteopontin-Mediated Neoplastic Transformations. *Org. Lett.* **2009**, *11* (6), 1341–1344. https://doi.org/10.1021/ol900133v.

(17) Hama, N.; Matsuda, T.; Sato, T.; Chida, N. Total Synthesis of (−)-Agelastatin A: The Application of a Sequential Sigmatropic Rearrangement. *Org. Lett.* **2009**, *11* (12), 2687–2690. https://doi.org/10.1021/ol900799e.

(18) Wehn, P. M.; Du Bois, J. A Stereoselective Synthesis of the Bromopyrrole Natural Product (−)-Agelastatin A. *Angew. Chem. Int. Ed.* **2009**, *48* (21), 3802–3805. https://doi.org/10.1002/anie.200806292.

(19) Movassaghi, M.; Siegel, D. S.; Han, S. Total Synthesis of All (−)-Agelastatin Alkaloids. *Chem. Sci.* **2010**, *1* (5), 561–566. https://doi.org/10.1039/C0SC00351D.

(20) Reyes, J. C. P.; Romo, D. Bioinspired Total Synthesis of Agelastatin A. *Angew. Chem. Int. Ed.* **2012**, *51* (28), 6870–6873. https://doi.org/10.1002/anie.201200959.

(21) Garigipati, R. S.; Freyer, A. J.; Whittle, R. R.; Weinreb, S. M. Diastereoselective Synthesis of Unsaturated Vicinal Amino Alcohols via Diels-Alder Reactions of N-Sulfinyl Dienophiles. *J. Am. Chem. Soc.* **1984**, *106* (25), 7861–7867. https://doi.org/10.1021/ja00337a036.

(22) Sharpless, K. B.; Hori, T. Allylic Amination of Olefins and Acetylenes by Imido Sulfur Compounds. *J. Org. Chem.* **1976**, *41* (1), 176–177. https://doi.org/10.1021/jo00863a051.

(23) Stang, P. J.; Zhdankin, V. *J. Am. Chem. Soc.* **1991**, *113* (12), 4571–4576. https://doi.org/10.1021/ja00012a028.

(24) Hale, K. J.; Domostoj, M. M.; Tocher, D. A.; Irving, E.; Scheinmann, F. Enantiospecific Formal Total Synthesis of the Tumor and GSK-3β Inhibiting Alkaloid, (−)-Agelastatin A. *Org. Lett.* **2003**, *5* (16), 2927–2930. https://doi.org/10.1021/ol035036l.

(25) Yoakim, C.; Ogilvie, W. W.; Cameron, D. R.; Chabot, C.; Guse, I.; Haché, B.; Naud, J.; O'Meara, J. A.; Plante, R.; Déziel, R. β-Lactam Derivatives as Inhibitors of Human Cytomegalovirus Protease. *J. Med. Chem.* **1998**, *41* (15), 2882–2891. https://doi.org/10.1021/jm980131z.

(26) Davis, F. A.; Zhang, Y.; Andemichael, Y.; Fang, T.; Fanelli, D. L.; Zhang, H. Improved Synthesis of Enantiopure Sulfinimines (Thiooxime *S* -Oxides) from *p* -Toluenesulfinamide and Aldehydes and Ketones. *J. Org. Chem.* **1999**, *64* (4), 1403–1406. https://doi.org/10.1021/jo9820622.

(27) Davis, F. A.; Deng, J. Asymmetric Synthesis of *s Yn* -(2 *R* ,3 *S*) - and *a Nti* -(*2S* ,3 *S*)-Ethyl Diamino-3-Phenylpropanoates from *N* -(Benzylidene)- *p* -

Toluenesulfinamide and Glycine Enolates. *Org. Lett.* **2004**, *6* (16), 2789–2792. https://doi.org/10.1021/ol048981y.

(28) Fructos, M. R.; Belderrain, T. R.; de Frémont, P.; Scott, N. M.; Nolan, S. P.; Díaz-Requejo, M. M.; Pérez, P. J. A Gold Catalyst for Carbene-Transfer Reactions from Ethyl Diazoacetate. *Angew. Chem. Int. Ed.* **2005**, *44* (33), 5284–5288. https://doi.org/10.1002/anie.200501056.

(29) Yadav, J. S.; Subba Reddy, B. V.; Mahesh Kumar, G.; Murthy, V. S. R. INDIUM TRICHLORIDE PROMOTED REGIOSELECTIVE RING OPENING OF AZIRIDINES WITH TMS AZIDE. *Synth. Commun.* **2002**, *32* (12), 1797–1802. https://doi.org/10.1081/SCC-120004058.

(30) Fosterj, B.; Webber, M.; Westwood, J. H. [19631 B.Ukhari, Foster, Lehmanlz, Webber, and Westwood. 229. 5.

(31) Crich, D. One Pot Selective 5′-Oxidation/Olefination of 2′-Deoxynucleosides. *Synlett* **1999**, *1999* (1), 67–68. https://doi.org/10.1055/s-1999-2550.

(32) Soai, K.; Ookawa, A.; Kaba, T.; Ogawa, K. Catalytic Asymmetric Induction. Highly Enantioselective Addition of Dialkylzincs to Aldehydes Using Chiral Pyrrolidinylmethanols and Their Metal Salts. *J. Am. Chem. Soc.* **1987**, *109* (23), 7111–7115. https://doi.org/10.1021/ja00257a034.

(33) Ichikawa, Y. J. Chem. Soc., Perkin Trans. 1 1992, 2135

(34) Dinsmore, A.; Mandy, K.; Michael, J. P. Total Synthesis of Two Novel 5,6,7,8-Tetrahydroindolizine Alkaloids, Polygonatines A and B. *Org. Biomol. Chem.* **2006**, *4* (6), 1032–1037. https://doi.org/10.1039/B517573A.

(35) Mashiko, T.; Hara, K.; Tanaka, D.; Fujiwara, Y.; Kumagai, N.; Shibasaki, M. En Route to an Efficient Catalytic Asymmetric Synthesis of AS-3201. *J. Am. Chem. Soc.* **2007**, *129* (37), 11342–11343. https://doi.org/10.1021/ja0752585.

(36) Deardorff, D. R.; Shambayati, S.; Myles, D. C.; Heerding, D. Studies on the Synthesis of (-)-Neplanocin A. Homochiral Preparation of a Key Cyclopentanoid Intermediate. *J. Org. Chem.* **1988**, *53* (15), 3614–3615. https://doi.org/10.1021/jo00250a040.

(37) Nishikawa, T.; Asai, M.; Ohyabu, N.; Isobe, M. Improved Conditions for Facile Overman Rearrangement1. *J. Org. Chem.* **1998**, *63* (1), 188–192. https://doi.org/10.1021/jo9713924.

(38) Okada, M.; Iwashita, S.; Koizumi, N. Efficient General Method for Sulfamoylation of a Hydroxyl Group. *Tetrahedron Lett.* **2000**, *41* (36), 7047–7051. https://doi.org/10.1016/S0040-4039(00)01130-8.

(39) Espino, C. G.; Fiori, K. W.; Kim, M.; Du Bois, J. Expanding the Scope of C−H Amination through Catalyst Design. *J. Am. Chem. Soc.* **2004**, *126* (47), 15378–15379. https://doi.org/10.1021/ja0446294.

(40) Jefford, C. W.; de Villedon de Naide, F.; Sienkiewicz, K. The Synthesis of Chiral 1-(1H-Pyrrole) Derivatives. *Tetrahedron Asymmetry* **1996**, *7* (4), 1069–1076. https://doi.org/10.1016/0957-4166(96)00111-5.

(41) Knapp, S.; Hale, J. J.; Bastos, M.; Gibson, F. S. Amino Protection Using Triazones. *Tetrahedron Lett.* **1990**, *31* (15), 2109–2112. https://doi.org/10.1016/0040-4039(90)80084-Y.

(42) Wittenberg, R.; Srogl, J.; Egi, M.; Liebeskind, L. S. Ketone Synthesis under Neutral Conditions. Cu(I) Diphenylphosphinate-Mediated, Palladium-Catalyzed Coupling of Thiol Esters and Organostannanes. *Org. Lett.* **2003**, *5* (17), 3033–3035. https://doi.org/10.1021/ol034962x.

(43) Otter, B. A.; Falco, E. A.; Fox, J. J. Nucleosides. LXI. Transformations of Pyrimidine Nucleosides in Alkaline Media. IV. Conversion of 5-Hydroxyuridines into Imidazoline Nucleosides. *J. Org. Chem.* **1969**, *34* (9), 2636–2642. https://doi.org/10.1021/jo01261a032.

(44) Müller, S.; Liepold, B.; Roth, G. J.; Bestmann, H. J. An Improved One-Pot Procedure for the Synthesis of Alkynes from Aldehydes. *Synlett* **1996**, *1996* (06), 521–522. https://doi.org/10.1055/s-1996-5474.

(45) Nicolaou, K. C.; Li, Y.; Fylaktakidou, K. C.; Mitchell, H. J.; Wei, H.-X.; Weyershausen, B. Total Synthesis of Apoptolidin: Part 1. Retrosynthetic Analysis and Construction of Building Blocks. *Angew. Chem. Int. Ed.* **2001**, *40* (20), 3849–3854. https://doi.org/10.1002/1521-3773(20011015)40:20<3849::AID-ANIE3849>3.0.CO;2-M.

(46) Garzan, A.; Jaganathan, A.; Salehi Marzijarani, N.; Yousefi, R.; Whitehead, D. C.; Jackson, J. E.; Borhan, B. Solvent-Dependent Enantiodivergence in the Chlorocyclization of Unsaturated Carbamates. *Chem. – Eur. J.* **2013**, *19* (27), 9015–9021. https://doi.org/10.1002/chem.201300189.

(47) Snyder, S. A.; Tang, Z.-Y.; Gupta, R. Enantioselective Total Synthesis of (−)-Napyradiomycin A1 via Asymmetric Chlorination of an Isolated Olefin. *J. Am. Chem. Soc.* **2009**, *131* (16), 5744–5745. https://doi.org/10.1021/ja9014716.

(48) Jaganathan, A.; Garzan, A.; Whitehead, D. C.; Staples, R. J.; Borhan, B. A Catalytic Asymmetric Chlorocyclization of Unsaturated Amides. *Angew. Chem. Int. Ed.* **2011**, *50* (11), 2593–2596. https://doi.org/10.1002/anie.201006910.

(49) Whitehead, D. C.; Yousefi, R.; Jaganathan, A.; Borhan, B. An Organocatalytic Asymmetric Chlorolactonization. *J. Am. Chem. Soc.* **2010**, *132* (10), 3298–3300. https://doi.org/10.1021/ja100502f.

(50) Denmark, S. E.; Kuester, W. E.; Burk, M. T. Catalytic, Asymmetric Halofunctionalization of Alkenes—A Critical Perspective. *Angew. Chem. Int. Ed.* **2012**, *51* (44), 10938–10953. https://doi.org/10.1002/anie.201204347.

(51) Cresswell, A. J.; Eey, S. T.-C.; Denmark, S. E. Catalytic, Stereoselective Dihalogenation of Alkenes: Challenges and Opportunities. *Angew. Chem. Int. Ed.* **2015**, *54* (52), 15642–15682. https://doi.org/10.1002/anie.201507152.

(52) Tan, C. K.; Zhou, L.; Yeung, Y.-Y. Organocatalytic Enantioselective Halolactonizations: Strategies of Halogen Activation. *Synlett* **2011**, *2011* (10), 1335–1339. https://doi.org/10.1055/s-0030-1260578.

(53) Cheng, Y. A.; Yu, W. Z.; Yeung, Y.-Y. Recent Advances in Asymmetric Intra- and Intermolecular Halofunctionalizations of Alkenes. *Org Biomol Chem* **2014**, *12* (15), 2333–2343. https://doi.org/10.1039/C3OB42335B.

(54) Tan, C. K.; Yeung, Y.-Y. Recent Advances in Stereoselective Bromofunctionalization of Alkenes Using N-Bromoamide Reagents. *Chem. Commun.* **2013**, *49* (73), 7985. https://doi.org/10.1039/c3cc43950j.

(55) Ashtekar, K. D.; Marzijarani, N. S.; Jaganathan, A.; Holmes, D.; Jackson, J. E.; Borhan, B. A New Tool To Guide Halofunctionalization Reactions: The Halenium Affinity (*HalA*) Scale. *J. Am. Chem. Soc.* **2014**, *136* (38), 13355–13362. https://doi.org/10.1021/ja506889c.

(56) Denmark, S. E.; Burk, M. T.; Hoover, A. J. On the Absolute Configurational Stability of Bromonium and Chloronium Ions. *J. Am. Chem. Soc.* **2010**, *132* (4), 1232–1233. https://doi.org/10.1021/ja909965h.

(57) Olah, G. A.; Bollinger, J. M. Stable Carbonium Ions. Lvii Catalysts with Olefins.Ang. .Ang. *J. Am. Chem. Soc.* **1968**, *90* (4), 947–953. https://doi.org/10.1021/ja01006a019.

(58) Olah, G. A.; Peterson, P. E. Stable Carbonium Ions. LXVII. Halonium Ion Formation via 1,4-Halogen Participation. Five-Membered-Ring Tetramethylenehalonium, 2-Methyltetramethylenehalonium, and 2,5-Dimethyltetramethylenehalonium Ions. *J. Am. Chem. Soc.* **1968**, *90* (17), 4675–4678. https://doi.org/10.1021/ja01019a030.

(59) Olah, G. A.; Bollinger, J. M.; Brinich, J. *J. Am. Chem. Soc.* **1968**, *90* (25), 6988–6992. https://doi.org/10.1021/ja01027a017.

(60) Zhang, D.; Ghosh, A.; Süling, C.; Miller, M. J. Efficient Functionalization of Acylnitroso Cycloadducts: Application to the Syntheses of Carbocyclic Nucleoside Precursors. *Tetrahedron Lett.* **1996**, *37* (22), 3799–3802. https://doi.org/10.1016/0040-4039(96)00692-2.

(61) Cesario, C.; Tardibono, L. P.; Miller, M. J. Titanocene(III) Chloride-Mediated Reductions of Oxazines, Hydroxamic Acids, and N-Hydroxy Carbamates. *J. Org. Chem.* **2009**, *74* (1), 448–451. https://doi.org/10.1021/jo802184y.

(62) Diéguez, H. R.; López, A.; Domingo, V.; Arteaga, J. F.; Dobado, J. A.; Herrador, M. M.; Quílez del Moral, J. F.; Barrero, A. F. Weakening C−O Bonds: Ti(III), a New Reagent for Alcohol Deoxygenation and Carbonyl Coupling Olefination. *J. Am. Chem. Soc.* **2010**, *132* (1), 254–259. https://doi.org/10.1021/ja906083c.

(63) Trost, B. M.; Dong, G. New Class of Nucleophiles for Palladium-Catalyzed Asymmetric Allylic Alkylation. Total Synthesis of Agelastatin A. *J. Am. Chem. Soc.* **2006**, *128* (18), 6054–6055. https://doi.org/10.1021/ja061105q.

(64) Cincinelli, R.; Musso, L.; Merlini, L.; Giannini, G.; Vesci, L.; Milazzo, F. M.; Carenini, N.; Perego, P.; Penco, S.; Artali, R.; Zunino, F.; Pisano, C.; Dallavalle, S. 7-Azaindole-1-Carboxamides as a New Class of PARP-1 Inhibitors. *Bioorg. Med. Chem.* **2014**, *22* (3), 1089–1103. https://doi.org/10.1016/j.bmc.2013.12.031.

(65) Tian, H.; Ermolenko, L.; Gabant, M.; Vergne, C.; Moriou, C.; Retailleau, P.; Al-Mourabit, A. Pyrrole-Assisted and Easy Oxidation of Cyclic α-Amino Acid- Derived Diketopiperazines under Mild Conditions. *Adv. Synth. Catal.* **2011**, *353* (9), 1525–1533. https://doi.org/10.1002/adsc.201100112.

(66) Nakatsuji, H.; Ueno, K.; Misaki, T.; Tanabe, Y. General, Robust, and Stereocomplementary Preparation of β-Ketoester Enol Tosylates as Cross-Coupling Partners Utilizing TsCl−N-Methylimidazole Agents. *Org. Lett.* **2008**, *10* (11), 2131–2134. https://doi.org/10.1021/ol800480d.

(67) Nguyen, H. N.; Huang, X.; Buchwald, S. L. The First General Palladium Catalyst for the Suzuki−Miyaura and Carbonyl Enolate Coupling of Aryl Arenesulfonates. *J. Am. Chem. Soc.* **2003**, *125* (39), 11818–11819. https://doi.org/10.1021/ja036947t.

(68) Lam, K. C.; Marder, T. B.; Lin, Z. Mechanism of the Palladium-Catalyzed Borylation of Aryl Halides with Pinacolborane. *Organometallics* **2010**, *29* (7), 1849–1857. https://doi.org/10.1021/om9010802.

(69) Ishiyama, T.; Murata, M.; Miyaura, N. Palladium(0)-Catalyzed Cross-Coupling Reaction of Alkoxydiboron with Haloarenes: A Direct Procedure for Arylboronic Esters. *J. Org. Chem.* **1995**, *60* (23), 7508–7510. https://doi.org/10.1021/jo00128a024.

(70) Hofstra, J. L.; Poremba, K. E.; Shimozono, A. M.; Reisman, S. E. Nickel-Catalyzed Conversion of Enol Triflates into Alkenyl Halides. *Angew. Chem. Int. Ed.* **2019**, *58* (42), 14901–14905. https://doi.org/10.1002/anie.201906815.

(71) L. Buchwald, S.; R. Naber, J.; P. Fors, B.; Wu, X.; T. Gunn, J. Stille Cross-Coupling Reactions of Aryl Mesylates and Tosylates Using a Biarylphosphine Based Catalyst System. *HETEROCYCLES* **2010**, *80* (2), 1215. https://doi.org/10.3987/COM-09-S(S)105.

(72) Roberts, I.; Kimball, G. E. The Halogenation of Ethylenes. *J. Am. Chem. Soc.* **1937**, *59* (5), 947–948. https://doi.org/10.1021/ja01284a507.

(73) Chung, W.; Vanderwal, C. D. Stereoselective Halogenation in Natural Product Synthesis. *Angew. Chem. Int. Ed.* **2016**, *55* (14), 4396–4434. https://doi.org/10.1002/anie.201506388.

(74) Landry, M. L.; Burns, N. Z. Catalytic Enantioselective Dihalogenation in Total Synthesis. *Acc. Chem. Res.* **2018**, *51* (5), 1260–1271. https://doi.org/10.1021/acs.accounts.8b00064.

(75) Whitehead, D. C.; Yousefi, R.; Jaganathan, A.; Borhan, B. An Organocatalytic Asymmetric Chlorolactonization. *J. Am. Chem. Soc.* **2010**, *132* (10), 3298–3300. https://doi.org/10.1021/ja100502f.

(76) Garzan, A.; Jaganathan, A.; Salehi Marzijarani, N.; Yousefi, R.; Whitehead, D. C.; Jackson, J. E.; Borhan, B. Solvent-Dependent Enantiodivergence in the Chlorocyclization of Unsaturated Carbamates. *Chem. – Eur. J.* **2013**, *19* (27), 9015–9021. https://doi.org/10.1002/chem.201300189.

(77) Yousefi, R.; Sarkar, A.; Ashtekar, K. D.; Whitehead, D. C.; Kakeshpour, T.; Holmes, D.; Reed, P.; Jackson, J. E.; Borhan, B. Mechanistic Insights into the Origin of Stereoselectivity in an Asymmetric Chlorolactonization Catalyzed by (DHQD)2PHAL. *J. Am. Chem. Soc.* **2020**, *142* (15), 7179–7189. https://doi.org/10.1021/jacs.0c01830.

(78) Yousefi, R.; Ashtekar, K. D.; Whitehead, D. C.; Jackson, J. E.; Borhan, B. Dissecting the Stereocontrol Elements of a Catalytic Asymmetric Chlorolactonization: Syn Addition Obviates Bridging Chloronium. *J. Am. Chem. Soc.* **2013**, *135* (39), 14524–14527. https://doi.org/10.1021/ja4072145.

(79) Burés, J. Variable Time Normalization Analysis: General Graphical Elucidation of Reaction Orders from Concentration Profiles. *Angew. Chem. Int. Ed.* **2016**, *55* (52), 16084–16087. https://doi.org/10.1002/anie.201609757.

(80) Nielsen, C. D.-T.; Burés, J. Visual Kinetic Analysis. *Chem. Sci.* **2019**, *10* (2), 348–353. https://doi.org/10.1039/C8SC04698K.

(81) Burés, J. What Is the Order of a Reaction? *Top. Catal.* **2017**, *60* (8), 631–633. https://doi.org/10.1007/s11244-017-0735-y.

(82) Sarkar, A. CATALYTIC ASYMMETRIC CHLOROFUNCTIONALIZATION REACTIONS: MECHANISTIC DISCOVERIES AND ADVANCEMENTS. 230.

(83) Ashtekar, K. D.; Vetticatt, M.; Yousefi, R.; Jackson, J. E.; Borhan, B. Nucleophile-Assisted Alkene Activation: Olefins Alone Are Often Incompetent. *J. Am. Chem. Soc.* **2016**, *138* (26), 8114–8119. https://doi.org/10.1021/jacs.6b02877.

(84) Denmark, S. E.; Ryabchuk, P.; Burk, M. T.; Gilbert, B. B. Toward Catalytic, Enantioselective Chlorolactonization of 1,2-Disubstituted Styrenyl Carboxylic Acids. *J. Org. Chem.* **2016**, *81* (21), 10411–10423. https://doi.org/10.1021/acs.joc.6b01455.

(85) Zeng, H.; Hua, R. Palladium-Catalyzed Hydrophenylation of Alkynes with Sodium Tetraphenylborate under Mild Conditions. *J. Org. Chem.* **2008**, *73* (2), 558–562. https://doi.org/10.1021/jo7020554.

(86) Marzijarani, N. S.; Yousefi, R.; Jaganathan, A.; Ashtekar, K. D.; Jackson, J. E.; Borhan, B. Absolute and Relative Facial Selectivities in Organocatalytic Asymmetric Chlorocyclization Reactions. *Chem. Sci.* **2018**, *9* (11), 2898–2908. https://doi.org/10.1039/C7SC04430E